Investigating the Intracellular Trafficking of Polymeric Vehicles for Gene Delivery

Julie Shi

A dissertation
submitted in partial fulfillment of the
requirements for the degree of

Doctor of Philosophy

University of Washington

2013

Supervisory Committee:

Suzie Pun, Ph.D., Chair

Patrick Stayton, Ph.D.

Oliver Press, M.D., Ph.D.

Dustin Maly, Ph.D.

Program Authorized to Offer Degree:
Bioengineering

University of Washington

Abstract

Investigating the Intracellular Trafficking of Polymeric Vehicles for Gene Delivery

Julie Shi

Chair of the Supervisory Committee
Associate Professor Suzie Pun, Ph.D.
Bioengineering

Gene therapy has the potential to revolutionize the treatment of diseases caused by genetic mutations. The development of effective, biocompatible synthetic gene delivery vectors can be improved by understanding the intracellular trafficking processes of these vectors. Part I focuses on the mechanistic evaluation of parameters that may be important for nonviral gene delivery. Chapter 1 provides a short introduction to nonviral gene delivery, methods used to determine the intracellular distribution of nonviral vectors, and general development of fractionation methods for determining the intracellular distribution of biologics. Chapter 2 uses the methods optimized in Chapter 1 to determine the bulk intracellular distribution of a synthetic cationic polymer carrier and cargo DNA in a cultured cell line. Chapter 3 is a mechanistic evaluation of the role of particle morphology on gene transfer. In Part II, we describe the development of peptide-functionalized materials for gene delivery. Chapter 4 is a review of the synthetic peptide-polymers developed in the Pun lab. Chapter 5 describes the incorporation of degradable segments into the peptide-polymers, while Chapter 6 describes the incorporation of an endosomal buffering peptide into these polymers. Finally, a new approach to identifying intracellular targeting ligands to a model organelle is described in Chapter 7. Chapter 8 concludes with recommendations for future work based on our findings.

TABLE OF CONTENTS

LIST OF FIGURES

LIST OF TABLES

ACKNOWLEDGMENTS

This thesis is the culmination of the efforts of many people who have given me support and guidance throughout my entire education. I cannot fully express my gratitude to everyone who has contributed to the completion of this Ph.D. thesis, including my mentors prior to graduate school, as well as numerous friends and family, but I would like to highlight those people particularly involved in my graduate school career.

I would first like to thank my advisor, Suzie Pun, for all her guidance, support, and scientific insight. She is truly a wonderful mentor and great role model. She displays a sense of optimism about her students' research despite the numerous trials of failed experiments in the lab. I cannot fathom how she is able to do all that she does, even with having young children at home. She is an inspiring example for women who want to be successful academics, as well as raise a family.

I would also like to thank the members of my reading committee: Dr. Patrick Stayton, Dr. Oliver Press, and Dr. Dustin Maly for their guidance and advice, as well as collaborative research relationships. I would also like to thank Eve Riskin, whom I have worked with on my endeavors outside of research, such as the UW Women's Initiative. She has been supportive in promoting women in engineering and I truly value her service to the university as well as the community.

I would definitely like to thank my previous and current labmates, with whom I have spent the bulk of the last five years:

- Ester Kwon, for being my first mentor in the lab and a great role model for a graduate student. Even after she graduated, she has been happy to answer my questions about the post-doctoral search process;

- Rob Burke, for asking tough questions and helping me work out various logistics with

radioactive work even though he was already in the working world for a couple of years;

- Tae Hee Kim, whose dedication to research (while her family lived far away) and ability to mentor undergraduate students inspired me to also become a good mentor and maintain a good attitude towards work in general;

- Kat Wang, for always being so nice and supportive, and providing a happy working environment;

- Russ Johnson, for being my primary mentor for my polymer work;

- Joan Schellinger, for her sunny disposition and working with me on the polymer work, as well as being a great chemist and mentor;

- Dave Chu, for commiserating with me during all the peptide and polymer synthesis, working together on projects, and for being extremely handy in fixing equipment;

- Leslie Chan and Maryelise Cieslewicz, for being my officemates and making up the "BFF club" (termed by Dave), hanging out with me outside of lab, and engaging in random conversations about science and life;

- Christine Wang, for being my unwilling "protégé", being Sergio's sous-chef, and hanging out with me in general;

- Kevin Tan, Chayanon Ngambenjawong, Nataly Kacherovsky, Paul Elias, and Hua Wei for making lab a little bit more interesting;

- The members of the Stayton lab and the Woodrow lab, for popping into our lab to have conversations (scientific and otherwise), letting me use their equipment, lending me their scientific expertise, and overall, forming great collaborative partnerships;

- and the undergraduates who have worked with me, for being flexible and hard-working, as I would not be able to complete all of my research endeavors without them:
  - Brian Chou, who helped with most of the optimization and method development of the fractionation work;
  - Jennifer Choi, for her unbelievably chipper and happy temperament, and for always being eager to do lots of rather tedious work;
  - Anh Ta, for working hard and taking the initiative to start new projects, even with relatively little expertise;
  - and Ersilia Anghel, a summer Amgen student, for adding some character to the lab, and for contributing to the polymer project in a relatively short amount of time.

I could not do this without the support of my family. My mother and father have been role models in what hard work can do to achieve the "American Dream", and instilled a sense of hard work in me at a young age. My younger siblings, Sharon, Nancy, and Nicholas, always thought I was the nerdy older sister, and for them, I have always felt the need to do well and be a good role model, and to try to inspire them about how cool science can be (although, in that respect, they still think science is boring).

And, of course, I would like to thank my husband, Sergio, who always reminded me that I had a life outside of work. He put up with my many complaints and woes during graduate school, and at the same time, made sure I was fed and mostly sane. He always expects the best from me, and pushes me to do better and achieve greater things.

Lastly, I would also like to thank my friends outside of lab, Tom Long, Austin Day, Joe Phan, and Jing Shang with whom I would sing karoake, eat at Musashi's, go hiking, watch movies, try new restaurants, or play board and video games.

DEDICATION

to my husband, Sergio,

and family,

dad, mom, Sharon, Nancy, and Nicholas

Part I

UNDERSTANDING THE INTRACELLULAR BARRIERS TO GENE DELIVERY WITH POLYMERIC VECTORS

The first section is focused on the development of quantitative tools for probing the intracellular trafficking barriers to non-viral gene delivery, particularly with the use of cationic polymeric vectors, and using these methods to investigate the intracellular distribution of various polymeric vectors and their cargo. There are three chapters in this section:

- Chapter 1 introduces the current methods for probing the intracellular delivery of macromolecules, with a focus on nucleic acids, as well as general method development for fractionation techniques used to separate intracellular organelles in cultured cell lines, with an application to determine the intracellular distribution of a polymer-antibody drug conjugate;

- Chapter 2 applies the fractionation methods developed in Chapter 1 to investigate the intracellular trafficking of polyethylenimine gene carriers and their plasmid DNA cargo;

- and Chapter 3 investigates the role of particle morphology on subsequent gene transfection by examining various steps in the trafficking process, such as cellular uptake, intracellular trafficking kinetics and distribution, and cargo unpackaging.

Chapter 1

DEVELOPMENT OF SUBCELLULAR FRACTIONATION METHODS FOR PROBING THE INTRACELLULAR DISTRIBUTION OF POLYMERIC VECTORS AND CARGO

Julie Shi, Brian Chou, Jennifer L. Choi, Geoffrey Y. Berguig, Oliver W. Press, Patrick S. Stayton, and Suzie H. Pun

Abstract

Subcellular fractionation can be a powerful method for tracking delivery vehicles and their cargo in intracellular organelles. The aim of this work is to establish a quantitative method for determining the intracellular distribution ofpolymer/DNA complexes ("polyplexes") in cultured cell lines using subcellular fractionation techniques. Separation of cytosol and organelle compartments using a combination of differential and density-gradient centrifugation was confirmed by marker enzyme assays and western blotting. Fluorescent-labeling and radiolabeling were also evaluated for tracking polyplex distribution. To demonstrate the versatility of these methods, fractionation studies were carried out to determine the cytosolic distribution of a radiolabeled antibody-polymer conjugate.[1] Fractionation and labeling methods were optimized, and are used to quantify the distribution of both cationic polymer and plasmid DNA in Chapter 2.

[1]Reproduced with permission from Berguig, G.Y., *et al.*, Intracellular delivery and trafficking dynamics of a lymphoma-targeting antibody-polymer conjugate, *Molecular Pharmaceutics*, **9**, pp. 3506-14.

1.1 Introduction

1.1.1 Non-viral gene therapy

Gene therapy involves the use of plasmid DNA to introduce transgenes into cells that inherently lack the ability to produce the protein that the transgene is programmed to generate. As a result, gene therapy has potential to be used in many therapeutic applications. The first federally approved human gene therapy protocol was initiated in 1990 for the treatment of X-linked severe combined immunodeficiency (SCID) [1]. In 2009, scientists reported the successful long-term gene-therapy-based treatment for SCID due to adenosine deaminase deficiency [2]. Patients with Leber congenital amaurosis, a form of congenital blindness, are showing continued visual improvement three years after a single unilateral injection of the gene vector [3]. Currently, diseases with complex etiologies such as cancer, infectious diseases, cardiovascular diseases, and neurodegenerative diseases are also being targeted for gene therapy [4].

There are two main approaches to gene delivery: viral and non-viral. Gene therapy that employs viruses as carriers of DNA has proved successful because viral vectors enable high transfection efficiencies and promote long-term gene expression. However, viral vectors tend to be toxic, cause inflammatory responses, become resistant after repeated uses, and are limited in cargo capacity. The use of non-viral vectors, such as polymers, may resolve these issues. Non-viral vectors are more stable than viral vectors, cause fewer adverse physiological effects, and are not limited by genome size.

In particular, the use of cationic polymers as vectors for gene therapy is promising because of their low toxicity, high biocompatibility, and ease of preparation [5]. Cationic polymers bind to anionic DNA molecules to form positively charged nanoparticles. Because the cell surface is negatively charged, the positively charged surface of polymeric nanoparticles can improve non-specific DNA uptake by cells. Unfortunately, vectors consisting of DNA and polycations, called "polyplexes", are much less efficient in gene transfer than viral vectors. To improve efficiency, polyplexes have been engineered to overcome several barriers to non-viral gene therapy such as cellular uptake, endo-lysosomal degradation, translocation to the nucleus, and transcription of the delivered DNA construct. However, our current

knowledge of how well these engineered constructs are overcoming these obstacles is limited.

Here we describe the current technologies available for analyzing the cellular distribution of biologics, with an emphasis on synthetic gene delivery vectors and associated cargo. The intracellular dynamics of nanomedicines, including non-viral carriers, and overviews of various methods for investigating these dynamics has been recently reviewed by several groups [6–10]; thus, the focus of this brief review will be focused on the methodologies currently under development for tracking biologics delivery vectors.

1.1.2 Quantitative analysis tools for probing polyplex cellular uptake and intracellular processing

Small molecule drugs going through the FDA approval process must undergo a series of extensive pharmacokinetic studies to determine drug biodistribution. However, in contrast to small-molecule drugs, complex biological drugs such as gene delivery vectors are composed of several elements due to their multifunctional nature, and quantitative knowledge must be acquired about the whereabouts of each constituent of the drug. To complicate matters, the target site of these complex biologics is often in the cell. Current methods of understanding the intracellular trafficking of complex biologics are limited; nonetheless, recent progress in developing quantitative tools to understand intracellular processes have allowed further insight into this aspect of gene delivery vectors and their cargo. New approaches and techniques in organelle fractionation and analysis were recently reviewed [11], so this section will focus on the application of these techniques for tracking biologics in intracellular organelles.

Subcellular fractionation

Subcellular fractionation methods allow for the separation of organelles based on mass, size, electrophoretic mobility, and density [12], and have been extensively used for determining the quantitative intracellular distribution of polymeric carriers and their therapeutic cargo. Although initially developed for isolation of organelles from rat liver, subcellular fractionation techniques have been adapted for use with tissue cultured cell lines. Subcellular frac-

tionation involves two main steps: (1) efficient yet gentle homogenization of cells, and (2) separation of organelles, most often *via* centrifugation. The simplest method for subcellular fractionation, called differential centrifugation, uses increasing g-forces to pellet organelles based on mass and size. However, this process results in cross-contamination between organelles and the potential to inadvertently lyse organelle compartments due to repeated centrifugation and pelleting steps. More recently, density-gradient centrifugation, which separates organelles based on buoyant density, has allowed for increased resolution and decreased cross-contamination between organelle compartments [13]. However, the process is tedious, and resolution between organelles of common buoyant density (*e.g.* endosomes and lysosomes) is low.

During instances where endosomal and lysosomal separation is not imperative, density gradients can be used to determine the intracellular distribution of polymer-drug conjugates. A density gradient using Percoll, a density medium that uses colloidal silica particles to self-generate gradients, was used in determining the intracellular distribution of HPMA copolymers conjugated to mesochlorin e_6 monoethylenediamine (Mce_6), a photosensitizer used to target solid tumors which has enhanced damaging capabilities in late endosomes and plasma membrane [14]. The same gradient was also used in determining the efficiency of HPMA-Tat conjugates to localize in the cytoplasm, rather than lysosomes [15]. However, the organelle distribution of conjugates was determined against the organelle distribution of an untreated cell control. An iodixanol gradient was used to determine the subcellular localization of fluorescently-labeled polyethylene glycol (PEG)-polyester dendron G4; addition of the conjugates perturbed the distribution of endocytic organelles [16]. Similar methods were also used in determining the intracellular distribution of branched polyethylenimine (bPEI)/plasmid DNA polplexes, and the distribution of organelles in density gradients were also shifted upon polyplex treatment [17]. Therefore, it is important to determine organelle populations with treated cells to attain accurate analyses.

Several techniques to overcome the lack of resolution between endosomes and lysosomes use density-shift methods [18], immunoisolation [19], or selective hypotonic lysis [20]. Many studies have used horseradish peroxidase (HRP) to increase the density of endosomes in order to separate them from lysosomes. Similarly, treatment of animals with Triton WR-

1339 has also improved the isolation of lysosomes from rat liver [21]. Also, the density of plasma membranes was increased when labeled with colloidal gold before homogenization. However, these methods require perturbation of the natural state of the cell, and can potentially affect quantification when using these methods for tracking of complex biologics. In contrast, immunoisolation allows the isolation of organelles based on antibody affinity, and has been effective in isolating pure populations of organelles. Unfortunately, since the capture efficiencies are rarely 100%, it would be difficult to use this technique for quantifying the intracellular distributions of biologics. Schröter *et al.* reported the optimization of a relatively quick differential centrifugation method where selective hypotonic lysis of lysosomes was used to separate endosomes and lysosomes [20]. However, cross-contamination between compartments can be an issue without careful washing.

Other methods, such as electrophoresis, take advantage of charge differences between organelles for separation. Several electrophoresis methods, such as free-flow electrophoresis (FFE) [22], capillary zone electrophoresis (CZE) [23], and density-gradient electrophoresis (DGE) [24] have been used to effectively separate endosomes and lysosomes; the latter method was also recently used to determine the intracellular distribution of non-viral vectors [25]. In FFE, acidifying organelles are separated by their electrophoretic mobility since they generate a membrane potential. In DGE, differences in both the density and charge of proteins, cells, and organelles are exploited by driving electromigration of the charged species through a viscous medium that varies in density in the same dimension as the applied electrical potential [26]. As a result, this method is particularly useful for separating and collecting different classes of endosomes and lysosomes, which have differential surface protein expression and membrane composition [24, 27–31]. However, some studies have shown considerable overlap between early endosomes and other organelles, such as Golgi, ER, and plasma membrane. Microfluidics (micro-FFE) have also been used to circumvent excessive Joule heating caused by the electric currents necessary for organelle separation in electrophoretic setups, and has been successful used for the isolation of mitochondria [32–35].

The use of antibodies can also enable the isolation of very pure populations of organelles. For example, endosomes have been isolated using immunoisolation, a method where an organelle-specific antibody (*e.g.* anti-EEA1 for endosomes) is used to capture

endosomes from crude organelle preparations [19]. However, this method is impractical to use for studying the intracellular distribution of drugs across multiple organelles. Organelle-specific antibodies are also used in fluorescence-activated organelle sorting (FAOS). Similarly to fluorescence-activated cell sorting (FACS), FAOS uses fluorescently-labeled antibodies to tag particular organelles, which are then separated using flow cytometry. This method is particularly useful in determining the subcellular localization of fluorescently-labeled conjugates [36]; however, affinity-based methods are dependent on the efficiency of the antibody to capture its target, and so, differential binding between antibodies can potentially skew results.

Few studies to date have attempted to use subcellular fractionation to quantify the intracellular distribution of biologics. There are multiple reasons for this: (1) separation techniques are complicated and tedious, often requiring specialized equipment, (2) the scale on which these experiments occur often require large amounts of material and are ill-suited for high-throughput analysis of conjugates, and (3) meaningful data can be obfuscated by contamination between organelle populations. Nevertheless, quantitative assessment of the intracellular distribution of therapeutics can provide valuable insight into the intracellular trafficking of these materials, leading to more accurate model predictions [37, 38] and a quantitative understanding of how the organelle distribution of synthetic vectors are affected by slight chemical modifications.

In particular, quantitative data about the localization of plasmids delivered using non-viral vectors can be crucial in understanding potential barriers to gene delivery [39]. Cohen *et al.* isolated nuclei and quantified the number of intranuclear plasmids delivered by lipoplexes and polyplexes [40]. By doing this, it was discovered that although similar amounts of plasmid was delivered to nuclei, protein expression was higher for lipoplexes, indicating that intranuclear polyplex unpackaging was inefficient. Other studies have also used subcellular fractionation to quantify plasmid DNA delivered to the nucleus using PEI [41], liposomes [42, 43], or adenovirus [44]. Quantitative analyses can also be used in developing predictive models for gene delivery [45]. For example, plasmids delivered using a water-soluble lipopolymer (WSLP) were quantified in plasma membrane, cytosol, lysosomes, and nuclei using real-time polymerase chain reaction (RT-PCR) and the results were applied

to a multi-compartment mathematical model [38]. Plasmids isolated from nuclei were also quantified and used to perform sensitivity analyses with trafficking rate constants for PEI, Lipofectamine, and adenoviral vectors [37]. In addition, radiolabeled plasmid DNA complexed with an RGD-oligolysine peptide and cationic liposomes was tracked in endosomes and lysosomes separated using a Percoll gradient and density-shift of endosomes [46]. An increase in intact DNA was found in the nuclear fraction when liposomes were used over just the peptide alone.

Simpler differential centrifugation techniques have also been used to verify the efficient endosomal release of therapeutic antibodies. For example, anti-CD3, an antibody that is taken up *via* receptor-mediated endocytosis in Jurkat T-cell lymphoma cells and rapidly degraded in lysosomal compartments, was detected in vesicular fractions after a simple cytosolic/vesicular separation [47]. When the antibody was conjugated to a pH-sensitive polymer that became membrane-lytic at endosomal pH, the antibody was seen in the cytosolic fraction as well. However, the study was only semi-quantitative, using western blotting as verification.

Whole-cell quantification methods

Due to the potential leakage of organelles during subcellular fractionation, recent progress in developing quantitative whole-cell techniques involving fluorescence microscopy have been made. In particular, Harashima and coworkers used confocal scanning laser microscopy to quantify fluorescently-labeled polyplexes and lipoplexes in nuclei, cytosol, endosomes, and lysosomes [48]. Since fluorescence intensity is not quantifiable, pixel number was used instead to quantify rhodamine-labeled plasmid DNA in confocal microscopy slices. Using this method, it was determined that the major barrier to delivery of plasmid DNA with oligoarginine (R_8) was entrapment in endosomes/lysosomes, which were labeled with LysoSensor. This method was also used to determine differences in subcellular distribution between lipoplexes and adenovirus [49, 50]. However, using fluorescence as a quantitative tool has been well-criticized due to the sensitivity of fluorophores to environmental factors, such as ionic strength [51], pH [52], and temperature [53].

Techniques without the need for fluorescently or radiolabeling the material include confocal Raman microscopy and secondary mass spectrometry [6, 54, 55]. However, most of these methods have only been applied to small molecule drugs, such as paclitaxel [56]. More tedious methods have also been used, such as quantifying gold nanoparticle uptake in isolated organelles by electron microscopy [55]. A high-throughput version of this method was recently used to quantify the intracellular distribution of gold-labeled siRNA/lipid nanoparticles [57].

1.2 Objectives

Cellular fractionation was developed to isolate organelles, initially from rat liver [58], and then from cultured cell lines and other tissue types [59]. Fractionation methods have been optimized to extract particular organelles, or to determine the relative separation of a variety of organelles. Due to the robustness of fractionation methods, we sought to optimize cellular fractionation methods for determining the intracellular distribution of a labeled polymeric carrier and its cargo in organelles involved in intracellular trafficking, namely the plasma membrane, cytosol, endosomes, and lysosomes. Previous reports have demonstrated the use of cellular fractionation methods to determine the intracellular distribution of polymer-drug conjugates [14–16] as well as gene delivery vectors [40, 41, 46].

We propose to optimize subcellular fractionation methods to track polymeric carriers and their cargo DNA in a cultured cell line. Subcellular fractionation techniques will be developed to isolate nuclei, cytosol, endosomes, and lysosomes. Polyplexes will then be incubated with cells for various amounts of time and quantified in collected fractions, which will correspond to different intracellular compartments. In addition, we will evaluate different labeling methods to determine the optimal labeling of the polymer and DNA for these fractionation studies.

1.3 Materials and methods

1.3.1 Materials

60% (w/v) OptiPrep (iodixanol) was purchased from Axis-Shield (Norton, MA). HALT protease inhibitor cocktail was purchased from Thermo Fisher Scientific (Pittsburgh, PA). Amine-reactive Alexa Fluor 647 was purchased from Invitrogen (Grand Island, NY). 10X Tris/glycine/SDS running buffer, polyacrylamide gels, and filter paper were purchased from Bio-Rad (Hercules, CA). PVDF membrane was purchased either from Bio-Rad (Hercules, CA) or Millipore (Billerica, MA). Horseradish Peroxidase (HRP)-conjugated goat anti-mouse (no. 554002), mouse anti-*EEA1* (250 μg/mL, no. 610457) mouse anti-*Rab5* (250 μg/mL, no. 610725) antibodies were purchased from BD Biosciences (San Diego, CA). Mouse anti-*LAMP2* antibody was purchased from the Developmental Studies Hybridoma Bank (supernatant, no. H4B4, Iowa City, IA). All cell culture medium and supplements were purchased from Cellgro/Mediatech (Fisher Scientific, Pittsburgh, PA). All chemical reagents, including poly(ethylenimine) (PEI, 25,000 g/mol, branched), were reagent-grade or better and were purchased from Sigma-Aldrich (St. Louis, MO) unless otherwise noted. Endotoxin-free plasmid pCMV-Luc2 was prepared by using the pGL4.10 vector (Promega, Madison, WI) and inserting the CMV promoter/intron region from the gWiz Luciferase (Aldevron, Madison, WI). The plasmid was isolated and produced with the Qiagen Plasmid Giga kit (Qiagen, Germany) according to the manufacturer's instructions.

1.3.2 Cell culture

HeLa (human cervical carcinoma) cells were grown in minimum essential medium (MEM) supplemented with 10% FBS and 100 IU penicillin, 100 μg/mL streptomycin, and 0.25 μg/mL amphotericin B. Cells were passaged when they reached ~80% confluency.

Ramos-AW (human EBV-positive Burkitt's lymphoma B cells) were grown in RPMI-1640 medium supplemented with 20 mM HEPES, 2 mM L-glutamine, 10% FBS, and 100 IU penicillin, 100 μg/mL streptomycin. Cell density was maintained at 3×10^5 cells per mL. All cells were grown at 37 °C, 5% CO_2.

1.3.3 Labeling of PEI with Alexa Fluor 647

To label PEI with Alexa Fluor 647, 3.21 mg of branched PEI (25 kD) was reacted at a 1:3 molar ratio with Alexa Fluor 647 carboxylic acid, succinimidyl ester (Invitrogen) in 1 M sodium biocarbonate, pH 8.3, for 1 h at room temperature in the dark. Excess dye was removed by applying the labeling solution to a PD-10 column (GE Healthcare), and the eluent, containing the labeled polymer, was lyophilized. The resulting polymer was reconstituted in 0.1X PBS and the pH was adjusted to 6.5 by adding 0.1 N HCl. The labeled polymer was characterized using a standard curve of dye alone to determine labeling efficiency and the Cu(II) acetate assay, as previously described [60], for the determination of PEI concentration.

1.3.4 Acetylation of PEI with [^{14}C]- or [^{3}H]- acetic anhydride

Branched polyethylenimine (bPEI, MW 25,000 $^{g}/_{mol}$) was reacted *via* acetylation of amines to obtain [^{14}C]- or [^{3}H]-labeled polymer. 20 mg of bPEI was dissolved in 100 μL dioxane and incubated with 5 molar eq. of [^{14}C]acetic anhydride (50 $^{mCi}/_{mL}$) and 20 molar eq. of *N,N*-diisopropylethylamine (DIPEA) per 25 kDa polymer for 2 h at room temperature. The reaction was quenched by adding 500 μL 0.1% glacial acetic acid (in dH_2O). Unreacted acetic anhydride and DIPEA was removed by applying the reaction mixture through a desalting spin column (Zeba, 7k MWCO, Thermo Fisher Scientific, Rockford, IL). The resulting eluent was characterized for the final bPEI concentration using a Cu(II) acetate assay [60] and by scintillation counting. The final polymer concentration was measured to be 3.7 $^{g}/_{L}$ at $\sim 7 \times 10^4$ $^{cpm}/_{\mu L}$. The polymer was diluted to a stock of 1 $^{mg}/_{mL}$ in 0.1X PBS, acidified to pH 6 with 0.1 N HCl, and stored at 4 °C. Further dilution of the polymer was carried out in dH_2O.

1.3.5 Treatment of cells with fluorescently-labeled polyplexes

A stock solution of PEI was prepared at 10 $^{mg}/_{mL}$ in 0.1X phosphate buffered saline (PBS), and the pH was adjusted to 6.5 by adding 0.1 N HCl. To formulate polyplexes, pCMV-Luc2 plasmid DNA was diluted to 0.1 $^{mg}/_{mL}$ in DNase/RNase-free H_2O and mixed with an equal volume of Alexa Fluor 647-labeled PEI at an amine to DNA phosphate (N/P)

ratio of 5. Polyplexes were then allowed to incubate for 10 min at room temperature in the dark. For fractionation studies, 2 mL of the polyplex solution (containing 100 μg DNA) was mixed with 18 mL of Opti-MEM medium (Invitrogen). For each time point, 10 million HeLa cells were grown in 15-cm plates at a concentration of 5 million cells per plate. Cells were washed once with PBS and incubated with 10 mL of polyplexes in OptiMEM for 0, 2, or 4 h at 37 °C, 5% CO_2. Following incubation with polyplexes, cells were prepared for cellular fractionation.

1.3.6 Preparation of iodixianol gradients

Continuous iodixanol gradients were prepared either as previously described [16], with some modifications, or as described in Axis-Shield application sheet S44. As described in Manunta *et al.*, a stock solution of 60% iodixanol (OptiPrep) was diluted to a working stock solution of 50% (v/v) iodixanol with a sucrose buffer (0.25 M sucrose, 6 mM EDTA, 60 mM HEPES-NaOH, pH 7.4). The working solution was further diluted to either 5% or 20% iodixanol with TES buffer (0.25 M sucrose, 10 mM triethanolamine, 1 mM EDTA, pH 7.4). 5-20% continuous iodixanol gradients were prepared by layering 5.5 mL 5% iodixanol on top of 5.5 mL 20% iodixanol in a 13 mL ultracentrifuge tube and preparing continuous gradients using a Gradient Master (Biocomp, New Brunswick, Canada).

As described in Axis-Shield application sheet S44, a stock solution of 60% iodixanol was diluted to a working stock solution of 40% with solution A (235 mM KCl, 12 mM $MgCl_2$, 25 mM $CaCl_2$, 30 mM EGTA, 150 mM HEPES-NaOH, pH 7.0). The working solution was further diluted to either 5% or 20% iodixanol with solution B (78 mM KCl, 4 mM $MgCl_2$, 8.4 mM $CaCl_2$, 10 mM EGTA, 50 mM HEPES-NaOH, pH 7.0). 5-20% continuous iodixanol gradients were prepared as described above.

1.3.7 Cellular fractionation of HeLa cells using differential centrifugation

Differential centrifugation to separate nuclei, plasma membrane, cytosol, endosomes, and lysosomes was carried out as described previously [20], with some modifications. Briefly, two 15-cm plates of 5×10^6 HeLa cells per plate were seeded overnight at 37 °C, 5% CO_2.

All subsequent steps were completed at 4 °C, on ice, and with pre-chilled reagents. Cells were washed three times with PBS, gently lifted off the plates in 5 mL PBS, washed off the plates several times with PBS, and transferred into pre-chilled conical tubes. Cells were then pelleted at 500g for 5 min, and resuspended in 10 mL PBS. Cells were pelleted again and then resuspended in 5 mL TES buffer (0.25 M sucrose, 10 mM triethanolamine, 1 mM EDTA, pH 7.4, with added 1X protease inhibitors). Cells were then homogenized by passing through a 25 5/8-gauge needle until greater than 90% cell lysis was achieved, as determined with trypan blue staining. Cell debris and unbroken cells were pelleted at 2000g for 2 min (fraction De). The supernatant was collected in a new tube and pelleted again at 2000g for 2 min. The supernatants were combined and centrifuged at 4000g for 2 min to pellet a crude fraction of plasma membrane and nuclei (fraction PN). The supernatant was then transferred into a new tube and pelleted again at 4000g for 2 min. The combined supernatants were centrifuged at 100,000g for 2 min to pellet mitochondria, endosomes, and lysosomes (EL). The supernatant was collected in a new tube and centrifuged again at 100,000g for 2 min. The supernatant was designated as the cytosol (fraction C). The resulting pellet (fraction EL) was resuspended in dH_2O and incubated for 10 min. The solution was centrifuged again at 100,000g for 2 min, resulting in a pellet of mitochondria and endosomes (fraction E) and a supernatant of lysosomes (fraction L).

1.3.8 Cellular fractionation of HeLa cells using iodixanol gradients

Two 15-cm plates of 5 $\times$ 10^6 HeLa cells per plate were seeded overnight at 37 °C, 5% CO_2. In some experiments, cells were treated with polyplexes for various times at 37 °C, 5% CO_2 prior to cell harvesting. All subsequent steps were completed at 4 °C, on ice, and with pre-chilled reagents. Cells were washed three times with PBS, gently lifted off the plates in 5 mL PBS, washed off the plates several times with PBS, and transferred into pre-chilled conical tubes. Cells were then pelleted at 500g for 5 min, and resuspended in 10 mL PBS. Cells were pelleted again and then resuspended in 5 mL TES buffer (0.25 M sucrose, 10 mM triethanolamine, 1 mM EDTA, pH 7.4, with added 1X protease inhibitors). Cells were then homogenized by passing through a 25 5/8-gauge needle until greater than

90% cell lysis was achieved, as determined with trypan blue staining. Nuclei and unbroken cells were pelleted at 1000g for 5 min. In other experiments, after washing in PBS, cells were resuspended in 5 mL homogenization medium (0.25 M sucrose, 78 mM KCl, 4 mM $MgCl_2$, 8.4 mM $CaCl_2$, 10 mM EGTA, 50 mM HEPES-NaOH, pH 7.0), pelleted, and homogenized in 1 mL homogenization medium. The resulting post-nuclear supernatant (PNS) was subjected to various fractionation procedures, as follows.

For separation of cytosol and vesicular organelles, PNS (2 mL) was layered on top of a step-gradient of 5% (300 μL) and 20% (200 μL) iodixanol and centrifuged at 200,000g for 2 h at 4 °C. 200 μL fractions were collected from the top and stored at -80 °C for further analysis. In other experiments, the PNS instead was layered on top of 10 μL cushion of 2.5 M sucrose and centrifuged 100,000g for 30 min at 4 °C. The supernatant, containing the cytosol, was transferred and the resulting pellet was resuspended in 500 μL TES buffer, layered on top of another 10 μL 2.5 M sucrose cushion, and centrifuged again at 100,000g for 10 min at 4 °C. The supernatants were combined and the resulting pellet was resuspended in 500 μL TES buffer. Aliquots of the samples were snap-frozen in liquid nitrogen and stored at -80 °C for further analysis.

For separation of endosomes and lysosomes, either PNS or the bottom 3 fractions from the initial cytosolic/vesicular fractionation were layered on top of a 5-20% continuous iodixanol gradient. Each time, a control gradient was prepared with equal volume of TES buffer instead of cell lysate. The tubes were then centrifuged at 114,000g or 90,000g (SW41) for 16-18 h at 4 °C. Twenty-eight 500 μL fractions were collected from the top of the gradient using an automated fraction collector (Brandel). Collected fractions were placed immediately on ice, aliquoted, and stored at -80 °C until further analysis.

1.3.9 Cellular fractionation of Ramos-AW cells

Cytosolic and endosomal/lysosomal fractions containing HD39 antibody/streptavidin (SA) conjugates [61] were separated by cellular homogenization and fractionation. Briefly, hot antibody was complexed with poly(propylacrylic acid) (PPAA) as previously described [61]. 3×10^7 cells were treated with 25 nM [^{3}H]HD39/SA or [^{3}H]HD39/SA-PPAA for 1 h pulse

and 5 h chase. 100 μL of media containing cells and conjugate were collected at the beginning of the pulse for scintillation counting. All further steps were completed at 4 °C, on ice, or with pre-chilled reagents. After treatment, cells were washed twice in 10 mL PBS and pelleted each time at 500g for 5 min. Cells were resuspended in 5 mL TES buffer and pelleted at 1000g for 6 min. The cells were homogenized by passing through a 26^1/$_2$-gauge needle until greater than 90% cell lysis was achieved, as determined with trypan blue staining. Nuclei and unbroken cells were pelleted at 1000g for 5 min. The resulting PNS was layered on top of 10 μL cushion of 2.5 M sucrose and centrifuged 100,000g for 30 min at 4 °C. The supernatant, containing the cytosol, was transferred and the resulting pellet was resuspended in 500 μL TES buffer, layered on top of another 10 μL 2.5 M sucrose cushion, and centrifuged again at 100,000g for 10 min at 4 °C. The supernatants were combined and the resulting pellet was resuspended in 500 μL TES buffer. Aliquots of the samples were snap-frozen in liquid nitrogen and stored at -80 °C for further analysis. Fractions were dissolved in Ultima Gold scintillation fluid (Perkin Elmer, Santa Clara, CA) to measure tritium on a scintillation counter (Beckman LS-6500).

1.3.10 Determination of gradient density

The density of the control gradient fractions was determined by measuring the refractive index (refractometer manufacturer). The density of the gradient was calculated using:

$$\rho = A\eta - B$$

where ρ is the density of the gradient fraction (g/mL), η is the refractive index, A and B are coefficients for ionic and non-ionic media, and are equal to 3.459 and 3.622, respectively [62].

1.3.11 Marker enzyme assays

All fractions were analyzed for lactate dehydrogenase activity (cytosol) [63], N-acetyl-β-glucosaminidase activity (lysosomes) [64], and protein content.

For lactate dehydrogenase activity, 1 μL of each fraction was added to 100 μL NADH/Tris/NaCl (0.244 mM NADH, 81.3 mM Tris, 203.2 mM NaCl, pH 7.2) and equilibrated to 30 °C.

At t_0, 20 μL of Tris/ NaCl/Na-pyruvate (81.3 mM Tris, 203.2 mM NaCl, pH 7.2, 9.76 mM Na-pyruvate) was added to each sample and the absorbance at 339 nm was measured every 10 min for 1 h at 30 °C using a plate reader (Tecan Safire^2). The linear portion of the slope A_{339} *vs.* time was compared to a standard of lactate dehydrogenase enzyme.

For *N*-acetyl-β-glucosaminidase activity, 10 μL of each fraction was added to 70 μL of citrate-phosphate buffer containing substrate (100 mM citrate-phosphate, pH 4.7, 7.5 mM *p*-nitrophenol-*N*-acetyl-β-D-glucosaminide) and incubated for 1 h at 37 °C. To stop the reaction, 200 μL of borate buffer (200 mM borate buffer, pH 9.8) was added to each sample. The specific enzyme activity was calculated by measuring the absorbance at 405 nm using a plate reader and comparing the released *p*-nitrophenol to a standard of *p*-nitrophenol.

Protein content was measured using a protein assay kit (Bio-Rad) according to the manufacturer's instructions, using immunoglobulin as a standard.

For studies with Alexa Fluor 647-labeled PEI, the fluorescence of each fraction was determined using a plate reader (ex. 647/20 nm, em. 670/20 nm).

1.3.12 Protein precipitation using trichloroacetic acid (TCA) and sodium deoxycholate (DOC)

To increase protein loading for SDS-PAGE, aliquots of fractions (250-300 μL) were precipitated using 100% TCA and 2% (w/v) DOC. $^1/_{100^{th}}$ volume eq. of 2% DOC was added to 1 volume eq. of protein sample. The sample was then vortexed and incubated on ice for 30 min. $^1/_{10^{th}}$ volume eq. was added to each sample and incubated overnight at 4 °C. The samples were then centrifuged at 15,000*g* for 15 min at 4 °C, and the supernatant was removed. The protein pellets were washed twice with ice-cold acetone, vortexed, and repelleted. The pellets were allowed to dry and then resuspended in 1X Laemmli sample buffer prior to SDS-PAGE.

1.3.13 Immunoblotting

Aliquots from each fraction were diluted with 5X reducing sample buffer (Pierce) and applied to a pre-cast 4-20% polyacrylamide gel (Bio-Rad). In other experiments, protein from equi-

volume aliquots were precipitated using TCA and DOC, and diluted in 1X Laemmli sample buffer (Bio-Rad) prior to loading onto a gel. Gels were run in a standard Tris/glycine/SDS buffer (25 mM Tris, 192 mM glycine, 0.1% SDS, pH 8.3) at 100 V for ~45 min. Proteins were then transferred onto a PVDF membrane using standard conditions (25 mM Tris, 192 mM glycine, 0.1% SDS, 10% methanol) for 1.5 h at 100 V. Non-specific binding sites were blocked by incubation in blocking buffer (Superblock, Pierce) for 1 h at room temperature. Membranes were then either probed with mouse anti-*Rab5* (1:1000) or anti-*LAMP2* (1:500) in blocking buffer overnight at 4 °C. After 3 × 10 min washes with Tris-buffer saline, pH 7.6, 0.1% Tween-20 (TBS-T), membranes were probed with HRP-conjugated goat anti-mouse antibody (1:100,000) in blocking buffer for 1 h at room temperature. Membranes were washed 3 × 10 min with TBS-T and developed with chemiluminescent substrate (West Femto, Pierce). Chemiluminescence was detected using a Kodak imager (Image Station 4000MM, Rochester, NY).

1.3.14 In vitro transfection with labeled polymer

HeLa cells were seeded at 30,000 cells/mL per well overnight at 37 °C, 5% CO_2 prior to transfection. Polyplexes were formulated with either unlabeled bPEI, Alexa Fluor 647-labeled bPEI, or radiolabeled bPEI (~1 × 10^5 cpm [^{14}C]bPEI + ~1 × 10^5 cpm [^{3}H]bPEI) at N/P 5 by adding eqivolumes of polymer to plasmid DNA (0.1 g/L), pipetting up and down to mix, and incubating for 10 min at room temperature. After the polyplexes were formed, 20 μL (containing 1 μg DNA) was mixed with 180 μL of Opti-MEM medium (Invitrogen). Seeded cells were washed once with PBS and then treated with 200 μL of polyplexes in Opti-MEM, which was added dropwise on top of the cells. After a 8 h incubation at 37 °C, 5% CO_2 in a humidified environment, the cells were washed once again with PBS and incubated in 500 μL of fresh complete medium for an additional 40 h. Cells were harvested and assayed for luciferase expression at 48 h. This was done by washing cells once with PBS, adding of 200 μL reporter lysis buffer (Promega, Madison, WI), and then performing one freeze-thaw cycle to complete the lysis of cells. Lysates were collected and centrifuged at 14,000g for 2 min. Luminescence was carried out following the manufacturers instructions (Promega,

Madison, WI). Luciferase activity is reported in relative light units (RLU) normalized by mg protein (RLU/mg), as measured by a microBCA Protein Assay Kit (Pierce).

1.4 Results and discussion

1.4.1 Fractionation using differential centrifugation

As a first approach, a differential centrifugation scheme was used to separate nuclei and plasma membrane (fraction PN), cytosol (fraction Mi/C), endosomes (fraction E), and lysosomes (fraction L) (Figure 1.1A). Due to the multiple washes and centrifugation steps, only 50% of the total protein was recovered after the separation. Of the recovered protein, 29.3% remained in fraction De, 5.55% in fraction PN, 51.4% in fraction Mi/C, 6.2% in fraction E, and 7.56% in fraction L (Figure 1.1B). Lysosomes, as detected by hexosaminidase activity, were found in all fractions to varying degrees, but mostly in fraction Mi/C and L, indicating incomplete separation of cytosol and lysosomes (Figure 1.1C). Cytosol, as detected by lactate dehydrogenase (LDH) activity, was found mostly in fraction Mi/C (Figure 1.1D). These results indicate that lysosomes did not pellet efficiently from the cytosolic fraction.

1.4.2 Fractionation using a 5-20% continuous iodixanol gradient

Since differential centrifugation resulted in significant organellar contamination between fractions, a density-gradient centrifugation scheme was used instead (Figure 1.2A). To separate organelles involved in the endocytic pathway (cytosol, endosomes, lysosomes), the post-nuclear supernatant was applied onto a 5-20% continuous iodixanol gradient and the fractions collected were analyzed for cytosolic, lysosomal, and protein content (Figure 1.2B). Protein was mostly detected in the lesser dense fractions (fractions 2-8) and distributed throughout the rest of the gradient. LDH activity was detected mostly in fractions 2-7, while hexosaminidase activity was distributed into two peaks, a less dense (fractions 1-9) and denser (fractions 11-22) peak. Further analysis by immunoblotting for EEA1, a protein associated with early endosomes, indicated that endosomes were localized to fraction 4 (Figure 1.2C). Immunoblotting for LAMP1, a lysosomal membrane protein, indicated the denser peak detected by the hexosaminidase assay were indeed lysosomes (data not shown);

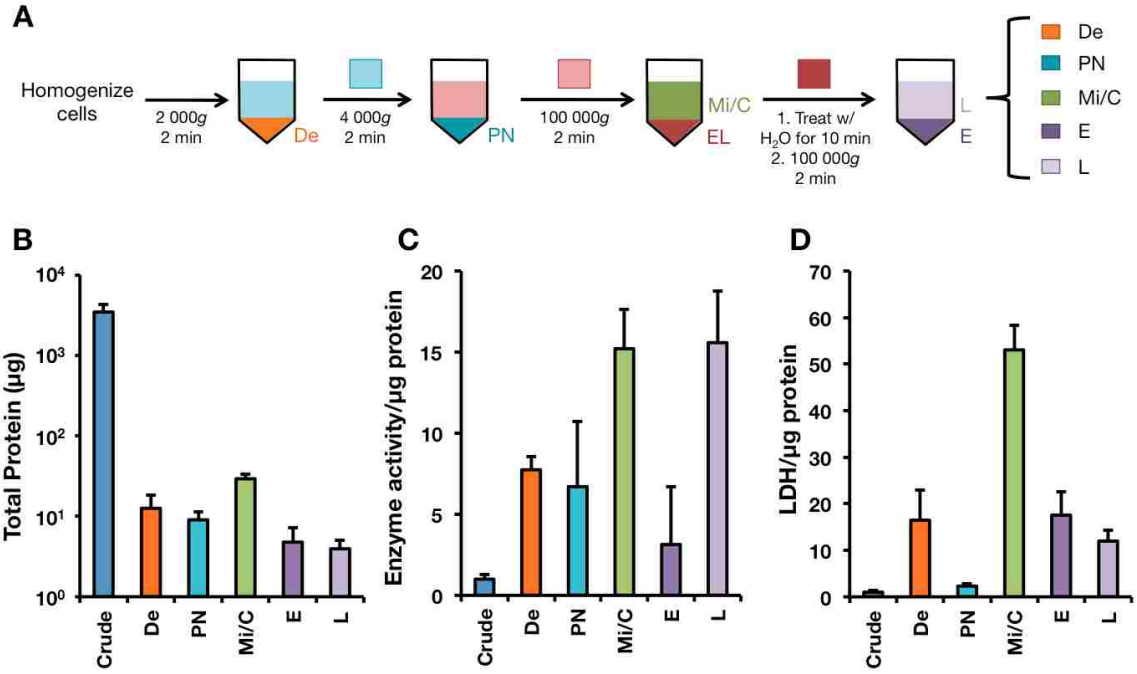

Figure 1.1: **Cellular fractionation using differential centrifugation.** (A) Schematic for differential centrifugation. Ten million HeLa cells were homogenized (crude), centrifuged to pellet destroyed cells (De) sequentially centrifuged at increasing g-forces to separate nuclei/plasma membrane (PN), microsomes/cytosol (Mi/C), endosomes (E), and lysosomes (L). (B) Total protein in collected fractions. (C) Hexosaminidase enzyme activity normalized to protein content in collected fractions. (D) Lactate dehydrogenase enzyme activity normalized to protein content in collected fractions. Data are represented as mean ± S.D., $n = 3$.

however, LAMP1 was not detected in lighter fractions. These results indicate that cytosol and endosomes are co-eluting in the lesser dense section of the gradient and separation was achieved between endosomes and lysosomes.

1.4.3 Subcellular distribution of fluorescently-labeled polymer/DNA complexes

To determine if polyplexes could be tracked in gradients, a model polymer, branched polyethylenimine (bPEI), was fluorescently labeled with Alexa Fluor 647 and incubated with cells for 2 h prior to fractionation on a 5-20% iodixanol gradient. Similarly to the fractionation without polyplex treatment, LDH activity was detected in the lesser dense

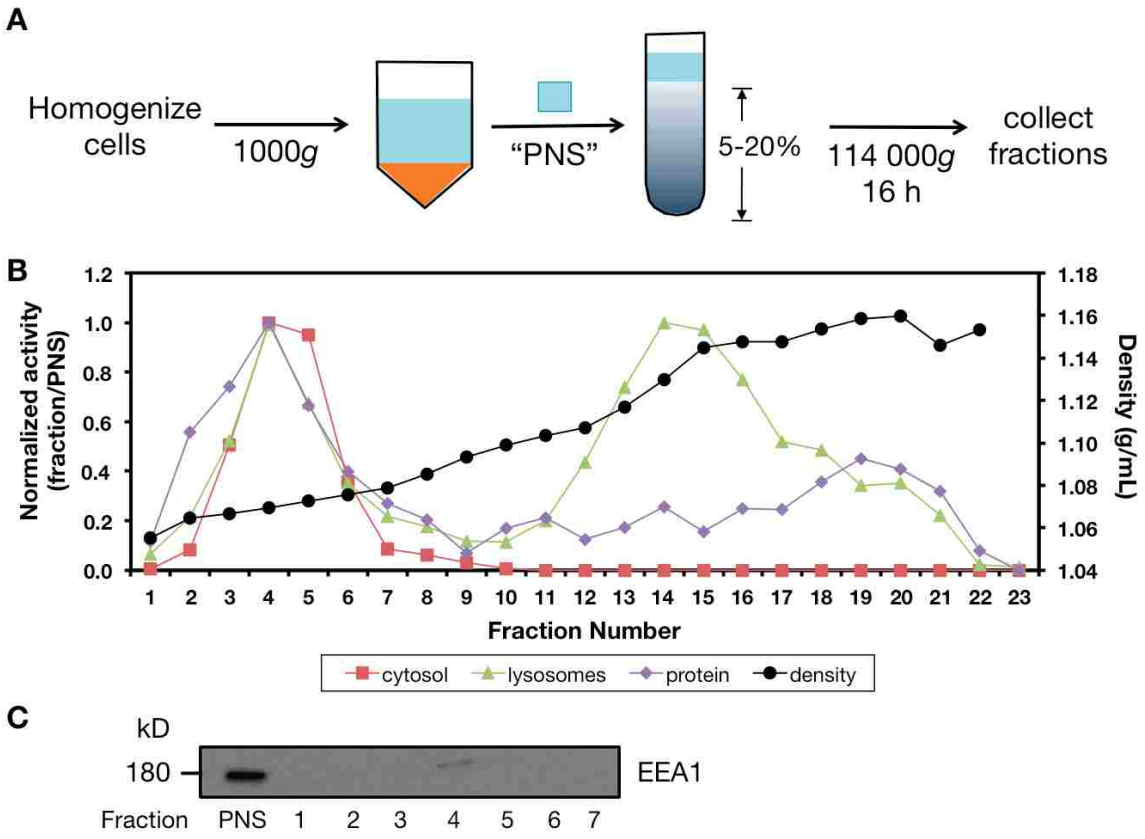

Figure 1.2: **Cellular fractionation using a 5-20% continous iodixanol gradient.** (A) Schematic for density-gradient centrifugation using a 5-20% continous iodixanol gradient. Ten million HeLa cells were homogenized, centrifuged to pellet destroyed cells and nuclei, and the resulting post-nuclear supernatant (PNS) was placed onto a 5-20% continous iodixanol gradient. Fractions were collected after organelles reached their equilibrium bouyant density. (B) Lactate dehydrogenase enzyme activity (red squares), hexosaminidase enzyme activity (green triangles), total protein (purple diamonds), and gradient density (black circles) in collected fractions. (C) Immunoblotting for EEA1 in fractions 1-7.

section of the gradient (fractions 2-8) while hexosaminidase activity was distributed into a lesser dense (fractions 2-8) and denser peak (fractions 11-20) (Figure 1.3). Interestingly, the denser peak of the hexosaminidase activity seemed less broad than the denser peak without polyplex treatment. Polyplexes, detected by fluorescence measurements, were detected throughout the gradient, with a sharp peak at the denser end of the gradient (fractions 18-22). Initial density-gradient studies using a Hoechst 33258 as a marker for nuclei showed

a peak positive for Hoechst at fractions 17-24, suggesting that polyplexes may be associated with nuclei that did not pellet during the initial centrifugation. However, Hoechst dyes have also been shown to stain isolated mitochondria [65].

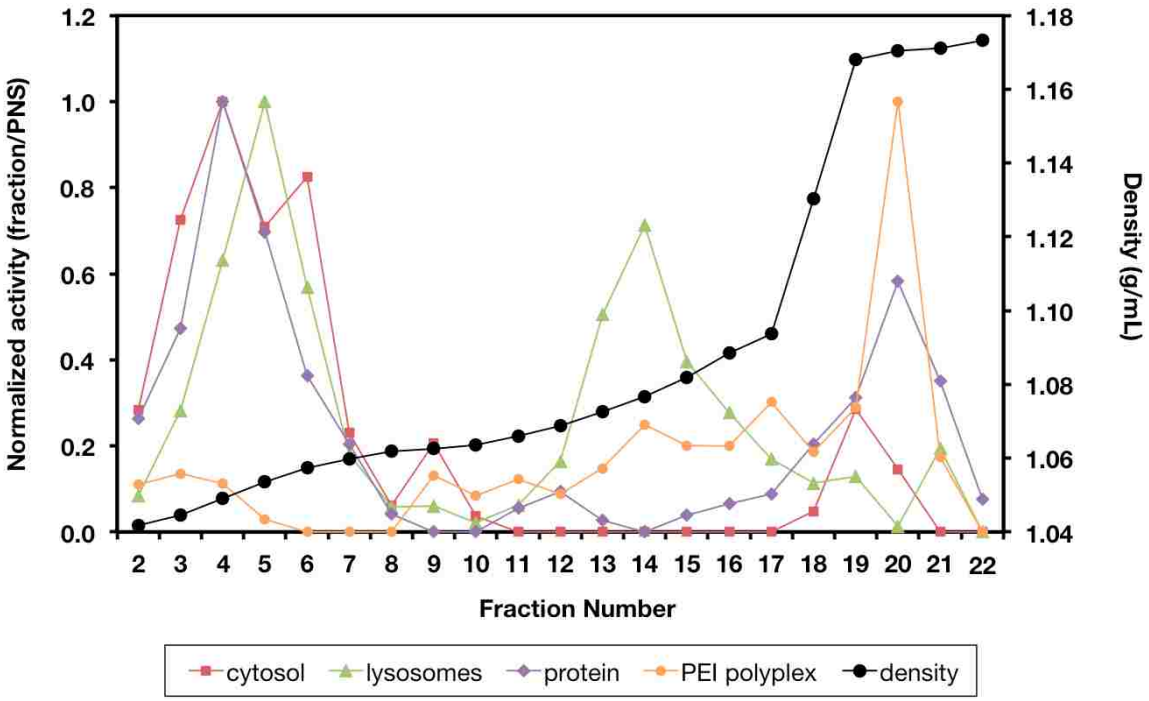

Figure 1.3: **Subcellular distribution of Alexa Fluor 647-labeled PEI polyplexes.** Ten million HeLa cells were incubated for 2 h with Alexa Fluor 647-labeled PEI polyplexes and fractionated using a 5-20% continous iodixanol gradient. Lactate dehydrogenase enzyme activity (red squares), hexosaminidase enzyme activity (green triangles), total protein (purple diamonds), PEI polyplex fluorescence (orange circles), and gradient density (black circles) in collected fractions.

1.4.4 Fractionation using a 2-step procedure

In order to separate cytosol and endosomes, a two-step fractionation procedure combining differential and density-gradient centrifugation was used (Figure 1.4A). Crude preparations of nuclei/plasma membrane, microsomes/cytosol, and endosomes/lysosomes were prepared using differential centrifugation, and each fraction was then placed onto a 5-20% iodixanol gradient (Figure 1.4B) to further separate endosomes and lysosomes. LDH was found mostly

in the Mi/C fraction and was distributed in the lesser dense portion of the gradient (Figure 1.4C). Hexosaminidase activity was found mostly in the Mi/C and EL fractions (Figure 1.4D). Hexosaminidase activity was again split into a lesser dense and denser peak, with the lesser dense peak in the Mi/C fraction and the denser peak in the EL fraction. Further analysis by immunoblotting showed that early endosomes remained in the Mi/C fraction (Figure 1.4E), indicating incomplete endosomal pelleting in the last step of differential centrifugation.

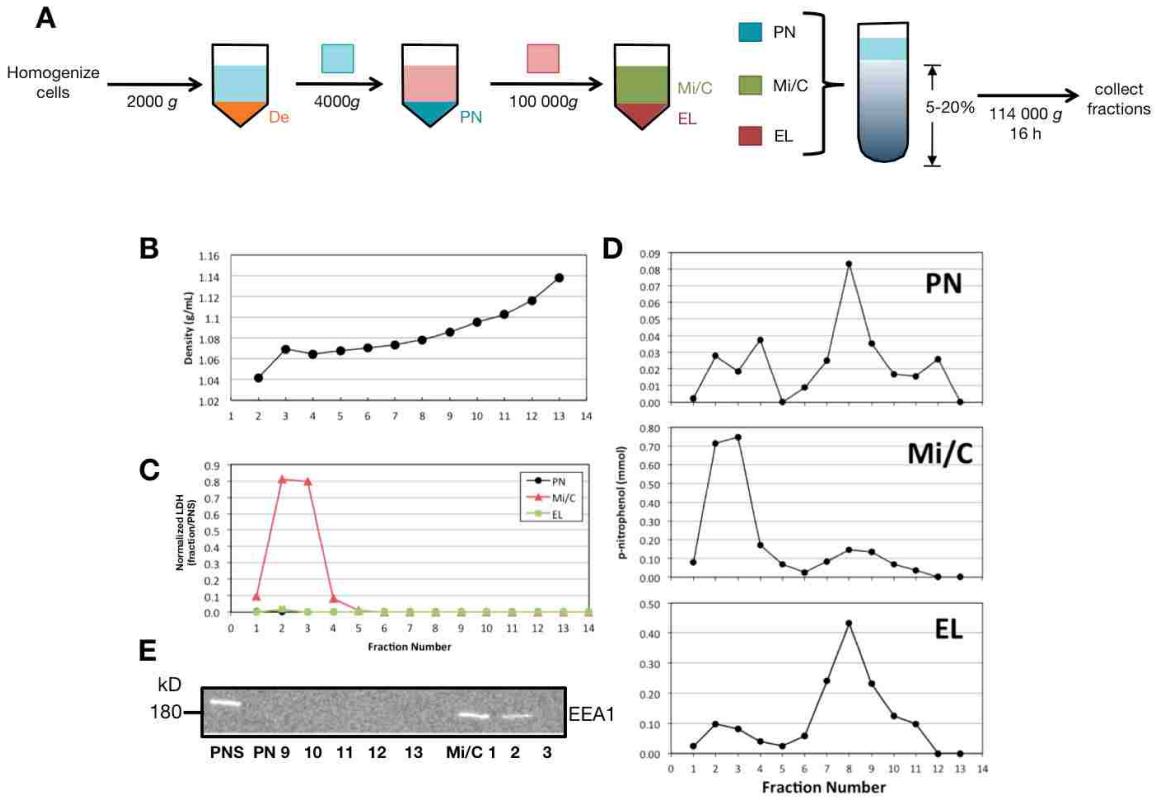

Figure 1.4: **Cellular fractionation using a 2-step procedure.** (A) Schematic for 2-step fractionation procedure. Ten million HeLa cells were subjected to an initial differential centrifugation step prior to fractionation using a 5-20% continous iodixanol gradient. (B) Gradient density in collected fractions. (C) Lactate dehydrogenase enzyme activity in collected fractions from samples PN (black circles), Mi/C (red triangles), and EL (green squares). (D) Hexosaminidase enzyme activity in collected fractions from samples PN, Mi/C, and EL. (E) Immunoblotting for EEA1 in collected fractions.

Previous studies have shown that introducing horseradish peroxidase (HRP) into endosomes could increase the buoyant density of endosomes, thereby allowing endosomes to appear in denser portions of the density gradient [18]. To determine if polyplex treatment could have the same effect as HRP, fluorescently-labeled PEI polyplexes were incubated with cells for 30 min, 2 h, or 4 h and subsequently fractionated using the two-step fractionation procedure. At 30 min, LDH activity was mostly found in fractions 1-2 in the Mi/C fraction (Figure 1.5), but seemed more dispersed throughout the entire gradient than previously detected (Figure 1.4C). The denser peak of hexosaminidase activity was also shifted slightly downwards (Figure 1.5). After 2 h, LDH activity appeared in three distinct peaks while hexosaminidase activity appeared as two characteristic lesser dense and denser peaks. By 4 h, the two denser peaks of LDH activity seemed more diffuse and less intense while hexosaminidase activity remained relatively unchanged. These results suggest that polyplexes may be interacting with soluble cytosolic proteins and subsequently perturbing cytosolic density in the gradient. Furthermore, immunoblotting for EEA1 showed that endosomes still remained in the Mi/C fraction (data not shown). Unfortunately, fluorescence of the labeled polymer could not be detected in any fraction, suggesting that fluorescence may not be sensitive enough for these fractionation studies.

1.4.5 Optimizing cytosolic vs. vesicular fractionation

As a first approach to optimize for the separation of cytosol and endosomes, cytosol and membrane-bound organelles were separated by centrifugation of the PNS at 150,000g for 1 h in a swinging-bucket rotor. However, the resulting pellet was difficult to resuspend and was unusable for further separation. Therefore, a small buffer layer of 20% iodixanol was placed underneath the PNS during centrifugation so that membrane-bound organelles could remain intact (Figure 1.6A). Since EEA1 can also be detected in the cytosol [66], the protein Rab5 was used as an early endosomal marker instead. Immunoblotting for Rab5 showed a small percentage of endosomes remained in the cytosol (fraction C) (Figure 1.6B). To increase cytosolic and early endosomal separation, an additional layer of 5% iodixanol was added in between the PNS and 20% iodixanol layer, the centrifugation was increased to

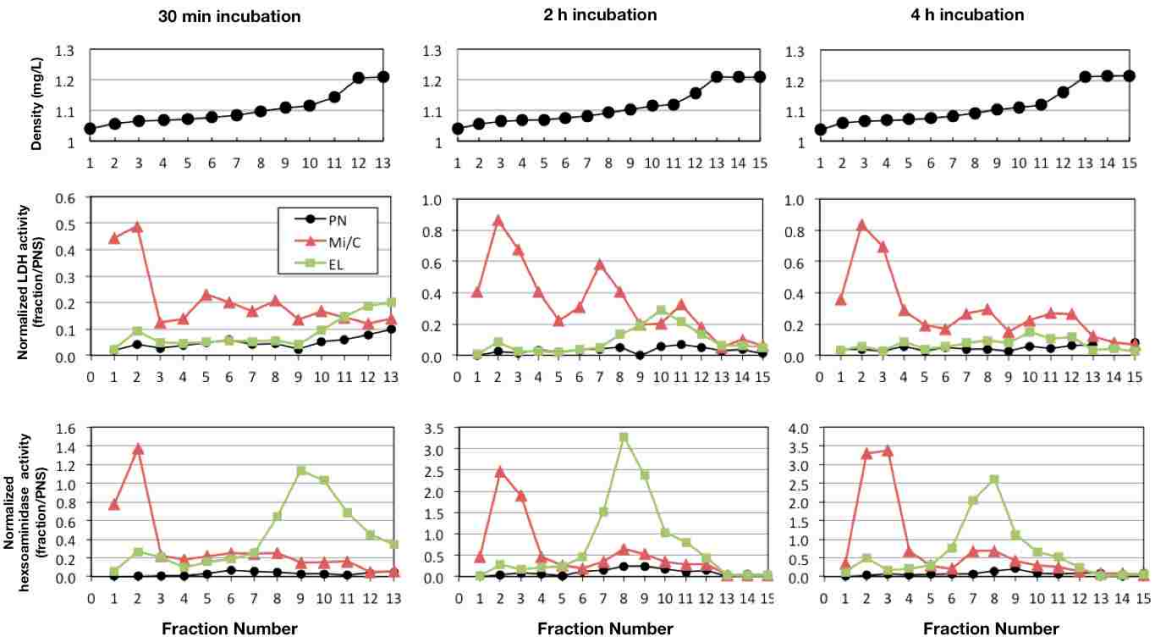

Figure 1.5: **Cytosolic and lysosomal distribution after treatment with PEI polyplexes for up to 4 h.** Ten million HeLa cells were incubated with PEI polyplexes for 30 min, 2 h, or 4 h at 37 °C before fractionation using a 2-step procedure. Gradient density is shown in the top row. Lactate dehydrogenase enzyme activity in collected fractions from samples PN (black circles), Mi/C (red triangles), and EL (green squares).

200,000g for 2 h, and 10-100 μL fractions were taken from the top of the discontinuous step gradient (Figure 1.7A). Early endosomes, as detected by Rab5, appeared mostly in fractions 9-10 (Figure 1.7B), although LDH activity seemed distributed throughout the middle of the gradient, peaking around fraction 6 (Figure 1.7C). To further separate endosomes and lysosomes, fractions 9-10 were placed onto a 5-20% continuous iodixanol gradient (Figure 1.8A). LDH activity remained in fractions C1-C8 while hexosaminidase activity was detected in one major peak at fractions 12-18 (Figure 1.8B). However, separation of cytosol and endosomes in the initial fractionation step was not reproducible since a repeated experiment showed a large amount of LDH in lighter fractions of the continuous iodixanol gradient (Figure 1.8C).

The fractionation procedure of cytosol and membrane-bound organelles was further modified to include a wash step so that residual cytosol would be removed from the vesicular

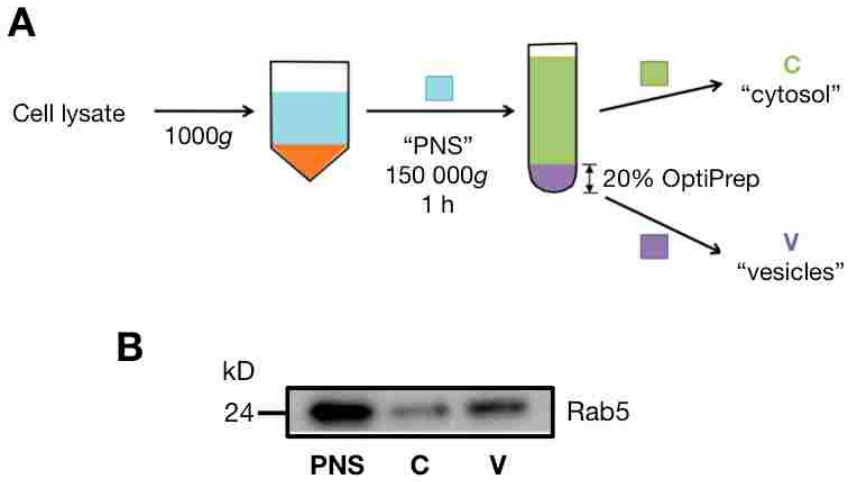

Figure 1.6: **Optimizing cytosolic *vs.* vesicular separation using a small cushion of 20% iodixanol.** (A) Schematic for cytosolic *vs.* vesicular separation. The post-nuclear supernatant (PNS) from 10 million HeLa cells were centrifuged on top of a small cushion of 20% iodixanol to separate cytosol from vesicles. (B) Immunoblotting for Rab5 in PNS, cytosolic, and vesicular fractions.

pellet (Figure 1.9A). In addition, a fixed angle rotor was used instead of a swinging-bucket rotor since the necessary volume for centrifugation was reduced, facilitating further separation on a density gradient, and separation time was shortened due to increased centrifugal forces. Immunoblotting for Rab5 and LAMP2, a lysosomal-associated membrane protein, demonstrated that endosomes were pelleted with the vesicular fraction (Figure 1.9B). Furthermore, greater than 99% of the total LDH activity was seen in the cytosolic fraction (data not shown), indicating little contamination of cytosol in the vesicular fraction.

1.4.6 Cytosolic and vesicular distribution of antibody-polymer conjugates in Ramos-AW cells

To demonstrate that materials could be quantified after cellular fractionation, the cytosolic and vesicular distribution of a model antibody-polymer conjugate [61] was determined using the fractionation procedure in Figure 1.9A. HD39 is an anti-CD22 internalizing monoclonal antibody (mAb) developed for the treatment of Non-Hodgkin lymphoma [67]. The

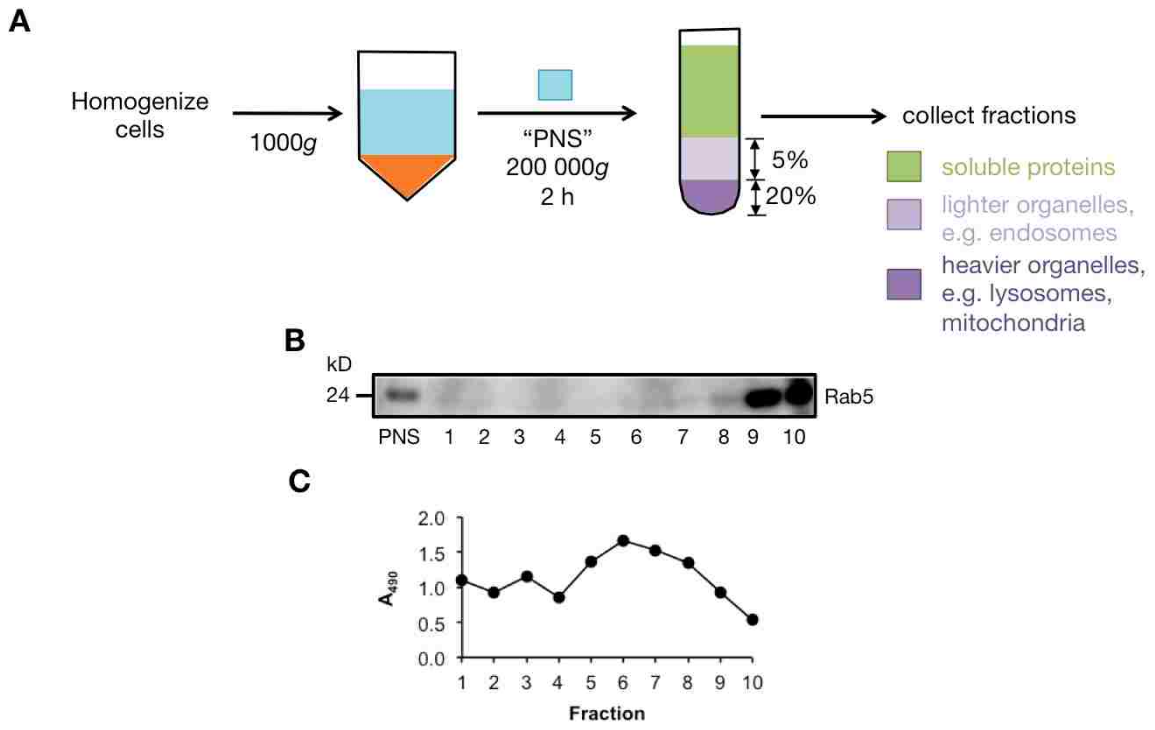

Figure 1.7: **Optimizing cytosolic *vs.* vesicular separation using a small cushion of 5 and 20% iodixanol.** (A) Schematic for cytosolic *vs.* vesicular separation. The post-nuclear supernatant (PNS) from 10 million HeLa cells were centrifuged on top of a small cushion of 5 and 20% iodixanol to increase separation of cytosol from vesicles. (B) Immunoblotting for Rab5 in PNS and collected fractions. (C) LDH activity in collected fractions.

antibody is taken up *via* receptor-mediated endocytosis, where it is trafficked to lysosomes for degradation. In order to increase cytosolic release and therapeutic effect, pH-responsive polymers, such as poly(propylacrylic acid) (PPAA), have been conjugated to mAbs and demonstrated increased efficacy [68]. Using the fractionation procedure in Figure 1.9A with untreated Ramos-AW cells, an EBV-positive lymphoma B-cell line, most of the endosomes were pelleted in the vesicular fraction (Figure 1.10A), and the vesicular fraction was devoid of LDH activity (data not shown). Biotinylated HD39 was radiolabeled with tritium, conjugated to either streptavidin (SA) or PPAA-SA, pulsed with Ramos-AW cells for 1 h, and then chased with fresh media for an additional 5 h. After the 1 h pulse, ~95% of the total applied HD39 or HD39/SA-PPAA appeared in the removed media and washes. After the

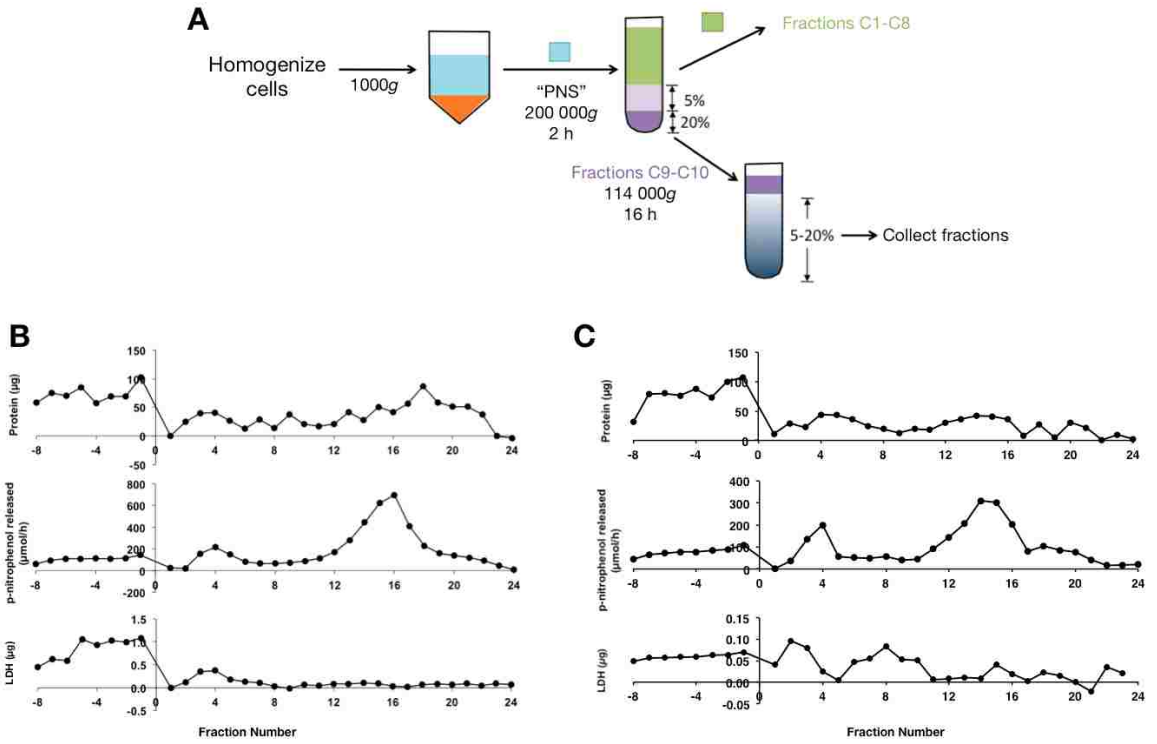

Figure 1.8: **Cellular fractionation using a 2-step procedure.** (A) Schematic for revised 2-step fractionation procedure. Ten million HeLa cells were subjected to an initial differential centrifugation step to separate cytosol and vesicular organelles prior to fractionation of the vesicular fraction using a 5-20% continous iodixanol gradient. (B) Total protein, hexosaminidase enzyme activity, and lactate dehydrogenase enzyme activity in collected fractions from one experiment. (C) Total protein, hexosaminidase enzyme activity, and lactate dehydrogenase enzyme activity in a repeated experiment.

5 h chase, only ~0.1-0.15% of the initial treatment was taken up by cells. Despite the low percentage of uptake, radiolabeled antibody was still detected in subsequent fractionation samples. Conjugation of PPAA to the antibody increased cytosolic release 3.5-fold (Figure 1.10B). However, a small amount of Rab5 was detected in the cytosolic fraction (Figure 1.10C). These results indicate that radiolabeled materials can be quantified successfully after cellular fractionation.

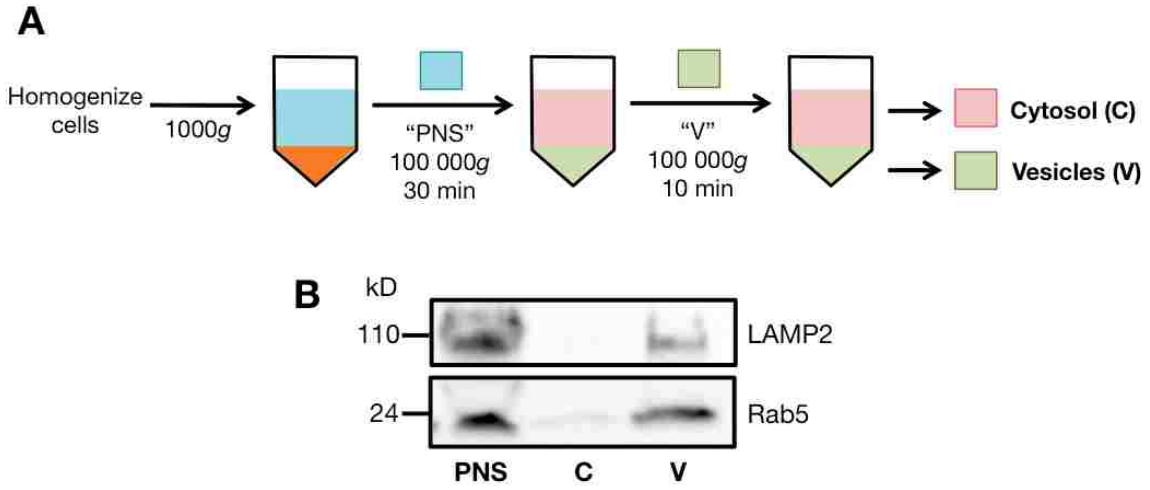

Figure 1.9: **Optimizing cytosolic *vs.* vesicular separation using a small cushion of 2.5 M sucrose.** (A) Schematic for cytosolic *vs.* vesicular separation. Ten million HeLa cells were subjected to a differential centrifugation step to separate cytosol and vesicular organelles. The post-nuclear supernatant (PN) was centrifuged onto a 10 μL cushion of 2.5 M sucrose, and the resulting pellet was washed, resuspended in buffer, and centrifuged again to obtain a pure cytosolic supernatant and a vesicular pellet. (B) Immunoblotting for Rab5 and LAMP2 in post-nuclear supernatant (PNS), cytosolic (C), and vesicular (V) fractions.

1.4.7 Fractionation using an improved 2-step procedure

To further separate endosomes and lysosomes, the vesicular fraction was resuspended and placed onto a 5-20% iodixanol gradient (Figure 1.11A). Immunoblotting for Rab5 and LAMP2 showed complete overlap of endosomes and lysosomes (fractions 14-18), indicating that organelles may be aggregating together (Figure 1.11B). In order to decrease potential organellar aggregation, salts were added to the homogenization buffer [69]. As a control, the PNS was also directly applied to the continuous iodixanol gradients to determine if the initial differential centrifugation step influenced endosomal/lysosomal distribution (Figure 1.11C). Without the initial centrifugation step, Rab5 was seen in two sections of the gradient, a lesser dense section (fractions 2-6) and a denser section (fractions 14-16), while LAMP2 was distributed throughout the middle of the gradient (fractions 11-17). When just the vesicular fraction was applied to the gradient (Figure 1.11D), LAMP2 distribu-

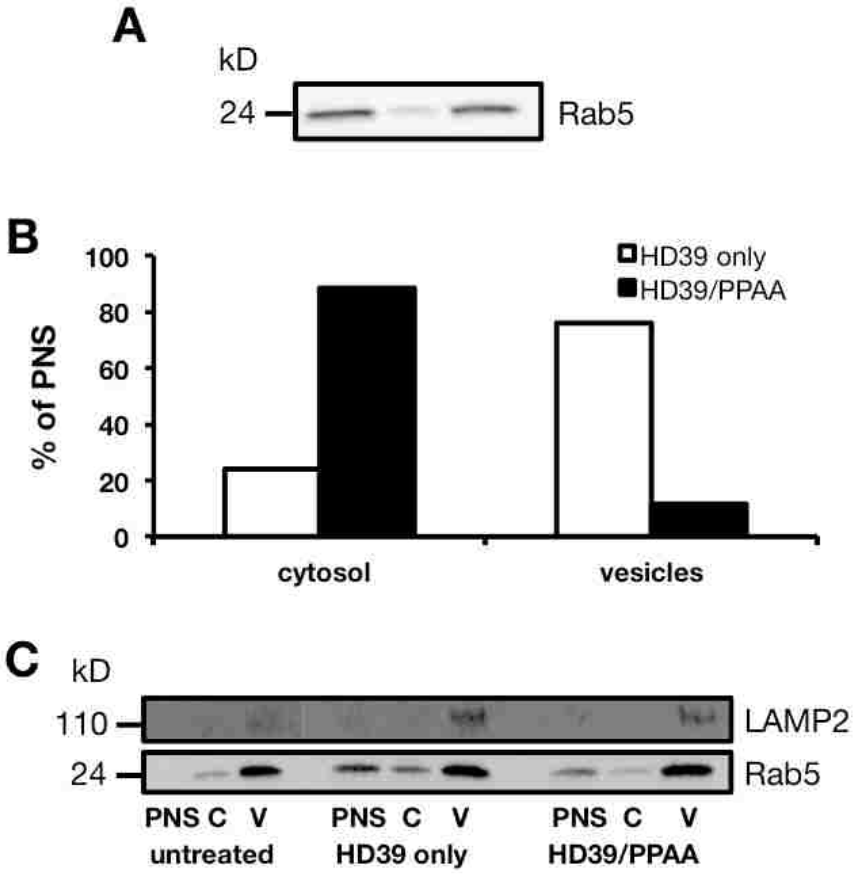

Figure 1.10: **Cytosolic *vs.* vesicular distribution of HD39 and HD39/PPAA in treated Ramos-AW cells.** (A) Thirty million Ramos-AW cells were fractionated according to the schematic in Figure 1.9A. Immunoblotting for *Rab5* in the post-nuclear supernatant (PNS), cytosolic (C), and vesicular (V) fractions. (B) Thirty million Ramos-AW cells were pulsed with tritium-labeled HD39 or HD39/PPAA conjugates for 1 h and then chased for an additional 5 h. Cells were then separated into cytosolic and vesicular fractions, and radiolabeled antibody was detected in both fractions for each sample. (C) Immunoblotting for Rab5 and LAMP2 in untreated, HD39-treated, and HD39/PPAA-treated cell fractions.

tion remained unchanged while Rab5 was seen mostly in the cytosolic fraction. However, previous studies have indicated that Rab5 exists in both soluble and insoluble states, and that the soluble version does not pellet [70]. These results indicate that separation between endocytic organelles could be further optimized. Other reports have also indicated that separation between endosomes and lysosomes is difficult. Chin *et al.* reported greater

resolution between early endosomes, recycling endosomes, and lysosomes by reducing the volume of fractions collected off the gradient [70]. Sequential differential centrifugation combined with continuous sucrose or glycerol gradients [71] was used to study the intracellular trafficking of chemoattractant receptors in Chinese hamster ovary (CHO) cells; sucrose gradients allowed the separation of endocytic organelles based on buoyant density while glycerol gradients allowed organelle separation based on size. However, continuous iodixanol gradients previously have been used to study the intracellular trafficking of the transferrin receptor [72], polymer-drug conjugates [16], and proteins involved in the endocytic pathway [70, 73]. Therefore, this density-gradient centrifugation method, verified with results from differential centrifugation methods, may be sufficient for tracking the polymer carrier and cargo DNA throughout various organelles.

1.4.8 Effect of polymer labeling method on transfection efficiency

Labeling method has been shown to influence the transfection efficiency for DNA [74], but it is unknown how labeling methods of the polymer affect transfection rates, which may indicate differential intracellular trafficking kinetics between labeled and unlabeled materials. To determine if fluorescently- or radio-labeled polymer transfected cells similarly to unlabeled polymer, the Alexa Fluor 647-labeled bPEI and radiolabeled bPEI (a mixture of [^{14}C]- and [^{3}H]-labeled) were used to formulated polyplexes, and applied to HeLa cells. Fluorescently-labeled bPEI transfected much less efficiently than unlabeled (5.9% of unlabeled) while radiolabeled bPEI transfected only slightly less efficiently (59.4% of unlabeled) (Figure 1.12A). Interestingly, labeling the polymer reduced cytotoxicity, with radiolabeled polymer being the least toxic (Figure 1.12B). Thus, radiolabeling the polymer was detemined to be the optimal method with the least impact on transfection efficiency.

1.5 Conclusions

Subcellular fractionation is a powerful tool that can be used to quantify the intracellular distribution of non-viral vectors, such as polyplexes. Since quantification relies on accurate separation of organelles, methods using differential centrifugation, density-gradient centrifugation, or a combination of both, were assessed for separation of plasma membrane,

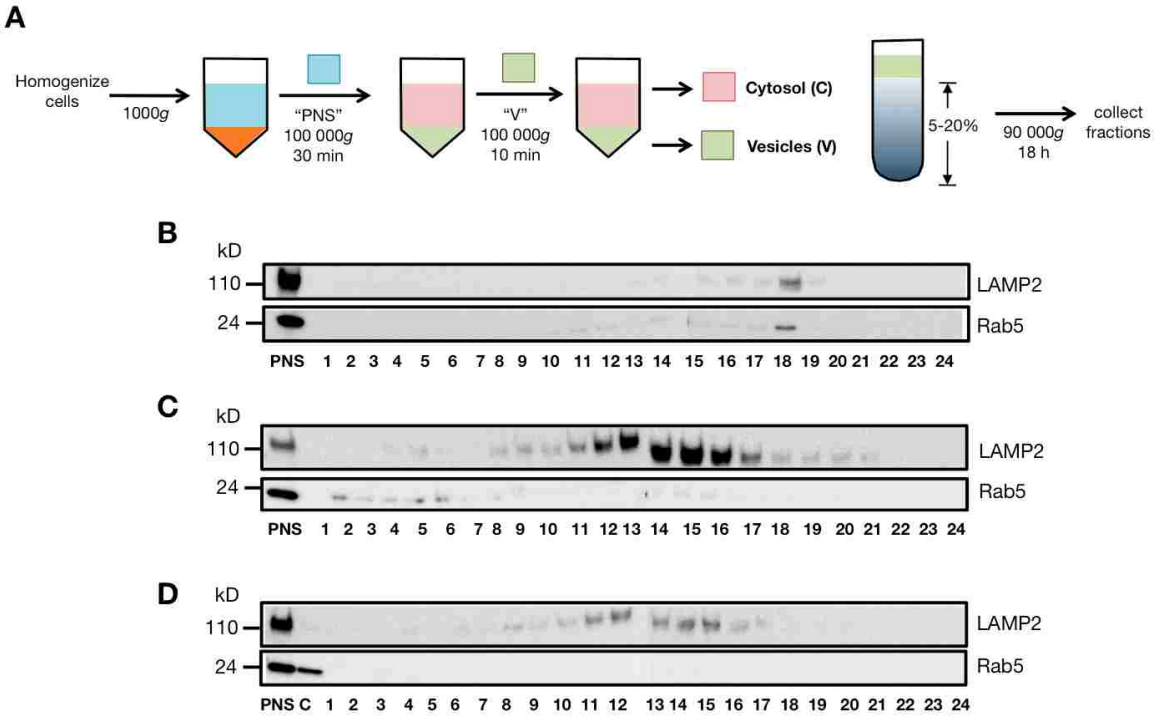

Figure 1.11: **Cellular fractionation using an improved 2-step procedure.** (A) Schematic for improved 2-step fractionation procedure. Ten million HeLa cells were subjected to an initial differential centrifugation prior to the vesicular (V) fraction being separated on a 5-20% continuous iodixanol gradient. (B) Immunoblotting for Rab5 and LAMP2 in collected fractions. (C) Immunoblotting for Rab5 and LAMP2 in collected fractions from a PNS-loaded sample using a buffer including salts to help eliminate organelle aggregation. (D) Immunoblotting for Rab5 and LAMP2 in collected fractions from a vesicular pellet-loaded sample using a buffer including salts to help eliminate organelle aggregation.

endosomes, lysosomes, and nuclei. Furthermore, we evaluated different labeling methods of the polymer and DNA to determine the optimal method for tracking both components during the fractionation process. We found that an inital separation of cytosol and vesicular organelles by differential centrifugation, followed by a density gradient to separate the remaining vesicular organelles, provided the best organellar resolution and reduced cross-contamination between organelle populations. We also found that radiolabeling rather than fluorescent-labeling was the more accurate in tracking the polymer and DNA. Therefore, these optimized methods will be used to track bPEI polyplexes in Chapter 2.

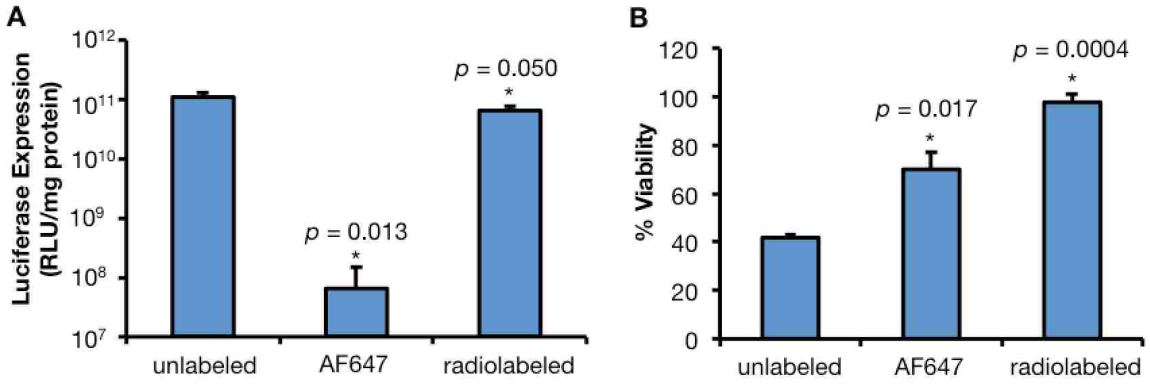

Figure 1.12: **Transfection in HeLa cells with differentially labeled polymer.** Polyplexes were formulated with either unlabeled, Alexa Fluor 647-labeled, or radiolabeled bPEI at N/P 5, and applied to cells for 8 h. At 48 h post-transfection, cells were washed and assessed for (A) luciferase reporter expression, and (B) protein content. Data are presented as the mean ± S.D., $n = 3$, (*) $p < 0.05$, as determined by two-tailed Student's t-test.

References

[1] Cavazzana-Calvo, M., Hacein-Bey, S., de Saint Basile, G., Gross, F., Yvon, E., Nusbaum, P., Selz, F., Hue, C., Certain, S., and Casanova, J.-L. (2000) Gene Therapy of Human Severe Combined Immunodeficiency (SCID)-X1 Disease. *Science*, **288**, 669–672.

[2] Aiuti, A., et al. (2009) Gene therapy for immunodeficiency due to adenosine deaminase deficiency. *N. Engl. J. Med.*, **360**, 447–458.

[3] Testa, F., et al. (2013) Three-Year Follow-up after Unilateral Subretinal Delivery of Adeno-Associated Virus in Patients with Leber Congenital Amaurosis Type 2. *Ophthalmology*, **120**, 1283–1291.

[4] Ginn, S. L., Alexander, I. E., Edelstein, M. L., Abedi, M. R., and Wixon, J. (2013) Gene therapy clinical trials worldwide to 2012 - an update. *J. Gene Med.*, **15**, 65–77.

[5] Pack, D. W., Hoffman, A. S., Pun, S., and Stayton, P. S. (2005) Design and development of polymers for gene delivery. *Nat. Rev. Drug Discov.*, **4**, 581–593.

[6] Zheng, N., Tsai, H. N., Zhang, X., and Rosania, G. R. (2011) The subcellular distribution of small molecules: from pharmacokinetics to synthetic biology. *Mol. Pharm.*, **8**, 1619–1628.

[7] Sahay, G., Alakhova, D. Y., and Kabanov, A. V. (2010) Endocytosis of nanomedicines. *J. Control. Release*, **145**, 182–195.

[8] Duncan, R. and Richardson, S. C. W. (2012) Endocytosis and intracellular trafficking as gateways for nanomedicine delivery: opportunities and challenges. *Mol. Pharm.*, **9**, 2380–2402.

[9] Vercauteren, D., Rejman, J., Martens, T. F., Demeester, J., De Smedt, S. C., and Braeckmans, K. (2012) On the cellular processing of non-viral nanomedicines for nucleic acid delivery: mechanisms and methods. *J. Control. Release*, **161**, 566–581.

[10] El-Sayed, A. and Harashima, H. (2013) Endocytosis of Gene Delivery Vectors: From Clathrin-dependent to Lipid Raft-mediated Endocytosis. *Mol. Ther.*, **21**, 1118–1130.

[11] Satori, C. P., Kostal, V., and Arriaga, E. A. (2012) Review on recent advances in the analysis of isolated organelles. *Anal. Chim. Acta*, **753**, 8–18.

[12] Pasquali, C., Fialka, I., and Huber, L. A. (1999) Subcellular fractionation, electromigration analysis and mapping of organelles. *J. Chromatogr. B Biomed. Sci. Appl.*, **722**, 89–102.

[13] Graham, J. M. (2001) Purification of a crude mitochondrial fraction by density-gradient centrifugation. *Curr Protoc Cell Biol*, **Chapter 3**, Unit 3.4.

[14] Tijerina, M., Kopečková, P., and Kopeček, J. (2003) Correlation of subcellular compartmentalization of HPMA copolymer-Mce6 conjugates with chemotherapeutic activity in human ovarian carcinoma cells. *Pharm. Res.*, **20**, 728–737.

[15] Nori, A., Jensen, K. D., Tijerina, M., Kopečková, P., and Kopeček, J. (2003) Tat-conjugated synthetic macromolecules facilitate cytoplasmic drug delivery to human ovarian carcinoma cells. *Bioconjug. Chem.*, **14**, 44–50.

[16] Manunta, M., Izzo, L., Duncan, R., and Jones, A. T. (2007) Establishment of subcellular fractionation techniques to monitor the intracellular fate of polymer therapeutics II. Identification of endosomal and lysosomal compartments in HepG2 cells combining single-step subcellular fractionation with fluorescent imaging. *J. Drug Target.*, **15**, 37–50.

[17] Shi, J., Chou, B., Choi, J. L., Ta, A. L., and Pun, S. H. (2013) Investigation of polyethylenimine/DNA polyplex transfection to cultured cells using radiolabeling and subcellular fractionation methods. *Mol. Pharm.*, **10**, 2145–2156.

[18] Ajioka, R. S. and Kaplan, J. (1987) Characterization of endocytic compartments using the horseradish peroxidase-diaminobenzidine density shift technique. *J. Cell Biol.*, **104**, 77–85.

[19] Burré, J., Zimmermann, H., and Volknandt, W. (2007) Immunoisolation and subfractionation of synaptic vesicle proteins. *Anal. Biochem.*, **362**, 172–181.

[20] Schröter, C. J., Braun, M., Englert, J., Beck, H., Schmid, H., and Kalbacher, H. (1999) A rapid method to separate endosomes from lysosomal contents using differential centrifugation and hypotonic lysis of lysosomes. *J. Immunol. Methods*, **227**, 161–168.

[21] Leighton, F., Poole, B., Beaufay, H., Baudhuin, P., Coffey, J. W., Fowler, S., and De Duve, C. (1968) The large-scale separation of peroxisomes, mitochondria, and lysosomes from the livers of rats injected with triton WR-1339. Improved isolation procedures, automated analysis, biochemical and morphological properties of fractions. *J. Cell Biol.*, **37**, 482–513.

[22] Fuchs, R. and Ellinger, I. (2002) Free-flow electrophoretic analysis of endosome subpopulations of rat hepatocytes. *Curr Protoc Cell Biol*, **Chapter 3**, Unit 3.11.

[23] Chen, Y., Xiong, G., and Arriaga, E. A. (2007) CE analysis of the acidic organelles of a single cell. *Electrophoresis*, **28**, 2406–2415.

[24] Tulp, A., Verwoerd, D., Fernandez-Borja, M., Neefjes, J., and Hart, A. A. (1996) High resolution density gradient electrophoresis of cellular organelles. *Electrophoresis*, **17**, 173–178.

[25] Tedford, N. C. (2007) Quantitative analysis of non-viral gene therapy in primary liver culture systems.

[26] Tulp, A. (1984) Density gradient electrophoresis of mammalian cells. *Methods Biochem Anal*, **30**, 141–198.

[27] Pol, A. and Enrich, C. (1997) Membrane transport in rat liver endocytic pathways: preparation, biochemical properties and functional roles of hepatic endosomes. *Electrophoresis*, **18**, 2548–2557.

[28] Pol, A., Ortega, D., and Enrich, C. (1997) Identification and distribution of proteins in isolated endosomal fractions of rat liver: involvement in endocytosis, recycling and transcytosis. *Biochem. J.*, **323 (Pt 2)**, 435–443.

[29] Pfeffer, S. (2003) Membrane domains in the secretory and endocytic pathways. *Cell*, **112**, 507–517.

[30] Ellinger, I., Klapper, H., Courtoy, P. J., Vaerman, J.-P., and Fuchs, R. (2002) Different temperature sensitivity of endosomes involved in transport to lysosomes and transcytosis in rat hepatocytes: analysis by free-flow electrophoresis. *Electrophoresis*, **23**, 2117–2129.

[31] Ellinger, I., Klapper, H., and Fuchs, R. (1998) Fluid-phase marker transport in rat liver: free-flow electrophoresis separates distinct endosome subpopulations. *Electrophoresis*, **19**, 1154–1161.

[32] Lu, H., Gaudet, S., Schmidt, M. A., and Jensen, K. F. (2004) A microfabricated device for subcellular organelle sorting. *Anal. Chem.*, **76**, 5705–5712.

[33] Kohlheyer, D., Eijkel, J. C. T., Schlautmann, S., van den Berg, A., and Schasfoort, R. B. M. (2007) Microfluidic high-resolution free-flow isoelectric focusing. *Anal. Chem.*, **79**, 8190–8198.

[34] Moschallski, M., et al. (2010) MicroPrep: chip-based dielectrophoretic purification of mitochondria. *Electrophoresis*, **31**, 2655–2663.

[35] Wolken, G. G., Kostal, V., and Arriaga, E. A. (2011) Capillary isoelectric focusing of individual mitochondria. *Anal. Chem.*, **83**, 612–618.

[36] Gonçalves, C., Mennesson, E., Fuchs, R., Gorvel, J.-P., Midoux, P., and Pichon, C. (2004) Macropinocytosis of polyplexes and recycling of plasmid via the clathrin-dependent pathway impair the transfection efficiency of human hepatocarcinoma cells. *Mol. Ther.*, **10**, 373–385.

[37] Varga, C. M., Tedford, N. C., Thomas, M., Klibanov, A. M., Griffith, L. G., and Lauffenburger, D. A. (2005) Quantitative comparison of polyethylenimine formulations and adenoviral vectors in terms of intracellular gene delivery processes. *Gene Ther.*, **12**, 1023–1032.

[38] Zhou, J., Yockman, J. W., Kim, S. W., and Kern, S. E. (2007) Intracellular kinetics of non-viral gene delivery using polyethylenimine carriers. *Pharm. Res.*, **24**, 1079–1087.

[39] Kamiya, H., Akita, H., and Harashima, H. (2003) Pharmacokinetic and pharmacodynamic considerations in gene therapy. *Drug Discovery Today*, **8**, 990–996.

[40] Cohen, R. N., van der Aa, M. A. E. M., Macaraeg, N., Lee, A. P., and Szoka, F. C. (2009) Quantification of plasmid DNA copies in the nucleus after lipoplex and polyplex transfection. *J. Control. Release*, **135**, 166–174.

[41] Oh, Y.-K., Suh, D., Kim, J. M., Choi, H.-G., Shin, K., and Ko, J. J. (2002) Polyethylenimine-mediated cellular uptake, nucleus trafficking and expression of cytokine plasmid DNA. *Gene Ther.*, **9**, 1627–1632.

[42] Tachibana, R., HARASHIMA, H., Shinohara, Y., and Kiwada, H. (2001) Quantitative studies on the nuclear transport of plasmid DNA and gene expression employing nonviral vectors. *Adv. Drug Deliv. Rev.*, **52**, 219–226.

[43] Tachibana, R., Harashima, H., Ide, N., Ukitsu, S., Ohta, Y., Suzuki, N., Kikuchi, H., Shinohara, Y., and Kiwada, H. (2002) Quantitative analysis of correlation between number of nuclear plasmids and gene expression activity after transfection with cationic liposomes. *Pharm. Res.*, **19**, 377–381.

[44] Miyazawa, N., Leopold, P. L., Hackett, N. R., Ferris, B., Worgall, S., Falck-Pedersen, E., and Crystal, R. G. (1999) Fiber swap between adenovirus subgroups B and C alters intracellular trafficking of adenovirus gene transfer vectors. *J. Virol.*, **73**, 6056–6065.

[45] Parra-Guillén, Z. P., González-Aseguinolaza, G., Berraondo, P., and Trocóniz, I. F. (2010) Gene therapy: a pharmacokinetic/pharmacodynamic modelling overview. *Pharm. Res.*, **27**, 1487–1497.

[46] Colin, M., et al. (2000) Cell delivery, intracellular trafficking and expression of an integrin-mediated gene transfer vector in tracheal epithelial cells. *Gene Ther.*, **7**, 139–152.

[47] Lackey, C. A., Press, O. W., Hoffman, A. S., and Stayton, P. S. (2002) A biomimetic pH-responsive polymer directs endosomal release and intracellular delivery of an endocytosed antibody complex. *Bioconjug. Chem.*, **13**, 996–1001.

[48] Akita, H., Ito, R., Khalil, I. A., Futaki, S., and Harashima, H. (2004) Quantitative three-dimensional analysis of the intracellular trafficking of plasmid DNA transfected by a nonviral gene delivery system using confocal laser scanning microscopy. *Mol. Ther.*, **9**, 443–451.

[49] Hama, S., Akita, H., Ito, R., Mizuguchi, H., Hayakawa, T., and Harashima, H. (2006) Quantitative comparison of intracellular trafficking and nuclear transcription between adenoviral and lipoplex systems. *Mol. Ther.*, **13**, 786–794.

[50] Hama, S., Akita, H., Iida, S., Mizuguchi, H., and Harashima, H. (2007) Quantitative and mechanism-based investigation of post-nuclear delivery events between adenovirus and lipoplex. *Nucleic Acids Res.*, **35**, 1533–1543.

[51] Baxter, D. F., Kirk, M., Garcia, A. F., Raimondi, A., Holmqvist, M. H., Flint, K. K., Bojanic, D., Distefano, P. S., Curtis, R., and Xie, Y. (2002) A novel membrane potential-sensitive fluorescent dye improves cell-based assays for ion channels. *J Biomol Screen*, **7**, 79–85.

[52] Jiang, X.-J., Lo, P.-C., Yeung, S.-L., Fong, W.-P., and Ng, D. K. P. (2010) A pH-responsive fluorescence probe and photosensitiser based on a tetraamino silicon(IV) phthalocyanine. *Chem. Commun.*, **46**, 3188–3190.

[53] Ogawa, H., Inouye, S., Tsuji, F. I., Yasuda, K., and Umesono, K. (1995) Localization, trafficking, and temperature-dependence of the Aequorea green fluorescent protein in cultured vertebrate cells. *Proc. Natl. Acad. Sci. U.S.A.*, **92**, 11899–11903.

[54] Olson, K. J., Ahmadzadeh, H., and Arriaga, E. A. (2005) Within the cell: analytical techniques for subcellular analysis. *Anal Bioanal Chem*, **382**, 906–917.

[55] Elsaesser, A., Barnes, C. A., McKerr, G., Salvati, A., Lynch, I., Dawson, K. A., and Howard, C. V. (2011) Quantification of nanoparticle uptake by cells using an unbiased sampling method and electron microscopy. *Nanomedicine (Lond)*, **6**, 1189–1198.

[56] Ling, J., Weitman, S. D., Miller, M. A., Moore, R. V., and Bovik, A. C. (2002) Direct Raman imaging techniques for study of the subcellular distribution of a drug. *Appl Opt*, **41**, 6006–6017.

[57] Gilleron, J., et al. (2013) Image-based analysis of lipid nanoparticle-mediated siRNA delivery, intracellular trafficking and endosomal escape. *Nat. Biotechnol.*, **31**, 638–646.

[58] Fleischer, S. and Kervina, M. (1974) Subcellular fractionation of rat liver. *Meth. Enzymol.*, **31**, 6–41.

[59] Howell, K. E., Devaney, E., and Gruenberg, J. (1989) Subcellular fractionation of tissue culture cells. *Trends Biochem. Sci.*, **14**, 44–47.

[60] von Harpe, A., Petersen, H., Li, Y., and Kissel, T. (2000) Characterization of commercially available and synthesized polyethylenimines for gene delivery. *J. Control. Release*, **69**, 309–322.

[61] Berguig, G. Y., Convertine, A. J., Shi, J., Palanca-Wessels, M. C., Duvall, C. L., Pun, S. H., Press, O. W., and Stayton, P. S. (2012) Intracellular delivery and trafficking dynamics of a lymphoma-targeting antibody-polymer conjugate. *Mol. Pharm.*, **9**, 3506–3514.

[62] Plonne, D., Cartwright, I., Linss, W., Dargel, R., Graham, J. M., and Higgins, J. A. (1999) Separation of the intracellular secretory compartment of rat liver and isolated rat hepatocytes in a single step using self-generating gradients of iodixanol. *Anal. Biochem.*, **276**, 88–96.

[63] Seib, F. P., Jones, A. T., and Duncan, R. (2006) Establishment of subcellular fractionation techniques to monitor the intracellular fate of polymer therapeutics I. Differential centrifugation fractionation B16F10 cells and use to study the intracellular fate of HPMA copolymer - doxorubicin. *J. Drug Target.*, **14**, 375–390.

[64] Wendeler, M. and Sandhoff, K. (2009) Hexosaminidase assays. *Glycoconj. J.*, **26**, 945–952.

[65] Barja, G. and Herrero, A. (2000) Oxidative damage to mitochondrial DNA is inversely related to maximum life span in the heart and brain of mammals. *FASEB J.*, **14**, 312–318.

[66] Mu, F. T., Callaghan, J. M., Steele-Mortimer, O., Stenmark, H., Parton, R. G., Campbell, P. L., McCluskey, J., Yeo, J. P., Tock, E. P., and Toh, B. H. (1995) EEA1, an early endosome-associated protein. EEA1 is a conserved alpha-helical peripheral membrane protein flanked by cysteine "fingers" and contains a calmodulin-binding IQ motif. *J. Biol. Chem.*, **270**, 13503–13511.

[67] Leonard, J. P. and Goldenberg, D. M. (2007) Preclinical and clinical evaluation of epratuzumab (anti-CD22 IgG) in B-cell malignancies. *Oncogene*, **26**, 3704–3713.

[68] Palanca-Wessels, M. C., Convertine, A. J., Cutler-Strom, R., Booth, G. C., Lee, F., Berguig, G. Y., Stayton, P. S., and Press, O. W. (2011) Anti-CD22 antibody targeting of pH-responsive micelles enhances small interfering RNA delivery and gene silencing in lymphoma cells. *Mol. Ther.*, **19**, 1529–1537.

[69] Graham, J. M. (2001) Isolation of lysosomes from tissues and cells by differential and density gradient centrifugation. *Curr Protoc Cell Biol*, **Chapter 3**, Unit 3.6.

[70] Chin, L. S., Raynor, M. C., Wei, X., Chen, H. Q., and Li, L. (2001) Hrs interacts with sorting nexin 1 and regulates degradation of epidermal growth factor receptor. *J. Biol. Chem.*, **276**, 7069–7078.

[71] Suvorova, E. S., Gripentrog, J. M., and Miettinen, H. M. (2005) Different endocytosis pathways of the C5a receptor and the N-formyl peptide receptor. *Traffic*, **6**, 100–115.

[72] Sheff, D. R., Daro, E. A., Hull, M., and Mellman, I. (1999) The receptor recycling pathway contains two distinct populations of early endosomes with different sorting functions. *J. Cell Biol.*, **145**, 123–139.

[73] Proikas-Cezanne, T., Gaugel, A., Frickey, T., and Nordheim, A. (2006) Rab14 is part of the early endosomal clathrin-coated TGN microdomain. *FEBS Lett.*, **580**, 5241–5246.

[74] Ho, Y.-P., Chen, H. H., Leong, K. W., and Wang, T.-H. (2006) Evaluating the intracellular stability and unpacking of DNA nanocomplexes by quantum dots-FRET. *J. Control. Release*, **116**, 83–89.

Chapter 2

INVESTIGATION OF POLYETHYLENIMINE/DNA POLYPLEX TRANSFECTION TO CULTURED CELLS USING RADIOLABELING AND SUBCELLULAR FRACTIONATION METHODS

Julie Shi, Brian Chou, Jennifer L. Choi, Anh L. Ta, and Suzie Pun

Abstract

Quantitative analysis of the intracellular trafficking of non-viral vectors provides critical information that can guide the rational design of improved cationic systems for gene delivery. Subcellular fractionation methods, combined with radiolabeling, produce quantitative measurements of the intracellular trafficking of non-viral vectors and the therapeutic payload. In this work, differential and density-gradient centrifugation techniques were used to determine the intracellular distribution of radiolabeled 25 kD branched polyethylenimine (bPEI)/plasmid DNA complexes ("polyplexes") in HeLa cells over time. By differential centrifugation, [^{14}C]bPEI was found mostly in the lighter fractions whereas [^{3}H]DNA was found mostly in the heavier fractions. A majority of the intracellular polymer (∼60%) and DNA (∼90%) were found in the nuclear fraction. Polymer and DNA also differed in their distribution to heavier and denser organelles (lysosomes, mitochondria) in density-gradient centrifugation studies. An unexpected finding from this study was that between 18-50% of the DNA applied to the cells became cell-associated (either with the cell membrane and/or internalized), while only 1-6% of the polymer did so, resulting in an effective N/P ratio of less than 1. These results suggest that a significant amount of cationic polymer is dissociated from the DNA cargo early on in the transfection process.[1]

---

[1]Reproduced with permission from Shi, J., *et al. Molecular Pharmaceutics*, **10**, pp. 2145-56.

2.1 Introduction

Non-viral vectors, such as cationic polymers and lipids, have been extensively investigated for gene delivery [1]. Although non-viral vectors are generally considered safer than viral vectors, they are much less efficient at delivering nucleic acids to cells than viruses [2–4]. Non-viral vectors encounter several barriers to gene delivery that viruses can readily overcome, such as cellular uptake, endosomal escape, cytoplasmic translocation, and gene expression. Various moieties, such as endosomal escape peptides [5, 6] and nuclear localization [7] sequences, have been incorporated into the design of non-viral vectors to overcome these barriers; however, there are only a few studies that extensively investigate the impacts of chemical modifications on the intracellular trafficking of synthetic vectors [8–11].

The intracellular fate of synthetic gene delivery vehicles has been studied by fluorescence imaging, the use of chemical inhibitors, and subcellular fractionation. Fluorescence imaging methods, such as confocal microscopy, have been used to determine the intracellular distribution of non-viral vectors through colocalization studies with organelle labels [12]. While informative, microscopy methods are only semi-quantitative, although several efforts to develop quantitative microscopy techniques have been explored [13–15]. Chemical inhibitors have also been used to selectively inhibit various endocytic pathways [16, 17], although the specificity and the effect of these inhibitors on normal cellular activity have been debated [18]. Subcellular fractionation methods can provide quantitative data on intracellular distribution of materials and have been used to determine amount of delivered DNA to the nucleus with liposomal formulations [19] and poly(ethylenimine) (PEI) [20–22], and to provide rate constants for quantitative models [4, 23, 24]. Some studies have also tracked radiolabeled polyplexes in additional organelles using subcellular fractionation methods. While fluorescence microscopy can be affected by environmental factors, such as pH and temperature [25], radioactivity can provide substantially increased sensitivity and robustness. Furthermore, the use of radiolabeled compounds allows for mass balance calculations, so that 100% of the material applied to the sample can be tracked. Laurent *et al.* demonstrated the use of differential and isopycnic centrifugation to track [^{35}S]DNA complexed with poly(lysine) *in vivo* [9]. Colin *et al.* also tracked radiolabeled plasmid DNA (pDNA)/RGD-

K_{16}/Lipofectamine complexes in Percoll gradients, but horseradish peroxidase (HRP) was used to shift endosomal density [10]. In addition, only the DNA was tracked in these studies, limiting our understanding of how the interplay between both carrier and DNA affects intracellular polyplex trafficking.

The goal of this work is to quantify the intracellular distribution of cationic polymer and pDNA complexes, or polyplexes, in native cell environments. We used differential and density-gradient subcellular fractionation methods combined with radiolabeling to track both branched poly(ethylenimine) (bPEI) and pDNA in HeLa cells, a commonly used cultured cell line. We describe here a detailed approach to intracellular polyplex quantification, in which, for the first time to our knowledge, both polymer carrier and cargo DNA are followed in major organelles involved in polyplex trafficking. Polymer and pDNA were found to differ slightly in their intracellular trafficking patterns, and thus, draws attention to the necessity of more quantitative methods to investigate polyplex trafficking. We were also able to quantify the cellular uptake, membrane association, and internalization of polymer and DNA. These studies elucidated that a surprisingly low amount of polymer was internalized into the cell relative to DNA, and suggest that further studies into the mechanism and role of polycation-facilitated gene delivery are necessary.

2.2 Materials and methods

2.2.1 Materials

60%(w/v) OptiPrep (iodixanol) was purchased from Axis-Shield (Norton, MA). HALT protease inhibitor cocktail was purchased from Thermo Fisher Scientific (Pittsburgh, PA). 10X Tris/glycine/SDS running buffer, polyacrylamide gels, and filter paper were purchased from Bio-Rad (Hercules, CA). PVDF membrane was purchased either from Bio-Rad (Hercules, CA) or Millipore (Billerica, MA). Horseradish Peroxidase (HRP)-conjugated goat anti-mouse (no. 554002), mouse anti-Rab5 (250 μg/mL, no. 610725), and mouse anti-CD49b (250 μg/mL, no. 611017) antibodies were purchased from BD Biosciences (San Diego, CA). Mouse anti-LAMP2 antibody was purchased from the Developmental Studies Hybridoma Bank (supernatant, no. H4B4, Iowa City, IA). All cell culture medium and

supplements were purchased from Cellgro/Mediatech (Fisher Scientific, Pittsburgh, PA). Acetic anhydride[^{14}C] was purchased from American Radiolabeled Chemicals (St. Louis, MO). 2'-Deoxycytidine-5'-triphosphate (dCTP), [5-^{3}H] (no. MT 847A), was purchased from Moravek Radiochemicals (Brea, CA). Ultima Gold XR scintillation fluid was purchased from Perkin Elmer (Waltham, MA). All other chemical reagents, including poly(ethylenimine) (PEI, 25,000 g/mol, branched), were reagent-grade or better and were purchased from Sigma-Aldrich (St. Louis, MO) unless otherwise noted. Endotoxin-free plasmid pCMV-Luc2 was prepared by using the pGL4.10 vector (Promega, Madison, WI) and inserting the CMV promoter/intron region from the gWiz Luciferase (Aldevron, Madison, WI). The plasmid was isolated and produced with the Qiagen Plasmid Giga kit (Qiagen, Germany) according to the manufacturer's instructions.

2.2.2 Cell culture

HeLa (human cervical carcinoma) cells were grown in minimum essential medium (MEM) supplemented with 10% fetal bovine serum (FBS) and 100 IU penicillin, 100 μg/mL streptomycin, and 0.25 μg/mL amphotericin B at 37 °C, 5% CO_2. Cells were passaged when they reached ~80% confluency.

2.2.3 Preparation of cell lysate for assessment of marker enzyme assays

For assessment of marker enzyme assays, a crude cell lysate was prepared. 20×10^6 HeLa cells were seeded in 150-mm plates (at 5×10^6 per plate) overnight at 37 °C, 5% CO_2. Cells were washed twice with cold phosphate-buffered saline (PBS), gently lifted off the plates in 5 mL cold PBS, washed off the plates once with PBS, and transferred into pre-chilled conical tubes. Cells were then pelleted at 500g for 5 min and resuspended in 10 mL cold PBS. Cells were pelleted again and then resuspended in 5 mL cold homogenization buffer (0.25 M sucrose, 10 mM HEPES-NaOH, 1 mM EDTA, pH 7.4). After centrifugation at 1000g for 6 min, the resulting pellet was resuspended in 2.5x the wet pellet mass of homogenization buffer (with 1X protease inhibitors added). Cells were then lysed with six freeze-thaw cycles. The protein concentration of the cell lysate was determined using a microBCA kit (Pierce)

according to the manufacturer's instructions.

2.2.4 Marker enzyme assays

Samples containing organelles were analyzed for hexosaminidase A activity (lysosomes) [26], lactate dehydrogenase activity (cytosol), alkaline phosphatase (plasma membrane), succinate dehydrogenase activity (mitochondria) [27], and total protein content.

For lactate dehydrogenase activity, 1 μL of each sample was added to 100 μL NADH/Tris/NaCl (0.244 mM NADH, 81.3 mM Tris, 203.2 mM NaCl, pH 7.2) and equilibrated to 30 °C. At t_0, 20 μL of Tris/NaCl/Na-pyruvate (81.3 mM Tris, 203.2 mM NaCl, pH 7.2, 9.76 mM Na-pyruvate) was added to each sample and the absorbance at 339 nm was measured every 10 min for 1 h at 30 °C using a plate reader (Tecan Safire^2). The linear portion of the slope of the absorbance at 339 nm *vs.* time was compared to a purified lactate dehydrogenase enzyme standard.

For hexosaminidase A activity, 10 μL of each sample was added to 70 μL of citrate-phosphate buffer containing substrate (100 mM citrate-phosphate buffer, pH 4.7, 7.5 mM *p*-nitrophenol-*N*-acetyl-β-D-glucosaminide) and incubated for 1 h at 37 °C. To stop the reaction, 200 μL of borate buffer (200 mM borate buffer, pH 9.8) was added to each sample.

For alkaline phosphatase activity, 20 μL of each sample was added to 140 μL borate buffer containing substrate (50 mM sodium borate, 1 M $MgCl_2$, pH 9.8, 16 mM *p*-nitrophenyl phosphate) and incubated for 1-4 h at 37 °C. The specific enzyme activity was calculated by measuring the absorbance at 405 nm using a plate reader and comparing the released *p*-nitrophenol to a standard of *p*-nitrophenol.

For succinate dehydrogenase activity, 20 μL of each sample was added to 140 μL of Tris-EDTA-succinate buffer containing substrate (20 mM Tris-HCl, pH 7.4, 100 μM EDTA, 200 mM sodium succinate, 203 mM NaCl, 2.5 $^{mg}/_{mL}$ 2-*p*-iodonitrotetrazolium violet (INT)) and incubated for 1-4 h at 37 °C. The specific enzyme activity was calculating by measuring the absorbance at 492 nm using a plate reader and comparing the reduced INT to a standard of formazan-INT.

Protein content was measured using a Bradford-based protein assay kit (Bio-Rad) ac-

cording to the manufacturer's instructions, using immunoglobulin as a standard.

2.2.5 Optimization of cell breakage

Since detergents can potentially displace polymer/DNA interactions, cell lysis was carried out using mechanical techniques. The optimization of mechanical shear-induced cell breakage through a 25-gauge needle was carried out as previously described [27], but with minor modifications. HeLa cells (20×10^6) were seeded into four 150-mm dishes overnight at 37 °C, 5% CO_2. All subsequent steps were completed at 4 °C, on ice, and with pre-chilled reagents. Cells were washed twice with PBS, gently lifted off the plates in 5 mL PBS, washed off the plates once with PBS, and transferred into pre-chilled conical tubes. Cells were then centrifuged at 500*g* for 5 min and resuspended in 10 mL PBS. Cells were pelleted again and then resuspended in 5 mL homogenization buffer (0.25 M sucrose, 10 mM HEPES-NaOH, 1 mM EDTA, pH 7.4). After centrifugation at 1000*g* for 6 min, the resulting pellet was resuspended in 2.5x the wet pellet mass of homogenization buffer (with 1X protease inhibitors added). The cell suspension was then passed through a 25-gauge needle up to 30 times, with 20 μL aliquots taken after a various number of passes. The samples were diluted with 100 μL 250 mM sucrose, vortexed for 30 s, and centrifuged at 2000*g* for 10 min. The supernatant was then used to determine lactate dehydrogenase activity, using cells treated with 0.1% (v/v) Triton X-100 as a reference for 100% cell breakage.

2.2.6 Acetylation of PEI with [^{14}C]acetic anhydride

Branched polyethylenimine (bPEI, MW 25,000 g/mol) was reacted *via* acetylation of amines to obtain [^{14}C]-labeled polymer. 20 mg of bPEI was dissolved in 100 μL dioxane and incubated with 5 molar eq. of [^{14}C]acetic anhydride (50 mCi/mL) and 20 molar eq. of *N,N*-diisopropylethylamine (DIPEA) per 25 kDa polymer for 2 h at room temperature. The reaction was quenched by adding 500 μL 0.1% glacial acetic acid (in dH_2O). Unreacted acetic anhydride and DIPEA was removed by applying the reaction mixture through a desalting spin column (Zeba, 7k MWCO, Thermo Fisher Scientific, Rockford, IL). The resulting eluent was characterized for the final bPEI concentration using a Cu(II) acetate assay [28] and

by scintillation counting. The final polymer concentration was measured to be 3.7 g/L at $\sim 7 \times 10^4$ cpm/μL. The polymer was diluted to a stock of 1 mg/mL in 0.1X PBS, acidified to pH 6 with 0.1 N HCl, and stored at 4 °C. Further dilution of the polymer was carried out in dH_2O.

2.2.7 Labeling of plasmid DNA with [^{3}H]dCTP

Plasmid DNA (pLuc2-CMV) was radiolabeled using nick translation and 2-deoxycytidine 5-triphosphate, [5-^{3}H] (2.5 mCi/mL), according to manufacturers instructions (GE Healthcare, Pittsburgh, PA). Purification of unreacted nucleotides was completed using G50 microspin columns (Probequant, GE Healthcare). The mass recovery was assumed to be 100% with a final concentration of 9.1 μg/mL at $\sim 9 \times 10^4$ cpm/μL.

2.2.8 Gel retardation assay

Polyplex condensation was determined using a gel retardation assay. An equivolume of polymer was added to 0.5 μg plasmid DNA at different charge ratios (N/P) and allowed to complex for 10 min at room temperature. Prior to loading into a 0.8% agarose gel containing TAE buffer (40 mM Tris-acetate, 1 mM EDTA), 10X BlueJuice loading buffer (Life Technologies, Carlsbad, CA) was added to the samples. The gel was then electrophoresed at 100 V for 30-45 min. Plasmid DNA was visualized using ethidium bromide staining *via* an UV transilluminator (laser-excited fluorescence gel scanner, Kodak, Rochester, NY).

2.2.9 Uptake of radiolabeled polyplexes

Cells were seeded in 24-well plates at 2×10^4 cells per mL per well 24 h prior to polyplex addition. Polyplexes were formulated at N/P 5 by mixing 10 μL of [^{3}H]DNA/unlabeled DNA mixture (final concentration of 0.1 g/L in water at $\sim 5 \times 10^6$ cpm/mL) with 10 μL bPEI (65.3 μg/mL) for 10 min at room temperature prior to 10-fold dilution in reduced serum media (Opti-MEM, Life Technologies, Carlsbad, CA). Cells were washed once with PBS, and then incubated with 200 μL polyplexes (in Opti-MEM) for 4 h at 37 °C, 5% CO_2. After the incubation period, cells were washed once with PBS, allowed to incubate with 200 μL

CellScrub (Genlantis, San Diego, CA) for 15 min at room temperature, washed twice with DPBS (without divalent cations), trypsinized, and then collected for scintillation counting. For other time points (6, 8, 12, 24 h), cells were washed once with PBS after the 4 h incubation with polyplexes and replaced with complete media. At various time points after media replacement (2, 4, 8, 20 h), cells were washed with PBS, CellScrub, DPBS, and trypsinized as above. All washes and solutions were collected and analyzed for radioactivity.

2.2.10 Treatment of cells with radiolabeled polyplexes for fractionation studies

For each time point, 5-20 $\times$ 10^6 cells were grown in 150-mm plates (5 $\times$ 10^6 cells per plate). Polyplexes were formulated at N/P 5 by mixing 1 mL of [^{3}H]DNA/unlabeled DNA mixture (final concentration of 0.1 g/L in water at $\sim$5 $\times$ 10^6 cpm/mL) with 1 mL [^{14}C]bPEI (65.3 μg/mL) for 10 min at room temperature. Polyplexes were then diluted with 18 mL Opti-MEM. Each plate was washed once with PBS and incubated with 20 mL of polyplexes in Opti-MEM for specified times at 37 °C, 5% CO_2. In pulse-chase experiments, cells were treated with radiolabeled polyplexes (in Opti-MEM) for 4 h at 37 °C, 5% CO_2, washed once with PBS, replenished with complete media, and incubated at 37 °C, 5% CO_2 for the chase period.

2.2.11 Preparation of post-nuclear supernatant (PNS) for subsequent fractionation

5-20 $\times$ 10^6 HeLa cells were seeded in 150-mm plates (at 5 $\times$ 10^6 per plate) overnight at 37 °C, 5% CO_2. In some experiments, cells were treated with polyplexes for various times at 37 °C, 5% CO_2 prior to cell harvesting. All subsequent steps were completed at 4 °C, on ice, and with pre-chilled reagents. To remove dead/compromised cells, cells were washed twice with PBS, gently lifted off the plates in 5 mL PBS, washed off the plates once with PBS, and transferred into pre-chilled conical tubes. Cells were then pelleted at 500g for 5 min and resuspended in 10 mL PBS. Cells were pelleted again and then resuspended in 5 mL homogenization buffer. After centrifugation at 1000g for 6 min, the resulting pellet was resuspended in 2.5x the wet pellet mass of homogenization buffer (with 1X protease inhibitors added). Cells were then homogenized by passing through a 25-gauge needle until

greater than 90% cell lysis was achieved, as confirmed by light microscopy. Nuclei and unbroken cells were pelleted at 1000g for 10 min. The pellet was resuspended in homogenization buffer and centrifuged again. The resulting post-nuclear supernatant (PNS) was combined from both washes and was subjected to various fractionation procedures.

2.2.12 Cellular fractionation of cytosolic and vesicular components

Separation of cytosol and vesicular organelles was carried out as previously described [29], but with minor modifications. The PNS was layered on top of 10 μL cushion of 2.5 M sucrose and centrifuged 100,000g for 30 min at 4 °C (Beckman TLS-100.3). The supernatant, containing the cytosol, was transferred and the resulting pellet was resuspended in 500 μL homogenization buffer, layered on top of another 10 μL 2.5 M sucrose cushion, and centrifuged again at 100,000g for 10 min at 4 °C. The supernatants were combined and the resulting pellet was resuspended in 500 μL homogenization buffer. In order to break up the vesicular pellet, the resuspended pellet was passed gently through a 25-gauge needle. For studies without additional fractionation, the sucrose cushion was omitted. Aliquots of samples were snap-frozen in liquid nitrogen and stored at -80 °C for further analysis.

2.2.13 Cellular fractionation via differential centrifugation

Cells were treated with radiolabeled polyplexes for 1 h at 4 °C to allow for binding prior to incubation for 30 min or 4 h at 37 °C, 5% CO_2. After polyplex incubation, a post-nuclear supernatant was prepared, and then centrifuged at 3000g for 10 min at 4 °C. The pellet (heavy mitochondrial fraction, or HM) was resuspended in 500 μL homogenization buffer and centrifuged again. The supernatants were combined and centrifuged at 15,000g for 10 min at 4 °C. The pellet (light mitochondrial fraction, or LM) was resuspended in 500 μL homogenization buffer and centrifuged again. The supernatants were combined again and centrifuged at 100,000g for 45 min at 4 °C (Beckman TLS-100.3). The pellet (microsomal fraction, or MF) was resuspended in 500 μL TES buffer and centrifuged again. The supernatants (cytosolic fraction, or C) were combined. All pellets were resuspended in 500 μL homogenization buffer and gently passed through a 25-gauge needle to break

up remaining aggregates. Aliquots of each fraction were stored at -80 °C for subsequent analyses.

2.2.14 Preparation of continuous iodixanol gradients

Continuous iodixanol gradients were prepared as previously described [30], with some minor modifications. A stock solution of 60% iodixanol (OptiPrep) was diluted to a working stock solution of 50% (v/v) iodixanol with a sucrose buffer (0.25 M sucrose, 6 mM EDTA, 60 mM HEPES-NaOH, pH 7.4). The working solution was further diluted to either 5% or 20% iodixanol with TES buffer (0.25 M sucrose, 10 mM triethanolamine, 1 mM EDTA, pH 7.4). 5-20% continuous iodixanol gradients were prepared by layering 5.5 mL 5% iodixanol on top of 5.5 mL 20% iodixanol in a 13 mL ultracentrifuge tube and preparing continuous gradients using a Gradient Master (Biocomp, New Brunswick, Canada).

2.2.15 Cellular fractionation via density-gradient centrifugation

For separation of plasma membrane, endosomes, and lysosomes, the resuspended vesicular pellet from an initial cytosolic/vesicular fractionation was layered on top of a 5-20% continuous iodixanol gradient. For each experiment, a control gradient was prepared with equal volume of homogenization buffer instead of cell lysate. The tubes were then centrifuged at 90,000g (Beckman SW41) for 16-18 h at 4 °C. Twenty-four 500 μL fractions were collected from the top of the gradient using an automated fraction collector (Brandel, Gaithersburg, MD). Collected fractions were placed immediately on ice, aliquoted, and stored at -80 °C until further analysis.

2.2.16 Determination of gradient density

The density of the control gradient fractions was determined by measuring the refractive index (Reichert AR200, Depew, NY). The density of the gradient was calculated using

$$\rho = A\eta - B$$

where ρ is the density of the gradient fraction (g/mL), η is the refractive index, A and B are coefficients for ionic and non-ionic media, and are equal to 3.459 and 3.622, respectively [31].

2.2.17 Determination of radioactivity

For optimization studies, 10 μL of polymer (N/P 5) was added to 10 μL [^{3}H]DNA/unlabeled pDNA mixture (final concentration of 0.1 g/L in water at $\sim 5 \times 10^6$ cpm/mL), mixed, and allowed to incubate for 10 min at room temperature. Polyplexes were then treated with an equivolume of either calf thymus DNA (0.5 g/L in dH_2O), 1 M NaOH, or 10X trypsin, and then allowed to incubate for 30 min prior to addition of scinitillation fluid. Samples from fractionation studies were diluted with an equivolume of 1 M NaOH to disrupt electrostatic interactions between the polymer and DNA. For samples collected from density-gradient fractionation, a 5-fold excess of dH_2O was added to the sample to dilute out quenching effects from the iodixanol gradient media. 4-5 mL of scintillation fluid was added to each vial and vigorously mixed prior to determining radioactivity levels on a liquid scintillation counter (Beckman LS6500). The total radioactivity (counts per minute, or cpm) in each sample was determined by combining the radioactivity found all collected washes and fractions. ^{3}H and ^{14}C measurements were analyzed using methods described elsewhere [32].

2.2.18 Protein precipitation and immunoblotting

To increase protein loading for SDS-PAGE, aliquots of fractions (250 μL) were subjected to trichloroacetic acid (TCA)-deoxycholate(DOC)/acetone precipitation. The pellets were then resuspended in Laemmli buffer (Bio-Rad) or reducing sample buffer (Pierce) prior to SDS-PAGE. Samples were then applied to a pre-cast 4-20% polyacrylamide gel (Bio-Rad) and electrophoresed through a standard Tris/glycine/SDS buffer (25 mM Tris, 192 mM glycine, 0.1% SDS, pH 8.3). Proteins were then transferred onto a PVDF membrane using standard conditions (25 mM Tris-base, 192 mM glycine, 0.1% SDS, 10% methanol) for 1.5 h at 100 V. Non-specific binding sites were blocked by incubation in blocking buffer (Superblock, Pierce) for 1 h at room temperature. Membranes were then either probed with mouse anti-Rab5 (1:1000), anti-LAMP2 (1:500), or anti-CD49b (1:500) in blocking

buffer overnight at 4 °C. After 3×10 min washes with TBS-T (20 mM Tris-HCl, 137 mM NaCl, 0.1% Tween-20), membranes were probed with HRP-conjugated goat anti-mouse antibody (1:100,000) in blocking buffer for 1 h at room temperature. Membranes were washed 3×10 min with TBS-T and developed with chemiluminescent substrate (West Femto, Pierce). Chemiluminescence was detected (10-15 min exposure) using a Kodak imager (Image Station 4000MM, Rochester, NY). Blots were stripped with stripping buffer according to manufacturer's instructions (Restore stripping buffer, Pierce), and re-probed for the different antibodies. The density of each band was calculated using ImageJ.

2.3 Results

2.3.1 Uptake of [^{3}H]DNA/bPEI polyplexes

As a first approach to determine the time dependency of cellular uptake and internalization of polyplexes, a pulse-chase experiment was performed using radiolabeled polyplexes. Cells were treated with bPEI polyplexes formulated with [^{3}H]DNA for 4 h, rinsed, and then replaced with fresh media for up to an additional 20 h. Cell-surface associated polyplexes were collected by a 15 min incubation with CellScrub buffer. During the 4 h pulse period, the rate of surface-association and cellular internalization of polyplexes, as determined by scintillation counting for the radiolabeled plasmid, appeared linear with time, with ~50% of polyplexes associating with cells after 4 h (Figure 2.1). During the chase period, the percentage of cell surface-associated polyplexes decreased over time, from 35.9% to 11.3%, as the percentage of internalized polyplexes increased over time, from 14.0% to 33.4%. The percentage of polyplexes also increased slightly in the chase media over time, from 4.8% after a 2 h chase to 9.1% after a 20 h chase, indicating possible gradual dissociation of polyplexes from the cell surface or polyplex exocytosis. These results suggest that the intracellular distribution of polyplexes is shifting from association with the plasma membrane to trafficking through intracellular organelles over the duration of 24 h.

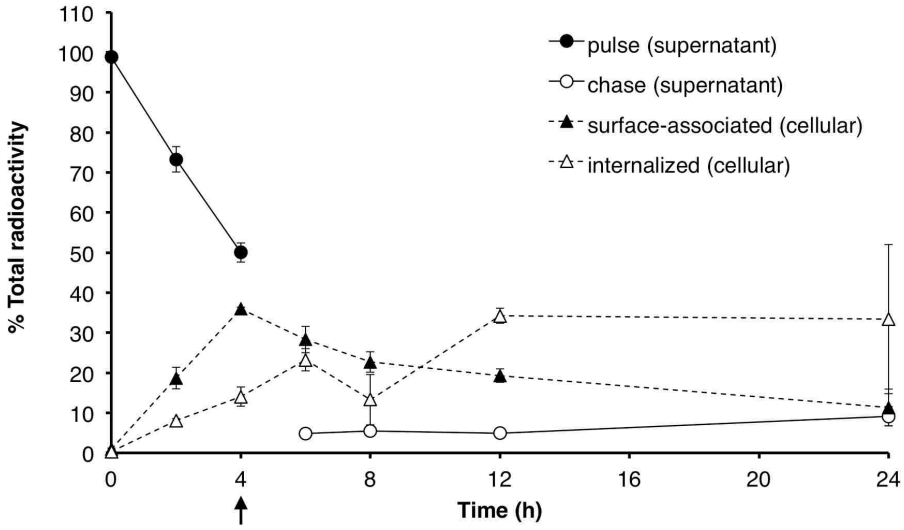

Figure 2.1: **Distribution of [^{3}H]DNA/bPEI polyplexes after pulse-chase in cells and cell supernatant.** HeLa cells (2×10^4) were pulsed with [^{3}H]DNA/bPEI polyplexes for 4 h and then chased (black arrow) in complete media for an additional 2, 4, 8, or 20 h. Media and washes collected during the pulse period was termed "pulse supernatant" (and similarly with the "chase supernatant", but with media and washes collected during the chase period). CellScrub and corresponding washes collected was termed as "surface-associated" polyplexes, while trypsinized cells was termed as "internalized" polyplexes. The radioactivity counts of the pulse supernatant, chase supernatant, surface-associated, and internalized samples were summed to calculate the total radioactivity. Data are presented as mean ± S.D., $n = 3$.

2.3.2 Validation of marker enzyme assays, optimization of cell breakage, and optimization of preparation of samples for scintillation counting

Cellular fractionation studies have been used to quantitatively assess the intracellular distribution of a number of polymer/liposome conjugates [10, 27, 30]. As an initial step, marker enzyme assays were validated with cell lysate and methods for efficient cell lysis were optimized in order to evaluate the organelle distribution after fractionation and maintain intact organelles during fractionation, respectively. Various marker enzyme assays were assessed for suitable limits-of-detection (LOD) using crude cell lysate. A linear relationship was found between indicator release and amount of cell lysate in assays for alkaline phosphatase (plasma membrane marker) (Figure 2.2A), hexosaminidase A (lysosomal marker) (Figure

2.2B), and succinate dehydrogenase (mitochondrial marker) (Figure 2.2C). Purified lactate dehydrogenase was used as a standard for lactate dehydrogenase activity (cytosolic marker) (Figure 2.2D). The LOD, defined as three standard deviations from the blank [33], was 0.34, 0.33, 3.9, and 0.35 μg protein in assays for alkaline phosphatase, hexosaminidase A, succinate dehydrogenase, and lactate dehydrogenase activity, respectively. An assay for 5'-nucleotidase, another commonly marker for plasma membrane, was also assessed, but the LOD was too high for use in fractionation experiments (data not shown).

Next, the minimum number of 25-gauge needle passes necessary to efficiently release organelles from whole cell suspensions was determined. A concentrated cell suspension was passed through a 25-gauge needle for 0-30 passes followed by analysis of the supernatant cytosolic leakage, as determined by lactate dehydrogenase release (Figure 2.3). A cell suspension treated with 0.1% (v/v) Triton X-100 was used as a reference for 100% cell breakage. Cell breakage through a 25-gauge needle was optimized at ~20 passes, which resulted in 92.1% release of lactate dehydrogenase. Attempts at gentle cell breakage using other traditional methods, such as a Dounce or Potter-Elvehjem homogenizer, yielded irreproducible and insufficient breakage (data not shown), as well as significant loss of cell lysate.

Furthermore, initial studies to determine the radioactivity in samples revealed that polyplex packaging influenced measurement readings. Therefore, poly-L-lysine (PLL) or bPEI polyplexes with [^{3}H]DNA were treated with a final concentration of either 0.5 g/L calf thymus DNA, 0.5 M NaOH, or 5X trypsin to restore radioactivity activity (Figure 2.4). Left untreated, polyplexes showed 6-12% decrease in radioactivity compared to DNA alone. Treatment with excess calf thymus DNA or trypsin did not restore measurements for both polymers; only treatment with excess base provided near 100% of the radioactivity of uncomplexed DNA. Therefore, samples were diluted with equivolume of excess base prior to radioactivity measurements.

2.3.3 Cytosolic and vesicular distribution of PEI polyplexes

Next, a simple fractionation method was used to separate nuclear, cytosolic, and vesicular components to determine intracellular polyplex distribution in these major compartments

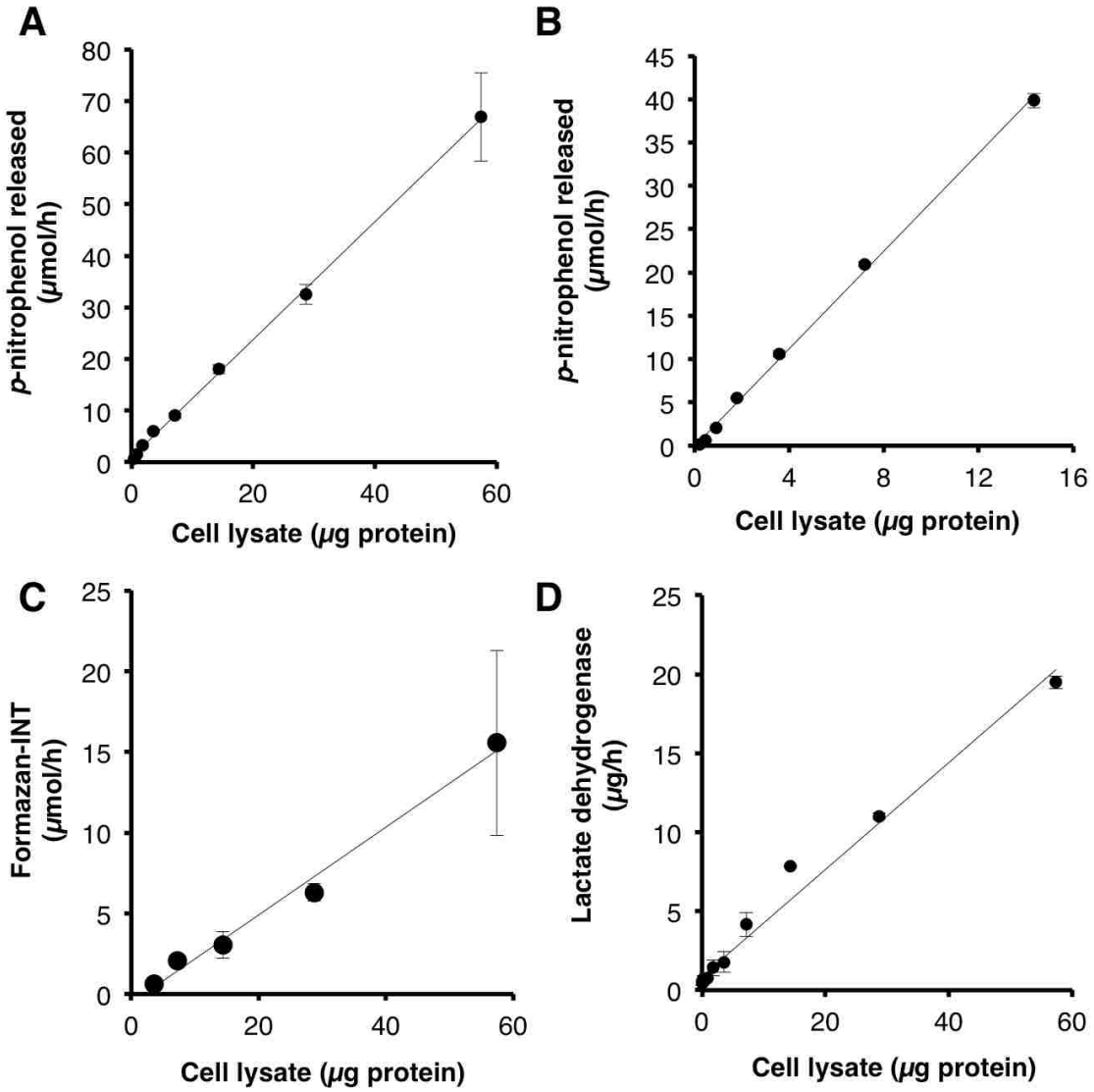

Figure 2.2: **Evaluation of marker enzyme assays.** (A) HeLa cells (2×10^7) were lysed through six freeze-thaw cycles and the resulting cell lysate was used to evaluate marker enzyme assays for (B) alkaline phosphatase (plasma membrane), (C) hexosaminidase A (lysosomes), (D) succinate dehydrogenase (mitochondria), and (e) lactate dehydrogenase (cytosol). Data are presented as mean ± S.D., $n = 3$.

over time. For sensitive tracking of both polymer and DNA, each component was radiolabeled, used to form polyplexes, applied to cells, and then detected in isolated organelle fractions. The partial acetylation of bPEI slightly affected polyplex condensation; complete

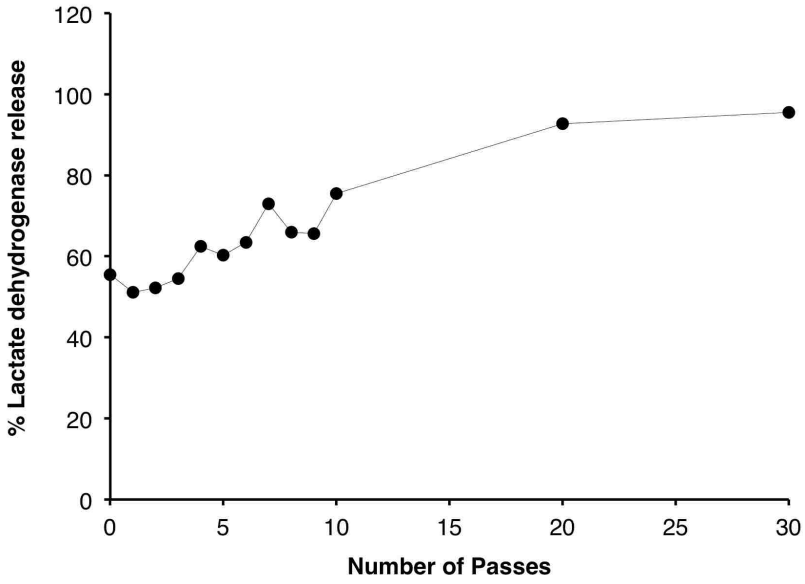

Figure 2.3: **Optimization of cell lysis with a needle and syringe.** HeLa cells (2×10^7) were lysed through a 25-gauge needle and the supernatant was measured for lactate dehydrogenase release after a various number of passages.

DNA retardation was observed at N/P 3 instead of N/P 2 in gel electrophoresis assays (Figure 2.5). Cells were pulsed with [^{14}C]bPEI/[^{3}H]DNA polyplexes for 4 h, rinsed, replaced with fresh media, and then fractionated into nuclear, cytosolic, and vesicular components after a 0, 2, 8, or 20 h chase period. The vesicular fraction contained membrane-associated organelles, such as the plasma membrane, endosomes, lysosomes, and mitochondria (data not shown). In general, the percentage of cell-associated [^{3}H]DNA decreased slightly over the chase period, from 30.2% to 25.6% (Figure 2.6A). This trend was also observed in Figure 2.1 by summing the percent [^{3}H]DNA in surface-associated and internalized samples. The percentage of cell-associated [^{14}C]bPEI also decreased slightly, from 4.5% to 3.4%. Meanwhile, a gradual increase in [^{3}H]DNA and [^{14}C]bPEI was observed in the chase media (Figure 2.6B). Of the total radioactivity found in the cell-associated fractions, 86.2-91.5% of [^{3}H]DNA (Figure 2.6C) and 57.9-65.0% of [^{14}C]bPEI (Figure 2.6D) were present in the nuclear fraction; however, since the nuclear fraction also contained up to 10% unbroken cells, these values may be greater than the actual amount of nuclear-associated material.

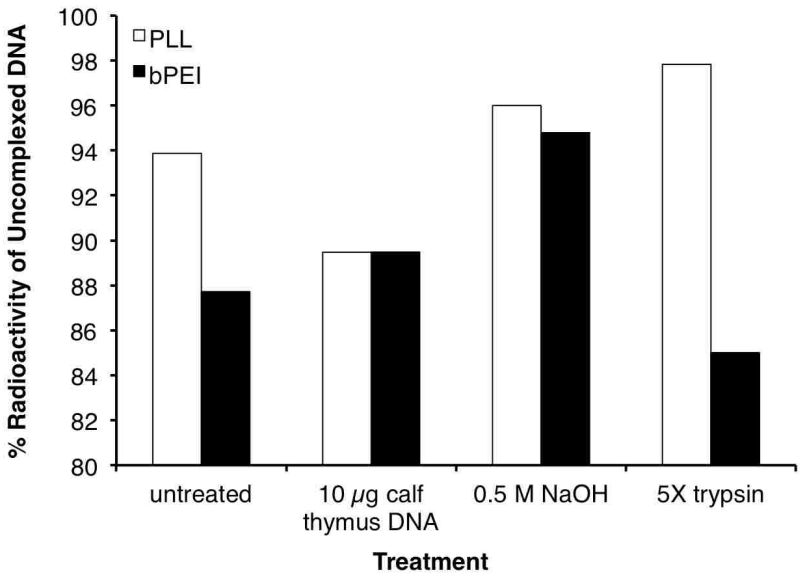

Figure 2.4: **Optimization of polyplex unpackaging for radioactivity measurements.** Polyplexes were formed with 1 μg [^{3}H]DNA/unlabeled DNA mixture and unlabeled polymer, and subsequently treated with either 10 μg calf thymus DNA (to compete off radiolabeled DNA), 0.5 M NaOH (to deprotonate amines on the polymer), and 5X trypsin (to degrade polymer). Radioactivity counts are expressed as a percentage of the radioactivity count from uncomplexed DNA.

[^{3}H]DNA and [^{14}C]bPEI were present in the cytosolic fraction at low concentrations (less than 10% of the post-nuclear fractions). The percentage of [^{3}H]DNA and [^{14}C]bPEI in the cytosolic fraction peaked after 8 h chase to 0.79% and 3.71%, respectively, with effective N/P ratios of 3.1-4.2 throughout the chase period. The percentage of [^{3}H]DNA and [^{14}C]bPEI in the vesicular fraction was highest at the beginning of the chase period (0 h) at 13.3% and 40.3%, respectively, and then gradually decreased over the 20 h chase period. The effective N/P ratios in the vesicular fraction was 2.4-2.8 throughout the chase period. In contrast, the percentage of [^{3}H]DNA and [^{14}C]bPEI in the nuclear fraction increased over time to reach 91.5% and 65.0%, respectively, after the 20 h chase period, with effective N/P ratios ranging from 0.45 to 0.53. These results indicate that most of the polymer and DNA remain in membrane-associated organelle fractions (nuclear, vesicular) while very little material is in the soluble cytosolic fraction. These results are consistent with polyplexes that remain

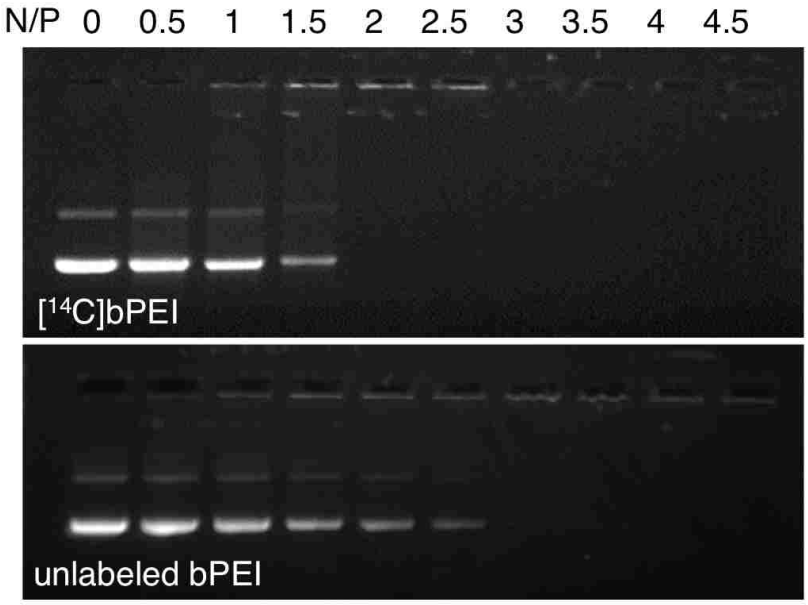

Figure 2.5: **Gel retardation assay of unlabeled and [^{14}C]-labeled bPEI.** [^{14}C]-labeled and unlabeled bPEI were complexed with unlabeled plasmid DNA at different charge ratios (N/P) and loaded onto 0.8% agarose gels. Plasmid DNA was visualized using ethidium bromide.

condensed in cytosolic and vesicular fractions, but disassemble prior to reaching the nuclear fraction.

2.3.4 Differential centrifugation after treatment with PEI polyplexes

Crude separation into nuclear, cytosolic, and vesicular components only allowed a superficial understanding of polyplex distribution. Therefore, more thorough fractionation procedures were explored to further determine polyplex distribution within different organelle compartments in more detail. Differential centrifugation, in which organelles are separated on the basis of mass, is commonly used to assess the relative distribution of materials in intracellular compartments [25, 27, 34, 35]. Cells were treated with dual-labeled polyplexes for 1 h at 4 °C to allow for polyplex binding to the cell surface but with minimal internalization (Figure 2.7A). Cells were then transferred to 37 °C for 30 min or 4 h to allow for polyplex internalization. We selected these times to investigate trafficking at an earlier

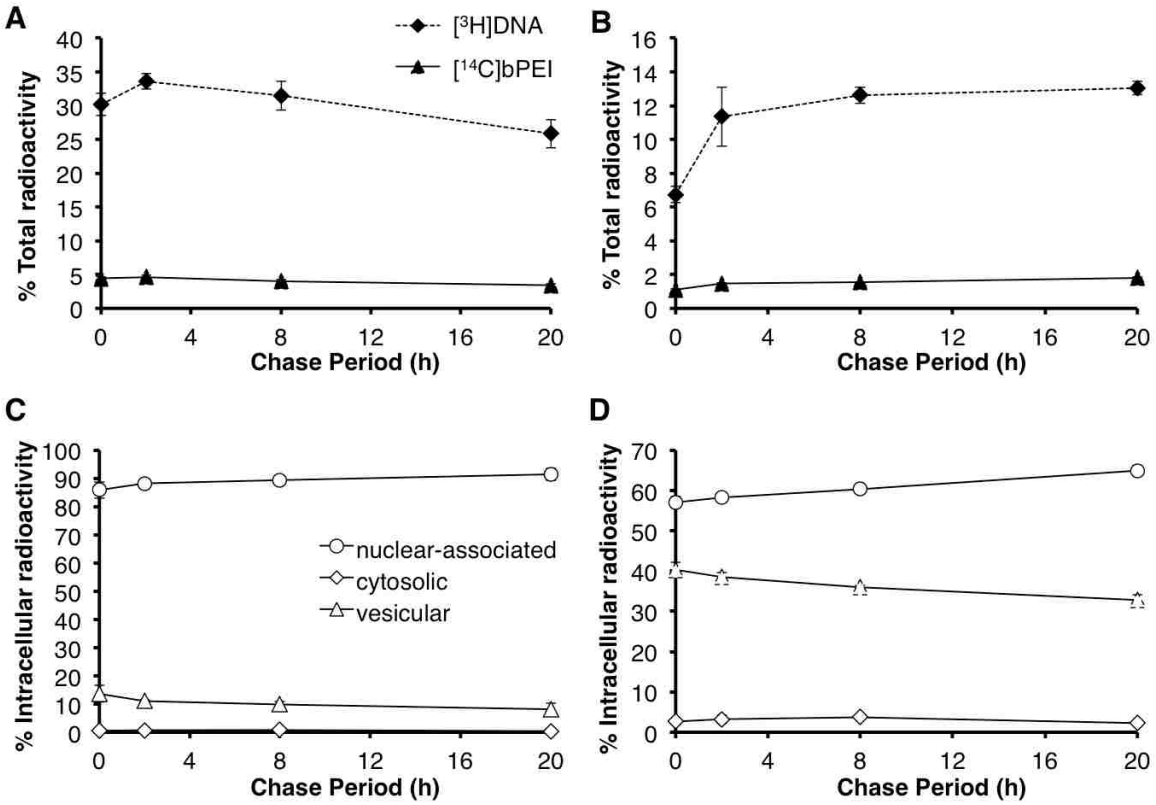

Figure 2.6: **Distribution of [^{3}H]DNA/[^{14}C]bPEI polyplexes after pulse-chase after cytosolic and vesicular fractionation.** HeLa cells (5×10^6) were pulsed with [^{3}H]DNA/[^{14}C]bPEI polyplexes for 4 h and then chased in complete media for an additional 2, 4, 8, or 20 h. All media, washes, and cells were collected to calculate the total radioactivity count in the sample. The percent of total radioactivity of [^{3}H]DNA/[^{14}C]bPEI measured in (A) cell-associated fractions and (B) chase supernatant. CellScrub and corresponding washes collected was termed as "surface-associated" polyplexes, while media and washes collected during the chase period was termed "chase supernatant". The radioactivity counts of all samples (media, washes, cells) were summed to calculate the total radioactivity. The nuclear-associated, cytosolic, and vesicular distribution of (C) [^{3}H]DNA and (D) [^{14}C]bPEI as a percent of the radioactivity found in intracellular fractions (nuclear, cytosolic, vesicular). Data are presented as mean ± S.D., $n = 3$.

time point (30 min) and at the same time point evaluated immediately after the pulse (4 h) in the aforementioned pulse-chase experiments. Afterwards, the cells were homogenized and fractionated according to the differential centrifugation schematic described in Figure 2.7B. After 30 min, the total percentage of [^{3}H]DNA and [^{14}C]bPEI associated with the cells

was 15.5% and 1.2%, respectively. After 4 h, the percentage increased to 48.0% and 5.6%, respectively. After both 30 min and 4 h, a majority of [^{3}H]DNA and [^{14}C]bPEI in cell-associated fractions was found in the nuclear fraction (for [^{3}H]DNA, 87.4% after 30 min, 93.0% after 4 h; for [^{14}C]bPEI, 73.2% after 30 min, 60.3% after 4 h) (Figure 2.7C-D). Of the post-nuclear fractions, [^{3}H]DNA was found mostly in the heavy mitochondrial fraction (HM) at 30 min (77.4% of total [^{3}H]DNA found in post-nuclear fractions) (Figure 2.7E), and then distributed slightly throughout the lighter fractions by 4 h. In contrast, [^{14}C]bPEI was found distributed throughout all fractions (Figure 2.7F), with more polymer found in the HM (40.6% of total [^{14}C]bPEI found in post-nuclear fractions) and light mitochondrial fraction (LM) (30.9%). By 4 h, [^{14}C]bPEI distributed to lighter fractions, with 31.9% found in the LM and 40.9% found in the microsomal fraction (MF). After 30 min, the effective N/P ratios were 0.34, 0.46, 1.4, 9.8, and 4.5 for NP, HM, LM, MF, and C fractions, respectively; after 4 h, the effective N/P ratios were 0.41, 1.3, 7.3, 10.3, and 3.9. The fold-increase of [^{3}H]DNA from 30 min to 4 h was 3.4, 1.4, 1.5, 12.9, and 12.7 for NP, HM, LM, MF, and C, respectively, while the fold-increase of [^{14}C]bPEI was 3.7, 3.5, 7.4, 12.5, and 10.0. In general, uptake of [^{3}H]DNA and [^{14}C]bPEI was significantly greater after 4 h than after 30 min. Interestingly, the fold-increase of [^{14}C]bPEI cellular association was slightly greater than that of [^{3}H]DNA (4.7 fold-increase for [^{14}C]bPEI *vs.* 3.1 fold-increase for [^{3}H]DNA) (Figure 2.8). Polymer accumulation in the HM and LM fractions was also greater than that of DNA. Most of the [^{14}C]bPEI did not become cell-associated (whole cell fraction, or WC) even though 48.0% of the [^{3}H]DNA was found in the WC fraction by 4 h.

To verify organelle distribution, post-nuclear fractions were analyzed for total protein content and marker enzyme activity. Most of the protein was found in the cytosolic fraction (C) (Figure 2.7G). Significant overlap of marker enzyme activity between the post-nuclear fractions was observed. Alkaline phosphatase activity (plasma membrane) was found distributed mostly in the HM and LM fractions (Figure 2.7H). Lactate dehydrogenase activity (cytosol) was found only in the C fraction (Figure 2.7I), while succinate dehydrogenase activity (mitochondria) was found mostly in the HM and LM fractions (Figure 2.7J). Endosomal and lysosomal distribution was assessed in fractions by immunoblotting for Rab5, a small GTPase required for early endosome fusion [36], and LAMP2, a lysosomal-associated

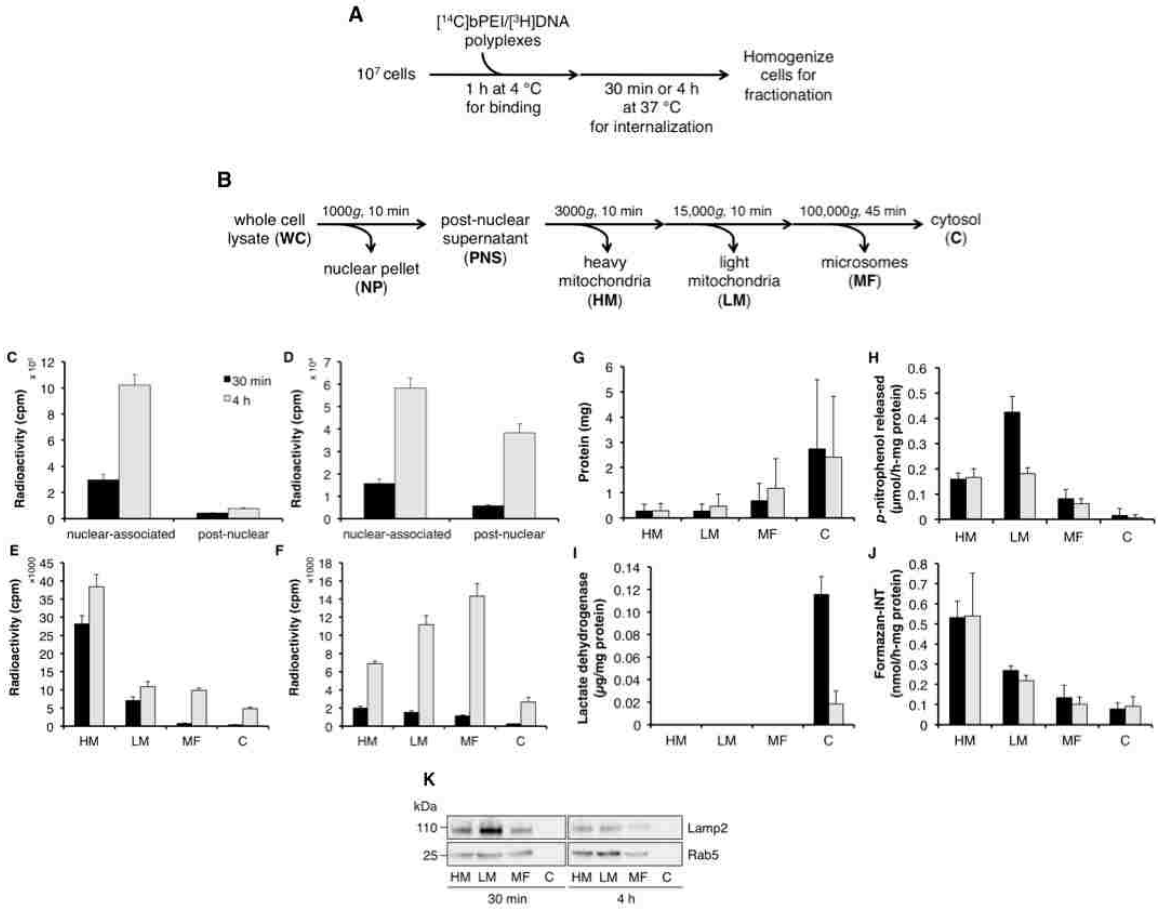

Figure 2.7: **Intracellular distribution of [^{3}H]DNA/[^{14}C]bPEI polyplexes in treated cells fractionated using differential centrifugation.** (A) HeLa cells (10^7) were incubated with [^{3}H]DNA/[^{14}C]bPEI polyplexes for 1 h at 4 °C to allow for binding and then at 37 °C for 30 min (black bars) or 4 h (grey bars) to allow for internalization prior to fractionation. (B) Schematic of differential centrifugation method used to separate organelle populations. Radioactivity counts of (C) [^{3}H]DNA and (D) [^{14}C]bPEI measured in cell-associated fractions. Radioactivity counts of (E) [^{3}H]DNA and (F) [^{14}C]bPEI in post-nuclear fractions. Post-nuclear fractions were also measured for (G) protein content, (H) alkaline phosphatase (plasma membrane), (I) lactate dehydrogenase (cytosol), and (J) succinate dehydrogenase (mitochondria) activity. Data are presented as mean ± S.D., $n = 3$. (K) Immunoblotting for LAMP2 (lysosomes) and Rab5 (endosomes) in post-nuclear fractions. 13 μg protein was loaded into each lane, and staining was visualized using HRP-conjugated secondary antibody and a chemiluminescent substrate.

membrane protein [37], respectively (Figure 2.7K). Both proteins were found in all post-nuclear fractions except for the C fraction, with slightly increased distribution in the HM

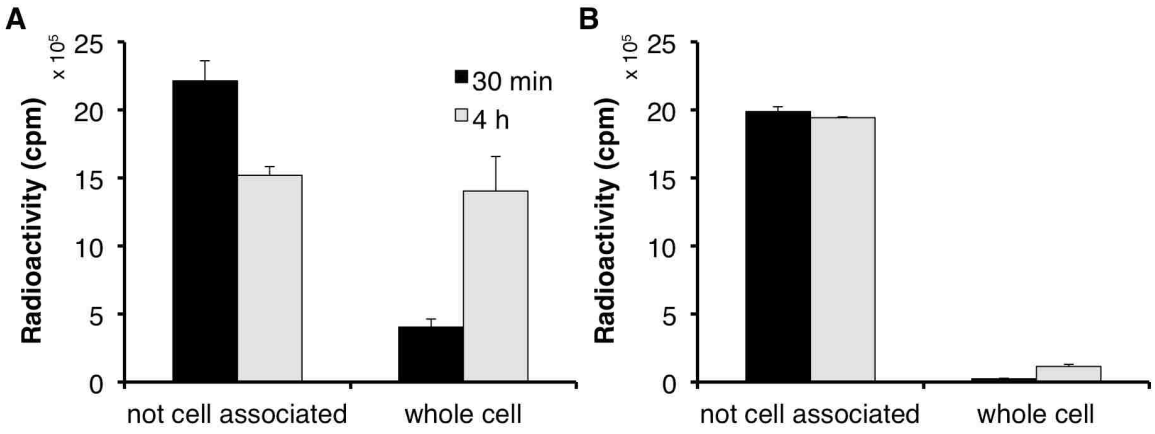

Figure 2.8: **Extracellular and cellular distribution of [^{3}H]DNA/[^{14}C]bPEI polyplexes in treated cells fractionated using differential centrifugation.** HeLa cells (10^7) were incubated with [^{3}H]DNA/[^{14}C]bPEI polyplexes for 1 h at 4 °C to allow for binding and then at 37 °C for 30 min (black bars) or 4 h (grey bars) to allow for internalization prior to fractionation. The radioactivity of (A) [^{3}H]DNA and (B) [^{14}C]bPEI measured in media and washes, which are "not cell associated", and whole cell fractions. Data are presented as mean ± S.D., $n = 3$.

and LM fractions. Due to the incomplete separation of organelles, differential centrifugation is not an effective method for quantification of intracellular polyplex distribution. Therefore, other subcellular fractionation methods were explored to confirm these findings.

2.3.5 Density-gradient centrifugation after treatment with PEI polyplexes

An alternative fractionation method, density-gradient centrifugation, in which organelles are separated by buoyant density, was evaluated for improved organelle separation. Density-gradient centrifugation using iodixanol as a density medium previously showed improved separation between various organelles [31]. Prior to density-gradient centrifugation, the cytosol was initially separated from the vesicular compartments (Figure 2.9A). To further investigate the polyplex distribution in the vesicular fraction, a 5-20% continuous iodixanol gradient was used to separate plasma membrane, endosomes, and lysosomes after cells were pulsed with polyplexes for 4 h, and then chased for either 0 or 20 h. The density of the control gradient (no cells) was linear over 1.04-1.19 g/mL (Figure 2.9B). As seen previously,

more DNA than polymer was cell-associated; 27.5-33.6% of the [^{3}H]DNA and 3.2-4.3% of the [^{14}C]bPEI of the total radioactivity was detected in the whole cell lysate at 4 h (Figure 2.10A-B). After the 20 h chase period, up to 22.2% of the [^{3}H]DNA and 2.2% of the [^{14}C]bPEI of the total radioactivity was detected in the chase media, indicating that about half of cell-associated materials (both DNA and polymer) is released back in the media over the 20 h chase period. Again, of the whole cell lysate, 92.9-93.4% of the [^{3}H]DNA and 73.6-74.7% of the [^{14}C]bPEI was found in the nuclear fraction (Figure 2.10C-D). Overall, a bimodal distribution of both DNA and polymer was detected in the vesicular fraction as a function of density. The first peak, found in the less dense portion of the gradient (fractions 2-5) (Figure 2.9C), corresponds to fractions enriched in plasma membrane and endosomes (Figure 2.9F-G). The second peak (fractions 11-21) was offset between DNA and polymer; the intensities of each component peaked in different fractions (fraction 17 for [^{3}H]DNA *vs.* fraction 15 for [^{14}C]bPEI) (Figure 2.9C). A tailed-distribution was seen in both components; for [^{3}H]DNA, the tail was in the less dense fractions (fraction 11-15), while for [^{14}C]bPEI, the tail was in the denser fractions (fraction 17-21). These results were reproducibly observed in multiple experiments; similar trends were also observed after a 20 h chase period (Figure 2.11).

Marker enzyme assays and immunoblotting for various organelles were completed to determine the organelle distribution in the iodixanol gradient. At both time points, protein was distributed throughout the gradient in a bimodal manner (Figure 2.9D, Figure 2.11B). Significantly higher protein amounts were found in the untreated samples after the 20 h chase period due to extensive cytotoxicity from polyplex treatment (Figure 2.11B). Lysosomes (hexosaminidase A activity) were found mostly in the denser portion of the gradient (fractions 12-20) (Figure 2.9E, Figure 2.11). Immunoblotting for CD49b (plasma membrane), LAMP2 (lysosomes), and Rab5 (early endosomes) were also completed to confirm assay results (Figure 2.9F-G, Figure 2.11D-E). Alkaline phosphatase activity was undetectable in fractions (data not shown). A slight difference in Rab5 distribution was observed with treated *vs.* untreated cells, with a slight shift of the protein to the lesser dense portion of the gradient after polyplex treatment. Most of the DNA and some polymer was also found in denser lysosomal compartments or compartments that were denser than lysosomes. Mi-

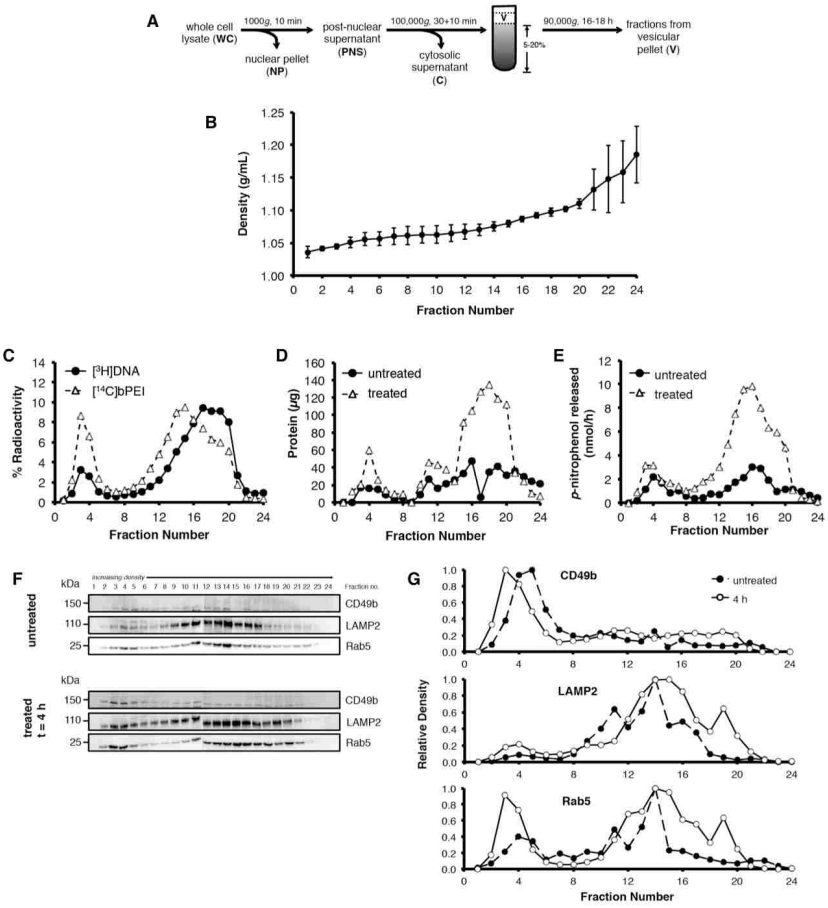

Figure 2.9: **Distribution of [^{3}H]DNA/[^{14}C]bPEI polyplexes after 4 h pulse in cells fractionated using a 5-20% continuous iodixanol density gradient.** (A) Schematic of density-gradient centrifugation method used to separate organelle populations. HeLa cells (2×10^7) were pulsed with [^{3}H]DNA/[^{14}C]bPEI polyplexes for 4 h, and then prepared for fractionation. A 5-20% continuous iodixanol gradient was used to separate vesicular organelles. (B) Density of control gradients. Data are presented as mean ± S.D., $n = 3$. (C) The percent radioactivity measured in fractions from the 5-20% gradient. 100% radioactivity is equal to the sum of the radioactivity found in all 24 fractions collected from the 5-20% gradient. (D) Total protein was measured in untreated and treated gradient fractions. (E) Hexosaminidase A (lysosome) activity was also measured in untreated and treated gradient fractions. (F) An equivolume (250 μL) of gradient fractions from untreated and treated samples was precipitated, concentrated, and probed for CD49b (plasma membrane), LAMP2 (lysosome), and Rab5 (endosome). (G) The optical density of each band was measured using ImageJ. Each time point presented is representative of duplicate experiments.

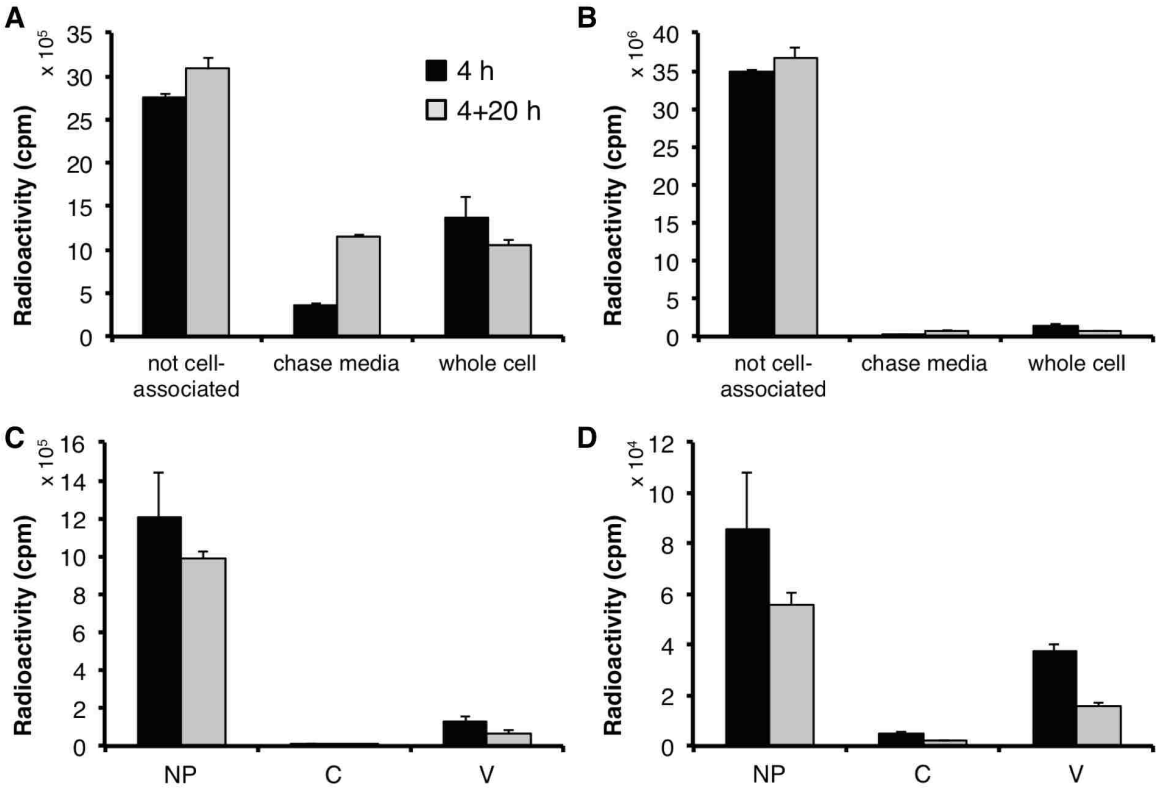

Figure 2.10: **Distribution of [^{3}H]DNA/[^{14}C]bPEI polyplexes in treated cells fractionated using density-gradient centrifugation.** HeLa cells (2×10^7) were pulsed with [^{3}H]DNA/[^{14}C]bPEI polyplexes for 4 h, and then prepared for fractionation. A 5-20% continuous iodixanol gradient was used to separate vesicular organelles.The radioactivity of (A) [^{3}H]DNA and (B) [^{14}C]bPEI measured in pulse media and washes, which are "not cell associated", chase media, and whole cell fractions. The radioactivity of (C) [^{3}H]DNA and (D) [^{14}C]bPEI measured in the nuclear, cytosolic, and vesicular fractions. Data are presented as mean ± average deviation (range divided by 2), $n = 2$.

tochondria have been found to distribute to denser portions of iodixanol gradients [38]; however, succinate dehydrogenase activity was undetectable in the fractions, possibly due to lack of assay sensitivity. These results also revealed that polyplex treatment affected organelle buoyancy and shifted organelle distribution in density gradients. Addition of polyplexes produced less dense endosomal fractions, potentially due to osmotic swelling of polyplex-containing endosomes [39]. Treatment with cationic lipoplexes and polymers has also been shown to shift organelle populations [30, 34, 40].

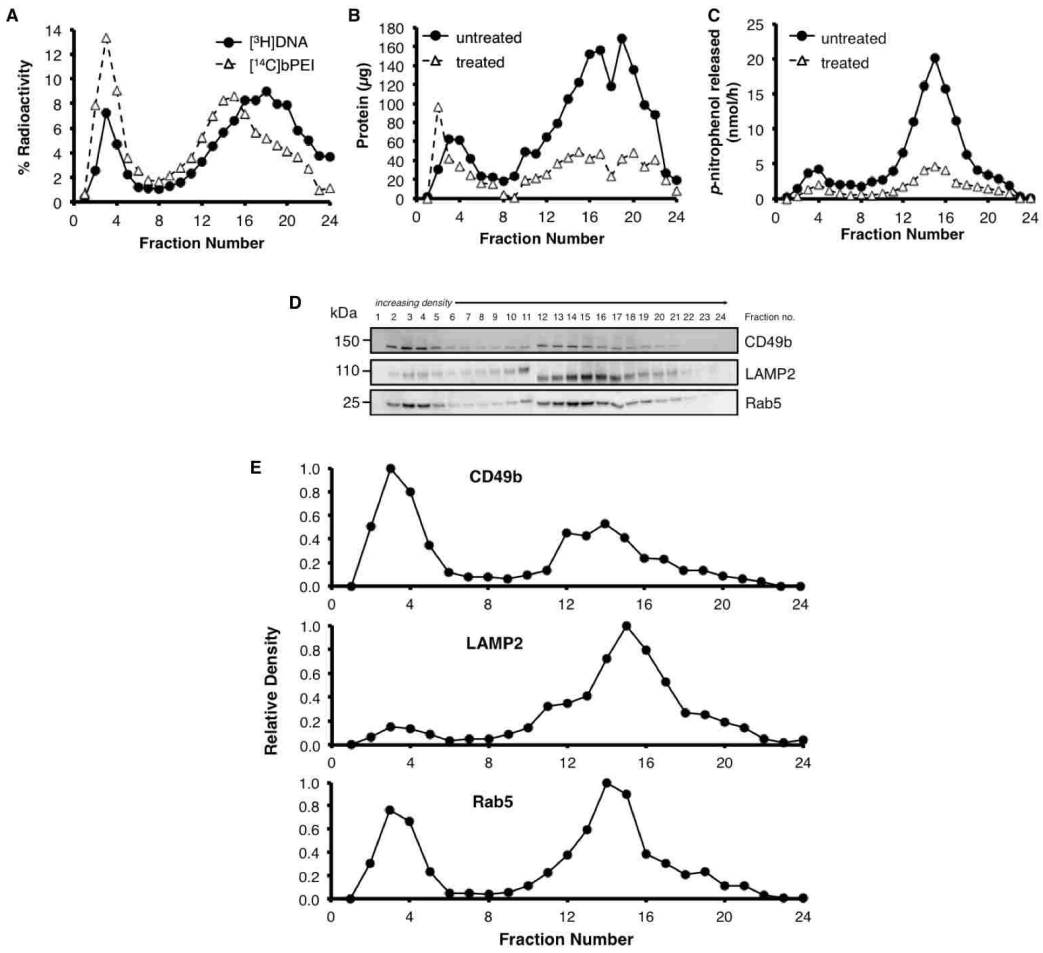

Figure 2.11: **Distribution of [^{3}H]DNA/[^{13}C]bPEI polyplexes after 4 h pulse-20 h chase in cells fractionated using a 5-20% co ntinuous iodixanol density gradient.** HeLa cells (2×10^7) were pulsed with [^{3}H]DNA/[^{14}C]bPEI polyplexes for 4 h, chased in complete media for 20 h, and then prepared for fractionation. A 5-20% continuous iodixanol gradient was used to separate vesicular organelles. (A) The percent radioactivity measured in fractions from the 5-20% gradient. 100% radioactivity is equal to the sum of the radioactivity found in all 24 fractions collected from the 5-20% gradient. (B) Total protein was measured in untreated and treated gradient fractions. (C) Hexosaminidase A (lysosome) activity was also measured in untreated and treated gradient fractions. (D) An equivolume (250 μL) of gradient fractions from treated samples was precipitated, concentrated, and probed for CD49b (plasma membrane), LAMP2 (lysosome), and Rab5 (endosome). (E) The optical density of each band was measured using ImageJ. Each time point presented is representative of duplicate experiments.

2.4 Discussion

Currently, most synthetic gene carriers in the development stage are tested by delivery of a reporter gene such as luciferase or green fluorescent protein. However, the delivery pathway is complex and reporter gene readouts only provide information about overall delivery efficiencies, leaving the details of specific steps to transfection hidden in the black box of the cell. The goal of this presented work is to improve our quantitative understanding of the intracellular trafficking of both the cargo DNA as well as the gene delivery vehicle itself. To accomplish this, we used radiolabeling and cellular fractionation strategies to track bPEI and the cargo plasmid DNA in extracellular and intracellular environments in cultured cells. Our main findings were that (1) overall cellular uptake of polymer was very low compared to the uptake of DNA; (2) nuclear association of intracellular polymer and DNA was high compared to other organelles; and (3) polymer and DNA traffic differently in intracellular vesicles.

The polycation PEI was radiolabeled by partial acetylation to gain quantitative insight into polymer cellular association and uptake, as well as intracellular distribution. Radiolabeling only slightly affected packaging ability, shifting full complexation of plasmid DNA to N/P 3 from N/P 2 (Figure 2.5). Alternative radiolabeling strategies, such as polymerizing [^{14}C]aziridine to synthesize [^{14}C]bPEI, leaves amine density unaffected compared to unlabeled PEI but would likely generate polymers with different polydispersity and molecular weights compared to commercially available PEI, which is one of the most frequently used polycations for gene transfer. In our studies, HeLa cells were treated at an N/P ratio of 5, which was optimal for transfection efficiency (data not shown), although the actual amount of polymer associated with DNA at N/P 5 was not determined. However, several groups have studied the complexation of 25 kD bPEI with plasmid DNA, and showed that at N/P 6, $<$ 50% of the bPEI is associated with DNA [41–43]. Specifically, Clamme *et al.* estimated by fluorescence correlation spectroscopy that PEI is associated with DNA at N/P $\sim$1 when formulated at N/P 6, and Boeckle *et al.* estimates this value to be 2.8 after polyplex purification by size exclusion chromatography [41, 42]. Surprisingly, only 1-6% of the applied polymer became associated with cells although 30-50% of the applied DNA was

cell-associated. This translates to an effective N/P ratio of 0.3-0.6, which is much lower than the expected N/P 1-3 of fully condensed polyplexes. This phenomenon was seen reproducibly throughout multiple experiments (Figure 2.6, Figure 2.8, Figure 2.10). Schaffer and Lauffenburger also noted low uptake of polyplexes by monitoring radiolabeled polycation, measuring that $> 90\%$ of [^{125}I]polylysine/DNA complexes were washed off the cell surface [44]; however, an effective N/P ratio was not calculated since the DNA was unlabeled. Despite an overall low uptake of polymer in our studies, the effective N/P ratios in the cytosolic and vesicular fractions was greater than 2 (Figures 2.6 and 2.7), indicating that intracellular polymer and DNA remain associated except at the nucleus. There are two possible explanations for such low overall cellular association of polymer: (1) rapid exocytosis of displaced polymer occurs after cellular uptake, or (2) polyplexes are partially unpackaged before cell uptake.

In order to gain insight into the first possibility, we analyzed radioactivity found in the collection of media from the chase periods in pulse-experiments. We found that the amount of polymer and DNA that was cell-associated after longer chase periods (*i.e.* 20 hours) was half that after shorter chase periods (*i.e.* 2 hours) (Figure 2.1, Figure 2.6, Figure 2.10A-B). This indicates that polymer is released back into the media from the cell with time, but the release does not appear to be preferential compared with DNA. Although polyplex exocytosis has received little attention, previous studies have indicated that up to 65% of internalized nanoparticles may be exocytosed fairly rapidly (within 30 min) depending on the nanoparticle concentration gradient across the cell membrane [45, 46]. In contrast, Seib *et al.* showed that bPEI alone did not exocytose significantly within 60 min in B16f10 melanoma cells [47]. Therefore, further studies to discern the role of polyplex exocytosis in cellular uptake should be pursued.

The second possibility is that polyplexes partially unpackage before cell uptake. Extracellular components, such as negatively-charged glycosaminoglycans (GAGs), have been shown to influence polyplex uptake and unpackaging by causing premature extracellular polyplex dissociation *via* electrostatic competition with GAGs [41, 43, 48–50]. However, previous studies using Förster resonance energy transfer (FRET) in which both the polymer carrier and cargo nucleic acid were labeled [15, 51] or the nucleic acid was dual-labeled [52–54]

showed that polyplexes remain intact, at least to some extent, in the cell. Furthermore, in our studies, a high N/P was also associated with the DNA in lighter and less dense organelles (Figures 2.7 and 2.9), indicating that the polymer and DNA separate during intracellular trafficking. Schubert *et al.* studied the complexation of plasmid DNA with linear PEI and found that "primary complexes" of PEI and DNA at N/P ~0.7 are first formed, which then merge into aggregates as more polymer is added [55]. These primary complexes are small in size (~30 nm) and can be internalized by cells. Clamme *et al.* also reported that in bPEI polyplexes formed at N/P 6, ~86% of the polymer existed freely in solution, and that these polyplexes were poorly compacted but can still transfect cells [42]. Therefore, it is possible that despite aggregate formation at N/P 5, the actual particles internalized by the cell are the primary complexes.

In addition to quantifying cellular uptake and association, intracellular polyplex nuclear distribution was measured by subcellular fractionation methods. Interestingly, most of the [^{3}H]DNA and [^{14}C]bPEI were found in the crude nuclear fraction, both at short times (30 min) (Figure 2.6C-D) and longer times (20 h) (Figure 2.10C-D). The effective N/P ratio in the nuclear fraction remained less than 1 throughout multiple studies (Figures 2.6 and 2.7, Figure 2.10C-D), indicating that the polymer dissociated from the DNA prior to reaching the nucleus. The percentage of cell-associated [^{3}H]DNA in the nuclear fractions increased with time, whereas the percentage of cell-associated [^{14}C]bPEI in these fractions decreased with time. The increase of [^{3}H]DNA in this fraction likely also includes accumulation of degraded plasmid in the nucleus, since DNA oligonucleotides (ODNs) undergo active nuclear import [56]. A fractionation study by Eboue *et al.* also found that up to 69% of PEI/[^{3}H]ODN complexes were found after 2.5 h in a purified nuclear fraction, indicating that a large percentage of polyplexes are nuclear-associated [11]. These results are in agreement with the large amount of [^{3}H]DNA we detected in the nuclear fraction (Figure 2.6C-D, Figure 2.7C-D, Figure 2.10C-D).

Incomplete separation of cytoskeletal filaments from nuclei during fractionation has been previously reported [57]. Cytoskeletal elements have been shown to mediate polyplex transfer to the perinuclear region [58, 59]. Bieber *et al.* also showed that, by fluorescence imaging, many PEI polyplexes locate in the perinuclear space rather than the cytosol, and thus pro-

posed that nuclear translocation remained a dominant barrier to efficient gene delivery [39]. Therefore, if cytoskeletal filaments separate with the nuclear fraction, this may explain why, in our studies, the cytosolic fraction contained such a small percentage of material despite the evidence for cytosolic distribution of PEI complexes [15]. It is difficult to discriminate polyplexes that are associated with the nuclear membrane from those that are intranuclear; Cohen *et al.* determined that a large amount of complexes still remained on the outer surface of the nuclear membrane using confocal microscopy despite treatment with excess cationic polymers and restriction enzymes [19]. Thus, the high percentage of intracellular DNA and polymer detected in our nuclear fractions does not necessarily indicate efficient delivery of intact plasmid DNA into the nucleus.

Despite a large fraction of [^{3}H]DNA and [^{14}C]bPEI in the nuclear fraction, differential distribution of each component was seen in post-nuclear organelles (Figures 2.7 and 2.9). In general, DNA was detected mostly in the heavier and denser fractions, which contained mostly lysosomes and mitochondria, while polymer was detected in mostly lighter and less dense fractions, which contained mostly plasma membrane, endosomes, and lysosomes. These findings may help explain the discrepancies between polymer and pDNA subcellular localization seen in other studies; in particular, ratiometric fluorescence studies demonstrated that the pH of compartments containing labeled DNA was higher than that of PEI [60] and histidylated polylysine [61]. Reports have also shown that lysosomal pH did not increase with labeled PEI [62] and that PEI in LAMP1-positive compartments also did not have increased pH [63]. These results may indicate an overall difference in the bulk polymer and DNA intracellular distribution, in which DNA is localized to mostly non-acidic organelles while polymer is mostly localized to acidified organelles. DNA was also seen split between two populations of denser organelles in a sucrose gradient by Laurent *et al.* [9]; they hypothesized that the non-lysosomal distribution of DNA in the denser regions of the gradient contained complexed plasmid DNA and that these structures may be phagosomes resulting from phagocytosis, a process that has been observed in HeLa cells [64]. The observation that polymer and DNA distribution remained largely unchanged over time indicates that polymer and/or polyplexes may be associating with vesicle-membrane lipids and traveling with these lipids during endocytosis. Since the exchange and transfer of ma-

terials through the endosomal/lysosomal pathway has been proposed to go through vesicle "kissing" and/or fusion [65], free cationic polymer may be traveling with the membrane lipids while the more neutrally-charged and water-soluble polyplexes (DNA-associated) are trafficked with the soluble contents of the vesicles. This may also help explain why, in our studies, the overall effective N/P ratio in cell-associated fractions was less than 1 while fractions containing mostly endocytic organelles (endosomes, lysosomes) had effective N/P ratios of ∼7-10 by 4 h (Figure 2.7). These results may also indicate that some polyplex unpackaging already occurs in the vesicular fractions, which was previously observed using FRET by Leong and coworkers [15]. In addition, poly-D-lysine, which is not degradable, exhibited similar unchanged subcellular distribution in denser organelles up to 14 h after injection into rats [9]. Similar trends were seen with [^{35}S]DNA complexed with bPEI [66]. When [^{125}I]bPEI alone was injected into rats, the polymer remained mostly in the lysosomal fraction after 4 and 18 h [67]. However, the extent of studies investigating polymer interaction with lipid membranes is focused on pore formation and membrane destabilization with non-biological lipid membranes [68, 69].

In summary, we demonstrate the use of subcellular fractionation methods to quantitatively assess both polymer and DNA in intracellular compartments. By radiolabeling both the synthetic carrier and the cargo DNA, we were able to quantify the amount of each component in the media, cell-associated fractions, as well as various intracellular organelles, such as the plasma membrane, nuclei, cytosol, endosomes, lysosomes, and mitochondria. These studies described general method development for the quantitative analysis of polyplex intracellular distribution, and will be applied for studying the effect of various chemical moieties on polymeric gene carriers.

2.5 Acknowledgments

This work is supported by the Center for the Intracellular Delivery of Biologics through the Washington State Life Sciences Discovery Fund Grant No. 2496490 and NIH 1R01NS064404. J.S. is supported by the National Science Foundation Graduate Research Fellowship under Grant No. DGE-0718124 and the Howard Hughes Medical Institute/UW Molecular Medicine Graduate Student Scholarship. B.C. was supported by a Mary Gates Undergrad-

uate Research Fellowship. We gratefully thank Dr. Drew Sellers for technical expertise and Dr. J. Paul Luzio (Professor of Molecular Membrane Biology, University of Cambridge), Dr. Oliver Press (Professor of Medicine, University of Washington and Fred Hutchinson Cancer Research Center), Dr. Patrick Stayton (Professor of Bioengineering, University of Washington), David Chu, and Dr. Joan Schellinger for helpful discussion.

References

[1] Pack, D. W., Hoffman, A. S., Pun, S., and Stayton, P. S. (2005) Design and development of polymers for gene delivery. *Nat. Rev. Drug Discov.*, **4**, 581–593.

[2] Suh, J., Wirtz, D., and Hanes, J. (2003) Efficient active transport of gene nanocarriers to the cell nucleus. *Proc. Natl. Acad. Sci. U.S.A.*, **100**, 3878–3882.

[3] Akita, H., Enoto, K., Masuda, T., Mizuguchi, H., Tani, T., and Harashima, H. (2010) Particle tracking of intracellular trafficking of octaarginine-modified liposomes: a comparative study with adenovirus. *Mol. Ther.*, **18**, 955–964.

[4] Varga, C. M., Tedford, N. C., Thomas, M., Klibanov, A. M., Griffith, L. G., and Lauffenburger, D. A. (2005) Quantitative comparison of polyethylenimine formulations and adenoviral vectors in terms of intracellular gene delivery processes. *Gene Ther.*, **12**, 1023–1032.

[5] Varkouhi, A. K., Scholte, M., Storm, G., and Haisma, H. J. (2011) Endosomal escape pathways for delivery of biologicals. *J. Control. Release*, **151**, 220–228.

[6] Funhoff, A. M., van Nostrum, C. F., Koning, G. A., Schuurmans-Nieuwenbroek, N. M. E., Crommelin, D. J. A., and Hennink, W. E. (2004) Endosomal escape of polymeric gene delivery complexes is not always enhanced by polymers buffering at low pH. *Biomacromolecules*, **5**, 32–39.

[7] Schaffert, D. and Wagner, E. (2008) Gene therapy progress and prospects: synthetic polymer-based systems. *Gene Ther.*, **15**, 1131–1138.

[8] Holmes, A., Dohrman, A., Ellison, A., Goncz, K., and Gruenert, D. (1999) Intracellular compartmentalization of DNA fragments in cultured airway epithelial cells mediated by cationic lipids. *Pharm. Res.*, **16**, 1020–1025.

[9] Laurent, N., Wattiaux-De Coninck, S., Mihaylova, E., Leontieva, E., Warnier-Pirotte, M. T., Wattiaux, R., and Jadot, M. (1999) Uptake by rat liver and intracellular fate of plasmid DNA complexed with poly-L-lysine or poly-D-lysine. *FEBS Lett.*, **443**, 61–65.

[10] Colin, M., et al. (2000) Cell delivery, intracellular trafficking and expression of an integrin-mediated gene transfer vector in tracheal epithelial cells. *Gene Ther.*, **7**, 139–152.

[11] Eboue, D., Auger, R., Angiari, C., Le Doan, T., and Tenu, J. P. (2003) Use of a simple fractionation method to evaluate binding, internalization and intracellular distribution of oligonucleotides in vascular smooth muscle cells. *Arch. Physiol. Biochem.*, **111**, 265–272.

[12] Watson, P., Jones, A. T., and Stephens, D. J. (2005) Intracellular trafficking pathways and drug delivery: fluorescence imaging of living and fixed cells. *Adv. Drug Deliv. Rev.*, **57**, 43–61.

[13] Akita, H., Ito, R., Khalil, I. A., Futaki, S., and Harashima, H. (2004) Quantitative three-dimensional analysis of the intracellular trafficking of plasmid DNA transfected by a nonviral gene delivery system using confocal laser scanning microscopy. *Mol. Ther.*, **9**, 443–451.

[14] Hama, S., Akita, H., Ito, R., Mizuguchi, H., Hayakawa, T., and Harashima, H. (2006) Quantitative comparison of intracellular trafficking and nuclear transcription between adenoviral and lipoplex systems. *Mol. Ther.*, **13**, 786–794.

[15] Chen, H. H., Ho, Y.-P., Jiang, X., Mao, H.-Q., Wang, T.-H., and Leong, K. W. (2008) Quantitative comparison of intracellular unpacking kinetics of polyplexes by a model constructed from quantum dot-FRET. *Mol. Ther.*, **16**, 324–332.

[16] Rejman, J., Bragonzi, A., and Conese, M. (2005) Role of clathrin- and caveolae-mediated endocytosis in gene transfer mediated by lipo- and polyplexes. *Mol. Ther.*, **12**, 468–474.

[17] von Gersdorff, K., Sanders, N. N., Vandenbroucke, R., De Smedt, S. C., Wagner, E., and Ogris, M. (2006) The internalization route resulting in successful gene expression depends on both cell line and polyethylenimine polyplex type. *Mol. Ther.*, **14**, 745–753.

[18] Vercauteren, D., Vandenbroucke, R. E., Jones, A. T., Rejman, J., Demeester, J., De Smedt, S. C., Sanders, N. N., and Braeckmans, K. (2010) The use of inhibitors to study endocytic pathways of gene carriers: optimization and pitfalls. *Mol. Ther.*, **18**, 561–569.

[19] Cohen, R. N., van der Aa, M. A. E. M., Macaraeg, N., Lee, A. P., and Szoka, F. C. (2009) Quantification of plasmid DNA copies in the nucleus after lipoplex and polyplex transfection. *J. Control. Release*, **135**, 166–174.

[20] Glover, D. J., Leyton, D. L., Moseley, G. W., and Jans, D. A. (2010) The efficiency of nuclear plasmid DNA delivery is a critical determinant of transgene expression at the single cell level. *J. Gene Med.*, **12**, 77–85.

[21] Hsu, C. Y. M., Hendzel, M., and Uludağ, H. (2011) Improved transfection efficiency of an aliphatic lipid substituted 2 kDa polyethylenimine is attributed to enhanced nuclear association and uptake in rat bone marrow stromal cell. *J. Gene Med.*, **13**, 46–59.

[22] Varga, C. M., Hong, K., and Lauffenburger, D. A. (2001) Quantitative analysis of synthetic gene delivery vector design properties. *Mol. Ther.*, **4**, 438–446.

[23] Banks, G. A., Roselli, R. J., Chen, R., and Giorgio, T. D. (2003) A model for the analysis of nonviral gene therapy. *Gene Ther.*, **10**, 1766–1775.

[24] Zhou, J., Yockman, J. W., Kim, S. W., and Kern, S. E. (2007) Intracellular kinetics of non-viral gene delivery using polyethylenimine carriers. *Pharm. Res.*, **24**, 1079–1087.

[25] Zheng, N., Tsai, H. N., Zhang, X., and Rosania, G. R. (2011) The subcellular distribution of small molecules: from pharmacokinetics to synthetic biology. *Mol. Pharm.*, **8**, 1619–1628.

[26] Wendeler, M. and Sandhoff, K. (2009) Hexosaminidase assays. *Glycoconj. J.*, **26**, 945–952.

[27] Seib, F. P., Jones, A. T., and Duncan, R. (2006) Establishment of subcellular fractionation techniques to monitor the intracellular fate of polymer therapeutics I. Differential centrifugation fractionation B16F10 cells and use to study the intracellular fate of HPMA copolymer - doxorubicin. *J. Drug Target.*, **14**, 375–390.

[28] von Harpe, A., Petersen, H., Li, Y., and Kissel, T. (2000) Characterization of commercially available and synthesized polyethylenimines for gene delivery. *J. Control. Release*, **69**, 309–322.

[29] Bartz, R., et al. (2011) Effective siRNA delivery and target mRNA degradation using an amphipathic peptide to facilitate pH-dependent endosomal escape. *Biochem. J.*, **435**, 475–487.

[30] Manunta, M., Izzo, L., Duncan, R., and Jones, A. T. (2007) Establishment of subcellular fractionation techniques to monitor the intracellular fate of polymer therapeutics II. Identification of endosomal and lysosomal compartments in HepG2 cells combining single-step subcellular fractionation with fluorescent imaging. *J. Drug Target.*, **15**, 37–50.

[31] Plonne, D., Cartwright, I., Linss, W., Dargel, R., Graham, J. M., and Higgins, J. A. (1999) Separation of the intracellular secretory compartment of rat liver and isolated rat hepatocytes in a single step using self-generating gradients of iodixanol. *Anal. Biochem.*, **276**, 88–96.

[32] L'Annunziata, M. F. (2012) *Handbook of Radioactivity Analysis*. Academic Press, 3 edn.

[33] Armbruster, D. A. and Pry, T. (2008) Limit of blank, limit of detection and limit of quantitation. *Clin Biochem Rev*, **29 Suppl 1**, S49–52.

[34] Richardson, S. C. W., Pattrick, N. G., Lavignac, N., Ferruti, P., and Duncan, R. (2010) Intracellular fate of bioresponsive poly(amidoamine)s in vitro and in vivo. *J. Control. Release*, **142**, 78–88.

[35] Duvvuri, M., Feng, W., Mathis, A., and Krise, J. P. (2004) A cell fractionation approach for the quantitative analysis of subcellular drug disposition. *Pharm. Res.*, **21**, 26–32.

[36] Gorvel, J. P., Chavrier, P., Zerial, M., and Gruenberg, J. (1991) rab5 controls early endosome fusion in vitro. *Cell*, **64**, 915–925.

[37] Eskelinen, E.-L. (2006) Roles of LAMP-1 and LAMP-2 in lysosome biogenesis and autophagy. *Molecular Aspects of Medicine*, **27**, 495–502.

[38] Graham, J. M. (2001) Isolation of lysosomes from tissues and cells by differential and density gradient centrifugation. *Curr Protoc Cell Biol*, **Chapter 3**, Unit 3.6.

[39] Bieber, T., Meissner, W., Kostin, S., Niemann, A., and Elsasser, H.-P. (2002) Intracellular route and transcriptional competence of polyethylenimine-DNA complexes. *J. Control. Release*, **82**, 441–454.

[40] Wattiaux, R., Jadot, M., Laurent, N., Dubois, F., and Wattiaux-De Coninck, S. (1996) Cationic lipids delay the transfer of plasmid DNA to lysosomes. *Biochem. Biophys. Res. Commun.*, **227**, 448–454.

[41] Boeckle, S., von Gersdorff, K., van der Piepen, S., Culmsee, C., Wagner, E., and Ogris, M. (2004) Purification of polyethylenimine polyplexes highlights the role of free polycations in gene transfer. *J. Gene Med.*, **6**, 1102–1111.

[42] Clamme, J. P., Azoulay, J., and Mély, Y. (2003) Monitoring of the formation and dissociation of polyethylenimine/DNA complexes by two photon fluorescence correlation spectroscopy. *Biophys. J.*, **84**, 1960–1968.

[43] Yue, Y., Jin, F., Deng, R., Cai, J., Chen, Y., Lin, M. C. M., Kung, H.-F., and Wu, C. (2011) Revisit complexation between DNA and polyethylenimine - Effect of uncomplexed chains free in the solution mixture on gene transfection. *J. Control. Release*, **155**, 67–76.

[44] Schaffer, D. V. and Lauffenburger, D. A. (1998) Optimization of cell surface binding enhances efficiency and specificity of molecular conjugate gene delivery. *J. Biol. Chem.*, **273**, 28004–28009.

[45] Panyam, J. and Labhasetwar, V. (2003) Dynamics of endocytosis and exocytosis of poly(D,L-lactide-co-glycolide) nanoparticles in vascular smooth muscle cells. *Pharm. Res.*, **20**, 212–220.

[46] Park, J. S., Han, T. H., Lee, K. Y., Han, Z., Hwang, J. J., Moon, D. H., Kim, S. Y., and Cho, Y. W. (2006) N-acetyl histidine-conjugated glycol chitosan self-assembled nanoparticles for intracytoplasmic delivery of drugs: endocytosis, exocytosis and drug release. *J. Control. Release*, **115**, 37–45.

[47] Seib, F. P., Jones, A. T., and Duncan, R. (2007) Comparison of the endocytic properties of linear and branched PEIs, and cationic PAMAM dendrimers in B16f10 melanoma cells. *J. Control. Release*, **117**, 291–300.

[48] Dai, Z., Gjetting, T., Mattebjerg, M. A., Wu, C., and Andresen, T. L. (2011) Elucidating the interplay between DNA-condensing and free polycations in gene transfection through a mechanistic study of linear and branched PEI. *Biomaterials*, **32**, 8626–8634.

[49] Bonner, D. K., Zhao, X., Buss, H., Langer, R., and Hammond, P. T. (2013) Crosslinked linear polyethylenimine enhances delivery of DNA to the cytoplasm. *J. Control. Release*, **167**, 101–107.

[50] Burke, R. S. and Pun, S. H. (2008) Extracellular barriers to in vivo PEI and PEGylated PEI polyplex-mediated gene delivery to the liver. *Bioconjug. Chem.*, **19**, 693–704.

[51] Ho, Y.-P., Chen, H. H., Leong, K. W., and Wang, T.-H. (2006) Evaluating the intracellular stability and unpacking of DNA nanocomplexes by quantum dots-FRET. *J. Control. Release*, **116**, 83–89.

[52] Itaka, K., Harada, A., Yamasaki, Y., Nakamura, K., Kawaguchi, H., and Kataoka, K. (2004) In situ single cell observation by fluorescence resonance energy transfer reveals fast intra-cytoplasmic delivery and easy release of plasmid DNA complexed with linear polyethylenimine. *J. Gene Med.*, **6**, 76–84.

[53] Matsumoto, Y., Itaka, K., Yamasoba, T., and Kataoka, K. (2009) Intranuclear fluorescence resonance energy transfer analysis of plasmid DNA decondensation from nonviral gene carriers. *J. Gene Med.*, **11**, 615–623.

[54] Alabi, C. A., Love, K. T., Sahay, G., Stutzman, T., Young, W. T., Langer, R., and Anderson, D. G. (2012) FRET-labeled siRNA probes for tracking assembly and disassembly of siRNA nanocomplexes. *ACS Nano*, **6**, 6133–6141.

[55] Schubert, U. S., Perevyazko, I., Pavlov, G., Hoeppener, S., Schubert, S., Bauer, M., and Fischer, D. (2012) Polyelectrolyte complexes of DNA and linear PEI: formation, composition and properties. *Langmuir*.

[56] Hartig, R., Shoeman, R. L., Janetzko, A., Grüb, S., and Traub, P. (1998) Active nuclear import of single-stranded oligonucleotides and their complexes with non-karyophilic macromolecules. *Biol. Cell*, **90**, 407–426.

[57] Staufenbiel, M. and Deppert, W. (1982) Intermediate filament systems are collapsed onto the nuclear surface after isolation of nuclei from tissue culture cells. *Exp. Cell Res.*, **138**, 207–214.

[58] de Bruin, K., Ruthardt, N., von Gersdorff, K., Bausinger, R., Wagner, E., Ogris, M., and Bräuchle, C. (2007) Cellular dynamics of EGF receptor-targeted synthetic viruses. *Mol. Ther.*, **15**, 1297–1305.

[59] Grosse, S., Aron, Y., Thévenot, G., Monsigny, M., and Fajac, I. (2007) Cytoskeletal involvement in the cellular trafficking of plasmid/PEI derivative complexes. *J. Control. Release*, **122**, 111–117.

[60] Akinc, A. and Langer, R. (2002) Measuring the pH environment of DNA delivered using nonviral vectors: implications for lysosomal trafficking. *Biotechnol. Bioeng.*, **78**, 503–508.

[61] Gonçalves, C., Pichon, C., Guérin, B., and Midoux, P. (2002) Intracellular processing and stability of DNA complexed with histidylated polylysine conjugates. *J. Gene Med.*, **4**, 271–281.

[62] Forrest, M. L. and Pack, D. W. (2002) On the kinetics of polyplex endocytic trafficking: implications for gene delivery vector design. *Mol. Ther.*, **6**, 57–66.

[63] Benjaminsen, R. V., Mattebjerg, M. A., Henriksen, J. R., Moghimi, S. M., and Andresen, T. L. (2012) The possible "proton sponge" effect of polyethylenimine (PEI) does not include change in lysosomal pH. *Mol. Ther.*.

[64] Kopatz, I., Remy, J.-S., and Behr, J.-P. (2004) A model for non-viral gene delivery: through syndecan adhesion molecules and powered by actin. *J. Gene Med.*, **6**, 769–776.

[65] Luzio, J. P., Parkinson, M. D. J., Gray, S. R., and Bright, N. A. (2009) The delivery of endocytosed cargo to lysosomes. *Biochem. Soc. Trans.*, **37**, 1019–1021.

[66] Wattiaux, R., Laurent, N., Wattiaux-De Coninck, S., and Jadot, M. (2000) Endosomes, lysosomes: their implication in gene transfer. *Adv. Drug Deliv. Rev.*, **41**, 201–208.

[67] Lecocq, M., Wattiaux-De Coninck, S., Laurent, N., Wattiaux, R., and Jadot, M. (2000) Uptake and intracellular fate of polyethylenimine in vivo. *Biochem. Biophys. Res. Commun.*, **278**, 414–418.

[68] Leroueil, P. R., Hong, S., Mecke, A., Baker, J. R., Orr, B. G., and Banaszak Holl, M. M. (2007) Nanoparticle interaction with biological membranes: does nanotechnology present a Janus face? *Acc. Chem. Res.*, **40**, 335–342.

[69] Nel, A. E., Mädler, L., Velegol, D., Xia, T., Hoek, E. M. V., Somasundaran, P., Klaessig, F., Castranova, V., and Thompson, M. (2009) Understanding biophysicochemical interactions at the nano-bio interface. *Nat. Mater.*, **8**, 543–557.

Chapter 3

EFFECT OF POLYPLEX MORPHOLOGY ON CELLULAR UPTAKE, INTRACELLULAR TRAFFICKING, AND TRANSGENE EXPRESSION

Julie Shi, Jennifer L. Choi, Brian Chou, and Suzie H. Pun

Abstract

Nanoparticle morphology has been shown to affect cellular uptake, but there are few studies investigating the impact of particle shape on biologic drug delivery. Recently, our group synthesized a series of *N*-(2-hydroxypropyl) methacrylamide (HPMA)-oligolysine brush polymers for nucleic acid delivery that varied in oligolysine peptide length and polymer molecular weight. Interestingly, a 50% longer peptide (K_{15}) transfected very poorly compared to the optimized polymer comprised of K_{10} peptide despite similar chemical composition and molecular weight. We hypothesized that differences in particle morphology contributed to the differences in plasmid DNA delivery. We found that particles formed with plasmid DNA and a polymer with the longer oligolysine peptide (pHK15) had larger aspect ratios than particles formed with the optimized polymer (pHK10). Even though both formulations showed similar percentages of cellular association, particles of a higher aspect ratio were internalized to a lesser extent. Furthermore, the rod-like particles accumulated more in endosomal/lysosomal compartments, leading to delayed nuclear delivery. Other parameters such as particle surface charge, unpackaging ability, uptake mechanism, intracellular trafficking, nor the presence of heparan sulfate proteoglycans significantly differed between the two polymer formulations. These results indicate that, for this system, polyplex morphology primarily impacts nucleic acid delivery efficiency through differences in cellular internalization rates.[1]

---

[1]Submitted for publication, currently under revision.

3.1 Introduction

Biologic drugs such as proteins, peptides, and nucleic acids are often encapsulated in delivery vehicles that both protect against premature degradation and facilitate uptake. Vehicles containing drugs with intracellular targets are generally internalized by cells through vesicular uptake mechanisms [1, 2]. The rate and mechanism of cellular internalization of these vehicles depends on the target cell type as well as on the physicochemical properties of the vehicles. The influence of particle shape and size on internalization mechanism has been studied in detail for several model nanoparticle systems, such as nanoparticles composed of polystyrene [3], poly(methacrylates) [4], silica [5, 6], gold [7, 8], and carbon [9]. However, there are few studies that have probed the influence of particle shape on the effectiveness of biologic drug delivery [3, 5].

Our group recently synthesized a series of HPMA-*co*-oligolysine comb-like polymers for nucleic acid delivery [10]. We found that two polymers with similar chemical composition but different comb lengths showed drastically different gene transfer efficiencies. Since several reports have indicated that polylysine peptides of different lengths complexed DNA into varying particle shapes [11, 12], we hypothesized that polycation structure could impact supramolecular morphology after complexation with a polyanion (termed "polyplexes"). Furthermore, the difference in particle morphology could affect downstream transfection efficiency. Particle size and shape has been shown to affect internalization rates for solid particles [3, 4, 6, 13]; however, it is unknown how the particle morphology of polyplexes influences cellular uptake and intracellular trafficking. In this work, the role of particle morphology on the various steps of intracellular nanoparticle delivery is investigated and quantified through a detailed analysis of uptake efficiency, endocytosis pathway, subcellular distribution, intracellular trafficking, and gene transfer efficiency. We find that particle morphology significantly impact rates of cellular uptake, but has minor influence on subsequent intracellular trafficking and processing. These results highlight the importance of considering polyplex morphology when designing nanoparticles for intracellular delivery.

3.2 Materials and methods

3.2.1 Materials

N-(2-hydroxypropyl)methacrylamide (HPMA) was purchased from Polysciences (Warrington, PA). The initiator VA-044 was purchased from Wako Chemicals USA (Richmond, VA). Chain transfer agent ethyl cyanovaleric trithiocarbonate (ECT) was a generous gift from Dr. Anthony Convertine (University of Washington). Rink amide resin was purchased from Merck Chemical Int. (Darmstadt, Germany). HBTU and Fmoc-protected lysine were purchased from Aapptec (Louisville, KY). *N*-succinimidyl methacrylate was purchased from TCI America (Portland, OR). Copper grids for electron microscopy studies were purchased from Electron Microscopy Sciences (Hatfield, PA). 2'-Deoxycytidine 5'-triphosphate tetraammonium salt, [5'-^{3}H], was purchased from Moravek Biochemicals and Radiochemicals (Brea, CA). Fluorescent dyes were purchased from Life Technologies (Green Island, NY). Ultima Gold scintillation fluid was purchased from Perkin-Elmer (Santa Clara, CA). All cell culture reagents were purchased from Cellgro/Mediatech (Fisher Scientific, Pittsburgh, PA). All other materials, including polylysine (PLL, 12,000 - 24,000 g/mol), were reagent grade or better and were purchased from Sigma-Aldrich (St. Louis, MO) unless otherwise stated. Endotoxin-free plasmid pCMV-Luc2 was prepared by using the pGL4.10 vector (Promega, Madison, WI) and inserting the CMV promoter/intron region from the gWiz Luciferase (Aldevron, Madison, WI). The plasmid was isolated and produced with the Qiagen Plasmid Giga kit (Qiagen, Germany) according to the manufacturer's instructions.

3.2.2 Synthesis and characterization of peptides and polymers

Synthesis of peptide monomers, methacrylated $AhxK_{10}$ ($MaAhxK_{10}$) and methacrylated $AhxK_{15}$ ($MaAhxK_{15}$) were completed exactly as described previously [10]. Briefly, peptide monomers were synthesized on a solid support of Rink amide following standard Fmoc/tBu chemistry and cleaved off the solid support with a solution of TFA/TIPS/1,3-dimethoxybenzene (92.5:2.5:5 v/v/v). Cleaved peptide monomers were precipitated in cold ether, dissolved in methanol, and reprecipitated in cold ether. Each peptide monomer was analyzed by RP-HPLC and MALDI-TOF MS and was shown to have greater than

95% purity after cleavage. MALDI-TOF MS calculated for $MaAhxK_{10}$ (MH^+) 1479.98, found 1479.85. MALDI-TOF MS calculated for $MaAhxK_{15}$ (MH^+) 2120.85, found 2120.19. Copolymers of HPMA and either $MaAhxK_{10}$ or $MaAhxK_{15}$ were synthesized *via* RAFT polymerization (DP 150) and characterized by size exclusion chromatography and amino acid analysis, as described previously [10].

3.2.3 Polyplex formulation and characterization

Stock solutions of polymers were prepared at 10 $^{mg}/_{mL}$ in 0.1X phosphate buffered saline (PBS), and the pH was adjusted to 6.5 by adding 0.1 N HCl. To formulate polyplexes, pCMV-Luc2 plasmid DNA was diluted to 0.1 $^{mg}/_{mL}$ in DNase/RNase-free H_2O and mixed with an equal volume of polymer at desired lysine to DNA phosphate (N/P) ratios. Polyplexes were then allowed to incubate for 10 min at room temperature prior to use for experiments. For ζ potential measurements, 20 μL of polyplexes were diluted with 180 μL dH_2O and 800 μL 10 mM NaCl prior to measuring ζ potential using a Zetasizer Nano ZS (Malvern Instruments Inc., Southborough, MA) using the Smoluchowsky model for aqueous suspensions.

3.2.4 Transmission electron microscopy

Polyplex morphology was imaged by electron microscopy on a hydrophilic surface. To render a hydrophilic surface, 400-mesh copper/formvar grids were treated with glow discharge for 45 s. Ten microliters of polyplexes (in dH_2O) was applied to the formvar-side of the grid for 30 min. The grid was washed four times in dH_2O, and then dipped in 4% (w/v) uranyl acetate (in dH_2O) to negatively stain the sample. Excess solution was wicked off the grid with filter paper, and the grid was allowed to dry overnight prior to imaging. Images of the sample grids were taken with a JEOL 1010 transmission electron microscope (Electron Microscopy Facility, Fred Hutchinson Cancer Research Center). Measurements of particle length were completed using ImageJ, and expressed in the text as the mean ± S.D.

3.2.5 Cell culture

HeLa (human cervical carcinoma) cells were grown in minimum essential medium (MEM) supplemented with 10% fetal bovine serum (FBS) and antibiotics/antimyotics (AbAm) (100 IU penicillin, 100 μg/mL streptomycin, and 0.25 μg/mL amphotericin B). CHO-K1 (Chinese Hamster ovary) cells were grown in F12K media supplemented with 10% FBS and AbAm. CHO-pgs-A745 cells were grown in F12K media supplemented with 10% FBS, 200 μM L-asparagine, 200 μM L-proline, and AbAm. Cells were passaged when they reached 80% confluency.

3.2.6 Labeling of plasmid DNA with tritium

Plasmid DNA was radiolabeled using nick translation and 2'-deoxycytidine 5'-triphosphate, [5-^{3}H], according to manufacturer's instructions (GE Healthcare). For uptake studies, [^{3}H]DNA was diluted with unlabeled plasmid so that the final concentration was 0.1 g/L at ∼1.67 pCi.

3.2.7 Uptake of tritium-labeled polyplexes

HeLa, CHO-K1, and CHO-pgs-A745 cells were seeded in 24-well plates at a density of 3×10^4 cells per well (1 mL per well) 24 h prior to polyplex addition. Cells were washed once with PBS and 200 μL of polyplexes, formulated at N/P 5 with [^{3}H]DNA (1 μg at 0.1 g/L, ∼1.67 pCi) in OptiMEM, were added on top of cells and allowed to incubate for up to 4 h at 37 °C, 5% CO_2. At various time points (0, 2, 4 h), cells were washed twice with PBS, allowed to incubate with 200 μL CellScrub (Genlantis) for 15 min at room temperature, washed twice with DPBS (without divalent cations), trypsinized, and then collected with scintillation counting. For other time points (6, 8, 12, 24 h), cells were washed once with PBS after 4 h incubation with polyplexes and replaced with complete media. At various time points after media replacement (2, 4, 8, 20 h), cells were washed with PBS, CellScrub, DPBS, and trypsinized as above. All washes and solutions were collected and analyzed for radioactivity. To determine radioactivity, samples were dissolved in Ultima Gold scintillation fluid and counted for 10 min on a scintillation counter (Beckman LS-6500).

3.2.8 In vitro transfection

HeLa, CHO-K1, and CHO-pgs-A745 cells were seeded overnight in 24-well plates at a density of 3×10^4 cells per well (1 mL per well) at 37 °C, 5% CO_2. Polyplexes were formulated as described above. After the polyplexes were formed, 20 μL (containing 1 μg DNA) was mixed with 180 μL of Opti-MEM medium (Invitrogen). Seeded cells were washed once with PBS and then treated with 200 μL of polyplexes in Opti-MEM, which was added dropwise on top of the cells. After a 4 h incubation at 37 °C, 5% CO_2 in a humidified environment, the cells were washed once again with PBS and incubated in 1 mL of fresh complete medium for an additional 44 h. Cells were harvested and assayed for luciferase expression at 48 h. This was done by washing cells once with PBS, adding of 200 μL reporter lysis buffer (Promega, Madison, WI), and then performing one freeze-thaw cycle to complete the lysis of cells. Lysates were collected and centrifuged at 14,000g for 5 min at 4 °C. Luminescence was carried out following the manufacturers instructions (Promega, Madison, WI). Luciferase activity is reported in relative light units (RLU) normalized by mg protein (RLU/mg), as measured by a microBCA Protein Assay Kit (Pierce).

3.2.9 In vitro transfection with chemical inhibitors

Stock solutions of genistein (5 $^{mg}/_{mL}$ in DMSO), chlorpromazine (1 $^{mg}/_{mL}$ in DMSO), and amiloride (2.5 $^{mg}/_{mL}$) were further diluted to working concentrations in OptiMEM (genistein, 50 $^{\mu g}/_{mL}$, chlorpromazine, 10 $^{\mu g}/_{mL}$, amiloride, 25 $^{\mu g}/_{mL}$), and used for transfections. For transfection with inhibitors, HeLa cells were seeded overnight in 24-well plates at a density of 3×10^4 cells per well (1 mL per well) at 37 °C, 5% CO_2. Polyplexes were formulated as described above. Cells were washed once with PBS and pre-treated with one of the chemical inhibitors (in OptiMEM) for 1 h at 37 °C, 5% CO_2 prior to polyplex transfection. 20 μL of polyplexes were then added to the cells and incubated for an additional 2 h at 37 °C, 5% CO_2. Cells were then washed once with PBS and incubated with fresh complete media for an additional 46 h. Cells were lysed and assayed for luciferase expression as described above.

3.2.10 Subcellular fractionation

Subcellular fractionation experiments were completed as previously described [14], with minor modifications. HeLa cells were seeded into 150 mm^2 dishes at 5×10^6 cells per dish 24 h prior to the start of the experiment. Cells were then treated with polyplexes formulated at N/P 5 with [^{3}H]DNA (100 μg at 0.1 g/L, dosed at ~1.67 pCi) for 4 h at 37 °C, 5% CO_2. To limit further intracellular trafficking and internalization, all future steps were done on ice, at 4 °C, and/or with pre-chilled reagents/equipment. Cells were washed once with PBS, incubated with CellScrub for 15 min at room temperature, washed twice in DPBS (no $MgCl_2$, $CaCl_2$), lifted off the plates in PBS, and then transferred to conical tubes. To remove dead/compromised cells, cells were then washed twice with PBS, pelleting cells at 500g for 5 min after each wash. The cells were then washed once with homogenization buffer (HB) (250 mM sucrose, 10 mM HEPES-NaOH, 1 mM EDTA, pH 7.4), pelleting the cells at 1000g for 6 min. The resulting pellet was then resuspended in 2.5x the wet pellet mass of HB (containing 1X protease inhibitors, Thermo Fisher HALT). Cells were then homogenized with a 25-gauge needle until greater than 90% cell lysis was achieved. Fractionation into a heavy mitochondrial (HM), light mitochondrial (LM), microsomal (MF), and cytosolic (C) fractions was then completed exactly as previously described [14]. Samples were stored at -80 °C. For radioactivity analysis, samples were mixed with an equivolume of 1 M NaOH prior to mixing with 4-5 mL Ultima Gold XR scintillation fluid (Perkin Elmer), and then analyzed for radioactivity using a scintillation counter (Beckman LS-6500).

3.2.11 Heparan sulfate competition assay

Ten microliters of polyplexes (in dH_2O) were treated with various amounts of heparan sulfate (5 g/L stock in dH_2O) and incubated at room temperature for 5 min. The entire sample was mixed with 10X BlueJuice loading buffer, loaded onto a 0.8% agarose gel containing TAE buffer (40 mM Tris-acetate, 1 mM EDTA) and ethidium bromide (0.5 μg/mL final concentration), and electrophoresed at 100 V. DNA was visualized using a UV transilluminator (laser-excited fluorescence gel scanner, Kodak, Rochester, NY).

3.2.12 Labeling of polymer with Alexa Fluor 568

To fluorescently label PLL, the polymer was reacted with Alexa Fluor 568 carboxylic acid, succinimidyl ester, in 1 M sodium bicarbonate, pH 8.3, at a 3:1 dye to polymer ratio for 1 h in the dark at room temperature. For labeling of pHK10 and pHK15, polymers were reacted with maleimide-functionalized Alexa Fluor 568 in PBS, containing 10 molar eq. of immobilized tris(2-carboxyethyl)phosphine) (TCEP), purged with N_2, and reacted for 2 h in the dark at room temperature. Excess dye was removed using a PD-10 column, using dH_2O as the eluent (GE Healthcare, Piscataway, NJ). Reaction efficiency was calculated by comparing the absorbance of the labeled polymer against a standard curve of the dye. Polymer concentration was calculated using a 2,4,6-trinitrobenzene sulfonic acid (TNBS) assay for primary amines, using the unlabeled polymer as a standard. Polymers were calculated to contain ∼1-2 dyes per polymer.

3.2.13 Multiple-particle tracking (MPT)

For multiple-particle tracking experiments, HeLa cells were seeded in 35 mm poly-L-lysine-treated glass-bottom petri dishes (MatTek, no. 1) at 4×10^4 cells per dish 24 h prior to the start of the experiment. Polyplexes were formulated with Alexa Fluor 568-labeled polymer and plasmid DNA (containing 0.25 μg DNA) at N/P 5 for 10 min at room temperature. The cells were washed with PBS and treated with polyplexes (in OptiMEM) for 30 min at 37 °C, 5% CO_2. Afterwards, cells were washed with PBS, and then placed in phenol red-free complete media for 2 h at 37 °C, 5% CO_2. After locating a cell under 100X magnification, 20 s videos (at 5 fps) were acquired using a monochromatic camera on an inverted fluorescent microscope (Nikon Ti-E, Melville, NY), using an appropriate filter set (ex. 560/40 nm, em. 630/75 nm, Chroma 49000 series, Rochingham, VT). Particles were then automatically tracked using Volocity v.6.2 (Perkin Elmer). Mean-squared-displacement was calculated using a custom-written MATLAB script (MathWorks, Natick, MA). Relative change (RC) values at short ($\tau_{reference} = 0.2$ s, $\tau_{probed} = 1$ s) and long time scales ($\tau_{reference} = 1$ s, $\tau_{probed} = 5$ s) were calculated and analyzed as previously described [15]. To characterize transport modes, trajectories of purely Brownian particles were created using a Monte Carlo

simulation, and confirmed by tracking 100 nm fluorescent polystyrene beads in glycerol. The effective diffusivity (D_{eff}) of the ensemble-average MSD was calculated using the following equation:

$$MSD = C + 4D_{eff}\tau^{\alpha}$$

where C is an adjustment factor dependent on the tracking resolution (μm^2), τ is the time lag (s), and α is an adjustment factor for subdiffusive motion ($\alpha = 1$ for diffusive motion) [16]. C was calculated to be 0.00657 ± 0.00445 μm^2.

3.3 Results

3.3.1 Polyplex morphology assessed by transmission electron microscopy (TEM)

pHK10 and pHK15 are comb-like HPMA-*co*-oligolysine polymers with similar chemical composition and molecular weight but different oligolysine brush length. The polymers are synthesized by reversible addition-fragmentation chain-transfer (RAFT) polymerization to provide high control over polymer molecular weight and composition [10]. Polylysine, a commercially-available linear polymer, was used for comparison. The polymer properties are summarized in Table 3.1. Despite the similarities in material composition and molecular weight, pHK10 and pHK15 showed significant differences in gene transfer efficiencies to cultured cells (Figure 3.1). At an amine to phosphate (N/P) ratio of 5, pHK10/DNA complexes (polyplexes) transfected HeLa cells as well as polyplexes with bPEI, the most commonly used cationic polymer for nonviral gene delivery, and with 42.3-fold higher transfection efficiency than pHK15 polyplexes; pHK15 polyplexes transfected similarly to PLL.

Previous reports have indicated a difference in polyplex morphology as a function of oligolysine length, ranging from loosely-complexed particles [11] to linear rods and oval-shaped particles [12]. Therefore, the polyplex morphology of pHK10, pHK15, and PLL polyplexes, formulated at N/P 5, was assessed by TEM. pHK10 polyplexes formed oblong particles, ~25 by ~74 nm (Figure 3.2A), while pHK15 particles formed longer rod-like particles (Figure 3.2B), with a width of ~18 nm and length of ~102 nm, toroids, or twisted particles. For comparison, PLL polyplexes formed either long, thin rods, around 38-191 nm

Table 3.1: Properties of HPMA-oligolysine polymers

polymer	targeted M_n (kD)[a]	determined M_n (kD)[a]	M_n/M_w[b]	mol % oligolysine monomer	mmol K/g polymer[b]
pHK10	61.85	65.51	1.141	20.5	4.92
pHK15	61.27	74.38	1.207	14	5

[a]Values determined by SEC coupled with laser light scattering and dRI detection. [b]Mol% of oligolysine and mmol lysine per gram polymer determined by amino acid analysis.

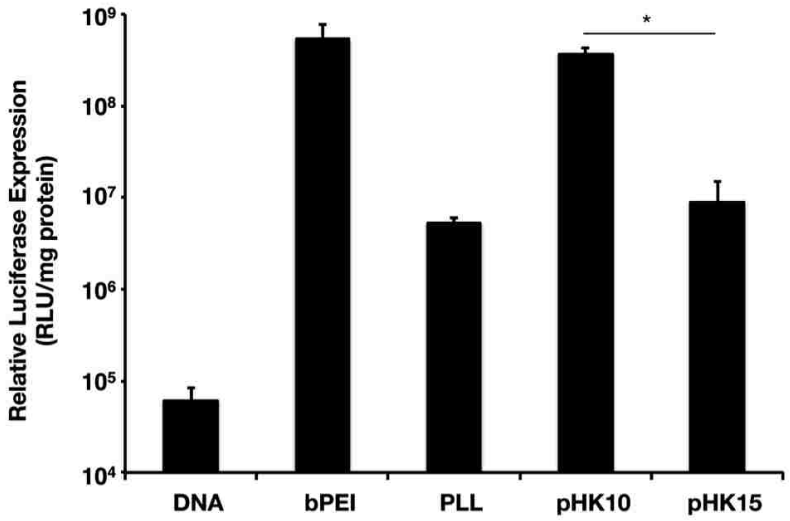

Figure 3.1: **Transfection efficiency of pHK10 and pHK15 polymers in HeLa cells.** HeLa cells were incubated with polyplexes formulated with bPEI, PLL, pHK10, or pHK15 and DNA (1 μg) for 4 h in serum-free conditions, replenished with complete media, and assessed for luciferase activity at 48 h. The data are represented as the mean $\pm$ S.D., $n = 3$. (*) denotes $p < 0.05$, as determined by a two-tailed, unpaired Student's t-test with unequal variance.

in length and 6-30 nm in width (~67% of all measured particles), or toroids, ~21-52 nm in diameter (~33% of all measured particles) (Figure 3.2C). The length of the minor axis decreased with increasing oligolysine length (Figure 3.2D), while the length of the major axis was larger in pHK15 particles than pHK10 (Figure 3.2E). The geometric mean of the aspect ratio, defined as the length of the major axis divided by the length of the minor axis, increased with oligolysine length (Figure 3.2F), and was 2.9, 5.6, and 6.3, for pHK10, pHK15,

and PLL (rods only) particles, respectively. These results somewhat differ from prior measurements of the hydrodynamic particle diameters, which indicated that HPMA-oligolysine copolymers formed slightly larger particles in water (100-150 nm) [10], possibly due to the non-spherical morphology of the lysine-based polymers. Polyplexes of a twisted morphology were also observed with PEGylated PLL dendrimers [17]; however, the researchers note that no distinct relationship between particle morphology and transfection was observed.

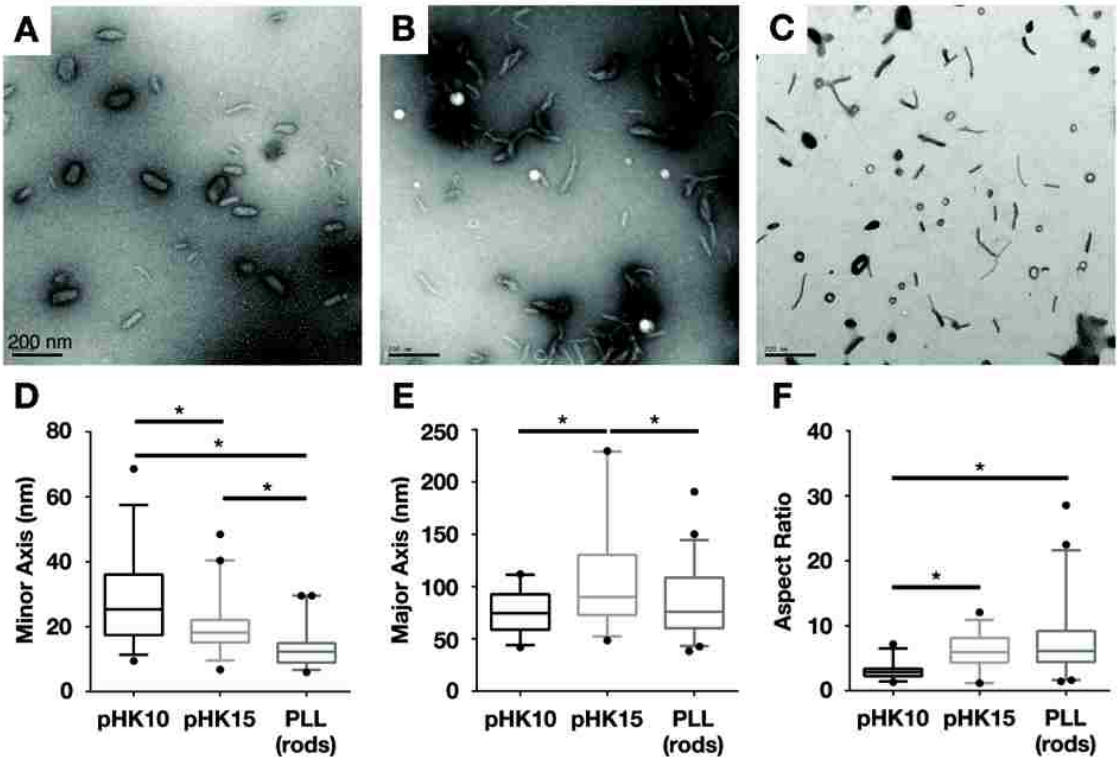

Figure 3.2: **Transmission electron micrographs of lysine-based polymers.** Particle morphology of (A) pHK10, (B) pHK15, and (C) PLL in water. The length of the (D) minor axis and (E) major axis were calculated for $n = 31$ for pHK10, $n = 39$ for pHK15, and $n = 44$ for PLL (rods only). (F) Aspect ratio was calculated by dividing the length of the major axis by the length of the minor axis. The line denotes the mean of each set of values. Statistical significance was determined using a Kruskall-Wallis test, where (*) $p < 0.05$.

3.3.2 Cellular uptake of polyplexes over time

Since particle morphology has been shown to affect the internalization pathway and efficiency of uptake into mammalian cells [5], the kinetics of pHK10, pHK15 and PLL polyplex uptake was determined using polyplexes formulated with radiolabeled plasmid DNA (Figure 3.3). Plasmid DNA was radiolabeled to provide a sensitive and quantitative method for detection. Cells were incubated with polyplexes for 4 h, and then washed and replaced with media for an additional 2, 4, 8, or 20 h. Internalization of polyplex after a 2 h incubation was also measured. After each time point, cells were incubated with CellScrub to reduce extracellularly-bound polyplexes. pHK10 showed the highest cellular association and cellular internalization after both 2 and 4 h compared to pHK15 and PLL. For example, after a 4 h incubation, pHK10 polyplex internalization efficiency was 4.09 ± 0.54%, followed by PLL (1.22 ± 0.33%), pHK15 (0.86 ± 0.04%), and DNA (0.32 ± 0.06%). Interestingly, the amount of internalized DNA continued to increase after polyplex removal at 4 h, suggesting continued internalization of surface-bound complexes not removed by CellScrub. At 24 h, pHK10 showed the highest uptake efficiency (3.73%), followed by PLL (2.19%), pHK15 (0.85%), and DNA (0.20%). A complete breakdown of polyplex distribution (solution, cell-associated, and internalized) is shown in Figure 3.4. The surface charge of particles were also determined by ζ potential measurements since cationic nanoparticles have been shown to bind to mammalian cells through electrostatic interactions. No significant differences were measured in the ζ potential of pHK10 and pHK15 polyplexes (Figure 3.5). Therefore, these results suggest that larger aspect ratios may reduce the rates of cellular internalization despite efficient cellular association.

3.3.3 Role of heparan sulfate proteoglycans on cellular uptake and transfection

Heparan sulfate proteoglycans (HSPGs) have been demonstrated to play an important role in the non-specific uptake and processing of cationic lipids and polyplexes [18–20]. In order to determine if differences in polyplex morphology affect electrostatic interactions with HSPGs, cellular uptake of polyplexes formulated with [^{3}H]DNA was assessed in wild-type Chinese hamster ovary (CHO) cell lines normally expressing HSPGs on their extracellu-

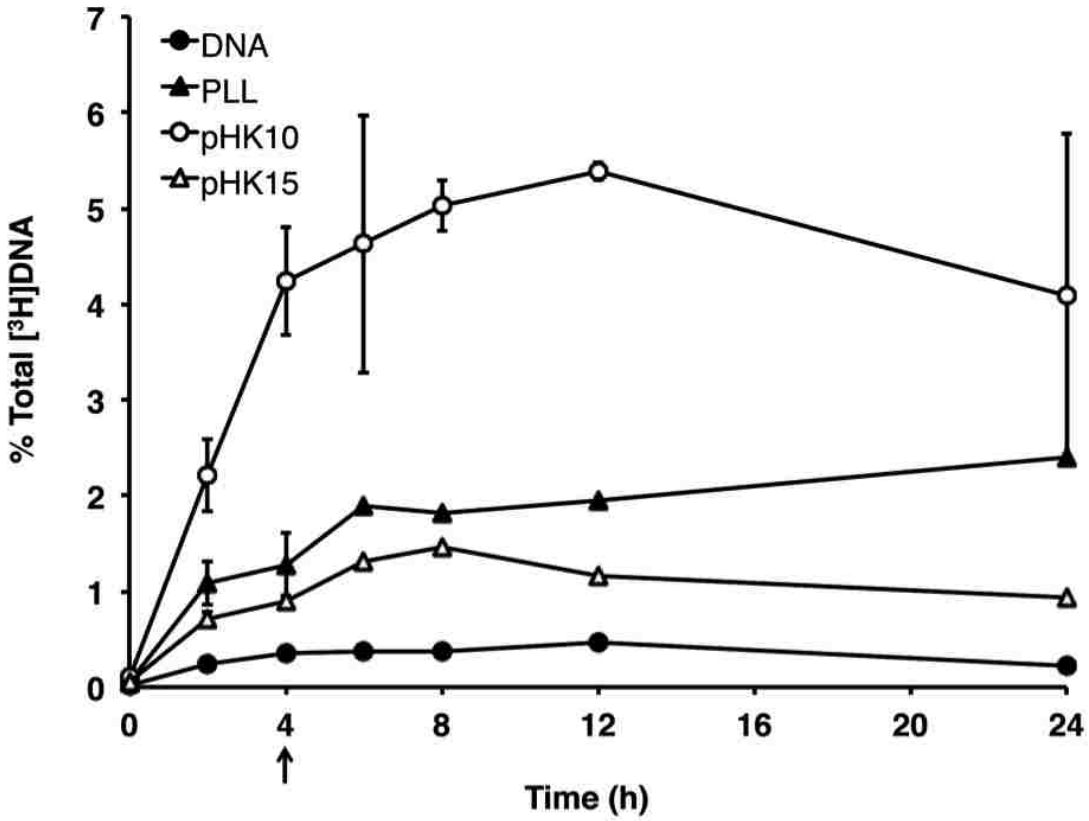

Figure 3.3: **Cellular uptake of [^{3}H]DNA/polymer complexes over time.** HeLa cells were treated with [^{3}H]DNA/polymer complexes (containing 1 μg DNA) for 4 h under serum-free conditions, rinsed, and replaced with complete media for up to an additional 20 h. The amount of internalized DNA as a function of total radioactivity (% total DNA) was determined for DNA alone (closed circles), PLL polyplexes (closed triangles), pHK10 polyplexes (open circles), and pHK15 polyplexes (open triangles). The data are represented as the mean $\pm$ S.D., $n = 3$.

lar surface (CHO-K1) or mutant CHO cells lacking the presence of HSPGs (CHO-pgs-A745) [19]. Surprisingly, polyplex uptake was 20.2% and 45.8% lower in wild-type CHO-K1 compared to CHO-pgs-A745 for pHK10 and pHK15, respectively, although gene expression levels were similar between the two cell lines (Figure 3.6A) in contrast to observations seen with other lysine-based vectors [21, 22]. As observed in Figure 3.1, the transfection efficiency of pHK15 polyplexes was 79-89% lower than that of pHK10 polyplexes in both CHO cell

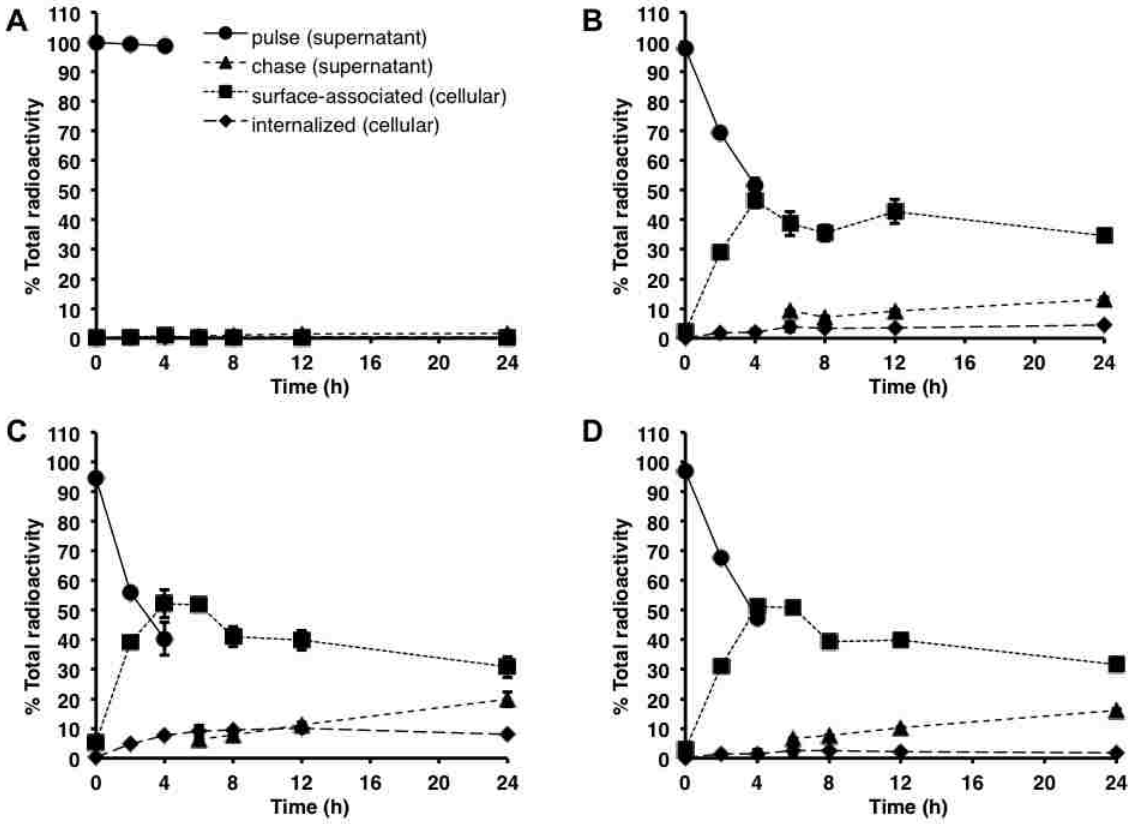

Figure 3.4: **[^{3}H]DNA/polymer complexes in pulse, chase, surface-associated, and internalized fractions over time.** HeLa cells were treated with [^{3}H]DNA/polymer complexes for 4 h in serum-free media, rinsed, and then allowed to incubate for an additional 20 h. In addition to trypsinized cells ("internalized"), the supernatant in both pulse and chase, as well as washes with CellScrub to remove extracellularly-bound polyplexes ("surface-associated"), was collected at various times for (A) DNA, (B) PLL, (C) pHK10, and (D) pHK15. Data are presented as mean ± S.D., $n = 3$.

lines (Figure 3.6B). Interestingly, the decreased cellular uptake of polyplexes in wild-type CHO cells did not translate to decreases in transfection efficiency. Therefore, HSPGs do not play a significant role in internalization of HPMA-*co*-oligolysine-based particles in these cultured cells. Instead, these particles may interact with a currently unknown receptor for cellular uptake.

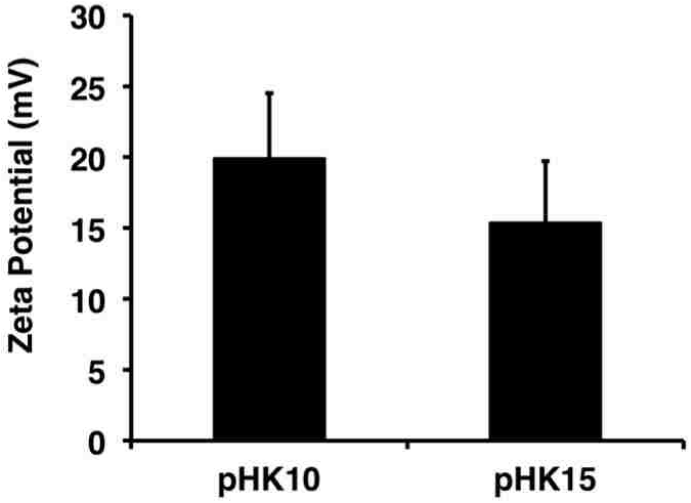

Figure 3.5: **ζ potential of pHK10 and pHK15 polyplexes.** Polyplexes were formulated at N/P 5 with 1 μg of DNA and diluted in 10 mM NaCl. Data are presented as mean $\pm$ S.D., $n = 3$.

3.3.4 In vitro transfection in the presence of endocytic inhibitors

The route of polyplex internalization has been shown to affect subsequent intracellular trafficking and ultimately transgene expression efficiency [23–25]. Therefore, the transfection of pHK10 and pHK15 polyplexes in HeLa cells was determined in the presence of inhibitors for major endocytic pathways for polyplexes [26], namely clathrin-mediated endocytosis (CME), caveolin-mediated endocytosis (CavME), and macropinocytosis. Cells were pretreated with either chlorpromazine, which inhibits CME by dissociating clathrin from the plasma membrane [27], genistein, which inhibits tyrosine-phosphorylation of Cav1 [28, 29], or amiloride, which inhibits Na^+/H^+ ion exchange in the plasma membrane [30], for 1 h prior to transfection and sustained inhibitor treatment during transfection with pHK10 and pHK15 polyplexes. Inhibitor concentrations were optimized using cell viability studies. For both polymers, only transfection in the presence of genistein, but not chlorpromazine or amiloride, affected transgene expression, suggesting that caveolin-mediated endocytosis is the primary internalization route of these particles in HeLa cells. Transfection efficiency was 70-89% lower than cells transfected without inhibitor treatment (Figure 3.7). Similar transfection trends with uptake inhibitors were observed with other HPMA-oligolysine polymers [31]. Since HSPGs have been shown to enter cells *via* a clathrin- and caveolin-independent pathway [32], these results also confirm HSPG-independent internalization.

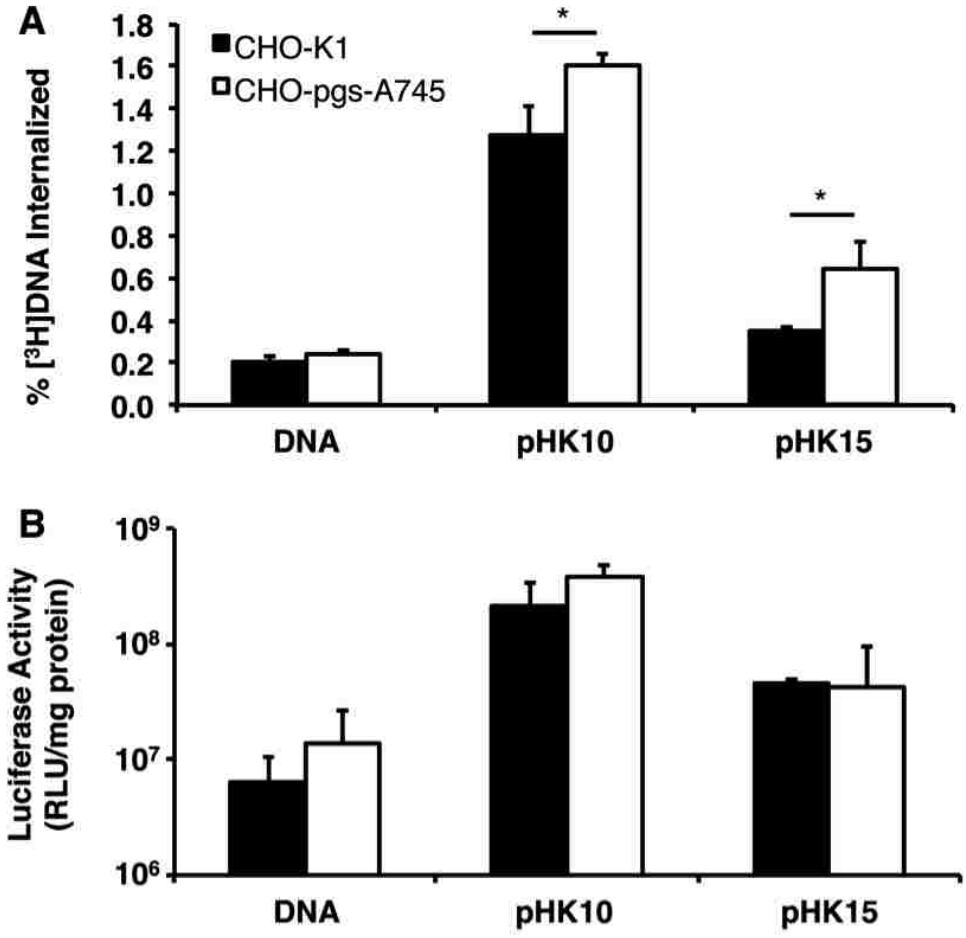

Figure 3.6: **Cellular uptake and transfection efficiency of pHK10 and pHK15 polyplexes in heparan sulfate proteoglycan (HSPG) normal and deficient cells.** (A) Cellular uptake of radiolabeled polyplexes. Cells were incubated with 1 μg of [^{3}H]DNA alone, pHK10/[^{3}H]DNA polyplexes, or pHK15/[^{3}H]DNA polyplexes for 4 h under serum-free conditions. The amount of internalized DNA as a function of total DNA (% [^{3}H]DNA internalized) was determined. (B) Transfection of HSPG normal (CHO-K1) and deficient (CHO-pgs-A745) cells. Cells were transfected with DNA (1 μg) at N/P 5 under serum-free conditions. Data are presented mean $\pm$ S.D., $n = 3$. (*) denotes $p < 0.05$, as determined by a two-tailed, unpaired Student's t-test with unequal variance.

Furthermore, differential internalization mechanisms does not account for the disparities in gene transfer observed between pHK10 and pHK15 materials.

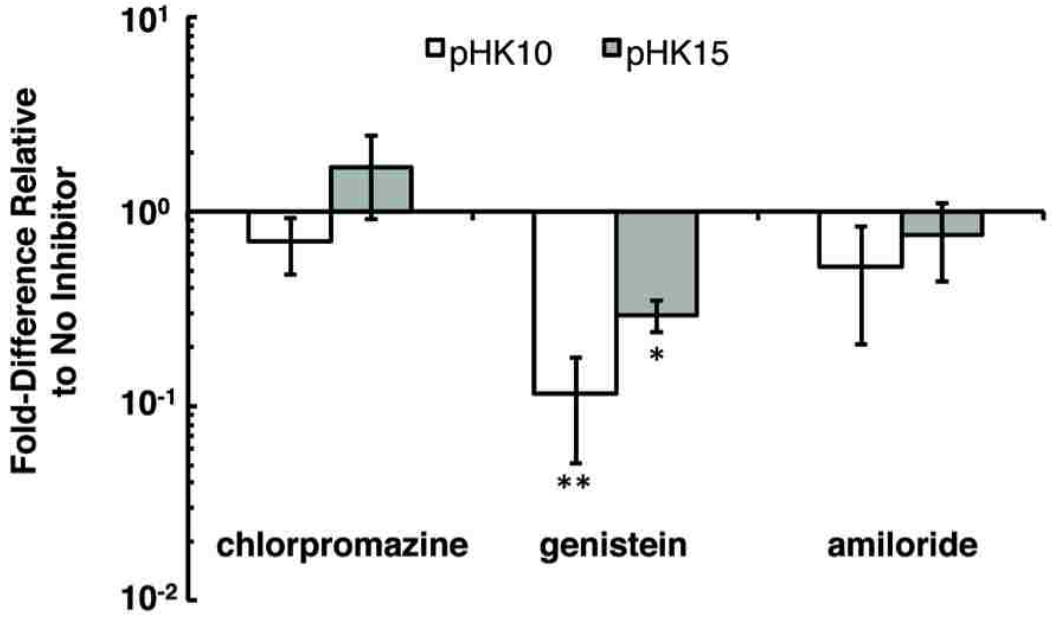

Figure 3.7: **Transfection efficiency of pHK10 and pHK15 polyplexes in HeLa cells in the presence of endocytic inhibitors.** Cells were pre-treated with chlorpromazine, genistein, or amiloride for 1 h prior to the addition of polyplexes formulated with DNA (1 μg) at N/P 5 under serum-free conditions. Data are presented mean ± S.D., $n = 4$. (*) denotes $p \leq 0.05$, (**) denotes $p < 0.1$, as determined by a two-tailed, unpaired Student's t-test with unequal variance.

3.3.5 Intracellular distribution via subcellular fractionation

To gain quantitative insight into the subcellular distribution of pHK10 and pHK15 polyplexes, HeLa cells were treated with polyplexes formulated with [^{3}H]DNA for 4 h, washed with CellScrub to reduce extracellularly-bound material, and subsequently fractionated into nuclear, heavy mitochondrial (HM), light mitochondrial (LM), microsomal (MF), and cytosolic (C) fractions. All media and washes were also collected to calculate a mass balance. Again, similar amounts of both pHK10 and pHK15 were found remaining in the media after incubation (Figure 3.8A). A higher percentage of pHK10/[^{3}H]DNA polyplexes were found internalized rather than surface-bound compared to pHK15/[^{3}H]DNA polyplexes. Interestingly, a higher percentage of pHK10 polyplexes were found in the nuclear fraction (80%) vs. pHK15 polyplexes (65%) (Figure 3.8B). There are several possible explanations

for this observation. Better nuclear delivery of DNA may be achieved using pHK10 polymers. Higher amounts of free DNA in the nucleus has led to higher transgene expression with polyphophoramidate vectors [33]. Enhanced nuclear accumulation may also indicate higher stability of pHK10 polyplexes against DNAse I [34]. Alternatively the high amount of [^{3}H]DNA in the nuclear fraction may be an artifact of degraded plasmid [35] or the presence of cytoplasmic filaments [14, 36]. Slightly more pHK15 polyplexes were also found in the LM and MF fractions, suggesting that pHK15 polyplexes are associated with endosomal and lysosomal compartments more than pHK10 polyplexes (Figure 3.8C) [14], although similar amounts of both formulations were found in the cytosolic fraction. These results may indicate that rod-like morphologies can preferentially accumulate in endosomal/lysosomal compartments and delay nuclear localization. A recent study demonstrated that the display of antibodies on rod-shaped particles resulted in higher cellular uptake, perhaps due to the multivalent interactions of antibodies with receptors on the cell surface [3]. Similarly, rod-like cationic polyplexes may also associate with the lipid membranes of endosomes and lysosomes due to greater surface area of the rod-shaped polyplexes.

3.3.6 Heparan sulfate decomplexation

Premature or delayed intracellular release of DNA can also lead to inefficient gene transfer [37]. Polymers were tested for their ability to release DNA using heparan sulfate for competitive displacement. Polyplex unpackaging was determined by adding various amounts of heparan sulfate with polyplexes formulated at N/P 5. Slight differences in polyplex unpackaging were seen between pHK10 and pHK15 formulations; pHK10 polyplexes were mostly unpackaged by 11 μg heparan sulfate, while pHK15 polyplexes needed at least 14 μg heparan sulfate to show unpackaging (Figure 3.9). However, neither formulation fully unpackaged, as determined by the amount of polyplex still left in the well, at 22 μg heparan sulfate (data not shown), the highest concentration tested. Fluorescence studies using YOYO-1 as a DNA intercalating agent and high NaCl concentrations to facilitate complete unpackaging also demonstrated that pHK10 and pHK15 unpackage DNA to similar extents (data not shown). Therefore, these results suggest that pHK10 and pHK15 polyplexes unpackage

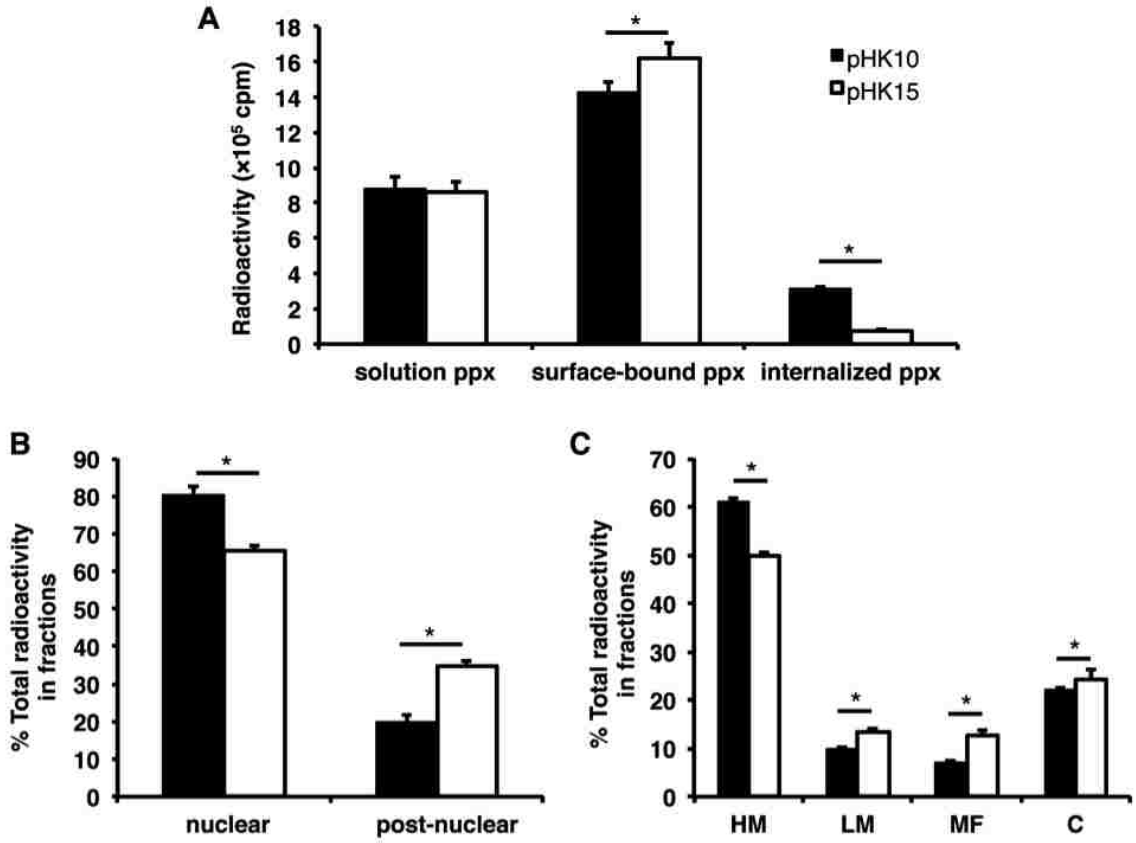

Figure 3.8: **Subcellular distribution of [^{3}H]DNA/polymer complexes in HeLa cells.** HeLa cells (5×10^6) were treated with pHK10 (black bars) or pHK15 (white bars) polyplexes (containing 100 μg DNA) for 4 h prior to being washed with CellScrub to remove extracellularly-bound polyplexes and fractionated into nuclear, heavy mitochondrial (HM), light mitochondrial (LM), microsomal (MF), and cytosolic (C) fractions. (A) The amount of [^{3}H]DNA found in solution (pulse), surface-bound (CellScrub), and internalized (trypsinized cells) fractions, (B) nuclear and post-nuclear fractions, and (C) post-nuclear fractions, composed of HM, LM, MF, C fractions. Data are presented as mean ± S.D., $n = 3$. (*) denotes $p \leq 0.05$, as determined by a two-tailed, unpaired Student's t-test with unequal variance.

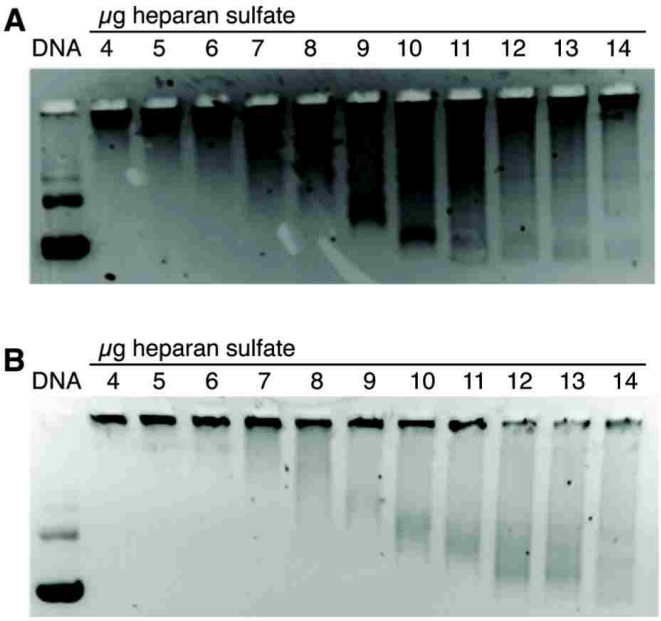

Figure 3.9: **Heparan sulfate decomplexation assay.** Polyplexes with (A) pHK10 and (B) pHK15 (containing 0.5 μg DNA) were treated with 4-14 μg heparan sulfate prior to gel electrophoresis. Free DNA is represented for comparison.

DNA to similar extents.

3.3.7 Intracellular particle trafficking via multiple-particle tracking

Multiple-particle tracking is a useful tool to measure the intracellular trafficking kinetics in live cells [16]. Previous differences in intracellular trafficking kinetics have been observed with the attachment of a targeting moiety [38] or PEG [39], and polyplexes undergoing non-degradative vs. degradative trafficking pathways [40, 41]. To determine if there were differences in intracellular polyplex trafficking between pHK10, pHK15, and PLL, cells were treated with Alexa Fluor 568-labeled polymer/DNA polyplexes for 1 h, rinsed, and then allowed to incubate with polyplexes for an additional 2 h after which 20 s videos of particle movement were captured. The effective diffusivity (D_{eff}) of the ensemble-average mean-squared displacement (MSD) for pHK10 (n = 139 in 5 cells), pHK15 (n = 154 in 5 cells), and PLL (n = 87 in 6 cells) was 4.04×10^{-3}, 6.27×10^{-3}, and 4.28×10^{-3} $\mu m^2/s$, respectively. The MSD for pHK15 was slightly greater than that of pHK10 (Figure 3.10). To further characterize particle transport, particle transport mode (hindered, diffusive, active) was determined by calculating a relative change (RC) value, defined as $D_{eff,probed}/D_{eff,reference}$

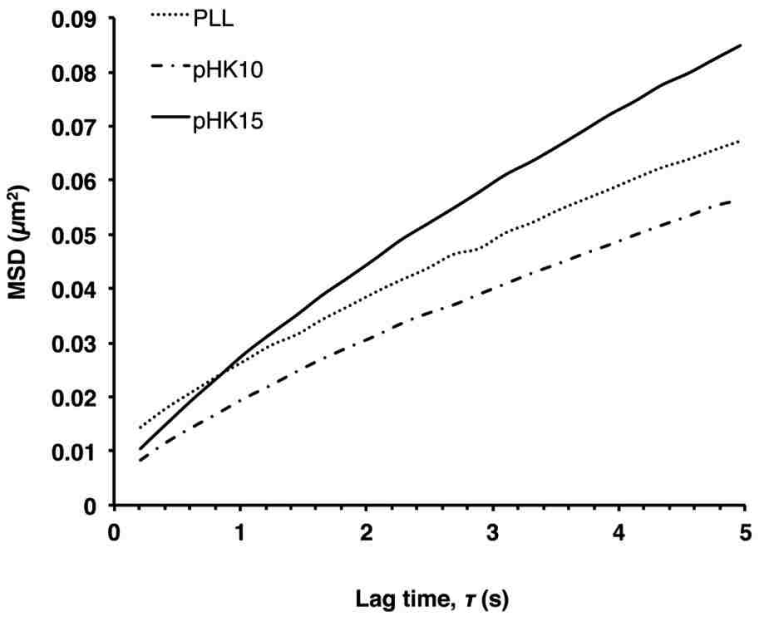

Figure 3.10: **Ensemble-average mean-squared displacement using multiple-particle tracking (MPT).** HeLa cells were incubated with Alexa Fluor 568-labeled polymer/DNA complexes for 1 h in serum-free media, rinsed, and then allowed to incubate in complete media for an additional 2 h. Afterwards, 20 s videos of particle trajectories were captured. Ensemble-average mean-squared displacement of PLL (n = 87 in 6 cells), pHK10 (n = 139 in 5 cells), pHK15 (n = 154 in 5 cells) particles.

(Figure 3.11). The average velocities of actively-transported particles were not statistically significant at long time scales by the Kruskall-Wallis test (geometric mean = 0.0720 μm/s for pHK10 vs. 0.0942 μm/s for pHK15). These results indicate that there are insignificant differences in the intracellular trafficking kinetics for these polymers.

3.4 Conclusions

In summary, HPMA-oligolysine copolymers of different peptide lengths (K_{10} and K_{15}) formed polyplexes that differed in particle morphology, leading to major differences in cellular uptake and transfection efficiency. The presence of HSPGs decreased cellular uptake for both polymer formulations, but did not affect transfection efficiency. Interestingly, pHK15 polyplexes accumulated more in endosomal/lysosomal compartments than pHK10 polyplexes. Furthermore, charge density, unpackaging ability, and intracellular trafficking kinetics did not differ significantly between pHK10 and pHK15. These results suggest that polyplex morphology may play an important role in determining the transfection efficiency

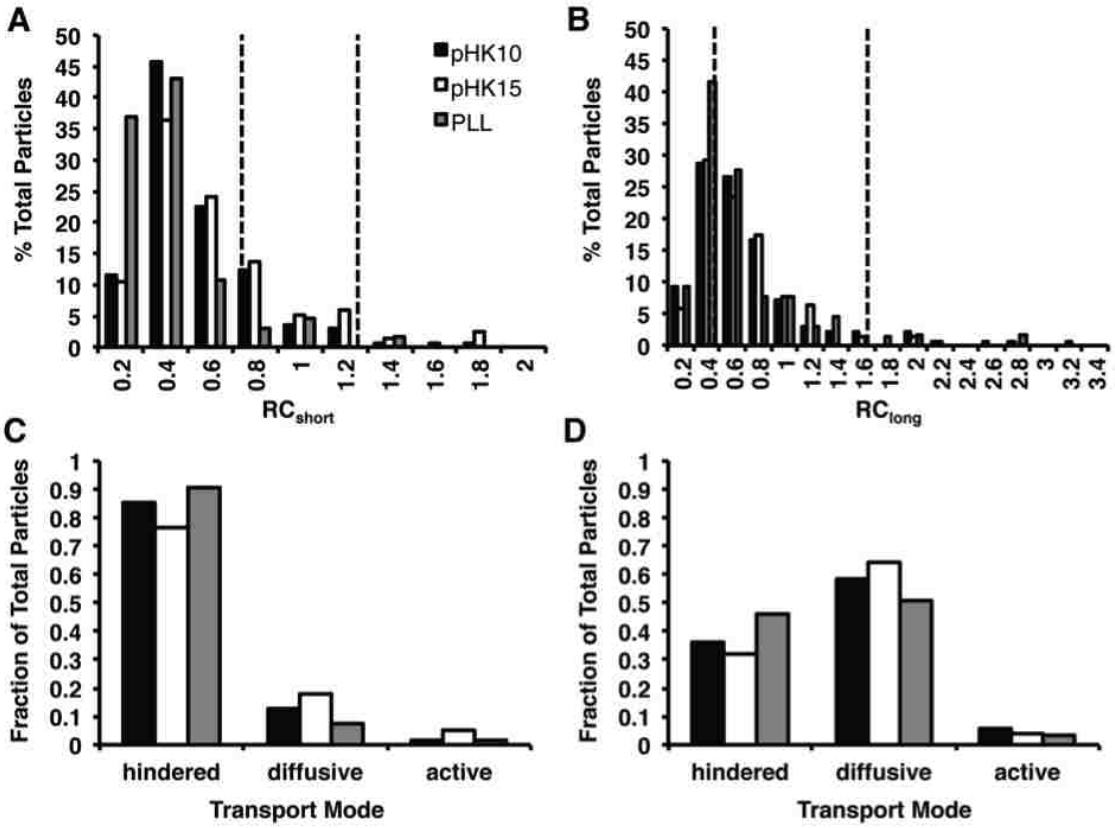

Figure 3.11: **Transport mode of pHK10, pHK15, PLL particles using multiple particle tracking (MPT).** HeLa cells were incubated with Alexa Fluor 568-labeled polymer/DNA complexes for 1 h in serum-free media, rinsed, and then allowed to incubate in complete media for an additional 2 h. Afterwards, 20 s videos of particle trajectories were captured. The relative change (RC) value for polymers calculated at (A) short time scales ($\tau = 0.2$ s) and (B) long time scales ($\tau = 5$ s), where dotted lines mark the bounds of random diffusive motion. The particle tracks were further characterized as hindered, diffusive, or active transport for (C) short and (D) long time scales.

of cationic gene carriers. Therefore, polyplex morphology should be considered when designing polymer structures as well as reproducible formulation conditions.

3.5 Acknowledgments

This work is supported by NIH/NINDS 1R01NS064404 and the Center for the Intracellular Delivery of Biologics through the Washington Life Sciences Discovery Fund Grant

No. 2496490. J.S. is supported by the National Science Foundation Graduate Research Fellowship under Grant No. DGE-0718124 and the Howard Hughes Medical Institute/UW Molecular Medicine Graduate Student Scholarship. J.L.C. and B.C. were supported by the Mary Gates Undergraduate Research Fellowship. We thank Sergio Haro for help on the MATLAB script, Profs. Patrick Stayton and Anthony Convertine (University of Washington) for the generous donation of the ECT reagent, Prof. Shaoyi Jiang (University of Washington) for use of his Malvern Zetasizer, Dr. Joan G. Schellinger and Dr. Russell Johnson for the polymer synthesis, and Dr. Bobbie Schneider (Electron Microscopy Services at the Fred Hutchinson Cancer Research Center) for her help and assistance with TEM imaging.

References

[1] Sahay, G., Alakhova, D. Y., and Kabanov, A. V. (2010) Endocytosis of nanomedicines. *J. Control. Release*, **145**, 182–195.

[2] Duncan, R. and Richardson, S. C. W. (2012) Endocytosis and intracellular trafficking as gateways for nanomedicine delivery: opportunities and challenges. *Mol. Pharm.*, **9**, 2380–2402.

[3] Barua, S., Ramos, J., Potta, T., Taylor, D., Huang, H.-C., Montanez, G., and Rege, K. Discovery of cationic polymers for non-viral gene delivery using combinatorial approaches. *Comb. Chem. High Throughput Screen*, **14**, 908–924.

[4] Gratton, S. E. A., Ropp, P. A., Pohlhaus, P. D., Luft, J. C., Madden, V. J., Napier, M. E., and DeSimone, J. M. (2008) The effect of particle design on cellular internalization pathways. *Proc. Natl. Acad. Sci. U.S.A.*, **105**, 11613–11618.

[5] Herd, H., Daum, N., Jones, A. T., Huwer, H., Ghandehari, H., and Lehr, C.-M. (2013) Nanoparticle geometry and surface orientation influence mode of cellular uptake. *ACS Nano*, **7**, 1961–1973.

[6] Huang, X., Teng, X., Chen, D., Tang, F., and He, J. (2010) The effect of the shape of mesoporous silica nanoparticles on cellular uptake and cell function. *Biomaterials*, **31**, 438–448.

[7] Chithrani, B. D., Ghazani, A. A., and Chan, W. C. W. (2006) Determining the size and shape dependence of gold nanoparticle uptake into mammalian cells. *Nano Lett.*, **6**, 662–668.

[8] Chithrani, B. D. and Chan, W. C. W. (2007) Elucidating the mechanism of cellular uptake and removal of protein-coated gold nanoparticles of different sizes and shapes. *Nano Lett.*, **7**, 1542–1550.

[9] Chaudhuri, P., Harfouche, R., Soni, S., Hentschel, D. M., and Sengupta, S. (2010) Shape effect of carbon nanovectors on angiogenesis. *ACS Nano*, **4**, 574–582.

[10] Johnson, R. N., Chu, D. S. H., Shi, J., Schellinger, J. G., Carlson, P. M., and Pun, S. H. (2011) HPMA-oligolysine copolymers for gene delivery: optimization of peptide length and polymer molecular weight. *J. Control. Release*, **155**, 303–311.

[11] Nayvelt, I., Thomas, T., and Thomas, T. J. (2007) Mechanistic differences in DNA nanoparticle formation in the presence of oligolysines and poly-L-lysine. *Biomacromolecules*, **8**, 477–484.

[12] Mann, A., Richa, R., and Ganguli, M. (2008) DNA condensation by poly-L-lysine at the single molecule level: role of DNA concentration and polymer length. *J. Control. Release*, **125**, 252–262.

[13] Yoo, J.-W., Doshi, N., and Mitragotri, S. (2010) Endocytosis and intracellular distribution of PLGA particles in endothelial cells: effect of particle geometry. *Macromol. Rapid Commun.*, **31**, 142–148.

[14] Shi, J., Chou, B., Choi, J. L., Ta, A. L., and Pun, S. H. (2013) Investigation of polyethylenimine/DNA polyplex transfection to cultured cells using radiolabeling and subcellular fractionation methods. *Mol. Pharm.*, **10**, 2145–2156.

[15] Lai, S. K. and Hanes, J. (2008) Real-time multiple particle tracking of gene nanocarriers in complex biological environments. *Methods Mol. Biol.*, **434**, 81–97.

[16] Kim, A. J. and Hanes, J. (2012) The emergence of multiple particle tracking in intracellular trafficking of nanomedicines. *Biophys. Rev.*, **4**, 83–92.

[17] Männistö, M., Reinisalo, M., Ruponen, M., Honkakoski, P., Tammi, M., and Urtti, A. (2007) Polyplex-mediated gene transfer and cell cycle: effect of carrier on cellular uptake and intracellular kinetics, and significance of glycosaminoglycans. *J. Gene Med.*, **9**, 479–487.

[18] Ruponen, M., Rönkkö, S., Honkakoski, P., Pelkonen, J., Tammi, M., and Urtti, A. (2001) Extracellular glycosaminoglycans modify cellular trafficking of lipoplexes and polyplexes. *J. Biol. Chem.*, **276**, 33875–33880.

[19] Mislick, K. A. and Baldeschwieler, J. D. (2005) Evidence for the role of proteoglycans in cation-mediated gene transfer. *Proc. Natl. Acad. Sci. U.S.A.*, **93**, 12349–12354.

[20] Ziraksaz, Z., Nomani, A., Ruponen, M., Soleimani, M., Tabbakhian, M., and Haririan, I. (2013) Cell-surface glycosaminoglycans inhibit intranuclear uptake but promote post-nuclear processes of polyamidoamine dendrimer-pDNA transfection. *Eur. J. Pharm. Sci.*, **48**, 55–63.

[21] Naik, R. J., Chandra, P., Mann, A., and Ganguli, M. (2011) Exogenous and cell surface glycosaminoglycans alter DNA delivery efficiency of arginine and lysine homopeptides in distinctly different ways. *J. Biol. Chem.*, **286**, 18982–18993.

[22] Åmand, H. L., Rydberg, H. A., Fornander, L. H., Lincoln, P., Nordén, B., and Esbjörner, E. K. (2012) Cell surface binding and uptake of arginine- and lysine-rich penetratin peptides in absence and presence of proteoglycans. *Biochim. Biophys. Acta*, **1818**, 2669–2678.

[23] McLendon, P. M., Fichter, K. M., and Reineke, T. M. (2010) Poly(glycoamidoamine) vehicles promote pDNA uptake through multiple routes and efficient gene expression via caveolae-mediated endocytosis. *Mol. Pharm.*, **7**, 738–750.

[24] Reilly, M. J., Larsen, J. D., and Sullivan, M. O. (2012) Polyplexes traffic through caveolae to the Golgi and endoplasmic reticulum en route to the nucleus. *Mol. Pharm.*, **9**, 1280–1290.

[25] Fichter, K. M., Ingle, N. P., McLendon, P. M., and Reineke, T. M. (2013) Polymeric nucleic acid vehicles exploit active interorganelle trafficking mechanisms. *ACS Nano*, **7**, 347–364.

[26] Vercauteren, D., Rejman, J., Martens, T. F., Demeester, J., De Smedt, S. C., and Braeckmans, K. (2012) On the cellular processing of non-viral nanomedicines for nucleic acid delivery: mechanisms and methods. *J. Control. Release*, **161**, 566–581.

[27] Wang, L. H., Rothberg, K. G., and Anderson, R. G. (1993) Mis-assembly of clathrin lattices on endosomes reveals a regulatory switch for coated pit formation. *J. Cell Biol.*, **123**, 1107–1117.

[28] Akiyama, T., Ishida, J., Nakagawa, S., Ogawara, H., Watanabe, S., Itoh, N., Shibuya, M., and Fukami, Y. (1987) Genistein, a specific inhibitor of tyrosine-specific protein kinases. *J. Biol. Chem.*, **262**, 5592–5595.

[29] Aoki, T., Nomura, R., and Fujimoto, T. (1999) Tyrosine phosphorylation of caveolin-1 in the endothelium. *Exp. Cell Res.*, **253**, 629–636.

[30] Hewlett, L. J., Prescott, A. R., and Watts, C. (1994) The coated pit and macropinocytic pathways serve distinct endosome populations. *J. Cell Biol.*, **124**, 689–703.

[31] Shi, J., Schellinger, J. G., Johnson, R. N., Choi, J. L., Chou, B., Anghel, E. L., and Pun, S. H. (2013) Influence of histidine incorporation on buffer capacity and gene transfection efficiency of HPMA-co-oligolysine brush polymers. *Biomacromolecules*, **14**, 1961–1970.

[32] Payne, C. K., Jones, S. A., Chen, C., and Zhuang, X. (2007) Internalization and trafficking of cell surface proteoglycans and proteoglycan-binding ligands. *Traffic*, **8**, 389–401.

[33] Chen, H. H., Ho, Y.-P., Jiang, X., Mao, H.-Q., Wang, T.-H., and Leong, K. W. (2008) Quantitative comparison of intracellular unpacking kinetics of polyplexes by a model constructed from quantum dot-FRET. *Mol. Ther.*, **16**, 324–332.

[34] Oh, Y.-K., Suh, D., Kim, J. M., Choi, H.-G., Shin, K., and Ko, J. J. (2002) Polyethylenimine-mediated cellular uptake, nucleus trafficking and expression of cytokine plasmid DNA. *Gene Ther.*, **9**, 1627–1632.

[35] Hartig, R., Shoeman, R. L., Janetzko, A., Grüb, S., and Traub, P. (1998) Active nuclear import of single-stranded oligonucleotides and their complexes with non-karyophilic macromolecules. *Biol. Cell*, **90**, 407–426.

[36] Staufenbiel, M. and Deppert, W. (1982) Intermediate filament systems are collapsed onto the nuclear surface after isolation of nuclei from tissue culture cells. *Exp. Cell Res.*, **138**, 207–214.

[37] Grigsby, C. L. and Leong, K. W. (2010) Balancing protection and release of DNA: tools to address a bottleneck of non-viral gene delivery. *J. R. Soc. Interface*, **7 Suppl 1**, S67–82.

[38] de Bruin, K., Ruthardt, N., von Gersdorff, K., Bausinger, R., Wagner, E., Ogris, M., and Bräuchle, C. (2007) Cellular dynamics of EGF receptor-targeted synthetic viruses. *Mol. Ther.*, **15**, 1297–1305.

[39] Suh, J., Choy, K.-L., Lai, S. K., Suk, J. S., Tang, B. C., Prabhu, S., and Hanes, J. (2007) PEGylation of nanoparticles improves their cytoplasmic transport. *Int. J. Nanomedicine*, **2**, 735–741.

[40] Lai, S. K., Hida, K., Chen, C., and Hanes, J. (2008) Characterization of the intracellular dynamics of a non-degradative pathway accessed by polymer nanoparticles. *J. Control. Release*, **125**, 107–111.

[41] Kim, A. J., Boylan, N. J., Suk, J. S., Lai, S. K., and Hanes, J. (2012) Non-degradative intracellular trafficking of highly compacted polymeric DNA nanoparticles. *J. Control. Release*, **158**, 102–107.

Part II

DEVELOPMENT OF PEPTIDE-BASED MATERIALS FOR ENHANCING THE INTRACELLULAR DELIVERY OF NUCLEIC ACIDS

The second section is focused on the development of peptide-functionalized polymers *via* living polymerization techniques for non-viral gene delivery, and the use of phage display technology to identify new ligands for targeting intracellular organelles, in particular the mitochondria. There are four chapters in this section:

- Chapter 4 is a review of the development of peptide-functionalized *N*-(2-hydroxypropyl) methacrylamide (HPMA) brush polymers, and the incorporation of various peptide moieties for nucleic acid condensation, degradability, endosomal escape, and targeting;
- Chapter 5 describes the incorporation of a reducible linker into HPMA-oligolysine brush polymers, and their evaluation for gene delivery;
- Chapter 6 describes the incorporation of an endosomal buffering peptide into HPMA-oligolysine brush polymers in two different polymer architectures, as well as their evaluation for gene delivery;
- and Chapter 7 illustrates the use of phage display technology for identifying potential targeting ligands to mitochondria.

Chapter 4

ENGINEERING BIODEGRADABLE AND MULTIFUNCTIONAL PEPTIDE-BASED POLYMERS FOR GENE DELIVERY

Julie Shi, Joan G. Schellinger, and Suzie H. Pun

Abstract

The complex nature of *in vivo* gene transfer establishes the need for multifunctional delivery vectors capable of meeting these challenges. An additional consideration for clinical translation of synthetic delivery formulations is reproducibility and scale-up of materials. In this review, we summarize our work over the last five years in developing a modular approach for synthesizing peptide-based polymers. In these materials, bioactive peptides that address various barriers to gene delivery are copolymerized with a hydrophilic backbone of *N*-(2-hydroxypropyl)methacrylamide (HPMA) using reversible-addition fragmentation chain-transfer (RAFT) polymerization. We demonstrate that this synthetic approach results in well-defined, narrowly-disperse polymers with controllable composition and molecular weight. To date, we have investigated the effectiveness of various bioactive peptides for DNA condensation, endosomal escape, cell targeting, and degradability on gene transfer, as well as the impact of multivalency and polymer architecture on peptide bioactivity.[1]

[1]Submitted for publication.

4.1 Introduction

Gene therapy has the potential to improve therapeutic outcomes for currently untreatable diseases. Viruses are naturally efficient vectors for gene therapy, but have encountered obstacles in clinical translation due to issues such as vector toxicity and immunogenicity, potential gene integration into oncogenic regions, and high production costs. Thus, nonviral materials, *e.g.* cationic lipids and polymers, have been extensively engineered as alternative gene delivery vectors and are attractive alternatives to viral vectors because they tend to have improved safety profiles and lower costs of production [1]. However, nonviral vectors have not been as successful in attaining high transgene expression efficiencies *in vivo*. In order to enhance the gene transfer efficiency of these materials, several groups have explored the use of bioactive peptides to address various extracellular and intracellular barriers to nonviral gene delivery, such as cellular uptake, endosomal escape, cargo unpackaging, and nuclear translocation [2–5]. These multicomponent synthetic materials have been engineered to overcome these barriers for various applications [6], including delivery to neurons [7] and hepatocytes [8].

Recent advances in living polymerization techniques, such as reversible-addition fragmentation chain transfer (RAFT), have allowed the development of well-defined polymers with controlled architectures and quantitative monomer incorporation [9–11]. Peptide-polymer conjugates containing multiple peptides can be synthesized by grafting peptides to preformed polymers or by polymerization of peptide monomers. The grafting technique has been extensively reviewed elsewhere [12–14]. The Klok group demonstrated the synthesis of peptide brush copolymers by RAFT polymerization of coiled coil peptide motifs in 2010 [15].

In this review, we summarize the work in the development of copolymers consisting of *N*-(2-hydroxypropyl)methacrylamide (HPMA) and multiple pendant oligopeptides for gene delivery (Figure 4.1). Cationic peptide moieties were explored and optimized for DNA condensation. To improve biodegradability, environmentally-responsive linkers were incorporated into the HPMA copolymers. In addition, both buffering and membrane-disruptive peptides were evaluated for enhancing endosomal escape of the polyplexes. Throughout

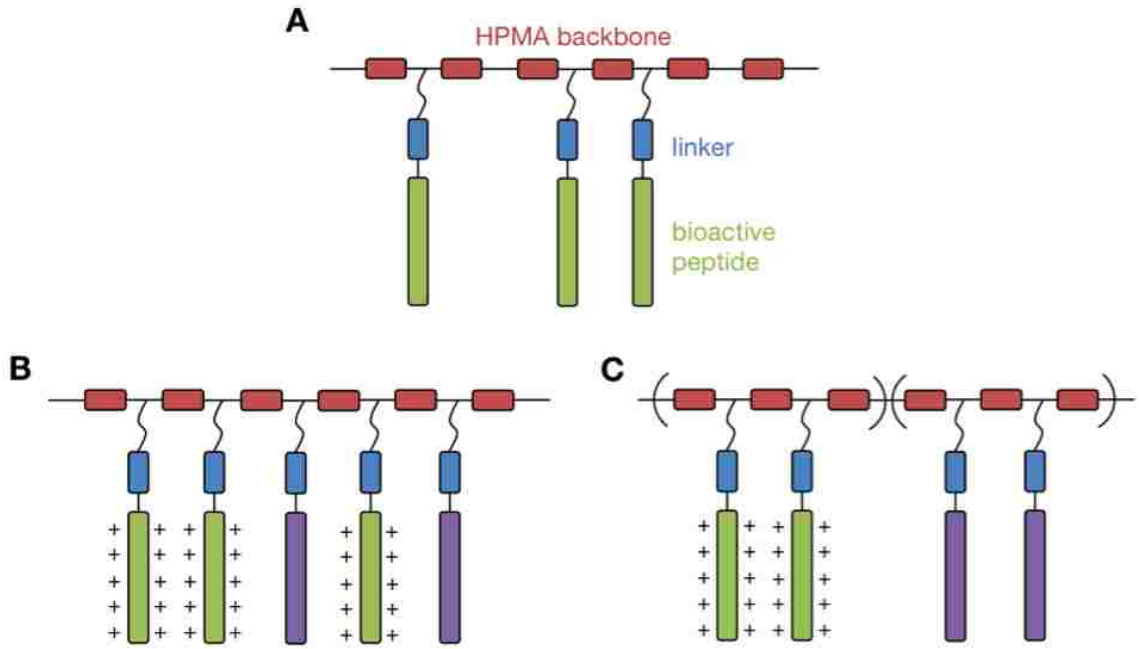

Figure 4.1: **Schematic of peptide-functionalized HPMA copolymers.** (A) Random-statistical copolymers of HPMA (red) and pendant bioactive peptides (green) with a linker (blue) between the hydrophilic backbone and the main peptide sequence. (B) Random-statistical copolymers of HPMA and multiple pendant peptides (cationic peptide in green; second bioactive peptide in purple). (C) Diblock copolymer of HPMA and multiple pendant peptides, where the cationic peptide is on one block, and a second bioactive peptide on a different block.

our work, we have also noted effects of polymer architecture and multivalency on transfection efficiency. Finally, we conclude with some therapeutic applications of this class of peptide-functionalized brush polymers that we have investigated.

4.2 Nucleic acid condensation using basic peptides

Cationic vectors can be used to form electrostatic complexes with anionic nucleic acid, termed "polyplexes", to protect the nucleic acid from serum and intracellular proteases. Early studies demonstrated the use of poly-L-lysine as a transfection agent to deliver plasmid DNA to achieve exogeneous protein expression [16]. Further work was conducted to optimize the oligolysine and polylysine residues for enhanced gene transfer, as well as introduce salt-

and serum-stability into these carriers [17]. Since then, a number of cationic polymers have been developed for gene delivery applications [1, 18]. In 1997, O'Brien-Simpson and coworkers reported a general method for the assembly of multi-peptide polymer constructs using acryloyl peptides by radical polymerization for vaccine development [19]. Thus, we hypothesized that this polymer architecture would enable a high incorporation of peptide moieties for the development of gene delivery vectors.

As a starting point, HPMA was chosen to compose the hydrophilic backbone. HPMA has been widely used for the synthesis of polymer-drug conjugates due to its biocompatibility, as well as its synthetic versatility and flexibility [20]. Therefore, we copolymerized short pendant oligolysine peptides with HPMA in a random-statistical brush polymer architecture using both free radical and RAFT polymerization approaches (Figure 4.2) [21, 22]. Polymers synthesized by RAFT polymerization exhibited more narrow polydispersity and better control over final polymer composition [23]. We next optimized the peptide length and molecular weight of these statistical polymers generated by RAFT polymerization, and found a peptide length of ten lysines, a composition of 5 mmol lysine per gram polymer, and a molecular weight of ~60 kDa was optimal for high transfection efficiencies (comparable to that of bPEI) and limited cytotoxicity [23]. Surprisingly, a 50% longer oligolysine peptide (K_{15}) demonstrated poor transfection efficiencies despite similar lysine composition and molecular weight. Extensive studies on the mechanism of enhanced transfection of the optimized polymer (p[HPMA-*co*-K_{10}]) over the poorly-performing polymer (p[HPMA-*co*-K_{15}]) showed that polyplexes of larger aspect ratios (more rod-like) greatly reduced cellular uptake and subsequent transfection efficiency [24]. Previous studies have reported that polylysine length correlates to the aspect ratio of the lysine/DNA complexes, thus highlighting the importance of understanding the biophysical interaction of plasmid DNA with various cationic moieties. In order to reduce cytotoxicity, we explored reducing charge density by alternating lysine residues with glycine spacers (p[HPMA-*co*-$(GK)_5$]). Interestingly, these polymers resulted in similar transfection efficiency compared with its pentamer counterpart (p[HPMA-*co*-K_5]) but actually demonstrated increased cytotoxicity [25].

Arginine is another cationic amino acid residue that has been explored as a complexation agent. The ability of arginine to exhibit cell-penetrating capabilities has allowed for

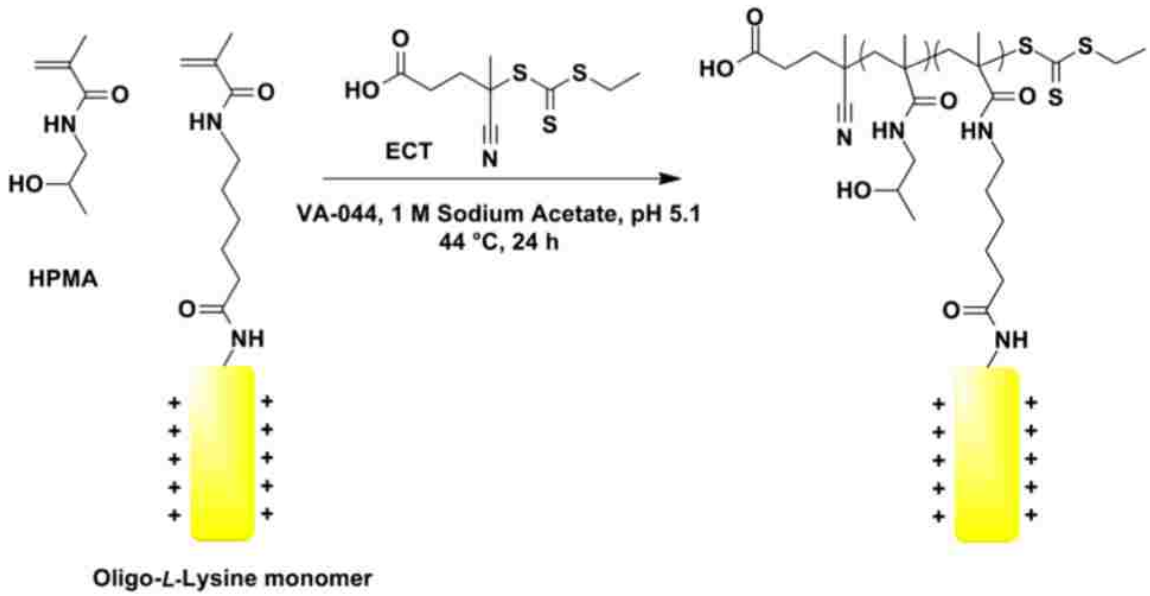

Figure 4.2: **Synthesis of statistical HPMA-oligolysine copolymers by RAFT polymerization.** HPMA and methacrylamido-functionalized oligolysine peptides are copolymerized under aqueous RAFT conditions using ethyl cyanovaleric trithiocarbonate (ECT) as the chain transfer agent (*CTA*) [26] and VA-044 as the initiator. The 6-carbon aminohexanoic acid (Ahx) is used as a linker between the pendant oligolysine peptide and the hydrophilic backbone.

enhanced cellular uptake [27]. Cell-penetrating peptides (CPP) such as the TAT protein transduction domain contain a number of arginine residues [28, 29]. Harashima and coworkers demonstrated that liposomes modified with an increasing density of octaarginine (R_8) peptides were taken up *via* macropinocytosis rather than clathrin-mediated endocytosis [30]. Therefore, arginine oligopeptides were also used as the complexation moiety in statistical HPMA brush polymers [25]. Similarly to previous reports comparing arginine motifs with lysine motifs [31–34], HPMA-oligoarginine polymers performed better in transfection efficiency when compared to a lysine analogue (~5-10 mmol lysine or arginine per gram polymer) but also caused increased cytotoxicity. Furthermore, due to challenges in synthesizing oligoarginine residues, guanidinylation of the lysine resides with *O*-methylisourea was also explored; guanidinylation has been shown to increase transfection efficiencies of various carriers [35–38] and cellular uptake of HPMA constructs [39]. Conversion of the lysine residues in HPMA-oligolysine polymers to homoarginines resulted in higher transfection efficiencies and lower cytotoxicity than branched PEI. Therefore, this method could be readily applied to other primary amine-based polymers to increase gene transfer efficiencies.

4.3 Degradability using environmentally-responsive elements

Biodegradability is a desirable attribute for the *in vivo* application of gene delivery vectors. Since higher polycation molecular weights can lead to increased toxicity [23, 40–42], linker chemistries have been used to introduce degradability into polymeric vectors. For example, environmentally-responsive linkages such as disulfide and acid-labile bonds can enable the release of cargo in specific intracellular compartments and promote degradability [43]. Likewise, specific amino acid sequences can be enzymatically degraded by various proteases [44–46]. We have explored both of these strategies for introducing a degradable segment into these HPMA-oligolysine polymers. Due to the relatively high levels of glutathione, a reducing agent, in the cytosolic environment compared to the extracellular space [47], the incorporation of disulfide linkages into polymeric carriers has been an attractive approach to increase biodegradability. To introduce reducibility, the six-carbon linker 6-aminohexanoic acid (Ahx) was exchanged with a linker containing a disulfide bond, 3-[(2-aminoethyl)dithio] propionic acid (Aedp) [48]. These reducible polymers were less cy-

totoxic, but achieved less efficient transfection efficiencies compared to the non-reducible analogue. However, a mixed formulation of reducible and non-reducible polymers achieved an intermediate level of transfection efficiency and reduced cytotoxicity. The high concentration of disulfide bonds within the polymer may lead to chemical instability, which was evidenced by partial improvement in transfection efficiency in the presence of EDTA to minimize metal-catalyzed redox/oxidation reactions.

As an alternative approach to enhancing degradability, we explored the use of enzymatically-cleavable peptide linkers, which have been used to introduce site-specific cleavage sites for the release of drugs and peptides [49–51]. A commonly used peptide linker sequence is cathepsin B-labile [12, 52]; cathepsin B is a lysosomal cysteine protease that exhibits endo- and exopeptidase activity [53]. We designed a cathepsin B-labile peptides sequence as a four amino acid sequence (FKFL), flanked by 6-carbon spacers (Ahx), and introduced the linker onto the N-terminus of the oligolysine motif between the HPMA backbone and the pendant cationic peptide [54]. The peptides demonstrated site-specific cleavage by cathepsin B within 15 minutes, while the polymers showed complete degradation of the pendant modified oligolysine motifs within 1 hour. In contrast to the reducible polymers in which transfection efficiencies were lower with polymers containing reducible linkers, the cathepsin B-labile polymers showed similar levels of transfection and were less toxic compared to a non-degradable analogue consisting of nondegradable D-amino acids. Therefore, this work demonstrates the possibility of using enzymatically-cleavable linkers to enable site-specific release and degradability for polyplex formulations.

4.4 Endosomal escape strategies

Once internalized, polyplexes are exposed to increasingly acidic environments in endosomes and lysosomes, and eventually are degraded by lysosomal proteases. To circumvent lysosomal degradation, various strategies have been investigated to induce endosomal escape, such as the incorporation of peptide moieties that enable proton buffering [55] or interaction with lipid membranes [56]. Virally-derived peptides, such as TAT, Antennapedia (Antp), and HGP, and membrane-disruptive peptides, such as melittin, have been used to increased delivery efficiencies of cargo due to their ability to interact with lipid membranes [3]. We

have used both of these approaches to enhance the endosomal escape abilities of our HPMA-oligolysine brush polymers, with varying success [57–59].

As a first approach, we drew inspiration from bPEI, which is commonly used as a transfection agent due to its ability to induce endosomal escape *via* the buffering of protons at pH ~6-7 [60, 61]. Several groups have mimicked this buffering strategy by incorporating histidine residues, which contain a protonable imidazole group at pH 6-7, into various gene carriers [55]. The addition of a second oligohistidine-containing peptide into statistical HPMA-oligolysine polymers demonstrated increased transfection efficiencies [22]. To further optimize the incorporation of oligohistidine peptides to increase transfection, statistical and diblock polymers were synthesized with varying incorporations of oligohistidine residues ranging in oligohistidine peptide incorporation (Figure 4.3) [57]. Interestingly, the polymer architecture affected the buffering range of the polymer in that diblock polymers buffered in the upper endosomal pH range (pH 5.6-7.4) whereas statistical polymers buffered in the lower endosomal pH range (pH 5.1-6.6). Despite improved buffering capabilities, only the statistical polymer containing 1.4 mmol histidine per gram polymer showed slight improvements in transfection ability over its non-histidylated analogue, possibly due to preferentially trafficking of the polyplexes through the non-acidifying caveolae-mediated endocytic pathway [62]. Furthermore, endosomal buffering requires a critical concentration threshold to be a viable strategy for endosomal escape, and thus, the use of more potent strategies may be beneficial.

Hydrophobic modification of polycationic polymers is another strategy for promoting endosomal escape. Xu and Szoka proposed that upon endocytosis, lipid-modified polycation/DNA complexes form ion pairs with the negatively-charged amphiphilic endosomal membrane, resulting in membrane destabilization and release of cargo [63]. Furthermore, incorporation of hydrophobic moieties allows for physical encapsulation of the genetic payload, enhanced serum stability, increased cell viability, and targeting ability [64]. Several reviews have been published regarding the advantages of lipid or hydrophobic modification of polycationic gene carriers [65, 66]. Previously, Abassi *et al.* reported various lipid-substituted polylysines as vectors for plasmid delivery and expression in skin fibroblasts. They showed that while all modified and unmodified polylysines demonstrated complete

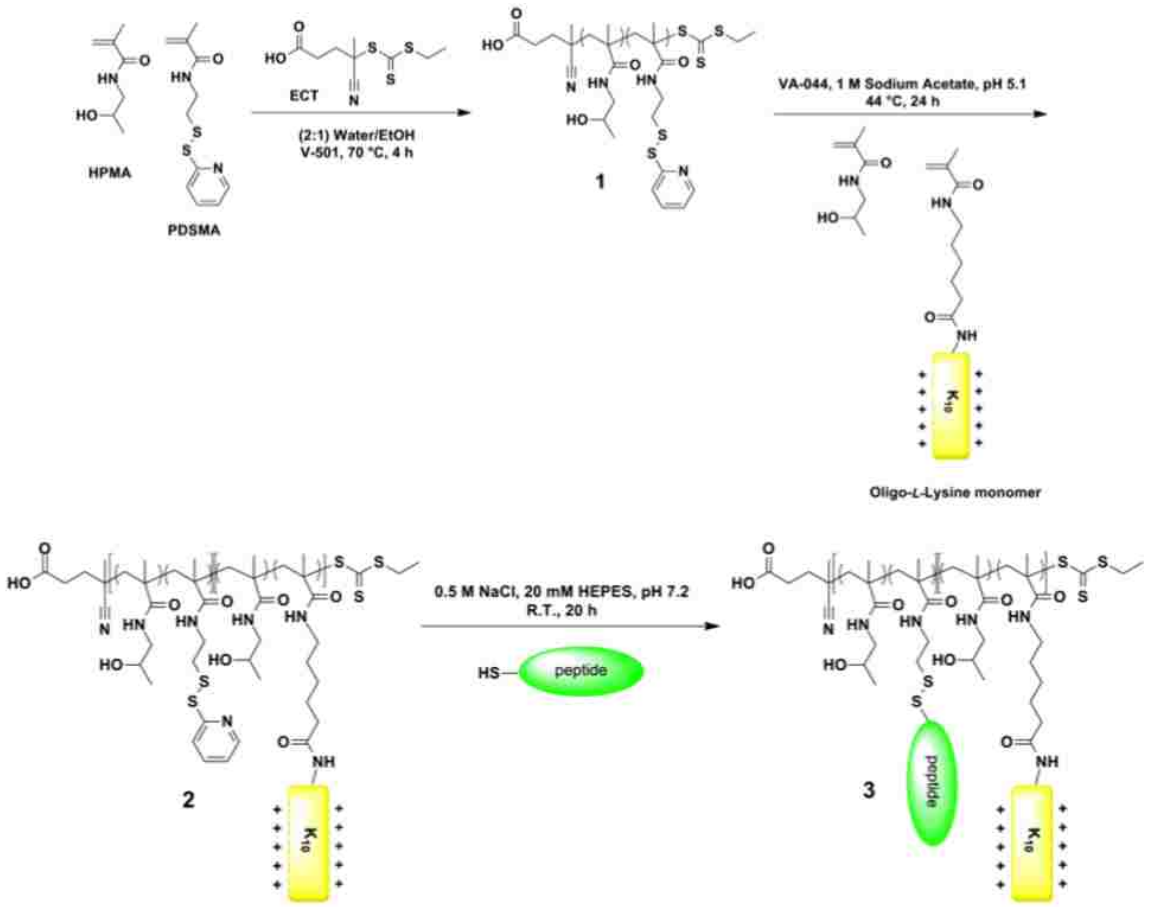

Figure 4.3: **Synthesis of diblock HPMA copolymers containing multiple pendant peptides.** RAFT polymerization of HPMA and PDSMA (molecule **1**), and then chain-extension with HPMA and oligo(L-lysine) to form the second block (molecule **2**). Disulfide exchange between the pyridyl disulfide on **2** and a cysteine-functionalized peptide yields a diblock polymer with two bioactive peptides (molecule **3**).

complexation with plasmid DNA, polymers with increased lipid substitution were more resistant to unpackaging with heparin treatment. Furthermore, most lipid-modified polymers exhibited increased pEGFP expression compared to native polylysine, with myristic and stearic acid lipid substituents demonstrating less cytotoxicity [67]. Inspired by this work, we prepared a panel of stearic acid-modified copolymers of HPMA and oligolysine. We grafted NHS-activated stearic acid (SA) onto the ϵ-amine of the lysine moiety of the previously optimized p[HPMA-*co*-K_{10}] copolymers at DP 190. The lipid substituent was grafted at various lipid to lysine ratios for optimization (Table 4.1). We then evaluated the polymers for gene transfection. There was no significant increase in gene transfection with these lipid-modified copolymers *in vitro* (Figure 4.4A); increasing lipid substitution also decreased transfection efficiency (Figure 4.4B). Interestingly, high lipid substitution showed decreased cytotoxicity. Thus, for these HPMA-oligolysine polymers, lipid substitution is not a viable method for increasing transfection efficiency.

Table 4.1: Characterization of lipid substitution on p[HPMA-*co*-K_{10}] copolymers

Polymer designation	Lys:Lipid molar ratio	Lipid/HPMA[a]	% Substituted Lys[b]
p[HPMA-*co*-K_{10}-*g*-SA] (10:1)	10:1	0.35	14
p[HPMA-*co*-K_{10}-*g*-SA] (20:1)	20:1	0.21	8.4
p[HPMA-*co*-K_{10}-*g*-SA] (40:1)	40:1	0.12	4.8

[a]Based on NMR integration of lipid -CH_2-CO (∼2.4 ppm) and HPMA -CH(OH)-CH_3 (∼3.7 ppm).
[b]Based on the theoretical mole ratio (∼20% AhxK_{10} and 80% HPMA): 2.5 mole Lys/1 mole HPMA.

Alternatively, membrane-active peptides have been promising for inducing endosomal escape due to their high disruptive potency [56]. We have investigated the use of melittin, a 26-mer derived from venom of the honey bee *Apis mellifera* [58], and sHGP, a shortened and optimized 15-mer peptide derived from the endodomain of the HIV gp41 region [59]. Melittin undergoes an α-helical conformational change at lipid membranes, allowing the peptide to insert into the membrane and induce pore formation [68, 69]. Polymeric carriers conjugated with melittin showed significantly increased transfection *in vitro* and *in vivo*

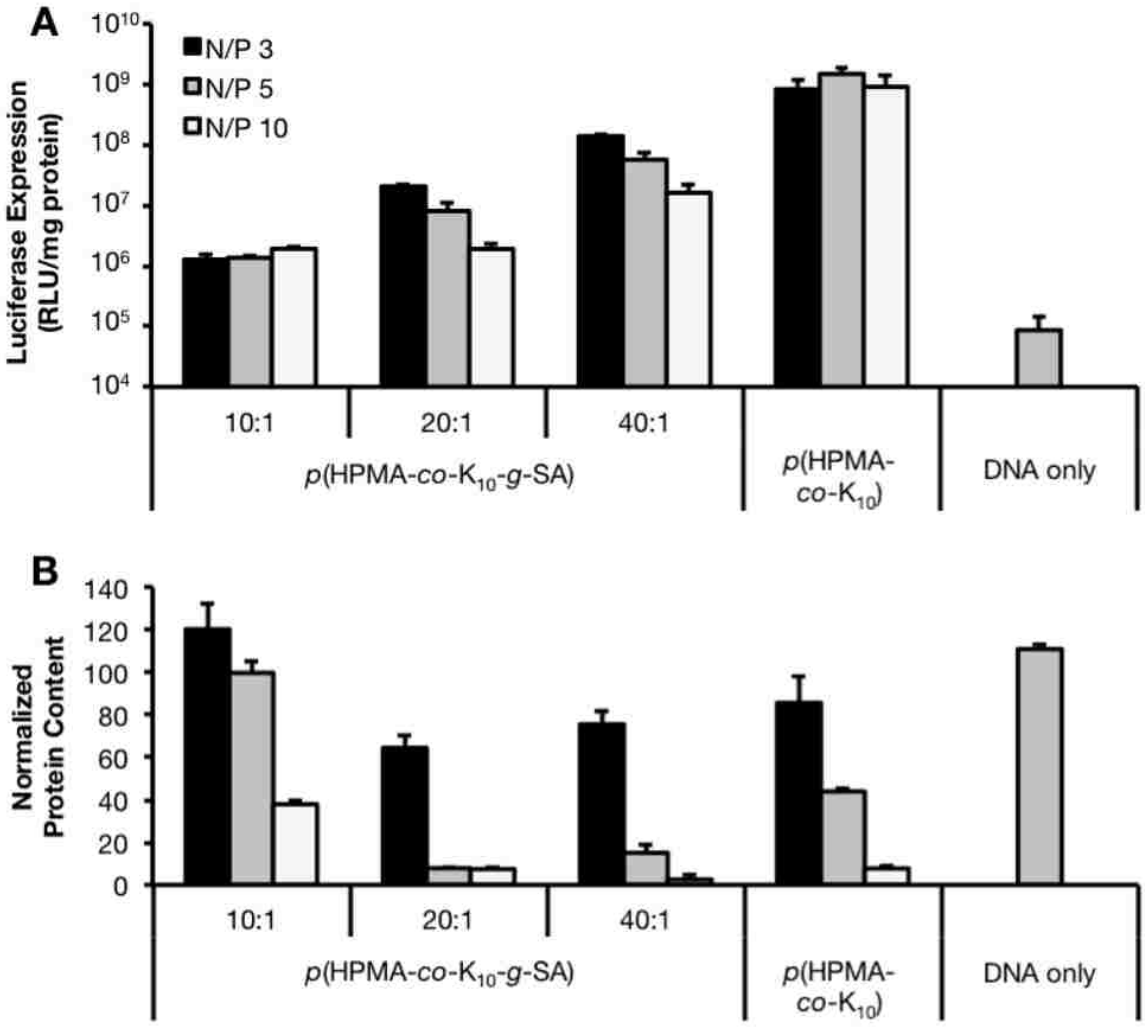

Figure 4.4: **Transfection of stearic acid (SA)-modified p[HPMA-*co*-K_{10}] polyplexes in HeLa cells.** HeLa cells were treated with polyplexes (containing 1 μg plasmid DNA) at charge ratios (N/P) of 3, 5, and 10 for 4 h in serum-free conditions, washed, and replenished with complete media. At 48 h post-transfection, cell lysates were assessed for (A) luciferase reporter gene expression and (B) protein content as an indicator for cytotoxicity. Data are presented as the mean ± S.D., $n = 3$.

[58, 70, 71]. Similarly to the HPMA-oligolysine-oligohistidine diblock copolymer, melittin was grafted onto a diblock of p[HPMA-*co*-PDSMA]-*b*-[HPMA-*co*-K_{10}], using PDSMA as the point of conjugation [58]. Incorporation of melittin into these brush polymers displayed hemolytic ability and significantly improved transfection efficiency over the base polymer, but also increased toxicity. To ameliorate some cytotoxicity, mixed formulations of the base polymer and the melittin-containing polymer were used for transfection and showed markedly improved toxicity profiles and even further improved transfection efficiencies to greater than that of branched PEI.

The incorporation of sHGP also helped increase the transfection efficiency of HPMA-oligolysine polymers [59]. sHGP was incorporated into HPMA-oligolysine polymers in a diblock architecture, similarly to melittin and the diblock oligohistidine-containing polymer, as well as a statistical architecture. Both polymer architectures demonstrated improved transfection efficiency compared to the base HPMA-oligolysine polymer, but the diblock polymer self-assembled into micelles, thereby sequestering the hydrophobic, membrane-lytic sHGP region. Interestingly, the diblock architecture resulted in less hemolytic activity and improved cytotoxicity profiles. Thus, these results suggest that the exposure of hemolytic regions under certain environmental conditions can lead to more efficient yet less toxic vectors. This strategy has previously been used in the design of synthetic polymers for siRNA delivery, where the exposure of a hydrophobic lytic domain occured under endosomal pH to facilitate cargo release into the cytosol [26]. To compare these different endosomal escape strategies, cells were transfected with p[HPMA-*co*-K_{10}] containing either oligohistidine, melittin, or sHGP peptides (Figure 4.5). All polymers that contained endosomal escape modalities performed better than the base polymer containing only oligolysine peptides. The statistical polymer containing oligohistidine peptides and the block polymer containing sHGP performed the best; however, the block sHGP polymer was the least toxic overall.

4.5 Delivery mechanisms of HPMA-peptide polymers

Salt stability is necessary for the systemic administration of polyplexes since polyplex aggregation can lead to *in vivo* toxicity [72]. The incorporation of HPMA as a hydrophilic

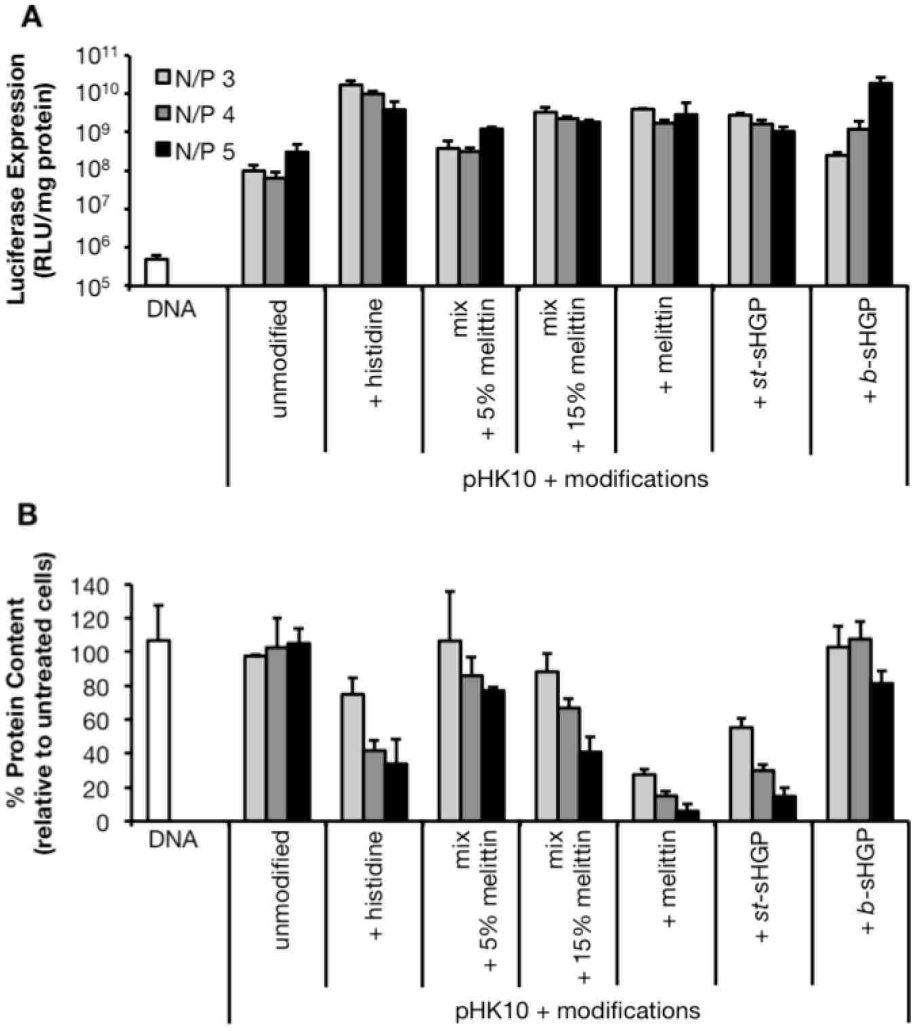

Figure 4.5: **Comparative transfection of *p*[HPMA-*co*-K_{10}] polymers ("pHK10") modified with various endosomal escape modalities in HeLa cells.** HeLa cells (3×10^4) were treated with polyplexes (containing 1 μg plasmid DNA) at charge ratios (N/P) of 3, 4, and 5 for 4 h in serum-free conditions, washed, and replenished with complete media. At 48 h post-transfection, cell lysates were assessed for (A) luciferase reporter gene expression and (B) protein content as an indicator for cytotoxicity. *pHK10 unmodified*: *p*[HPMA-*co*-K_{10}]; *pHK10 + histidine*: *p*[HPMA-*co*-K_{10}-*co*-K_5H_5] [57]; *pHK10 mix + 5% melittin*: a mixture of 95:5% (v/v) *p*[HPMA-*co*-K_{10}]:*p*[HPMA-*co*-melittin]-*b*-[HPMA-*co*-K_{10}] [58]; *pHK10 mix + 15% melittin*: a mixture of 85:15% (v/v) *p*[HPMA-*co*-K_{10}]:*p*[HPMA-*co*-melittin]-*b*-[HPMA-*co*-K_{10}]; *pHK10 + melittin*: *p*[HPMA-*co*-melittin]-*b*-[HPMA-*co*-K_{10}]; *pHK10 + st-sHGP*: *p*[HPMA-*co*-K_{10}-*co*-sHGP]; *pHK10 + b-sHGP*: *p*[HPMA-*co*-sHGP]-*b*-[HPMA-*co*-K_{10}]. Data are presented as the mean ± S.D., $n = 3$.

segment has reduced the salt-induced aggregation of multiple polymeric gene delivery systems [73–75]. We have also demonstrated increased salt stability of HPMA-oligolysine polyplexes when compared to lysine peptides or polylysine polyplexes [21–23]. In our optimization studies, salt stability decreased with increasing peptide incorporation [21, 22], larger polymer molecular weights, and longer oligolysine peptide lengths [23]. In particular, the latter trend was unexpected since polymers containing longer oligolysine peptides also had longer HPMA segments in the polymer backbone. The incorporation of a hydrophilic HPMA shell onto poly(glycidyl methacrylate-tetraethylenepentamine) (p[GMA-TEPA]) also reduced salt-induced aggregation of the polyplexes; in this case, longer hydrophilic segments further enhanced polyplex stability in physiological salt conditions [76]. As seen with polymers containing poly(ethylene glycol) (PEG) as a salt stabilizer [77], polymers containing the HPMA shell also demonstrated decreased *in vitro* transfection efficiencies. These results highlight the tradeoffs of incorporating hydrophilic segments into polymers for enhanced gene delivery *in vivo*.

In order to develop improved materials for nucleic acid delivery, it is important to understand the delivery mechanisms of engineered materials. To further characterize the HPMA-oligolysine polymers, we first determined the uptake efficiency of the optimized oligolysine-containing polymer (p[HPMA-*co*-K_{10}]) [24]. Despite much lower polyplex uptake efficiencies of the optimized polymer (p[HPMA-*co*-K_{10}]) *vs.* bPEI [78], the HPMA-oligolysine polymer achieved similar transfection efficiencies to that of bPEI [23]. Since alternative uptake routes have been implicated in improving polyplex transfection [62], transfection of the HPMA-oligolysine copolymers was also completed with the presence of various endocytic inhibitors [24, 57]. Transfection efficiencies were decreased in the presence of a small-molecule inhibitor for caveolae-mediated endocytosis, a pathway that circumvents the acidification process necessary for endosomal buffering. These results suggest that transfection may be more productive when HPMA-oligolysine polyplexes are routed *via* a non-acidifying endocytic route, similarly to other polycation systems [63, 79, 80]. Therefore, understanding the uptake pathway of various polymer formulations can aid in the rational design of improved materials.

4.6 Therapeutic applications

4.6.1 Stealth coatings for adenovirus-mediated gene delivery

Adenoviruses, especially adenovirus serotype 5 (Ad5), are effective gene delivery agents since they are able to transduce both dividing and non-dividing cells, and can be produced in large titers [81, 82]. However, Ad5 also induces a host immune response, limiting its use for systemic re-administration, and can only transduce cells expressing Coxsackievirus and Adenovirus Receptor (CAR) and αV integrins on their surface. To reduce the immunogenic response to the Ad5 capsid, as well as enhance the uptake of Ad5 in CAR-negative cell types, synthetic polymers using polyethylene glycol (PEG) and HPMA have been explored as stealth coatings [83]. We have also used HPMA-oligolysine brush polymers, varied in lysine peptide lengths, molecular weights, and degradability properties, to electrostatically interact with the negatively-charged viral capsid to form stealth coatings [84]. Interestingly, a peptide length of 10 lysines was optimal for increasing transduction of Ad5 under serum and serum-free conditions, similarly to the optimal polymer found for nonviral polyplex transfections [23]. The polymer coatings also enabled transduction of CAR-negative cells, which was mediated by the presence of heparan sulfate proteoglycans (HSPGs) on the cell surface. In particular, sulfated HSPGs have been implicated in enhancing cellular uptake of cationic materials through electrostatic interactions [85]. Furthermore, the stealth coating also significantly protected the virus from neutralizing antibodies, which inhibits efficient *in vivo* viral transduction, without reducing transduction efficiency; these results demonstrated the potential applicability of HPMA-oligolysine brush polymers to enhance Ad5 transduction *in vivo*.

4.6.2 Delivery to the central nervous system (CNS)

The delivery of therapeutic genes to the CNS can be beneficial for the treatment of neurological disorders [86, 87]. However, gene delivery to the CNS using nonviral vectors has not been successful due to the low transfection efficiencies achieved in non-dividing cells and low cellular uptake rates in terminally-differentiated neurons [88–90]. One approach to increase efficacy is to conjugate targeting ligands to polymeric vectors to enhance uptake by neuronal

subtypes [7, 91, 92]. We previously demonstrated that conjugation of Tet1, a 12-mer peptide identified by phage display to bind the Gtb1 ganglioside [93], to polyethylenimine (PEI) enhanced gene delivery to neural progenitor cells (NPCs) [94]. We found that ~0.6 Tet1 per polymer was sufficient to enhance transfection efficiency to NPCs *in vivo*. Recently, we have extended this work by exploring the effect of multivalency on targeting capability by varying ligand density of pendant Tet1 peptides in statistical HPMA-oligolysine copolymers [95]. We showed that there was an optimal ligand density for transfection of neuron-like PC-12 cells (~3 Tet1 per polymer), mainly due to increased toxicities seen with higher Tet1 ligand incorporation. Interestingly, high concentrations ($> 100\,\mu$M) of the Tet1 peptide alone did not cause significant cytotoxicity, suggesting that the incorporation of hydrophobic peptides such as Tet1 can increase the toxicity of cationic polymers [65].

Another approach for increasing transfection efficiency to neurons is to enhance endosomal escape of endocytosed polyplexes [96]. We have also demonstrated that melittin-containing HPMA polymer carriers enhanced effective bulk luciferase transfection to the brain over polymers without melittin after intraventricular injection [58].

4.7 Conclusions and future directions

In summary, we have demonstrated the synthesis of cationic polymers consisting of a hydrophilic HPMA backbone with multiple pendant peptides for DNA condensation, degradability, and endosomal escape. These HPMA-peptide brush polymers have also been used to improve adenovirus transduction and targeted delivery to the central nervous system. The relatively simple polymerization strategy used to synthesize these polymers have allowed the investigation of peptide multivalency, polymer architecture, and the use of various bioactive peptides for gene delivery applications.

4.8 Acknowledgements

This work is supported by NIH/NINDS 1R01NS064404, DMR 1206426, and the Center for the Intracellular Delivery of Biologics through the Washington Life Sciences Discovery Fund Grant No. 2496490. J.S. is supported by the National Science Foundation Graduate Research Fellowship under Grant No. DGE-0718124. We thank Dr. Russell Johnson and

David Chu for helpful discussion.

References

[1] Pack, D. W., Hoffman, A. S., Pun, S., and Stayton, P. S. (2005) Design and development of polymers for gene delivery. *Nat. Rev. Drug Discov.*, **4**, 581–593.

[2] Bergen, J. M. and Pun, S. H. (2005) Peptide-enhanced nucleic acid delivery. *MRS Bulletin*, **30**, 663–667.

[3] Gopal, V. (2013) Bioinspired peptides as versatile nucleic acid delivery platforms. *J. Control. Release*, **167**, 323–332.

[4] Martin, M. E. and Rice, K. G. (2007) Peptide-guided gene delivery. *AAPS J.*, **9**, E18–29.

[5] Levine, R. M., Scott, C. M., and Kokkoli, E. (2013) Peptide functionalized nanoparticles for nonviral gene delivery. *Soft Matter*, **9**, 985–1004.

[6] Kogure, K., Akita, H., Yamada, Y., and Harashima, H. (2008) Multifunctional envelope-type nano device (MEND) as a non-viral gene delivery system. *Adv. Drug Deliv. Rev.*, **60**, 559–571.

[7] Kwon, E. J., Bergen, J. M., Park, I. K., and Pun, S. H. (2008) Peptide-modified vectors for nucleic acid delivery to neurons. *J. Control. Release*, **132**, 230–235.

[8] Nishikawa, M., Yamauchi, M., Morimoto, K., Ishida, E., Takakura, Y., and Hashida, M. (2000) Hepatocyte-targeted in vivo gene expression by intravenous injection of plasmid DNA complexed with synthetic multi-functional gene delivery system. *Gene Ther.*, **7**, 548–555.

[9] Chu, D. S. H., Schellinger, J. G., Shi, J., Convertine, A. J., Stayton, P. S., and Pun, S. H. (2012) Application of living free radical polymerization for nucleic acid delivery. *Acc. Chem. Res.*, **45**, 1089–1099.

[10] Ahmed, M. and Narain, R. (2013) Progress of RAFT based polymers in gene delivery. *Prog. Polym. Sci.*.

[11] Xu, F. and Yang, W. (2011) Polymer vectors via controlled/living radical polymerization for gene delivery. *Prog. Polym. Sci.*, **36**, 1099–1131.

[12] Kopecek, J., Kopecková, P., Minko, T., and Lu, Z. (2000) HPMA copolymer-anticancer drug conjugates: design, activity, and mechanism of action. *Eur. J. Pharm. Biopharm.*, **50**, 61–81.

[13] Bulmus, V. (2011) RAFT polymerization mediated bioconjugation strategies. *Polym. Chem.*, **2**, 1463–1472.

[14] Gregory, A. and Stenzel, M. H. (2012) Progress in Polymer Science. *Prog. Polym. Sci.*, **37**, 38–105.

[15] Apostolovic, B., Deacon, S. P. E., Duncan, R., and Klok, H.-A. (2010) Hybrid polymer therapeutics incorporating bioresponsive, coiled coil peptide linkers. *Biomacromolecules*, **11**, 1187–1195.

[16] Wu, G. Y. and Wu, C. H. (1987) Receptor-mediated in vitro gene transformation by a soluble DNA carrier system. *J. Biol. Chem.*, **262**, 4429–4432.

[17] Toncheva, V., Wolfert, M. A., Dash, P. R., Oupický, D., Ulbrich, K., Seymour, L. W., and Schacht, E. H. (1998) Novel vectors for gene delivery formed by self-assembly of DNA with poly(L-lysine) grafted with hydrophilic polymers. *Biochim. Biophys. Acta*, **1380**, 354–368.

[18] Mintzer, M. A. and Simanek, E. E. (2009) Nonviral vectors for gene delivery. *Chem. Rev.*, **109**, 259–302.

[19] O'Brien-Simpson, N. M., Ede, N. J., Brown, L. E., Swan, J., and Jackson, D. C. (1997) Polymerization of unprotected synthetic peptides: A view toward synthetic peptide vaccines. *J. Am. Chem. Soc.*, **119**, 1183–1188.

[20] Kopeček, J. and Kopečková, P. (2010) HPMA copolymers: origins, early developments, present, and future. *Adv. Drug Deliv. Rev.*, **62**, 122–149.

[21] Burke, R. S. and Pun, S. H. (2010) Synthesis and characterization of biodegradable HPMA-oligolysine copolymers for improved gene delivery. *Bioconjug. Chem.*, **21**, 140–150.

[22] Johnson, R. N., Burke, R. S., Convertine, A. J., Hoffman, A. S., Stayton, P. S., and Pun, S. H. (2010) Synthesis of statistical copolymers containing multiple functional peptides for nucleic acid delivery. *Biomacromolecules*, **11**, 3007–3013.

[23] Johnson, R. N., Chu, D. S. H., Shi, J., Schellinger, J. G., Carlson, P. M., and Pun, S. H. (2011) HPMA-oligolysine copolymers for gene delivery: optimization of peptide length and polymer molecular weight. *J. Control. Release*, **155**, 303–311.

[24] Shi, J., Choi, J. L., Chou, B., Johnson, R. N., Schellinger, J. G., and Pun, S. H. (2013) Effect of polyplex morphology on cellular uptake, intracellular trafficking, and transgene expression. pp. 1–32.

[25] Carlson, P. M., Schellinger, J. G., Pahang, J. A., Johnson, R. N., and Pun, S. H. (2013) Comparative study of guanidine-based and lysine-based brush copolymers for plasmid delivery. *Biomat. Sci.*, **1**, 736–744.

[26] Convertine, A. J., Benoit, D. S. W., Duvall, C. L., Hoffman, A. S., and Stayton, P. S. (2009) Development of a novel endosomolytic diblock copolymer for siRNA delivery. *J. Control. Release*, **133**, 221–229.

[27] El-Sayed, A., Futaki, S., and Harashima, H. (2009) Delivery of macromolecules using arginine-rich cell-penetrating peptides: ways to overcome endosomal entrapment. *AAPS J.*, **11**, 13–22.

[28] Brooks, H., Lebleu, B., and Vives, E. (2005) Tat peptide-mediated cellular delivery: back to basics. *Adv. Drug Deliv. Rev.*, **57**, 559–577.

[29] Torchilin, V. P. (2008) Tat peptide-mediated intracellular delivery of pharmaceutical nanocarriers. *Adv. Drug Deliv. Rev.*, **60**, 548–558.

[30] Khalil, I. A., Kogure, K., Futaki, S., and Harashima, H. (2006) High density of octaarginine stimulates macropinocytosis leading to efficient intracellular trafficking for gene expression. *J. Biol. Chem.*, **281**, 3544–3551.

[31] Okuda, T., Sugiyama, A., Niidome, T., and Aoyagi, H. (2004) Characters of dendritic poly(L-lysine) analogues with the terminal lysines replaced with arginines and histidines as gene carriers in vitro. *Biomaterials*, **25**, 537–544.

[32] El-Sayed, A., Khalil, I. A., Kogure, K., Futaki, S., and Harashima, H. (2008) Octaarginine- and octalysine-modified nanoparticles have different modes of endosomal escape. *J. Biol. Chem.*, **283**, 23450–23461.

[33] Naik, R. J., Chandra, P., Mann, A., and Ganguli, M. (2011) Exogenous and cell surface glycosaminoglycans alter DNA delivery efficiency of arginine and lysine homopeptides in distinctly different ways. *J. Biol. Chem.*, **286**, 18982–18993.

[34] Åmand, H. L., Rydberg, H. A., Fornander, L. H., Lincoln, P., Nordén, B., and Esbjörner, E. K. (2012) Cell surface binding and uptake of arginine- and lysine-rich penetratin peptides in absence and presence of proteoglycans. *Biochim. Biophys. Acta*, **1818**, 2669–2678.

[35] Bromberg, L., Raduyk, S., Hatton, T. A., Concheiro, A., Rodriguez-Valencia, C., Silva, M., and Alvarez-Lorenzo, C. (2009) Guanidinylated polyethyleneimine-polyoxypropylene-polyoxyethylene conjugates as gene transfection agents. *Bioconjug. Chem.*, **20**, 1044–1053.

[36] Tziveleka, L.-A., Psarra, A.-M. G., Tsiourvas, D., and Paleos, C. M. (2007) Synthesis and characterization of guanidinylated poly(propylene imine) dendrimers as gene transfection agents. *J. Control. Release*, **117**, 137–146.

[37] Zhai, X., Sun, P., Luo, Y., Ma, C., Xu, J., and Liu, W. (2011) Guanidinylation: a simple way to fabricate cell penetrating peptide analogue-modified chitosan vector for enhanced gene delivery. *J. Appl. Polym. Sci.*, **121**, 3569–3578.

[38] Mattheis, C., Wang, H., Meister, C., and Agarwal, S. (2013) Effect of guanidinylation on the properties of poly(2-aminoethylmethacrylate)-based antibacterial materials. *Macromol Biosci*, **13**, 242–255.

[39] Treat, N. J., Smith, D., Teng, C., Flores, J. D., Abel, B. A., York, A. W., Huang, F., and McCormick, C. L. (2012) Guanidine-Containing Methacrylamide (Co)polymers via aRAFT: Toward a Cell Penetrating Peptide Mimic(). *ACS Macro Lett*, **1**, 100–104.

[40] Hwang, S. J., Bellocq, N. C., and Davis, M. E. (2001) Effects of structure of beta-cyclodextrin-containing polymers on gene delivery. *Bioconjug. Chem.*, **12**, 280–290.

[41] Fischer, D., Li, Y., Ahlemeyer, B., Krieglstein, J., and Kissel, T. (2003) In vitro cytotoxicity testing of polycations: influence of polymer structure on cell viability and hemolysis. *Biomaterials*, **24**, 1121–1131.

[42] de Wolf, H. K., de Raad, M., Snel, C., van Steenbergen, M. J., Fens, M. H. A. M., Storm, G., and Hennink, W. E. (2007) Biodegradable poly(2-dimethylamino ethylamino)phosphazene for in vivo gene delivery to tumor cells. Effect of polymer molecular weight. *Pharm. Res.*, **24**, 1572–1580.

[43] Ganta, S., Devalapally, H., Shahiwala, A., and Amiji, M. (2008) A review of stimuli-responsive nanocarriers for drug and gene delivery. *J. Control. Release*, **126**, 187–204.

[44] Dubowchik, G. M., Firestone, R. A., Padilla, L., Willner, D., Hofstead, S. J., Mosure, K., Knipe, J. O., Lasch, S. J., and Trail, P. A. (2002) Cathepsin B-labile dipeptide linkers for lysosomal release of doxorubicin from internalizing immunoconjugates: model studies of enzymatic drug release and antigen-specific in vitro anticancer activity. *Bioconjug. Chem.*, **13**, 855–869.

[45] Lévesque, S. G. and Shoichet, M. S. (2007) Synthesis of enzyme-degradable, peptide-cross-linked dextran hydrogels. *Bioconjug. Chem.*, **18**, 874–885.

[46] Grosse, S. M., Tagalakis, A. D., Mustapa, M. F. M., Elbs, M., Meng, Q.-H., Mohammadi, A., Tabor, A. B., Hailes, H. C., and Hart, S. L. (2010) Tumor-specific gene transfer with receptor-mediated nanocomplexes modified by polyethylene glycol shielding and endosomally cleavable lipid and peptide linkers. *FASEB J.*, **24**, 2301–2313.

[47] Meister, A. and Anderson, M. E. (1983) Glutathione. *Annu. Rev. Biochem.*, **52**, 711–760.

[48] Shi, J., Johnson, R. N., Schellinger, J. G., Carlson, P. M., and Pun, S. H. (2012) Reducible HPMA-co-oligolysine copolymers for nucleic acid delivery. *Int. J. Pharm.*, **427**, 113–122.

[49] Jiang, T., Olson, E. S., Nguyen, Q. T., Roy, M., Jennings, P. A., and Tsien, R. Y. (2004) Tumor imaging by means of proteolytic activation of cell-penetrating peptides. *Proc. Natl. Acad. Sci. U.S.A.*, **101**, 17867–17872.

[50] Hatakeyama, H., AKITA, H., Kogure, K., Oishi, M., Nagasaki, Y., Kihira, Y., Ueno, M., Kobayashi, H., Kikuchi, H., and HARASHIMA, H. (2007) Development of a novel systemic gene delivery system for cancer therapy with a tumor-specific cleavable PEG-lipid. *Gene Ther.*, **14**, 68–77.

[51] Ulijn, R. V. (2006) Enzyme-responsive materials: a new class of smart biomaterials. *J Mater Chem*, **16**, 2217–2225.

[52] Sutherland, M. S. K., et al. (2006) Lysosomal trafficking and cysteine protease metabolism confer target-specific cytotoxicity by peptide-linked anti-CD30-auristatin conjugates. *J. Biol. Chem.*, **281**, 10540–10547.

[53] Turk, V., Turk, B., and Turk, D. (2001) Lysosomal cysteine proteases: facts and opportunities. *EMBO J.*, **20**, 4629–4633.

[54] Chu, D. S. H., Johnson, R. N., and Pun, S. H. (2012) Cathepsin B-sensitive polymers for compartment-specific degradation and nucleic acid release. *J. Control. Release*, **157**, 445–454.

[55] Midoux, P., Pichon, C., Yaouanc, J.-J., and Jaffrès, P.-A. (2009) Chemical vectors for gene delivery: a current review on polymers, peptides and lipids containing histidine or imidazole as nucleic acids carriers. *Br. J. Pharmacol.*, **157**, 166–178.

[56] Wagner, E. (1999) Application of membrane-active peptides for nonviral gene delivery. *Adv. Drug Deliv. Rev.*, **38**, 279–289.

[57] Shi, J., Schellinger, J. G., Johnson, R. N., Choi, J. L., Chou, B., Anghel, E. L., and Pun, S. H. (2013) Influence of histidine incorporation on buffer capacity and gene transfection efficiency of HPMA-co-oligolysine brush polymers. *Biomacromolecules*, **14**, 1961–1970.

[58] Schellinger, J. G., Pahang, J. A., Johnson, R. N., Chu, D. S. H., Sellers, D. L., Maris, D. O., Convertine, A. J., Stayton, P. S., Horner, P. J., and Pun, S. H. (2013) Melittin-grafted HPMA-oligolysine based copolymers for gene delivery. *Biomaterials*, **34**, 2318–2326.

[59] Schellinger, J. G., Pahang, J. A., Shi, J., and Pun, S. H. (2013) Block Copolymers Containing a Hydrophobic Domain of Membrane-Lytic Peptides Form Micellar Structures and Are Effective Gene Delivery Agents. *ACS Macro Lett.*, **2**, 725–730.

[60] Kichler, A., Leborgne, C., Coeytaux, E., and Danos, O. (2001) Polyethylenimine-mediated gene delivery: a mechanistic study. *J. Gene Med.*, **3**, 135–144.

[61] Akinc, A., Thomas, M., Klibanov, A. M., and Langer, R. (2005) Exploring polyethylenimine-mediated DNA transfection and the proton sponge hypothesis. *J. Gene Med.*, **7**, 657–663.

[62] Reilly, M. J., Larsen, J. D., and Sullivan, M. O. (2012) Polyplexes traffic through caveolae to the Golgi and endoplasmic reticulum en route to the nucleus. *Mol. Pharm.*, **9**, 1280–1290.

[63] Xu, Y. and Szoka, F. C. (1996) Mechanism of DNA release from cationic liposome/DNA complexes used in cell transfection. *Biochemistry*, **35**, 5616–5623.

[64] Liu, Z., Zhang, Z., Zhou, C., and Jiao, Y. (2010) Hydrophobic modifications of cationic polymers for gene delivery. *Prog. Polym. Sci.*, **35**, 1144–1162.

[65] Incani, V., Lavasanifar, A., and Uludağ, H. (2010) Lipid and hydrophobic modification of cationic carriers on route to superior gene vectors. *Soft Matter*, **6**, 2124–2138.

[66] Zhu, L. and Mahato, R. I. (2010) Lipid and polymeric carrier-mediated nucleic acid delivery. *Expert Opin. Drug Deliv.*, **7**, 1209–1226.

[67] Abbasi, M., Uludağ, H., Incani, V., Hsu, C. Y. M., and Jeffery, A. (2008) Further investigation of lipid-substituted poly(L-Lysine) polymers for transfection of human skin fibroblasts. *Biomacromolecules*, **9**, 1618–1630.

[68] Juvvadi, P., Vunnam, S., and Merrifield, R. B. (1996) Synthetic melittin, its enantio, retro, and retroenantio isomers, and selected chimeric analogs: their antibacterial, hemolytic, and lipid bilayer action. *J. Am. Chem. Soc.*, **118**, 8989–8997.

[69] Raghuraman, H. and Chattopadhyay, A. (2007) Melittin: a membrane-active peptide with diverse functions. *Biosci. Rep.*, **27**, 189–223.

[70] Ogris, M., Carlisle, R. C., Bettinger, T., and Seymour, L. W. (2001) Melittin enables efficient vesicular escape and enhanced nuclear access of nonviral gene delivery vectors. *J. Biol. Chem.*, **276**, 47550–47555.

[71] Baumhover, N. J., Anderson, K., Fernandez, C. A., and Rice, K. G. (2010) Synthesis and in vitro testing of new potent polyacridine-melittin gene delivery peptides. *Bioconjug. Chem.*, **21**, 74–83.

[72] Ogris, M., Brunner, S., Schüller, S., Kircheis, R., and Wagner, E. (1999) PEGylated DNA/transferrin-PEI complexes: reduced interaction with blood components, extended circulation in blood and potential for systemic gene delivery. *Gene Ther.*, **6**, 595–605.

[73] Oupický, D., Howard, K. A., Konák, C., Dash, P. R., Ulbrich, K., and Seymour, L. W. (2000) Steric stabilization of poly-L-Lysine/DNA complexes by the covalent attachment of semitelechelic poly[N-(2-hydroxypropyl)methacrylamide]. *Bioconjug. Chem.*, **11**, 492–501.

[74] Oupický, D., Ogris, M., Howard, K. A., Dash, P. R., Ulbrich, K., and Seymour, L. W. (2002) Importance of lateral and steric stabilization of polyelectrolyte gene delivery vectors for extended systemic circulation. *Mol. Ther.*, **5**, 463–472.

[75] Šubr, V., Koňák, Č., Laga, R., and Ulbrich, K. (2006) Coating of DNA/poly(L-lysine) complexes by covalent attachment of poly[N-(2-hydroxypropyl)methacrylamide]. *Biomacromolecules*, **7**, 122–130.

[76] Wei, H., Pahang, J. A., and Pun, S. H. (2013) Optimization of brush-like cationic copolymers for nonviral gene delivery. *Biomacromolecules*, **14**, 275–284.

[77] Hatakeyama, H., Akita, H., and Harashima, H. (2011) A multifunctional envelope type nano device (MEND) for gene delivery to tumours based on the EPR effect: a strategy for overcoming the PEG dilemma. *Adv. Drug Deliv. Rev.*, **63**, 152–160.

[78] Shi, J., Chou, B., Choi, J. L., Ta, A. L., and Pun, S. H. (2013) Investigation of polyethylenimine/DNA polyplex transfection to cultured cells using radiolabeling and subcellular fractionation methods. *Mol. Pharm.*, **10**, 2145–2156.

[79] Fichter, K. M., Ingle, N. P., McLendon, P. M., and Reineke, T. M. (2013) Polymeric nucleic acid vehicles exploit active interorganelle trafficking mechanisms. *ACS Nano*, **7**, 347–364.

[80] McLendon, P. M., Fichter, K. M., and Reineke, T. M. (2010) Poly(glycoamidoamine) vehicles promote pDNA uptake through multiple routes and efficient gene expression via caveolae-mediated endocytosis. *Mol. Pharm.*, **7**, 738–750.

[81] Chailertvanitkul, V. A. and Pouton, C. W. (2010) Adenovirus: a blueprint for non-viral gene delivery. *Curr. Opin. Biotechnol.*, **21**, 627–632.

[82] Jang, J.-H., Schaffer, D. V., and Shea, L. D. (2011) Engineering biomaterial systems to enhance viral vector gene delivery. *Mol. Ther.*, **19**, 1407–1415.

[83] Kreppel, F. and Kochanek, S. (2008) Modification of adenovirus gene transfer vectors with synthetic polymers: a scientific review and technical guide. *Mol. Ther.*, **16**, 16–29.

[84] Wang, C.-H. K., Chan, L. W., Johnson, R. N., Chu, D. S. H., Shi, J., Schellinger, J. G., Lieber, A., and Pun, S. H. (2011) The transduction of Coxsackie and Adenovirus Receptor-negative cells and protection against neutralizing antibodies by HPMA-co-oligolysine copolymer-coated adenovirus. *Biomaterials*, **32**, 9536–9545.

[85] Ruponen, M., Rönkkö, S., Honkakoski, P., Pelkonen, J., Tammi, M., and Urtti, A. (2001) Extracellular glycosaminoglycans modify cellular trafficking of lipoplexes and polyplexes. *J. Biol. Chem.*, **276**, 33875–33880.

[86] Davidson, B. L. and Breakefield, X. O. (2003) Viral vectors for gene delivery to the nervous system. *Nat. Rev. Neurosci.*, **4**, 353–364.

[87] Rogers, M.-L. and Rush, R. A. (2012) Non-viral gene therapy for neurological diseases, with an emphasis on targeted gene delivery. *J. Control. Release*, **157**, 183–189.

[88] Pérez-Martínez, F. C., Guerra, J., Posadas, I., and Ceña, V. (2011) Barriers to non-viral vector-mediated gene delivery in the nervous system. *Pharm. Res.*, **28**, 1843–1858.

[89] Suk, J. S., Suh, J., Choy, K., Lai, S. K., Fu, J., and Hanes, J. (2006) Gene delivery to differentiated neurotypic cells with RGD and HIV Tat peptide functionalized polymeric nanoparticles. *Biomaterials*, **27**, 5143–5150.

[90] Bergen, J. M. and Pun, S. H. (2008) Analysis of the intracellular barriers encountered by nonviral gene carriers in a model of spatially controlled delivery to neurons. *J. Gene Med.*, **10**, 187–197.

[91] Zeng, J., Too, H.-P., Ma, Y., Luo, E. S. E., and Wang, S. (2004) A synthetic peptide containing loop 4 of nerve growth factor for targeted gene delivery. *J. Gene Med.*, **6**, 1247–1256.

[92] Oliveira, H., Fernandez, R., Pires, L. R., Martins, M. C. L., Simões, S., Barbosa, M. A., and Pêgo, A. P. (2010) Targeted gene delivery into peripheral sensorial neurons mediated by self-assembled vectors composed of poly(ethylene imine) and tetanus toxin fragment c. *J. Control. Release*, **143**, 350–358.

[93] Liu, J. K., Teng, Q., Garrity-Moses, M., Federici, T., Tanase, D., Imperiale, M. J., and Boulis, N. M. (2005) A novel peptide defined through phage display for therapeutic protein and vector neuronal targeting. *Neurobiol. Dis.*, **19**, 407–418.

[94] Kwon, E. J., Lasiene, J., Jacobson, B. E., Park, I.-K., Horner, P. J., and Pun, S. H. (2010) Targeted nonviral delivery vehicles to neural progenitor cells in the mouse subventricular zone. *Biomaterials*, **31**, 2417–2424.

[95] Chu, D. S. H., Schellinger, J. G., Bocek, M. J., Johnson, R. N., and Pun, S. H. (2013) Optimization of Tet1 ligand density in HPMA-co-oligolysine copolymers for targeted neuronal gene delivery. Tech. rep.

[96] Suk, J. S., Suh, J., Lai, S. K., and Hanes, J. (2007) Quantifying the intracellular transport of viral and nonviral gene vectors in primary neurons. *Exp. Biol. Med.*, **232**, 461–469.

Chapter 5

REDUCIBLE HPMA-*CO*-OLIGOLYSINE BRUSH COPOLYMERS FOR GENE DELIVERY

Julie Shi*, Russell N. Johnson*, Joan G. Schelllinger, Peter Carlson, and Suzie H. Pun

**Equally contributed to work*

Abstract

Biodegradability can be incorporated into cationic polymers *via* the use of disulfide linkages that are degraded in the reducing environment of the cell cytosol. In this work, *N*-(2-hydroxypropyl)methacrylamide (HPMA) and methacrylamido-functionalized oligo-L-lysine peptide monomers with either a non-reducible 6-aminohexanoic acid (AHX) linker or a reducible 3-[(2-aminoethyl)dithiol]propionic acid (AEDP) linker were copolymerized *via* reversible addition-fragmentation chain transfer (RAFT) polymerization. Both of the copolymers and a 1:1 (w/w) mixture of copolymers with reducible and non-reducible peptides were complexed with DNA to form polyplexes. The polyplexes were tested for salt stability, transfection efficiency, and cytotoxicity. The HPMA-oligolysine copolymer containing the reducible AEDP linkers was less efficient at transfection than the non-reducible polymer and was prone to flocculation in saline and serum-containing conditions, but was also not cytotoxic at charge ratios tested. Optimal transfection efficiency and toxicity was attained with mixed formulation of copolymers. Uptake studies indicated that blocking extracellular thiols did not restore transfection efficiency and that the decreased transfection of the reducible polyplex is not primarily caused by extracellular polymer reduction by free thiols. The decrease in transfection efficiency of the reducible polymers could be partially mitigated by the addition of 1 mM EDTA to prevent metal-catalyzed oxidation of reduced polymers.[1]

---

[1]Reprinted from *International Journal of Pharmaceutics*, Shi, J., *et al.*, Reducible HPMA-*co*-oligolysine brush copolymers for nucleic acid delivery, **427**, pp. 133-22, Copyright© 2012, with permission from Elsevier.

5.1 Introduction

Biodegradability is an important attribute of polycations used in nucleic acid delivery formulations for *in vivo* applications. Polyplexes (polycation and nucleic acid complexes) formed from higher molecular weight polycations are more stable in the extracellular environment [1] while intracellular nucleic acid release typically occurs by competitive displacement and therefore occurs more readily when shorter polycations are used [2]. In addition, polycation cytotoxicity has been shown to be reduced with decreasing polymer molecular weight [3–5]. To meet these two seemingly opposing material requirements, polycations that undergo triggered intracellular degradation have been employed. The two most commonly used strategies employed in design of degradable polycations are acid-labile bonds, such as hydrazones and esters, and reducible disulfide linkages [6–8]. The latter approach is particularly attractive because the disulfide bonds are stable in the oxidizing extracellular environment while the reducing environment of the cell cytoplasm triggers intracellular degradation.

Three major approaches have been used to incorporate reducible bonds in polyplex formulations: (1) crosslinking polyplexes using reactive thiols or disulfide-containing crosslinkers, (2) crosslinking low molecular weight polycations using the same approach, or (3) synthesizing cationic polymers with internal disulfide linkages. Disulfide bonds were first introduced to polyplex formulations by crosslinking preformed polyplexes to increase stability of polyplexes for *in vivo* applications [9–11]. In these examples, crosslinked polyplexes were shown to be more resistant to DNA release and colloidal aggregation. The second approach has been primarily applied to polyethylenimine (PEI); crosslinking of PEI has been shown to increase transfection efficiency of low molecular weight PEI while providing reduced toxicity compared with high molecular weight, non-degradable PEI in several reports [12–20]. Finally, reducible polymers, such as reducible poly(amidoamines) have been synthesized by using monomers containing an internal disulfide bond [21–25]. One major advantage of this approach is better control over final polymer architecture that may improve the reproducibility of polyplex formulations.

We previously synthesized HPMA-oligolysine copolymers that contain a reducible disul-

fide linker, 3-[(2-aminoethyl)dithio] propionic acid (AEDP), between the HPMA backbone and the oligolysine peptide *via* free radical polymerization [21]. Additionally, we recently demonstrated that the HPMA-oligolysine copolymers can be synthesized *via* reversible addition-fragmentation chain transfer (RAFT) polymerization, resulting in narrowly-disperse and well-defined polymers, as well as stoichiometric incorporation of peptide monomers. The oligolysine length, oligolysine content, and polymer molecular weight for this class of polymers was optimized for polymers ability to transfect cultured cells [26, 27]. Polymers composed of oligolysines with ten lysines (K_{10}) incorporated at 20 mole % showed comparable transfection efficiencies to that of polyethylenimine (PEI), but with reduced toxicity.

The goal of this work is to synthesize reducible HPMA-oligolysine polymers *via* controlled RAFT polymerization and to evaluate transfection efficiency and toxicity of these materials in several cultured cell lines. Because HPMA-oligolysine molecular weight and peptide loading can be well controlled using this approach, the effect of a reducible versus stable architecture can be studied directly by keeping these other factors, known to affect transfection efficiency, constant. Although the backbone of these HPMA-oligolysine polymers is not readily degradable, reduction results in release of oligolysine peptides from the main chain. Since the oligolysine component of the copolymers represents a majority of the mass ratio of the copolymer, complete reduction of disulfide linkers by releasing the oligolysine component from the polymer would result in a significantly diminished polymer molecular weight. Thus, polymers were designed to have molecular weights above the renal filtration threshold to promote polyplex stability during circulation but to degrade into fragments that can be easily excreted after disulfide reduction.

In this work we report the synthesis and evaluation of HPMA-oligolysine copolymers for the delivery of plasmid DNA. Copolymers of HPMA and oligolysine with either a nonreducible or a reducible linker were synthesized *via* RAFT polymerization. Polyplexes with these copolymers were evaluated for salt stability, and transfection efficiency and cytotoxicity various cell lines. Finally, flow cytometry and transfection studies with 5,5-dithiobis-(2-nitrobenzoic acid) (DTNB) assess the effect of free extracellular thiols on uptake and transfection efficiency using these copolymers.

5.2 Materials and methods

5.2.1 Materials

N-(2-hydroxypropyl)methacrylate (HPMA) was purchased from Polysciences (Warrington, PA). The initiator VA-044 was purchased from Wako Chemicals USA (Richmond, VA). Chain transfer agent ethyl cyanovaleric trithiocarbonate (ECT) was a generous gift from Dr. Anthony Convertine (University of Washington). Rink amide resin was purchased from Merck Chemical Int. (Darmstadt, Germany). HBTU and Fmoc-protected lysine were purchased from Aapptec (Louisville, KY). *N*-succinimidyl methacrylate was purchased from TCI America (Portland, OR). All cell culture reagents were purchased from Cellgro/Mediatech (Fisher Scientific, Pittsburgh, PA). All other materials, including poly(ethylenimine) (PEI, 25,000 g/mol, branched) and poly(L-lysine) (PLL, 12,000 - 24,000 g/mol), were reagent grade or better and were purchased from Sigma-Aldrich (St. Louis, MO) unless otherwise stated. Endotoxin-free plasmid pCMV-Luc2 was prepared by using the pGL4.10 vector (Promega, Madison, WI) and inserting the CMV promoter/intron region from the gWiz Luciferase (Aldevron, Madison, WI). The plasmid was isolated and produced with the Qiagen Plasmid Giga kit (Qiagen, Germany) according to the manufacturers instructions.

5.2.2 Synthesis of peptide monomers

N-(9-Fluorenylmethoxycarbonyl)-protected 3-[(2-aminoethyl)dithio] propionic acid (Fmoc-Aedp) was synthesized as previously described, but with some improvements [21]. Briefly, 616 mg (1.83 mmol, 2 eq.) of 9-fluorenylmethyl *N*-succinimidyl carbonate (Fmoc-OSu) was dissolved in 6 mL of dimethoxyethane (DME). An AEDP solution (2 eq. at 90 g/L in aqueous sodium bicarbonate) was then added dropwise to the Fmoc-OSu solution while stirring. The reaction mixture was allowed to proceed for 3 h at room temperature with vigorous stirring in the dark after which the solution was filtered through a 0.2 μm pore size PVDF filter and solvent removed *in vacuo*. The desired product was then extracted in chloroform as described previously. Crude material was then dissolved in minimum amount of dichloromethane and reprecipitated in cold hexane to give an off-white solid in quantitative yield.

Oligo-L-lysine (K_{10}) was synthesized on a solid support containing the Rink amide linker (100-200 mesh) using standard Fmoc/tBu chemistry on an automated PS3 peptide synthesizer (Protein Technologies, Phoenix, AZ). Prior to peptide cleavage from the resin, the N-terminus of the peptide was deprotected and modified with either Fmoc-protected 6-aminohexanoic acid (AHX) or Fmoc-AEDP. The N-terminus was then subsequently deprotected and reacted with *N*-succinimidyl methacrylate to provide a methacrylamido functionality on the peptide. The functionalized peptide monomers are referred to as $MaAhxK_{10}$ and $MaAedpK_{10}$. Synthesized peptides were cleaved from the resin by treating the solid support with a solution of trifluoroacetic acid (TFA)/dimethoxybenzene (DMB)/triisopropylsilane (TIS) (92.5:5:2.5 v/v/v) for 1.5 h with gentle mixing. Cleaved peptide monomers were then precipitated in cold ether, dissolved in methanol, and re-precipitated in cold ether. The peptide monomers were then frozen, lyophilized, and stored at -20 °C until polymer synthesis. If needed, peptide monomers were purified *via* reversed-phase high-performance liquid chromatography (RP-HPLC) using acetonitrile as the mobile phase and dH_2O (0.1 μm filtered) as the stationary phase. The peptide monomers were analyzed by RP-HPLC and MALDI-TOF mass spectrometry (MS) and were shown to have greater than 95% purity. The products were confirmed by MALDI-TOF MS. MALDI-TOF MS calculated for $MaAhxK_{10}$ (MH^+), [1479.98]; found, [1480.02]. MALDI-TOF MS calculated for $MaAedpK_{10}$ (MH^+), [1530.09]; found, [1530.09].

5.2.3 Synthesis of HPMA-co-AhxK$_{10}$ via free radical polymerization

A copolymer of HPMA-*co*-$AhxK_{10}$ was synthesized *via* free radical polymerization as previously described [21], with some modifications. Briefly, 20 mol% of $MaAhxK_{10}$ (0.027 mmol, or 40 mg) and 80 mol% of HPMA (0.108 mmol, or 15.5 mg) were dissolved in reaction buffer (6 M guanidine hydrochloride, 2 mM EDTA, 0.5 M Tris-base, buffered to pH 8.3 with HCl) to give a final monomer concentration of 85 $^{mg}/_{mL}$. The weight of the initiator (I) 2,2-azobis[2-(2-imidazolin-2-yl)propane]dihydrochloride (VA-044) used for the polymerization was calculated as 5% of the total mmole of the monomer (to give a theoretical degree of polymerization, or DP, of 190). The reaction mixture was added to an oven-dried 5 mL

pear-shaped reaction vessel, purged with N_2 gas for 15 min, and then sealed and heated to 44 °C for 48 h to generate 27 mg of copolymer after dialysis.

5.2.4 Synthesis of HPMA-co-AhxK$_{10}$ and HPMA-co-AedpK$_{10}$ via RAFT polymerization

Copolymers of HPMA-*co*-AhxK$_{10}$ and HPMA-*co*-AedpK$_{10}$ were synthesized *via* reversible-addition fragmentation chain transfer (RAFT) polymerization as previously described [26], using ethyl cyanovaleric trithiocarbonate (ECT, MW 263.4 g/mol) [28] as the chain transfer agent (*CTA*) and VA-044 as the initiator (*I*). Briefly, 20 mol % of either MaAhxK$_{10}$ or MaAedpK$_{10}$ (0.176 mmol, or 270.0 mg) and 80 mol% of HPMA (0.705 mmol, or 100.98 mg) were dissolved and sonicated in acetate buffer (1 M in dH_2O, pH 5.1) such that the final monomer concentration was 0.7 M. The molar ratio of $^{CTA}/_{I}$ was 10, and the DP used was 190. The reaction mixture was added to a 5 mL reaction vessel in the following order: ECT (100 $^{mg}/_{mL}$ in ethanol), 100% ethanol (10% of the final reaction volume), peptide monomer/HPMA mixture, and VA-044 (10 $^{mg}/_{mL}$ in acetate buffer). The reaction vessels were then sealed with a rubber septum and purged with N_2 gas for 10 min prior to incubation in an oil bath (44 °C) for 24 h. The copolymer solution was then dissolved in water, dialyzed against dH_2O to remove unreacted monomers and buffer salts, lyophilized, and stored at -20 °C. The final yield after dialysis was 58% of the theoretical yield.

5.2.5 Polymer characterization and degradation studies

Molecular weight analysis of the copolymers was carried out by gel permeation chromatography (GPC) as previously described, using a miniDAWN TREOS light scattering detector (Wyatt, Santa Barbara, CA) and an Optilab rEX refractive index detector (Wyatt). Absolute molecular weight averages M_n and M_w and $^{dn}/_{dc}$ values were calculated using ASTRA software (Wyatt). The dn/dc value for each copolymer was 0.133 $^{mL}/_{g}$. The content of K_{10} peptide within the HPMA copolymers were determined by amino acid analysis, as previously described [27].

Reduction of HPMA-MaAedpK$_{10}$ copolymers was carried out by dissolving the copolymers at a concentration of 10 $^{mg}/_{mL}$ in acetate buffer (150 mM, pH 4.4) with 1 mM EDTA.

Tris(2-carboxyethyl)phosphine) (TCEP) was added to the solution to a final concentration of 25 mM. The progress of the reaction was followed by GPC using methods described above.

5.2.6 Polyplex formulation and characterization

Stock solutions of polymers were prepared at 10 $^{mg}/_{mL}$ in 0.1X phosphate buffered saline (PBS), and the pH was adjusted to 6.5 by adding 0.1 N HCl. Polymer solutions were used within 2 weeks of preparation. To formulate polyplexes, pCMV-Luc2 plasmid DNA was diluted to 0.1 $^{mg}/_{mL}$ in DNase/RNase-free H_2O and mixed with an equal volume of polymer at desired lysine to DNA phosphate (N/P) ratios. Polyplexes were then allowed to incubate for 10 min at room temperature. For *in vitro* transfections, 20 μL of the polyplex solution (containing 1 μg DNA) was mixed with 180 μL of Opti-MEM medium (Invitrogen). The particle size of the polyplexes was determined by mixing 20 μL of the polyplex solution with either 20 μL of 0.2 μm-filtered dH_2O or 20 μL of 2X PBS. The polyplex solutions were incubated for 15 min at room temperature prior to particle sizing by dynamic light scattering (DLS) (ZetaPALS, Brookhaven Instruments Corp.).

For serum degradation studies, pCMV-Luc2 plasmid DNA was pre-stained with YOYO-1 iodide (Invitrogen), a known bis-intercalating dye, to yield a DNA concentration of 0.1 $^{mg}/_{mL}$ at a ratio of 5:1, DNA base pairs to dye molecules. The DNA-dye solution was allowed to incubate for 1 h at room temperature. Polyplexes were prepared by adding 10 μL of polymer solution to 10 μL of pDNA-dye solution (containing 1 μg DNA) at N/P of 5. Equal volumes (20 μL) of various fetal bovine serum (FBS) concentrations were added to the polyplex solution to give serum final concentrations of 50%, 25%, and 10%, and the polyplexes were allowed to incubate for 30 min. 20 μL aliquot samples, mixed with 1 μL of loading buffer, were then loaded onto a 0.8% agarose gel containing TAE buffer (40 mM Tris-acetate, 1 mM EDTA) and electrophoresed in the dark at 100 V. pDNA was then visualized using an UV transilluminator (laser-excited fluorescence gel scanner, Kodak, Rochester, NY).

5.2.7 Cell culture

HeLa (human cervical carcinoma), NIH/3T3 (mouse embryonic fibroblast), and CHO-K1 (Chinese hamster ovary) cells were grown in minimum essential medium (MEM), Dulbeccos modified eagle medium (DMEM), and F-12K medium, respectively, supplemented with 10% FBS and 100 IU penicillin, 100 μg/mL streptomycin, and 0.25 μg/mL amphotericin B. Cells were passaged when they reached ~80% confluency.

5.2.8 In vitro transfection

HeLa, NIH/3T3, and CHO-K1 cells were seeded overnight in 24-well plates at a density of 3×10^4 cells per well (1 mLwell) at 37 °C, 5% CO_2. Polyplexes were formed as described above. After the polyplexes were formed, 20 μL (containing 1 μg DNA) was mixed with 180 μL of Opti-MEM medium (Invitrogen) or complete cell medium (containing 10% FBS) for serum transfections. Seeded cells were washed once with PBS and then treated with 200 μL of polyplexes in Opti-MEM or complete medium, which was added dropwise on top of the cells. After a 4 h incubation at 37 °C, 5% CO_2 in a humidified environment, the cells were washed once again with PBS and incubated in 1 mL of fresh complete medium for an additional 44 h. For studies with DTNB, the cells were pre-incubated with 500 μL DTNB (5 mM in Opti-MEM) for 1 h, washed with PBS, and then incubated with polyplexes in Opti-MEM containing 5 mM DTNB for 4 h. For studies with EDTA, cells were treated with polyplexes in Opti-MEM containing 1 mM EDTA for 4 h; cells were collected, washed with PBS, pelleted, resuspended in complete media, and added back into the well for an additional 44 h. In all experiments cells were harvested and assayed for luciferase expression at 48 h. This was done by washing cells once with PBS, adding of 200 μL reporter lysis buffer (Promega, Madison, WI), and then performing one freeze-thaw cycle to complete the lysis of cells. Lysates were collected and centrifuged at 14,000g for 15 min. Luminescence was carried out following the manufacturers instructions (Promega, Madison, WI). Luciferase activity is reported in relative light units (RLU) normalized by mg protein (RLU/mg), as measured by a microBCA Protein Assay Kit (Pierce).

5.2.9 Cytotoxicity assay

The cytotoxicity of the polymers was evaluated *in vitro* using the MTS assay. HeLa, NIH/3T3, and CHO-K1 cells were plated overnight in 96-well plates at a density of 3 $\times$ 10^3 cells per well per 0.1 mL. Polymers were prepared in serial dilutions in dH_2O and then diluted 10-fold in Opti-MEM medium (Invitrogen). The cells were rinsed once with PBS and incubated with 40 μL of the polymer solution for 4 h at 37 °C, 5% CO_2. Cells were rinsed once with PBS and the medium was replaced with 100 μL complete growth medium. At 48 h, 20 μL of 3-(4,5-dimethylthiazol-2-yl)-5-(3-carboxymethoxyphenyl)-2-(4-sulfophenyl)-2*H*-tetrazolium (MTS) (Promega) were added to each well. Cells were then incubated at 37 °C, 5% CO_2 for 4 h. The absorbance of each well was measured at 490 nm using a microplate reader (TECAN Safire^2). IC_{50} values were computed using a nonlinear fit (four-parameter variable slope) in GraphPad Prism v.5 (San Diego, CA).

5.2.10 Flow cytometry

HeLa and NIH/3T3 cells were seeded overnight in 6-well plates at a density of 2 $\times$ 10^5 cells per well (2 $^{mL}/_{well}$) at 37 °C, 5% CO_2. Polyplexes were formulated with polymer and plasmid DNA labeled with TOTO-3 (1 dye per 25 base pairs). The polyplexes were then diluted 10-fold in Opti-MEM and the fluorescence of TOTO-3 were measured on a microplate reader (Tecan Safire^2). Seeded cells were washed once with PBS and treated with 1 mL of DTNB (5 mM in Opti-MEM) or Opti-MEM (for non-treated samples) for 1 h at 37 °C, 5% CO_2. Polyplexes were formulated with polymer and plasmid DNA labeled with TOTO-3 (1 dye per 25 base pairs). The cells were then incubated with 800 μL of Opti-MEM containing polyplexes (with 5 mM DTNB for treated samples) for 30 min at 37 °C, 5% CO_2. The cells were washed once again with PBS and treated with CellScrub (Genlantis) for 15 min at room temperature to remove extracellularly-bound polyplexes. Cells were then trypsinized and pelleted at 1000*g* for 5 min. Cell were pelleted again, washed with complete medium, and resuspended in 0.3 mL complete medium for flow cytometry. Flow cytometry analysis was completed at the Cell Analysis Facility (BD FACS Canto, University of Washington). TOTO-3 was excited at 633 nm and the emission was detected using a 660/20-nm band-pass

filter. A total of 10,000 events were collected per sample.

5.2.11 Statistical analysis

The data are represented as the mean and standard deviations. Differences were analyzed using the two-tailed Student's t-test and a p-value of less than or equal to 0.05 was taken as significant.

5.3 Results

5.3.1 Synthesis of HPMA-co-AhxK$_{10}$ and HPMA-co-AedpK$_{10}$

Synthesis of HPMA-*co*-MaAhxK$_{10}$ and HPMA-*co*-MaAedpK$_{10}$ copolymers was carried out by RAFT copolymerization of HPMA with oligolysine comonomers that contained either an AEDP or AHX linker. The principle difference between the two linkers is that AEDP contained an internal disulfide bond that can be degraded in reducing environments such as the cell cytosol. Copolymerization was carried out as illustrated in (Figure 5.1). The resulting polymers displayed properties that were close to targeted values (Table 5.1). The number molecular weight average, M_n, of HPMA-*co*-MaAedpK$_{10}$ was 80.2 kDa, which corresponded well to the targeted molecular weight of 79.5 kDa. Polydispersity of the copolymer was 1.11. Amino acid analysis of the HPMA-oligolysine copolymers demonstrated a near quantitative yield of the oligo-L-lysine peptide monomer in resulting copolymers (final mole %: 18.4). As a result, the concentration of lysine in each of the final copolymers. In both copolymers the targeted degree of polymerization (DP) was 190; as a consequence, the number of monomers per copolymer chain was similar and the lysine weight ratio was identical despite some difference in the final M_n of the two copolymers.

To compare polymers synthesized *via* RAFT and free radical polymerization, a copolymer of HPMA-*co*-MaAhxK$_{10}$ was also synthesized *via* free radical polymerization (Table 5.1). The parameters used in the synthesis were kept as similarly as possible to the synthesis of the RAFT polymers to generate a comparable material. However, despite a targeted DP of 190, the polymer synthesized *via* free radical polymerization had a very large M_n and also resulted in lower than expected incorporation of oligo-L-lysine peptide.

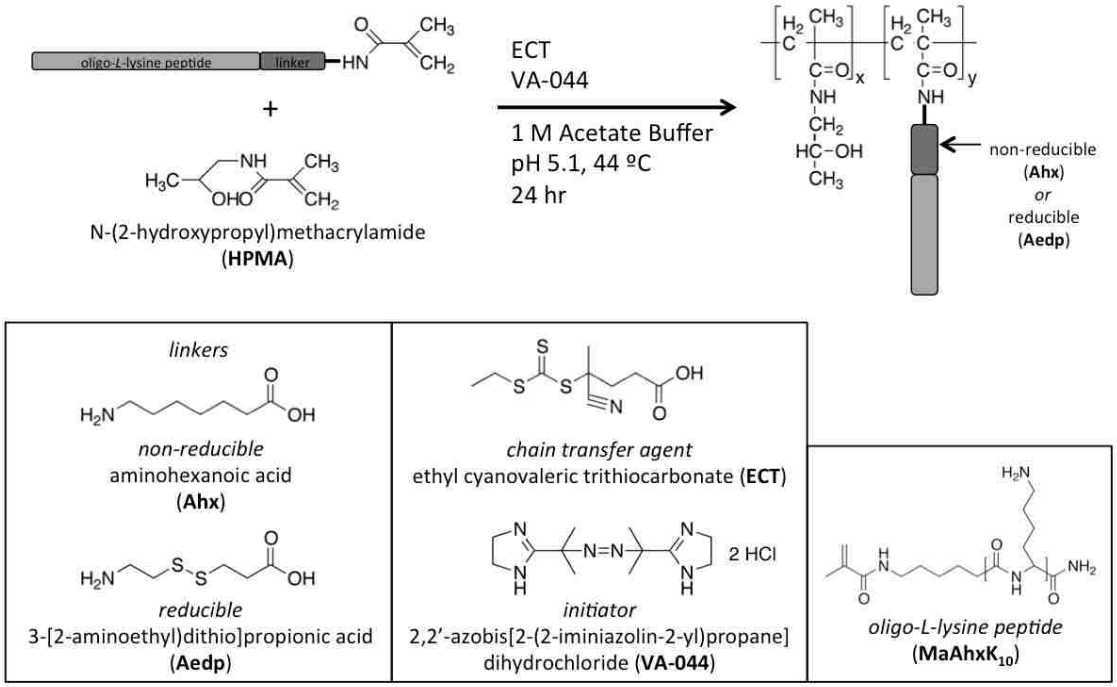

Figure 5.1: **Synthesis of reducible HPMA-co-oligolysine copolymers *via* reversible-addition fragmentation chain transfer (RAFT) polymerization.** Statistical polymers of HPMA and oligolysine were synthesized *via* RAFT polymerization using ECT as the chain transfer agent and VA-044 as the initiator. A *CTA* to *I* ratio of 10 and a degree of polymerization (DP) of 190 was used in all polymerizations. A non-reducible (Ahx) or a reducible (Aedp) linker was used in the synthesis of the oligolysine (K_{10}) peptide in order to introduce biodegradability into the polymer. Peptide monomers were functionalized with a methacrylamido group (Ma) for polymerization.

5.3.2 Polymer degradation with TCEP

The HPMA-*co*-MaAedpK$_{10}$ copolymer was treated with tris(2-carboxyethyl) phosphine (TCEP) to reduce the disulfide bond contained in the MaAedpK$_{10}$ component of the copolymers. Reduction was assessed by size exclusion chromatography. Degradation was done in the presence of EDTA (Figure 5.2A) or without EDTA (Figure 5.2B), a chelator that sequesters trace metals capable of oxidizing free sulfhydryls to disulfide bonds. The mass fraction of the degraded products was calculated by determining the area under the corresponding peaks. Figure 5.2A indicated that reduction of the disulfide bonds proceeded

Table 5.1: Properties of HPMA-oligolysine copolymers

polymer	targeted M_n (kD)	determined M_n (kD)[a]	M_n/M_w[a]	mol % K_{10} monomer[b]	mmol amine/g polymer[b]	IC_{50} (μg lys/mL)[c]	IC_{50} (μg lys/mL)[d]	IC_{50} (μg lys/mL)[e]
Polymer synthesized by free radical polymerization								
HPMA-AhxK_{10}	78.0	168.4	2.24	12.0	0.00713	0.114*	0.128*	0.0901*
Polymers synthesized by RAFT polymerization								
HPMA-AhxK_{10}	78.0	77.6	1.18	19.6	4.83	9.67*	8.23*	12.16*
HPMA-AedpK_{10}	79.5	80.2	1.11	19.4	4.79	13.03*	12.24*	12.25*
1:1 (w/w) mixture	–	–	–	–	–	12.24*	10.54*	12.25*
bPEI (25 kD)	–	–	–	–	23.22	1.85**	1.57**	1.45**
PLL (12-24 kD)	–	–	–	–	4.51	0.70**	0.72**	0.75**

[a]Values determined by GPC coupled with laser light scattering, and dRI detection. [b]Mol% of oligo-L-lysine and mmol amine/g polymer determined by amino acid analysis. [c]IC_{50} values determined using NIH/3T3 cells. [d]IC_{50} values determined using CHO-K1 cells. [e]IC_{50} values determined using HeLa cells. *Values were adjusted to lysine equivalent. **Values were adjusted to amine equivalent and IC_{50} values are in μg amine/mL.

quickly. At 15 min, the copolymer was 80.2% degraded and by 2 h, the polymer was 99.3% degraded. When EDTA was present, treatment with TCEP resulted in the generation of degraded copolymer and free oligolysine. However, when EDTA was not present, a high molecular weight fraction was also generated, the degraded copolymer appeared less uniform, and at least a portion of oligolysine appeared to dimerize.

5.3.3 Polyplex stability

Dynamic light scattering was used to measure the effective hydrodynamic diameter of HPMA-AhxK_{10} and HPMA-AedpK_{10} polyplexes at N/P ratios of 3, 5, and 10 in water, 150 mM PBS, and complete cell medium (DMEM + 10% FBS). Polyplexes of HPMA-AhxK_{10} formed small particles in water (150-186 nm), and particle size at N/P of 5 and 10 remained stable against salt-induced aggregation in 150 mM PBS (Figure 5.3). Polyplexes of HPMA-AedpK_{10} formed smaller particles in water (90-100 nm) compared to HPMA-AhxK_{10}, but were not salt stable even in the presence of 1 mM EDTA (data not shown). Polyplexes of a 1:1 (w/w) mixture of the non-reducible and reducible polymer formed small particles in water, similar to that of HPMA-AedpK_{10}, and were relatively salt stable like HPMA-AhxK_{10}. All polyplex formulations increased in size to an average hydrodynamic

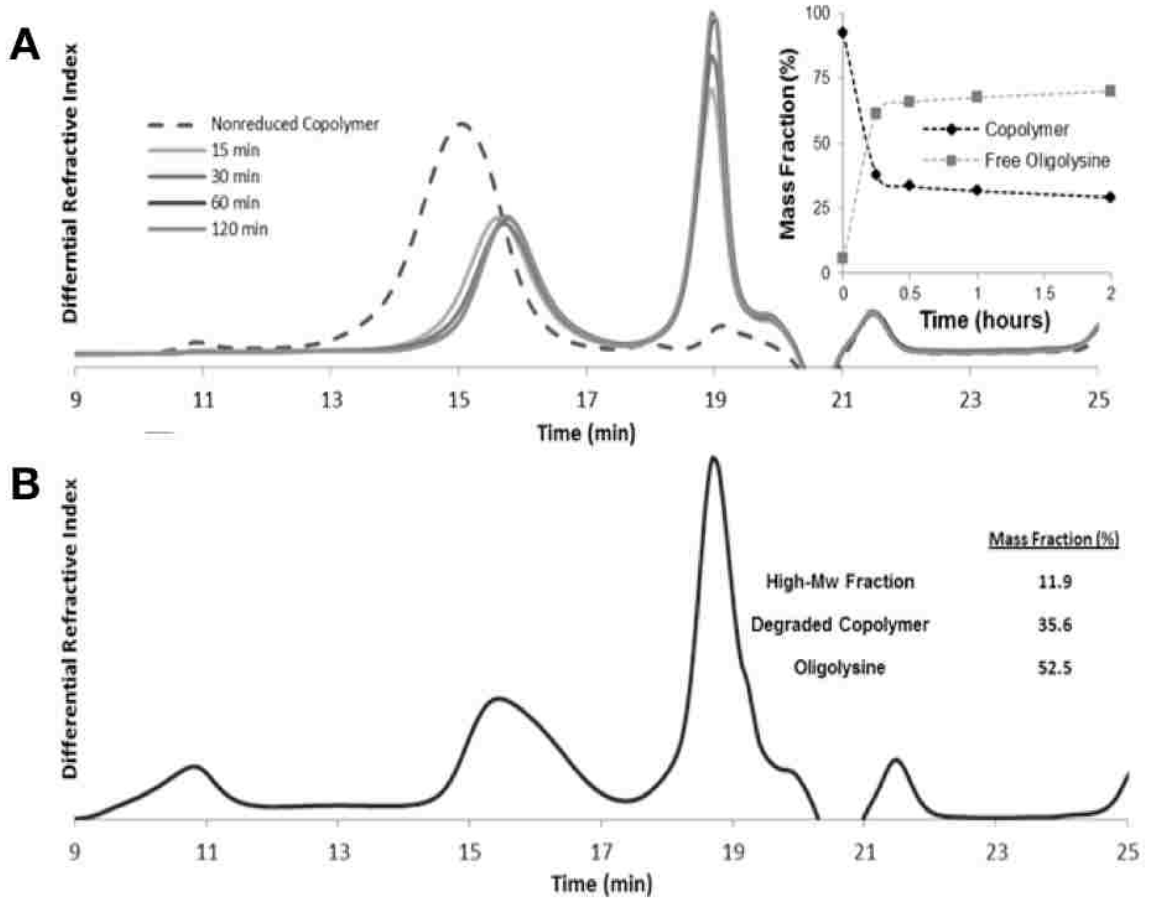

Figure 5.2: **Degradation of HPMA-AedpK$_{10}$ with TCEP.** HPMA-AedpK$_{10}$ was degraded over time in the presence of 25 mM TCEP. Reduced copolymers were applied to a GPC column to track changes in molecular weight at degradation of the copolymer occurred. (A) Reduction was done in the presence of EDTA. The insert indicates the mass fraction of degraded copolymer and free oligolysine. Degraded copolymer eluted between 14 to 17 min, while free oligolysine eluted from 18 to 20 mi. The insert shows the mass fraction of peptide and copolymer. Reduction done without EDTA (B) produced three eluted peaks in SEC. The first is a high molecular weight fraction (9 to 12 min), the second peak is degraded copolymer (14 to 17 min), and the third is oligolysine (18 to 20 min).

diameter $>$ 500 nm in 10% serum. These data suggest that although the reducible polymer does not form salt stable polyplexes, a mixture with non-reducible polymer increases polyplex salt stability. However, in the presence of 10% serum particles do not maintain their small size regardless of polymer composition.

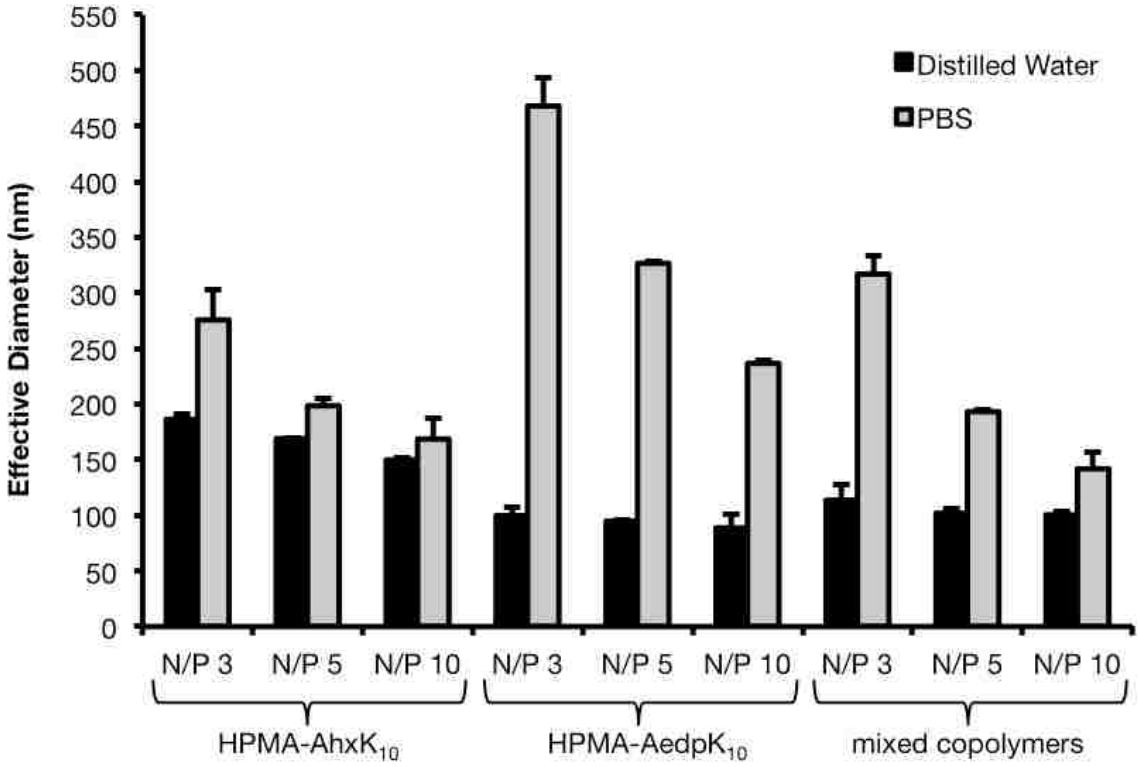

Figure 5.3: **Particle sizing of polyplexes by dynamic light scattering (DLS).** The effective diameter of polyplexes formulated with HPMA-AhxK_{10}, HPMA-AedpK_{10}, or a 1:1 (w/w) mixture was determined by DLS in water, PBS with an ionic strength of 150 mM, and DMEM medium supplemented with 10% FBS. Data are presented as mean ± S.D., n = 3.

The stability of HPMA-AhxK_{10} and HPMA-AedpK_{10} polyplexes in the presence of serum was also assessed by an agarose gel retardation assay. Because serum shows an intrinsic band similar to free DNA in an agarose gel containing ethidium bromide (data not shown), a YOYO-1 pre-labeled DNA was used instead. Free DNA incubated with various concentrations of serum (lanes 1, 5, 9 and 13) show streaking as a result of DNA degradation (Figure 5.4). HPMA-AedpK_{10}, HPMA-AhxK_{10} and a known protease-resistant copolymer, HPMA-Ahx(D)K_{10}, in which all lysines are D-lysines, were able to fully complex plasmid DNA in the presence of various serum concentrations as shown by the absence of bands corresponding to free DNA.

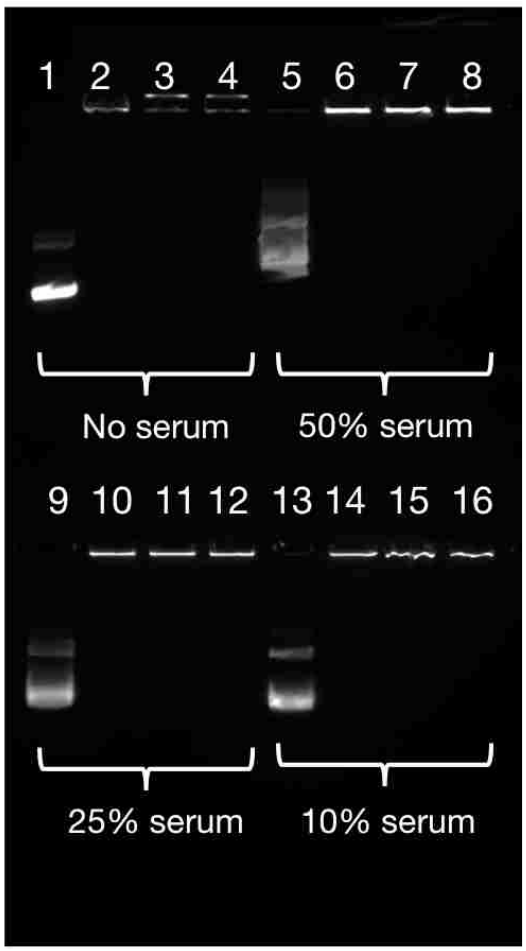

Figure 5.4: **Polyplex stability in serum *via* gel retardation assay.** Polyplexes complexed with YOYO-1-labeled plasmid DNA and either HPMA-AedpK$_{10}$, HPMA-AhxK$_{10}$, or HPMA-Ahx(d)K$_{10}$ were incubated with various concentrations of serum (50%, 25%, 10%). Free DNA (plasmid DNA not complexed with polymer) was used as a control.

5.3.4 Delivery of plasmid DNA to cultured cells

Polyplex transfection efficiency was determined by delivery of a luciferase plasmid, pCMV-Luc2, to cells in serum-free and serum-containing (10% FBS) conditions. For comparison against commonly used polymeric reagents, branched PEI (bPEI, 25 kD) and poly-L-lysine (PLL, 12-24 kD) polyplexes were also evaluated. Transfection was also conducted with HPMA-AhxK$_{10}$ synthesized by free radical polymerization (Figure 5.5). Polyplexes were

formed at N/P (nitrogen to phosphate) ratios of 3, 5, and 10, and evaluated for transfection efficiency under serum-free conditions in NIH/3T3, CHO-K1, and HeLa cells (Figure 5.6). N/P 5 was determined to be optimal for high transfection efficiency and low cytotoxicity; therefore, the rest of the studies were completed with polyplexes formulated at N/P 5. HPMA-AhxK_{10} transfected more efficiently than poly-L-lysine (PLL, 12-24 kD) in all cell lines (Figure 5.7A). The luciferase activity of cells transfected with HPMA-AedpK_{10} was decreased by at least one order of magnitude compared to its non-reducible analog in all cell types and showed very similar activity to PLL. When the two polymers were mixed prior to polyplex formation and applied to cells, the resulting transfection efficiencies were intermediate between those of the individual polymers in all tested cell types. These results suggest that while HPMA-AedpK_{10} is poor at transfection, a 1:1 (w/w) mixture of HPMA-AhxK_{10} and HPMA-AedpK_{10} can improve transfection efficiency. The HPMA copolymers were also evaluated for transfection efficiency in the presence of 10% serum (Figure 5.8). Transfection efficiency of all polymer formulations was decreased under serum conditions. In addition, transfection of HPMA-AhxK_{10} synthesized *via* RAFT had very similar transfection efficiency to HPMA-AhxK_{10} synthesized by free radical polymerization.

5.3.5 Polymer toxicity

Cytotoxicity of polyplexes and polymers was determined by the BCA and MTS assay, respectively. The BCA assay was conducted 48 h after transfection to determine the amount of total cellular protein in lysates of transfected cells. Untreated cells were used to determine 100% cell viability. Again, cytotoxicity of HPMA-AhxK_{10} synthesized by free radical polymerization was also determined as a comparison. Polyplexes of HPMA-AhxK_{10} and HPMA-AedpK_{10}, formulated at N/P 5, were nontoxic to NIH/3T3 cells. HPMA-AhxK_{10} decreased cell viability to 74.6% in CHO-K1 cells and 52.1% in HeLa cells (Figure 4b). A mixture of HPMA-AhxK_{10} and HPMA-AedpK_{10} reduced the toxicity of HPMA-AhxK_{10} alone. In comparison, PLL was very toxic to all cell types, decreasing cell viability to 43.8% in NIH/3T3 cells, 29.6% in CHO-K1 cells, and 48.8% in HeLa cells. PEI was relatively non-toxic for all cell types.

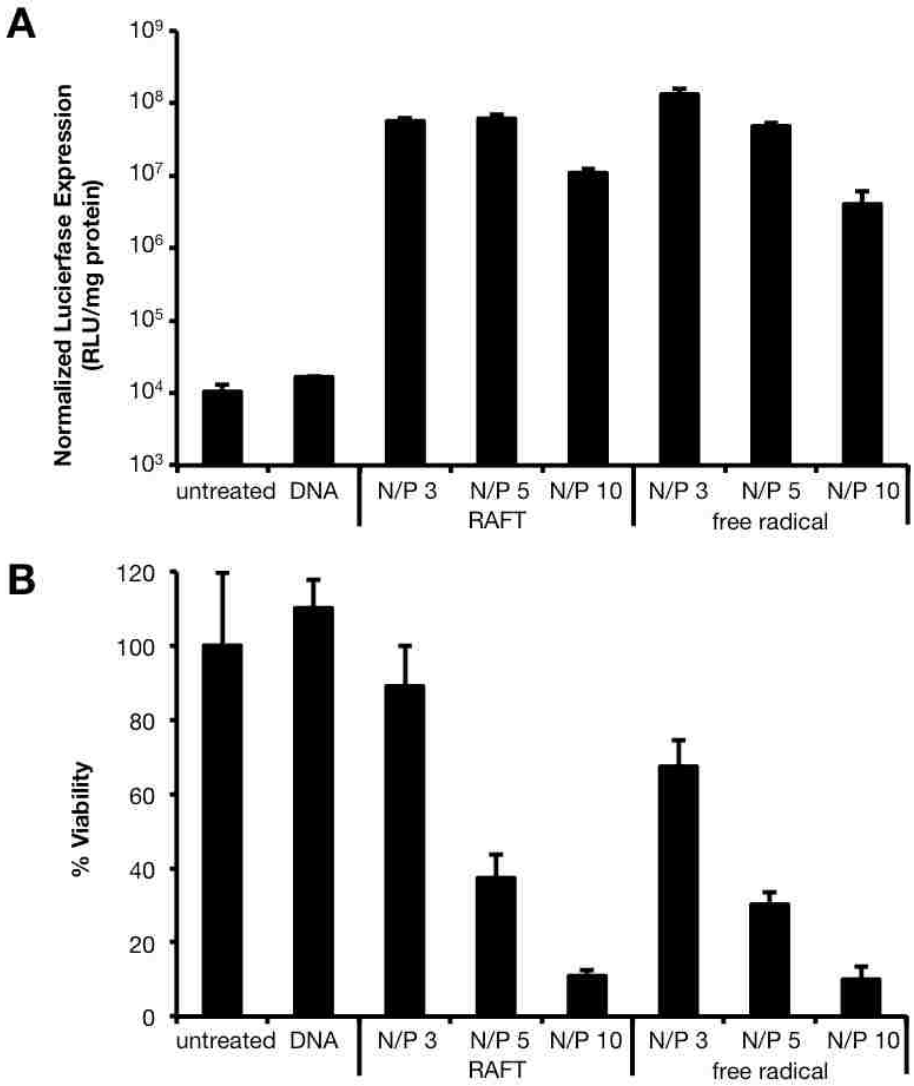

Figure 5.5: **Transfection and cell viability of free radical and RAFT HPMA copolymers in HeLa cells.** (A) Transfection efficiency and cell viability of HPMA-$AhxK_{10}$ copolymers in HeLa cells. Cells were treated with polyplexes at N/P of 3, 5 and 10 in serum-free conditions for 4 h. Luciferase activity was measured 48 h after transfection and normalized to total protein content in each sample. (B) Toxicity of the polyplexes was determined by measuring total protein content and designating untreated cells as 100% viable. *Untreated*: untreated controls; *RAFT*: HPMA-$AhxK_{10}$ synthesized by RAFT polymerization; and *free radical*: HPMA-$AhxK_{10}$ synthesized by free radical polymerization. Data are presented as mean ± S.D., $n = 3$.

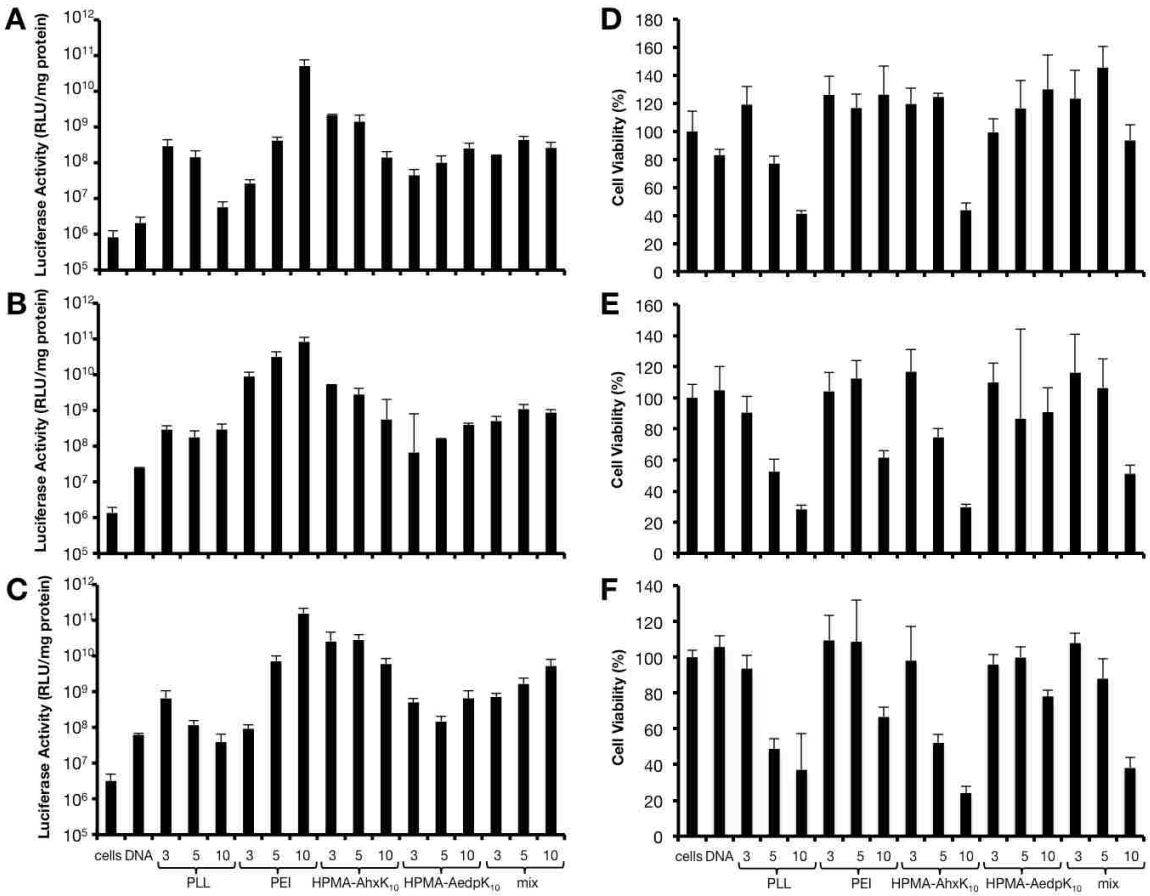

Figure 5.6: **Transfection efficiency and cell viability of HPMA-oligolysine copolymers in 3 cell types.** (A) NIH/3T3, (B) CHO-K1, and (C) HeLa cells were treated with polyplexes at N/P of 3, 5 and 10 in serum-free media for 4 h. Luciferase activity was measured 48 h after transfection and normalized to total protein content in each sample. Toxicity of the polyplexes in (D) NIH/3T3, (E) CHO-K1, and (F) HeLa cells was determined by measuring total protein content and designating untreated cells as 100% viable. *Cells*: untreated controls; *bPEI*: branched polyethylenimine (25 kD); *PLL*: poly-L-lysine (12-24 kD); *Mixed copolymers*: 1:1 (v/v) mixture of HPMA-AhxK$_{10}$ and HPMA-AedpK$_{10}$. DTNB stands for 5,5-dithiobis-(2-nitrobenzoic acid). Data are presented as mean ± S.D., $n = 4$.

To determine the IC$_{50}$ values of the polymers (concentration of polymers for 50% cell survival), cells were treated with a range of polymer concentrations in serum-free conditions to simulate transfection conditions. The MTS assay was used to assess the mitochondrial activity, an indicator of cell viability. Untreated cells were used to determine

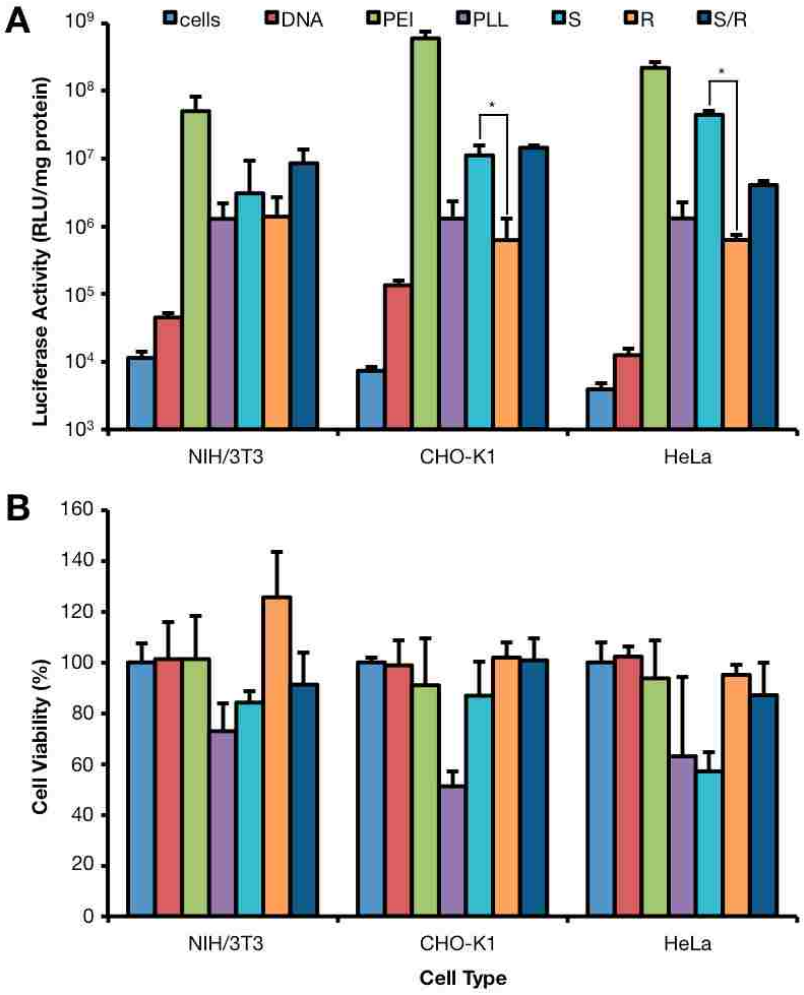

Figure 5.7: **Transfection and cell viability of HPMA copolymers in HeLa, NIH/3T3, and CHO-K1 cells.** (A) Transfection efficiency of HPMA copolymers in HeLa, NIH/3T3, and CHO-K1. Polyplexes (N/P 5) of copolymer and luciferase-encoding plasmid DNA were incubated with cells for 4 h in serum-free conditions. Luciferase activity was measured 48 h after transfection and normalized to total protein content in each sample. *Cells*: untreated controls; *bPEI*: branched polyethylenimine (25 kD); *PLL*: poly-L-lysine (12-24 kD); *S*: HPMA-AhxK$_{10}$; *R*: HPMA-AedpK$_{10}$; *S/R*: 1:1 (v/v) mixture of HPMA-AhxK$_{10}$ and HPMA-AedpK$_{10}$. (B) Polyplex cytotoxicity in HeLa, NIH/3T3, and CHO-K1. Toxicity of the polyplexes was determined by measuring total protein content and designating untreated cells as 100% viable. Data are presented as mean ± S.D., $n = 4$, (*) $p < 0.05$, as determined by two-tailed Student's t-test.

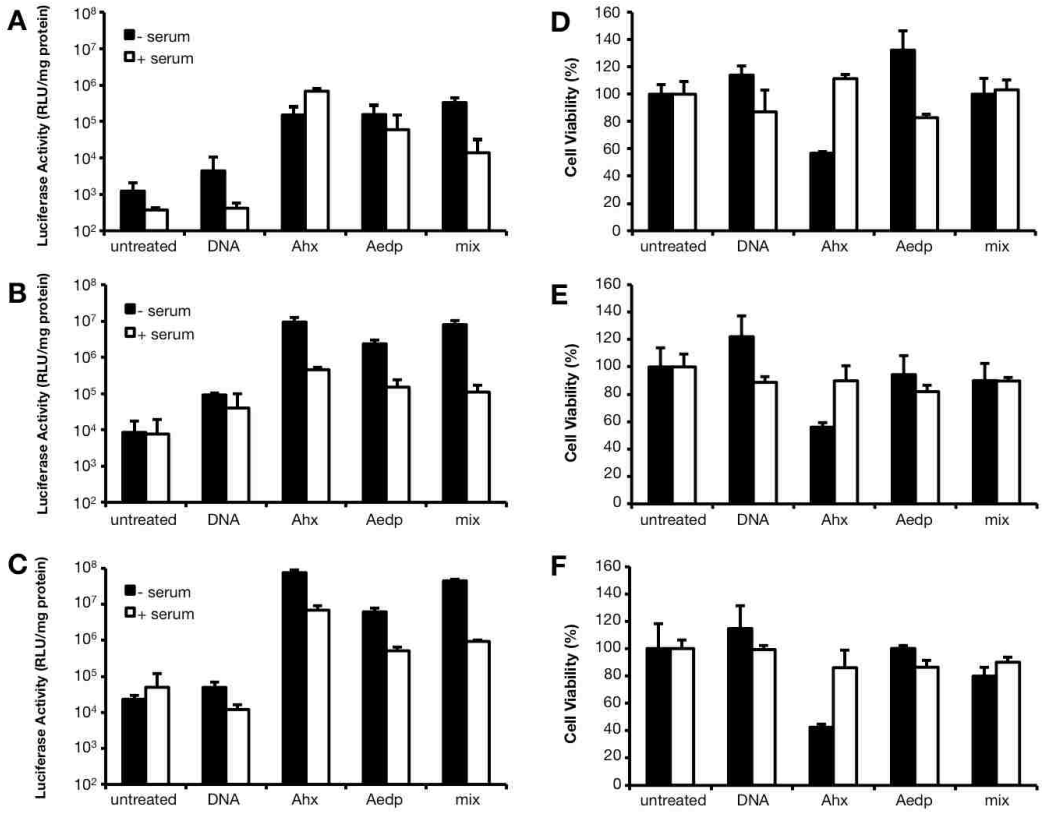

Figure 5.8: **Transfection efficiency and cell viability of HPMA-oligolysine copolymers in 3 cell types in serum-free and 10% serum media.** (A) NIH/3T3, (B) CHO-K1, and (C) HeLa cells were treated with polyplexes at N/P 5 in serum-free media or in 10% serum for 4 h. Luciferase activity was measured 48 h after transfection and normalized to total protein content in each sample. Toxicity of the polyplexes in (D) NIH/3T3, (E) CHO-K1, and (F) HeLa cells was determined by measuring total protein content and designating untreated cells as 100% viable. *Untreated*: untreated controls; *Ahx*: HPMA-AhxK$_{10}$; and *Aedp*: HPMA-AedpK$_{10}$. Data are presented as mean ± S.D., $n = 3$.

100% cell viability. The IC$_{50}$ values of both HPMA-AhxK$_{10}$ and HPMA-AedpK$_{10}$ copolymers were higher than both bPEI (IC$_{50}$ = 1.45-1.85 μg amine/mL) and PLL (~0.7 μg amine/mL) for all cell types tested (NIH/3T3, CHO-K1, HeLa) (Table 1). HPMA-AedpK$_{10}$ (13.0-20.2 μg lysine/mL) was slightly less toxic than HPMA-AhxK$_{10}$ (8.2-12.2 μg lysine/mL) for all cell types, and a mixture of the two copolymers in a 1:1 (w/w) ratio resulted in decreased toxicity in NIH/3T3 (12.2 μg lysine/mL) and CHO-K1 (10.5 μg lysine/mL) cells, but not in HeLa cells (12.3 μg lysine/mL). HPMA-AhxK$_{10}$ synthesized by free radical polymerization was more

toxic than HPMA-AhxK_{10} synthesized by RAFT polymerization in all cell types.

5.3.6 Cellular uptake and transfection of polyplexes incubated with DTNB

Redox proteins such as thioredoxin reductase and protein disulfide isomerase can reduce thiols at the cell surface [29, 30]; additionally, some cell types such as HeLa cells have been found to secrete thiols into the extracellular space [31]. To determine if the decrease in transfection efficiency in HeLa cells was due to the presence of extracellular thiols that may prematurely destabilize polyplexes, cells were pretreated with 5 mM 5,5-dithiobis-(2-nitrobenzoic acid) (DTNB), a cell-impermeable chemical that reacts with free thiols. Polyplexes of plasmid DNA labeled with TOTO-3 were then incubated with HeLa cells for 30 min with or without DTNB and cellular uptake was assessed by flow cytometry. Because the quantum yield of TOTO-3 in polyplexes is sensitive to the packaging state of the plasmid, the fluorescence of TOTO-3-labeled plasmid complexed with HPMA-AhxK_{10} and HPMA-AedpK_{10} was measured and confirmed to be similar in both formulations (Figure 5.9). Plasmid uptake was significantly lower from transfection with HPMA-AedpK_{10} polyplexes and mixed polyplexes compared to HPMA-AhxK_{10} polyplexes (Figure 5.10) although nearly all cells (97-99%) were positive for fluorescence (data not shown). When cells were treated with polyplexes in the presence of 5 mM DTNB, uptake of HPMA-AedpK_{10} polyplexes was still significantly less than uptake of its non-reducible analog; however, the decreased uptake was less drastic. Polyplexes of a 1:1 (w/w) mixture of the two polymers were taken up by cells more efficiently than reducible polymer alone. To confirm these results, transfection efficiency PLL, PEI, HPMA-AhxK_{10} and HPMA-AedpK_{10} to NIH/3T3, CHO-K1 and HeLa cells was also evaluated in the presence of DTNB. With DTNB treatment, transfection with the reducible material remained less efficient than with the non-reducible material in all cell types tested (Figure 5.11), demonstrating that blocking extracellular thiols does not restore transfection efficiency of the reducible material.

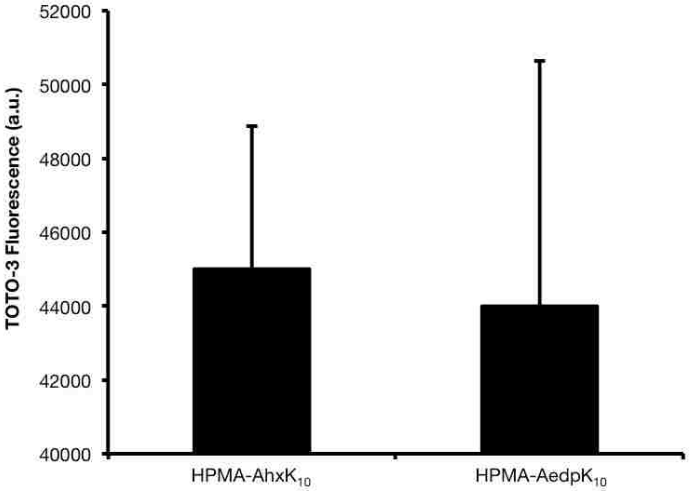

Figure 5.9: **TOTO-3 fluorescence of plasmid DNA complexed with HPMA copolymers.** Polyplexes of copolymer and TOTO-3 labeled plasmid DNA were formulated at N/P 5. TOTO-3 fluorescence was measured by excitation at 633 nm and emission at 670 nm. Data are presented as mean ± S.D., $n = 3$, (*) $p < 0.05$, as determined by two-tailed Student's t-test.

5.3.7 Delivery of plasmid DNA to cultured cells with EDTA treatment

Since reduced HPMA-AedpK$_{10}$ was shown to crosslink in the absence of EDTA (Figure 5.2B), we investigated the possibility that polymer oxidation by trace metals adversely affected transfection efficiency of these materials. To minimize metal-catalyzed redox/oxidation processes, cells were transfected with polyplexes in the presence of 1 mM EDTA. Again, HPMA-AedpK$_{10}$ showed diminished ability to transfect NIH/3T3 and HeLa cells (Figure 5.12). However, the difference in transfection efficiency between HPMA-AhxK$_{10}$ and HPMA-AedpK$_{10}$ was much less when transfections were conducted with 1 mM EDTA. In the absence of EDTA, luciferase expression in HPMA-AedpK$_{10}$-transfected cells was 193-fold, 14-fold, and 17-fold lower than HPMA-AhxK$_{10}$-transfected cells in HeLa, NIH/3T3, and CHO-K1 cells, respectively. However, with only 1 mM EDTA, luciferase expression in HPMA-AedpK$_{10}$-transfected cells was 9-fold, 4.8-fold, and 0.6-fold lower than HPMA-AhxK$_{10}$-transfected cells in HeLa, NIH/3T3, and CHO-K1 cells, respectively. In addition, the mixed copolymer formulation restored transfection efficiency to the efficiency levels of HPMA-AhxK$_{10}$.

5.4 Discussion

The incorporation of reducible moieties into cationic polymers for nucleic acid delivery has been shown as a viable method for introducing environmentally-responsive degradability.

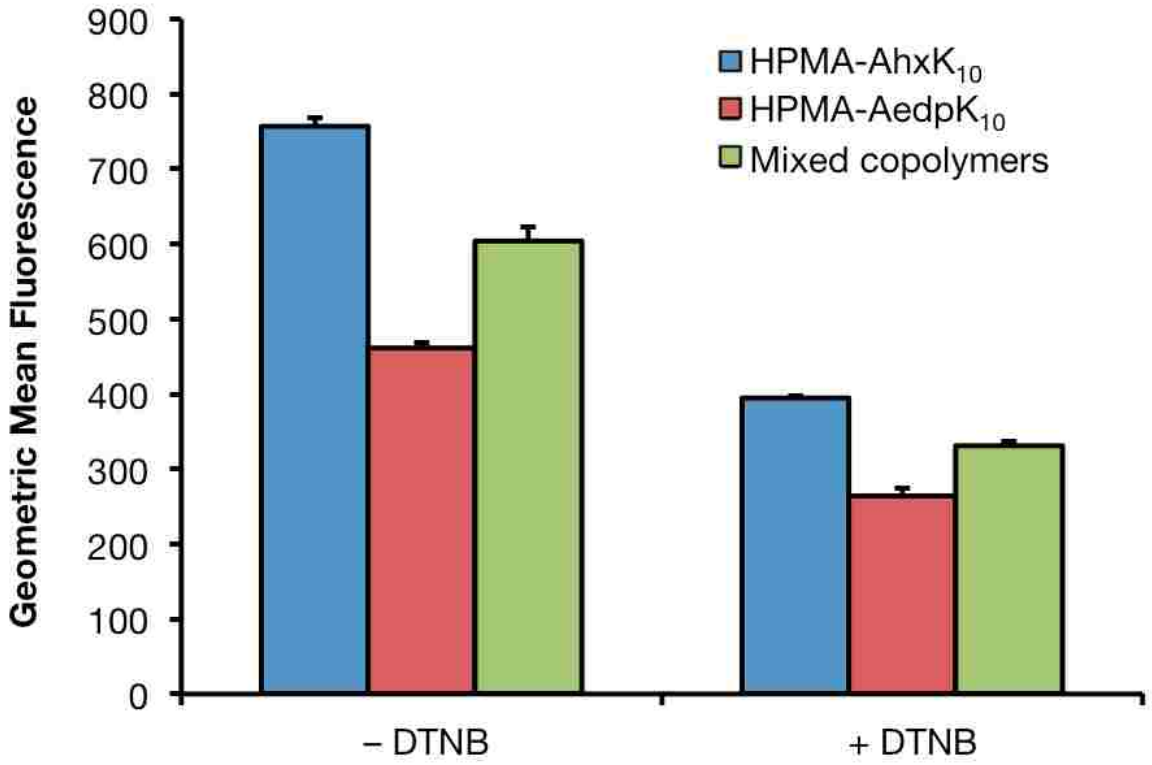

Figure 5.10: **Uptake of polyplexes in HeLa cells treated with DTNB.** Luciferase plasmid DNA was labeled with TOTO-3 prior to complexation with HPMA copolymers (HPMA-AhxK$_{10}$, HPMA-AedpK$_{10}$, or a 1:1 (w/w) mixture). HeLa cells pretreated with or without 5 mM DTNB in serum-free media for 1 h prior to transfection and then incubated with polyplexes for 30 min in serum-free media with or without 5 mM DTNB. Polyplex uptake was assessed by flow cytometry. DTNB stands for 5,5-dithiobis-(2-nitrobenzoic acid). Data are presented as mean ± S.D., $n = 3$, (*) $p < 0.05$, as determined by two-tailed Student's t-test.

In particular, use of disulfide bonds is attractive because of their relative stability in the extracellular environment; however, disulfide bonds can be destabilized in the presence of high concentrations of reductive intracellular agents, *e.g.* glutathione, which is 50-1000 times (in human liver, up to 10 mM) more concentrated in the cytosol than in the extracellular space [32]. We hypothesized that incorporating a disulfide linkage between the pendant oligolysine peptides and the HPMA backbone would facilitate the release of DNA from polyplexes while also limiting toxicity of the cationic polymer. We have previously

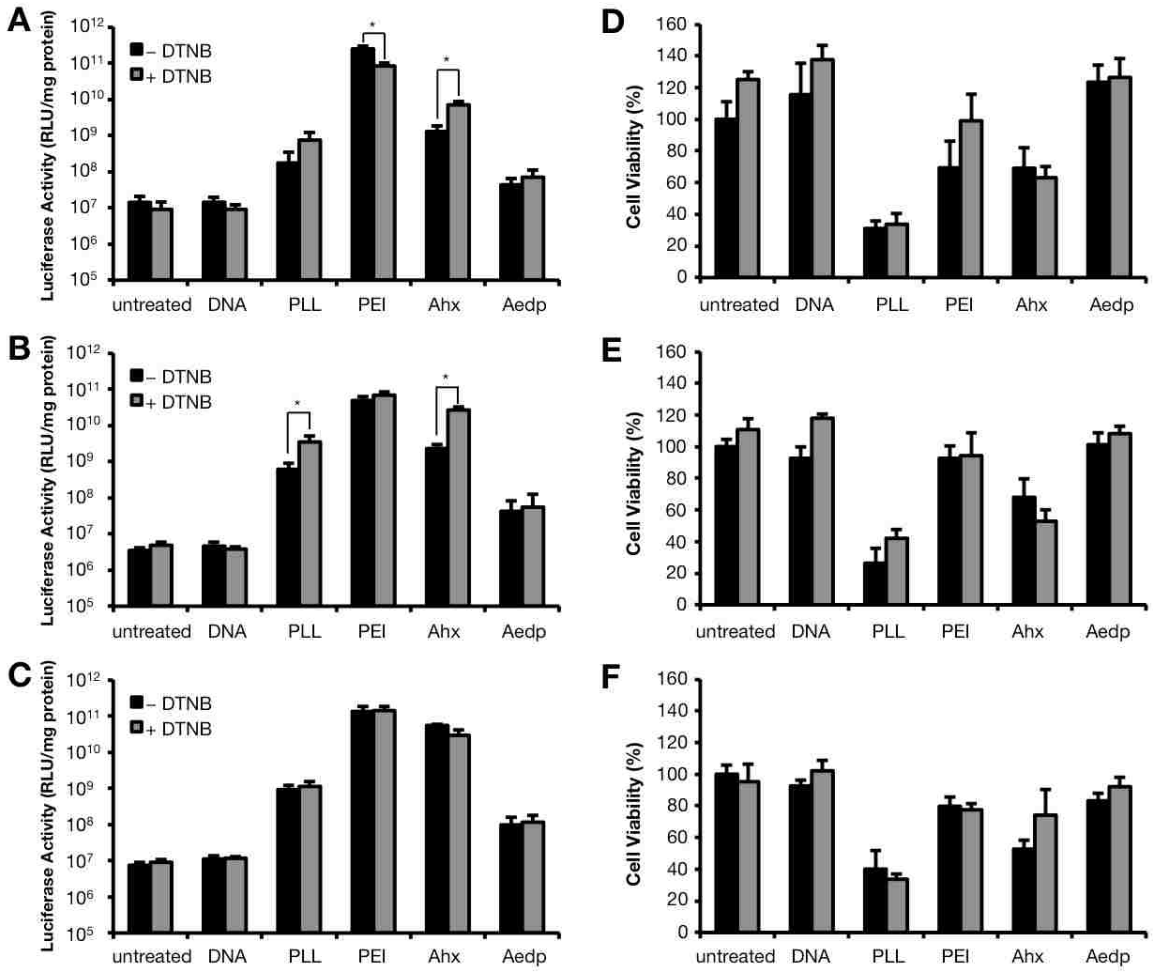

Figure 5.11: **Transfection efficiency and cell viability of cells treated with DTNB.** (A) NIH/3T3, (B) CHO-K1, and (C) HeLa cells were pretreated with or without 5 mM DTNB in serum-free media for 1 h prior to transfection. Polyplexes (N/P 5) of copolymer and luciferase-encoding plasmid DNA were incubated with cells for 4 h in serum-free media with 5 mM DTNB. Luciferase activity was measured 48 h after transfection and normalized to total protein content in each sample. Toxicity of the polyplexes in (D) NIH/3T3, (E) CHO-K1, and (F) HeLa cells was determined by measuring total protein content and designating untreated cells as 100% viable. *Cells*: untreated controls; *PEI*: branched polyethylenimine (25 kD); *PLL*: poly-L-lysine (12-24 kD); *Ahx*: HPMA-AhxK_{10}; *Aedp*: HPMA-AedpK_{10}. DTNB stands for 5,5-dithiobis-(2-nitrobenzoic acid). Data are presented as mean ± S.D., $n = 4$, (*) $p < 0.05$, as determined by two-tailed Student's t-test.

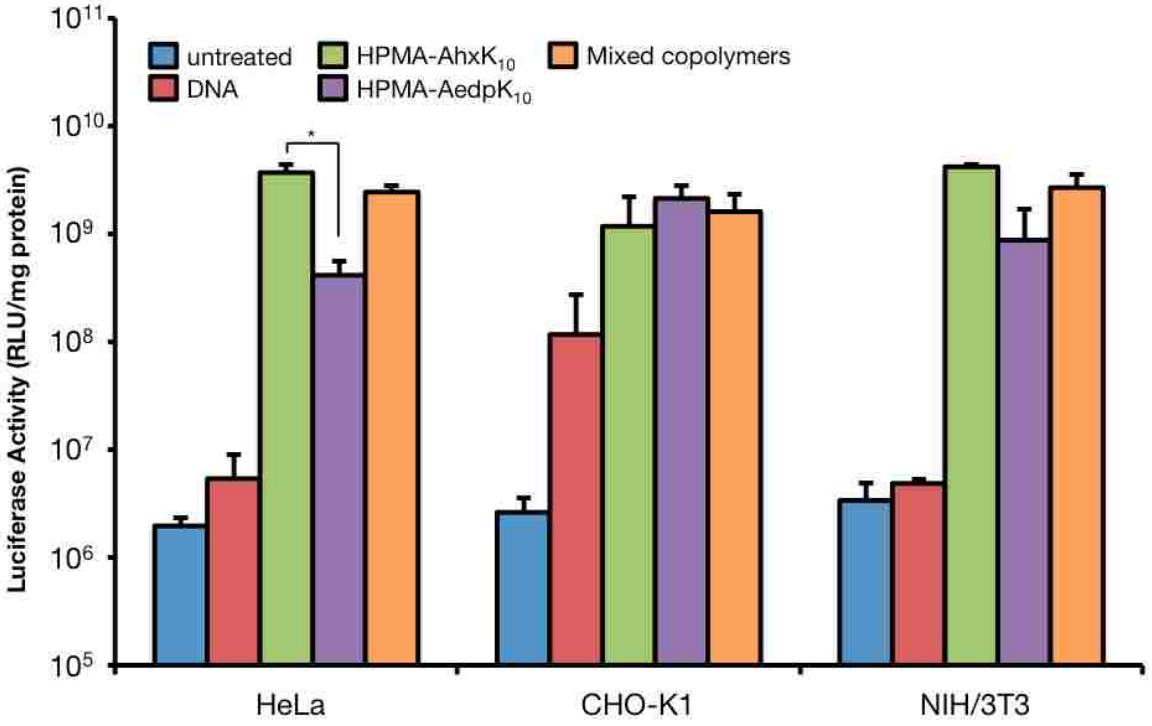

Figure 5.12: **Transfection efficiency of HPMA copolymers in HeLa, CHO-K1, and NIH/3T3 in the presence of 1 mM EDTA.** Polyplexes (N/P 5) of copolymer and luciferase-encoding plasmid DNA were incubated with cells for 4 h with 1 mM EDTA in serum-free conditions. Luciferase activity was measured 48 h after transfection and normalized to total protein content in each sample. *Untreated*: untreated controls; *Mixed copolymers*: 1:1 (w/w) mixture of HPMA-$AhxK_{10}$ and HPMA-$AedpK_{10}$. Data are presented as mean ± S.D., $n = 3$, (*) $p < 0.05$, as determined by two-tailed Student's t-test.

demonstrated that monomers of HPMA and oligolysine bearing an AEDP linker can be copolymerized *via* free radical polymerization, and that these copolymers were less toxic than their non-reducible counterpart [21]. Here, reducible and non-reducible analogues of HPMA-oligolysine copolymers were synthesized by RAFT polymerization. The resulting two polymers had similar molecular weights and peptide compositions. Surprisingly, aside from reduced cytotoxicity, the reducible HPMA-$AedpK_{10}$ polymer showed less attractive plasmid delivery properties compared to the non-reducible HPMA-$AhxK_{10}$ polymer. Specifically, polyplexes formed from HPMA-$AedpK_{10}$ were less salt stable, facilitated less plasmid uptake, and provided lower transfection efficiencies to three cultured cell lines.

First, HPMA-AhxK_{10} polymers synthesized by both free radical and RAFT polymerization were directly compared. RAFT polymerized polymers had controlled composition and molecular weight (19.6% K_{10} monomer incorporation, 77.6 kD) and were more homogenous, with polydispersities of 1.1-1.2 (Table 5.1). In contrast, HPMA-AhxK_{10} synthesized *via* free radical polymerization had low incorporation of K_{10} monomer (12%), high molecular weight (168.4 kD), and high polydispersity (2.2). Previous reports of polymers synthesized by free radical polymerization show similarly polydisperse materials [21, 33]. The transfection efficiency of these polymers were evaluated at N/P 3, 5, and 10 in HeLa cells using the target mass to charge ratios to calculate N/P ratios (Figure 5.5). Both polymers had similar transfection efficiencies; however, the IC_{50} values for the free radical polymer were much lower than those for the RAFT polymer. We have previously shown that cytotoxicity of HPMA-*co*-oligolysine polymers increases with increasing molecular weight [27]. The high molecular weight fraction of the polydisperse HPMA-AhxK_{10} synthesized *via* free radical polymerization is likely responsible for the observed toxicity. Therefore, HPMA-AhxK_{10} synthesized by RAFT polymerization results in more controlled and well-defined polymers with reduced cytotoxicity.

The ability for polyplexes to remain stable in physiological salt conditions is an important attribute for systemic delivery. We showed both previously and in this manuscript that polyplexes formulated with HPMA-AhxK_{10} are salt stable (Figure 5.3). Salt-induced increases in the particle size of polyplexes results from a disruption of the electrical double layer caused by the addition of counter ions. Several studies have demonstrated that incorporation of a hydrophilic but uncharged polymer, such as PEG, prevents flocculation through steric repulsion even after the electrical double layer has been disrupted by salts [34]. In this context, HPMA monomers were included as the backbone of both HPMA-AedpK_{10} and HPMA-AhxK_{10} copolymers to stabilize polyplexes in physiological conditions. However, polyplexes formed in the presence of 10% serum increased in size to > 500 nm regardless of polymer type and composition. Despite this increase in size, polyplexes in the presence of serum remain intact. Gel electrophoresis of polyplexes confirm that polyplexes were retained in the well, unlike free DNA that migrated and was degraded in the presence of serum (Figure 5.4). However, the fluorescence intensity of polplexes in the well increased

with increasing serum content. Since the YOYO-1 intercalating dye is quenched by intermolecular electronic interactions when plasmid DNA is condensed, this indicates that the polyplexes are loosened in the presence of serum. Interestingly, increasing N/P ratios resulted in the largest effective diameters, possibly due to interaction between excess polymer and serum proteins (Figure 5.3). Reduced transfection efficiency of these polymers in serum (Figure 5.8A-C) may be due to the inability of the excess polymer to mediate transfection, which has been shown to be important for efficient transfection [35, 36]. Polyplex toxicity was also reduced under serum conditions (Figure 5.8C-F), which further suggests that free polymer may be neutralized by serum proteins.

Multiple groups have reported that the incorporation of disulfide linkages does not affect polyplex stability in salt [8]. However, unlike HPMA-AhxK$_{10}$ polyplexes, polyplexes formed with HPMA-AedpK$_{10}$ were not salt stable. Particle size of the polyplexes increased from relatively small particles that were below 100 nm in water to particles with much larger effective diameters (Figure 5.3). Differences in stability between HPMA-AedpK$_{10}$ and HPMA-AhxK$_{10}$ polyplexes may be attributed to the increased concentration of disulfide bonds [37]. The more hydrophobic HPMA-AedpK$_{10}$ polymers may render the resulting polyplex more prone to flocculation from van der Waals attraction forces. Salt-induced flocculation of polyplexes formulated with HPMA-AedpK$_{10}$ copolymers may also indicate premature degradation of disulfide bonds in the AEDP linkers leading to intermolecular crosslinking or even loss of HPMA from the polyplex surface. Degradation of disulfide bonds can spontaneously occur through direct attack of the disulfide bond by hydroxyl anions or by α- and β-elimination reactions at neutral and basic conditions [38]. Also, it has been shown that spontaneous reduction of a single disulfide bond in proteins with several disulfide bonds can trigger other intermolecular reducing reactions, disrupting protein stability [39, 40]. In a similar manner, degradation of a disulfide bond in a polyplex formulated with HPMA-AedpK$_{10}$ copolymers could potentially lead to a chain-reduction of proximal disulfide bonds, which would have high local concentrations within a polyplex. Pichon and coworkers showed by TEM using their disulfide bond-containing poly[Lys-AEDTP] materials that particle fusion, hypothesized to result from intermolecular crosslinking, occurs quickly after polymer reduction followed by polyplex decomplexation [41]. However, it

should be noted that with our materials, particle flocculation in salt was not mitigated by addition of EDTA to prevent metal-catalyzed oxidation.

Polyplexes of the reducible polymer HPMA-AedpK$_{10}$ did not transfect cells as well as its non-reducible analog, HPMA-AhxK$_{10}$, but transfected similarly to PLL (Figure 5.7A). However, the reducible polymer was relatively non-toxic compared to the non-reducible polymer in HeLa and CHO-K1 cells, and PLL in all cell types tested (Figure 5.7B). These results show that the toxicity profile of the HPMA-oligolysine is improved by incorporating a disulfide linkage. At higher N/P ratios transfection efficiency with HPMA-AedpK$_{10}$ materials can approach that of HPMA-AhxK$_{10}$ (Figure 5.6). Increases of transfection at elevated charge ratios have been attributed to increased concentrations of free cationic polymer by promoting release of polyplexes from the endosomes and lysosomes [35].

Previous reports have identified that extracellular reduction can affect the uptake of disulfide-containing cationic peptides [42] or polymers [31]. To investigate if decreased transfection efficiency of HPMA-AedpK$_{10}$ was due to premature extracellular reduction, cellular uptake of HPMA-AhxK$_{10}$ and HPMA-AedpK$_{10}$ polyplexes in HeLa cells in the presence of the cell-impermeable reagent DTNB was assessed by flow cytometry. DTNB has been used previously to block reductive effects of free extracellular thiols [6]. Cellular uptake of polyplexes formulated with HPMA-AhxK$_{10}$, HPMA-AedpK$_{10}$, or a 1:1 (w/w) mixture of both copolymers reflected similar trends to those observed in transfection studies (Figure 5.10). DTNB treatment reduced uptake of all polyplexes, but showed similar trends as the uptake study completed without DTNB. Similarly, transfection with HPMA-AedpK$_{10}$ polyplexes did not improve with DTNB (Figure 5.11). These results suggest that extracellular reduction of HPMA-AedpK$_{10}$ by free thiols is not the major cause of decreased cellular uptake of the reducible polyplexes, and decreased cellular uptake may be caused by an alternative mechanism.

In instances where HPMA-AedpK$_{10}$ was dissolved as a stock solution and then stored at 4 °C for longer than 2 weeks, a higher molecular weight fraction was observed by GPC analysis (data not shown). A similar observation was also made when degradation studies using 25 mM TCEP to reduce HPMA-AedpK$_{10}$ copolymer was done without EDTA. These observations indicate that metal-catalyzed oxidation of free sulfhydryls influences the material

properties through nonspecific crosslinking of HPMA-AedpK_{10} copolymers. To control the effects of metal-catalyzed oxidation of free sulhydryl groups, transfections were done with fresh stock solutions of HMPA-AedpK_{10} and transfections were also done in the presence of EDTA. Treatment of cells with EDTA increased transfections in some instances (Figure 5.12). One possible explanation is that oxidation of degraded HPMA-AedpK_{10} copolymers could effectively cage proximal DNA, preventing its release from the polyplex and thereby limit the transfection efficiency of the materials. A study by Christensen and coworkers also demonstrated that diminished transfection efficiency of poly(amido ethyleneamine) that correlated with increased branching and disulfide content [43]. Furthermore, Miyata and coworkers also demonstrated that diminished transfection efficiency was observed at elevated disulfide crosslinkers in reducible PLL-PEI materials [37]. It may also be possible to achieve higher transfection efficiencies at higher N/P ratios. Wang and coworkers show that reducible linear cationic polymers prepared by click chemistry transfected better than their non-reducible counterparts, but at N/P ratios of 15 and higher [44]. Similar trends were observed for other polymer systems [25, 45]. For most practical applications in nucleic acid delivery, use of reducible materials requires greater stability that that presented by HPMA-AedpK_{10}. Improvements in polyplex stability were observed when mixtures of reducing and non-reducing HPMA-oligolysine copolymers were used. The polyplexes demonstrated improved salt stability, increased transfection efficiency, and were non-toxic at charge ratios tested. This formulation may prevent premature reduction of disulfide bonds and limit unwanted oxidation from occurring by spatial separation and/or steric hindrance. Alternatively, disulfide linkages have been stabilized by adding methyl groups [46] and/or benzene rings [45] around the disulfide bond in order to sterically hinder premature reduction before reaching the cytosol.

In summary, we describe the controlled synthesis of a reducible HPMA-oligolysine copolymer and evaluate the transfection efficiency of this polymer and its non-reducible counterpart in multiple cell lines. The reducible polymer was tolerated better than the non-reducible polymer but also showed lower transfection efficiency in cultured cells. Elimination of extracellular thiols did not restore transfection efficiency, indicating that premature extracellular reduction is not the primary cause of decreased transfection. However, stability of the

reducible polymer was improved with the addition of EDTA. In addition, a mixed formulation of reducible and non-reducible copolymers was able to partially restore transfection efficiency over that of the reducible polymer alone and maintain low toxicity. Chemical modifications to stabilize the disulfide bond may be explored to apply this polymer system *in vivo*.

5.5 Acknowledgments

This work is supported by NIH 1R01NS064404 and the Center for Intracellular Delivery of Biologics through the Washington State Life Sciences Discovery Fund Grant No. 2496490. J.S. is supported by the National Science Foundation Graduate Research Fellowship under Grant No. DGE-0718124. We gratefully thank Profs. Anthony Convertine and Patrick Stayton for generously providing the ECT chain transfer agent and Dr. Ester Kwon for preparing the pCMV-Luc2 plasmid.

References

[1] Tang, R., Palumbo, R. N., Nagarajan, L., Krogstad, E., and Wang, C. (2010) Well-defined block copolymers for gene delivery to dendritic cells: probing the effect of polycation chain-length. *J. Control. Release*, **142**, 229–237.

[2] Schaffer, D. V., Fidelman, N. A., Dan, N., and Lauffenburger, D. A. (2000) Vector unpacking as a potential barrier for receptor-mediated polyplex gene delivery. *Biotechnol. Bioeng.*, **67**, 598–606.

[3] de Wolf, H. K., de Raad, M., Snel, C., van Steenbergen, M. J., Fens, M. H. A. M., Storm, G., and Hennink, W. E. (2007) Biodegradable poly(2-dimethylamino ethylamino)phosphazene for in vivo gene delivery to tumor cells. Effect of polymer molecular weight. *Pharm. Res.*, **24**, 1572–1580.

[4] Fischer, D., Li, Y., Ahlemeyer, B., Krieglstein, J., and Kissel, T. (2003) In vitro cytotoxicity testing of polycations: influence of polymer structure on cell viability and hemolysis. *Biomaterials*, **24**, 1121–1131.

[5] Hwang, S. and Davis, M. E. (2001) Cationic polymers for gene delivery: Designs for overcoming barriers to systemic administration. *Current Opinion in Molecular Therapeutics*, **3**, 183–191.

[6] Bauhuber, S., Hozsa, C., Breunig, M., and Göpferich, A. (2009) Delivery of nucleic acids via disulfide-based carrier systems. *Adv. Mater. Weinheim*, **21**, 3286–3306.

[7] Ganta, S., Devalapally, H., Shahiwala, A., and Amiji, M. (2008) A review of stimuli-responsive nanocarriers for drug and gene delivery. *J. Control. Release*, **126**, 187–204.

[8] Ouyang, D., Shah, N., Zhang, H., Smith, S. C., and Parekh, H. S. (2009) Reducible disulfide-based non-viral gene delivery systems. *Mini Rev Med Chem*, **9**, 1242–1250.

[9] McKenzie, D. L., Smiley, E., Kwok, K. Y., and Rice, K. G. (2000) Low molecular weight disulfide cross-linking peptides as nonviral gene delivery carriers. *Bioconjug. Chem.*, **11**, 901–909.

[10] McKenzie, D. L., Kwok, K. Y., and Rice, K. G. (2000) A potent new class of reductively activated peptide gene delivery agents. *J. Biol. Chem.*, **275**, 9970–9977.

[11] Trubetskoy, V. S., Loomis, A., Slattum, P. M., Hagstrom, J. E., Budker, V. G., and Wolff, J. A. (1999) Caged DNA does not aggregate in high ionic strength solutions. *Bioconjug. Chem.*, **10**, 624–628.

[12] Breunig, M., Lungwitz, U., Liebl, R., Klar, J., Obermayer, B., Blunk, T., and Goepferich, A. (2007) Mechanistic insights into linear polyethylenimine-mediated gene transfer. *Biochim. Biophys. Acta*, **1770**, 196–205.

[13] Choi, S. and Lee, K.-D. (2008) Enhanced gene delivery using disulfide-crosslinked low molecular weight polyethylenimine with listeriolysin o-polyethylenimine disulfide conjugate. *J. Control. Release*, **131**, 70–76.

[14] Deng, R., Yue, Y., Jin, F., Chen, Y., Kung, H.-F., Lin, M. C. M., and Wu, C. (2009) Revisit the complexation of PEI and DNA — How to make low cytotoxic and highly efficient PEI gene transfection non-viral vectors with a controllable chain length and structure? *J. Control. Release*, **140**, 40–46.

[15] Gosselin, M. A., Guo, W., and Lee, R. J. (2001) Efficient gene transfer using reversibly cross-linked low molecular weight polyethylenimine. *Bioconjug. Chem.*, **12**, 989–994.

[16] Kloeckner, J., Wagner, E., and Ogris, M. (2006) Degradable gene carriers based on oligomerized polyamines. *Eur. J. Pharm. Sci.*, **29**, 414–425.

[17] Liu, J., Jiang, X., Xu, L., Wang, X., Hennink, W. E., and Zhuo, R. (2010) Novel reduction-responsive cross-linked polyethylenimine derivatives by click chemistry for nonviral gene delivery. *Bioconjug. Chem.*, **21**, 1827–1835.

[18] Neu, M., Sitterberg, J., Bakowsky, U., and Kissel, T. (2006) Stabilized nanocarriers for plasmids based upon cross-linked poly(ethylene imine). *Biomacromolecules*, **7**, 3428–3438.

[19] Peng, Q., Zhong, Z., and Zhuo, R. (2008) Disulfide cross-linked polyethylenimines (PEI) prepared via thiolation of low molecular weight PEI as highly efficient gene vectors. *Bioconjug. Chem.*, **19**, 499–506.

[20] Wang, Y., Chen, P., and Shen, J. (2006) The development and characterization of a glutathione-sensitive cross-linked polyethylenimine gene vector. *Biomaterials*, **27**, 5292–5298.

[21] Burke, R. S. and Pun, S. H. (2010) Synthesis and characterization of biodegradable HPMA-oligolysine copolymers for improved gene delivery. *Bioconjug. Chem.*, **21**, 140–150.

[22] Chen, J., Wu, C., and Oupický, D. (2009) Bioreducible hyperbranched poly(amido amine)s for gene delivery. *Biomacromolecules*, **10**, 2921–2927.

[23] Dai, F., Sun, P., Liu, Y., and Liu, W. (2010) Redox-cleavable star cationic PDMAEMA by arm-first approach of ATRP as a nonviral vector for gene delivery. *Biomaterials*, **31**, 559–569.

[24] Lin, C., Zhong, Z., Lok, M. C., Jiang, X., Hennink, W. E., Feijen, J., and Engbersen, J. F. J. (2006) Linear poly(amido amine)s with secondary and tertiary amino groups and variable amounts of disulfide linkages: synthesis and in vitro gene transfer properties. *J. Control. Release*, **116**, 130–137.

[25] Ou, M., Wang, X.-L., Xu, R., Chang, C.-W., Bull, D. A., and Kim, S. W. (2008) Novel biodegradable poly(disulfide amine)s for gene delivery with high efficiency and low cytotoxicity. *Bioconjug. Chem.*, **19**, 626–633.

[26] Johnson, R. N., Burke, R. S., Convertine, A. J., Hoffman, A. S., Stayton, P. S., and Pun, S. H. (2010) Synthesis of statistical copolymers containing multiple functional peptides for nucleic acid delivery. *Biomacromolecules*, **11**, 3007–3013.

[27] Johnson, R. N., Chu, D. S. H., Shi, J., Schellinger, J. G., Carlson, P. M., and Pun, S. H. (2011) HPMA-oligolysine copolymers for gene delivery: optimization of peptide length and polymer molecular weight. *J. Control. Release*, **155**, 303–311.

[28] Convertine, A. J., Benoit, D. S. W., Duvall, C. L., Hoffman, A. S., and Stayton, P. S. (2009) Development of a novel endosomolytic diblock copolymer for siRNA delivery. *J. Control. Release*, **133**, 221–229.

[29] Mandel, R., Ryser, H. J., Ghani, F., Wu, M., and Peak, D. (1993) Inhibition of a reductive function of the plasma membrane by bacitracin and antibodies against protein disulfide-isomerase. *Proc. Natl. Acad. Sci. U.S.A.*, **90**, 4112–4116.

[30] Rubartelli, A., Bajetto, A., Allavena, G., Wollman, E., and Sitia, R. (1992) Secretion of thioredoxin by normal and neoplastic cells through a leaderless secretory pathway. *J. Biol. Chem.*, **267**, 24161–24164.

[31] Sun, W. and Davis, P. B. (2010) Reducible DNA nanoparticles enhance in vitro gene transfer via an extracellular mechanism. *J. Control. Release*, **146**, 118–127.

[32] Meister, A. and Anderson, M. E. (1983) Glutathione. *Annu. Rev. Biochem.*, **52**, 711–760.

[33] Layman, J. M., Ramirez, S. M., Green, M. D., and Long, T. E. (2009) Influence of polycation molecular weight on poly(2-dimethylaminoethyl methacrylate)-mediated DNA delivery in vitro. *Biomacromolecules*, **10**, 1244–1252.

[34] Oupický, D., Parker, A. L., and Seymour, L. W. (2002) Laterally stabilized complexes of DNA with linear reducible polycations: strategy for triggered intracellular activation of DNA delivery vectors. *J. Am. Chem. Soc.*, **124**, 8–9.

[35] Thibault, M., Astolfi, M., Tran-Khanh, N., Lavertu, M., Darras, V., Merzouki, A., and Buschmann, M. D. (2011) Excess polycation mediates efficient chitosan-based gene transfer by promoting lysosomal release of the polyplexes. *Biomaterials*.

[36] Boeckle, S., von Gersdorff, K., van der Piepen, S., Culmsee, C., Wagner, E., and Ogris, M. (2004) Purification of polyethylenimine polyplexes highlights the role of free polycations in gene transfer. *J. Gene Med.*, **6**, 1102–1111.

[37] Miyata, K., Kakizawa, Y., Nishiyama, N., Harada, A., Yamasaki, Y., Koyama, H., and Kataoka, K. (2004) Block catiomer polyplexes with regulated densities of charge and disulfide cross-linking directed to enhance gene expression. *J. Am. Chem. Soc.*, **126**, 2355–2361.

[38] Trivedi, M. V., Laurence, J. S., and Siahaan, T. J. (2009) The role of thiols and disulfides on protein stability. *Curr. Protein Pept. Sci.*, **10**, 614–625.

[39] Kelly, S. T. and Zydney, A. L. (1994) Effects of intermolecular thiol-disulfide interchange reactions on bsa fouling during microfiltration. *Biotechnol. Bioeng.*, **44**, 972–982.

[40] Tous, G. I., Wei, Z., Feng, J., Bilbulian, S., Bowen, S., Smith, J., Strouse, R., McGeehan, P., Casas-Finet, J., and Schenerman, M. A. (2005) Characterization of a novel modification to monoclonal antibodies: thioether cross-link of heavy and light chains. *Anal. Chem.*, **77**, 2675–2682.

[41] Pichon, C., LeCam, E., Guérin, B., Coulaud, D., Delain, E., and Midoux, P. (2002) Poly[Lys-(AEDTP)]: a cationic polymer that allows dissociation of pDNA/cationic polymer complexes in a reductive medium and enhances polyfection. *Bioconjug. Chem.*, **13**, 76–82.

[42] Aubry, S., Burlina, F., Dupont, E., Delaroche, D., Joliot, A., Lavielle, S., Chassaing, G., and Sagan, S. (2009) Cell-surface thiols affect cell entry of disulfide-conjugated peptides. *FASEB J.*, **23**, 2956–2967.

[43] Christensen, L. V., Chang, C.-W., Kim, W. J., Kim, S. W., Zhong, Z., Lin, C., Engbersen, J. F. J., and Feijen, J. (2006) Reducible poly(amido ethylenimine)s designed for triggered intracellular gene delivery. *Bioconjug. Chem.*, **17**, 1233–1240.

[44] Wang, Y., Zhang, R., Xu, N., Du, F.-S., Wang, Y.-L., Tan, Y.-X., Ji, S.-P., Liang, D.-H., and Li, Z.-C. (2011) Reduction-Degradable Linear Cationic Polymers as Gene Carriers Prepared by Cu(I)-Catalyzed Azide-Alkyne Cycloaddition. *Biomacromolecules*, **12**, 66–74.

[45] Son, S., Singha, K., and Kim, W. J. (2010) Bioreducible BPEI-SS-PEG-cNGR polymer as a tumor targeted nonviral gene carrier. *Biomaterials*, **31**, 6344–6354.

[46] Kellogg, B. A., et al. (2011) Disulfide-linked antibody-maytansinoid conjugates: optimization of in vivo activity by varying the steric hindrance at carbon atoms adjacent to the disulfide linkage. *Bioconjug. Chem.*, **22**, 717–727.

Chapter 6

INFLUENCE OF HISTIDINE INCORPORATION ON BUFFER CAPACITY AND GENE TRANSFECTION EFFICIENCY OF HPMA-*CO*-OLIGOLYSINE BRUSH POLYMERS

Julie Shi, Joan G. Schellinger, Russell N. Johnson, Jennifer L. Choi, Brian Chou, Ersilia L. Anghel, and Suzie H. Pun

Abstract

One of the major intracellular barriers to non-viral gene delivery is efficient endosomal escape. The incorporation of histidine residues into polymeric constructs has been found to increase endosomal escape *via* the proton sponge effect. Statistical and diblock copolymers of *N*-(2-hydroxypropyl)methacrylamide (HPMA), oligolysine, and oligohistidine were synthesized *via* reversible-addition fragmentation chain transfer (RAFT) polymerization, and tested for *in vitro* transfection efficiency, buffering ability, and polyplex uptake mechanism *via* the use of chemical endocytic inhibitors. Interestingly, histidine-containing statistical and diblock polymers exhibited increased buffer capacity in different endosomal pH ranges. Statistical copolymers transfected better than block copolymers that contained similar amounts of histidine. In addition, only the polymer containing the highest incorporation of oligohistidine residues led to increases in transfection efficiency over the HPMA-oligolysine base polymer. Thus, for these polymer architectures, high histidine incorporation may be required for efficient endosomal escape. Furthermore, uptake studies indicate that non-acidified caveolae-mediated endocytosis may be the primary route of transfection for these copolymers, suggesting that alternative approaches for increasing endosomal escape may be beneficial for enhancing transfection efficiency with these HPMA-oligolysine copolymers.[1]

---

[1]Reproduced with permission from Shi, J., *et al. Biomacromolecules*, **14**, 1961-70.

6.1 Introduction

Non-viral vectors, such as lipids and polymers, have been used frequently for the delivery of nucleic acids because of their ease of use *in vitro* and improved safety profiles *in vivo* over viral vectors [1]. However, transfection efficiencies from these systems are generally lower than their viral counterparts. Non-viral vectors have achieved limited success in gene delivery because of multiple intracellular barriers [1, 2]. In particular, one of the major barriers to efficient non-viral gene delivery is trapping of internalized particles in endo/lysosomal compartments [3, 4]. One proposed mechanism for endosomal release of polymers is the proton sponge effect whereby polymers that buffer within the pH range of 5-7 facilitate an osmotic swelling of endosomes that leads to content release [5]. A commonly used cationic polymer, branched polyethylenimine (bPEI), is composed of repeating monomers containing weakly basic amines to facilitate the proton sponge effect. PEI is hypothesized to achieve high transfection efficiencies due to its ability to escape endosomal compartments [6].

Several reports have studied the use of histidine-based materials as gene carriers since the imidazole ring is a weak base with pK_a ~6 [7, 8]. These studies have shown that the incorporation of histidine into polymeric gene delivery vehicles increases the endosomal buffering capacity of the polymer, improving the efficiency of endosomal escape [9, 10]. For example, poly(L-lysine) (PLL) grafted with 18-mer of poly(L-histidine) residues resulted in increased transfection efficiency over PLL alone [11]. Branched polymers consisting of a lysine core and lysine-histidine peptide branches also showed increased transfection efficiency with higher histidine content [12]. Other chemical gene delivery vectors modified with histidine or imidazole have been extensively reviewed elsewhere [8].

We have previously shown that statistical copolymers of *N*-(2-hydroxypropyl)methacrylamide (HPMA), oligo(L-lysine), and oligo(L-histidine) can be synthesized *via* reversible addition-fragmentation chain transfer (RAFT) polymerization [13]. The use of living radical polymerization techniques, such as RAFT polymerization, has been gaining in popularity in gene transfer applications due to the ability to synthesize narrowly-disperse, well-defined polymers [14, 15]. Recently, optimized formulations of HPMA-oligolysine copolymers showed transfection efficiencies almost as high as those of bPEI even though the HPMA

copolymers did not contain a moiety for endosomal escape [16].

Previous reports have demonstrated that various polymer architectures significantly affect transfection efficiency and cellular toxicity [17–20]. The objective of this study is to further improve the gene delivery ability of HPMA-oligolysine copolymers through the incorporation of histidine moieties. In this work, several statistical or block brush-like copolymers were synthesized with varying percentages of histidine-containing peptides. Evaluation of these materials included investigation of buffering capacity, mechanism of cellular uptake and transfection efficiency, and toxicity profiles to cultured cells.

6.2 Materials and methods

6.2.1 Materials

N-(2-hydroxypropyl)methacrylamide (HPMA) was purchased from Polysciences (Warrington, PA). The initiator VA-044 was purchased from Wako Chemicals USA (Richmond, VA). Chain transfer agent ethyl cyanovaleric trithiocarbonate (ECT) was a generous gift from Dr. Anthony Convertine (University of Washington). Rink amide resin was purchased from Merck Chemical Int. (Darmstadt, Germany). HBTU, Fmoc-protected lysine, and Trt-protected histidine were purchased from Aapptec (Louisville, KY). All cell culture reagents were purchased from Cellgro/Mediatech (Fisher Scientific, Pittsburgh, PA). All other materials, including poly(ethylenimine) (PEI, 25,000 g/mol, branched), poly(L-lysine) (PLL, 12,000 24,000 g/mol), chlorpromazine hydrochloride, genistein (synthetic), amiloride hydrochloride, bafilomycin A_1, and chloroquine disphosphate salt were reagent grade or better and were purchased from Sigma-Aldrich (St. Louis, MO) unless otherwise stated. Endotoxin-free plasmid pCMV-Luc2 was prepared by using the pGL4.10 vector (Promega, Madison, WI) and inserting the CMV promoter/intron region from the gWiz Luciferase (Aldevron, Madison, WI). The plasmid was isolated and produced with the Qiagen Plasmid Giga kit (Qiagen, Germany) according to the manufacturers instructions.

6.2.2 Synthesis of peptide monomers

Oligo(L-lysine) (K_{12} and K_{10}) and oligo(L-histidine) (K_6H_5 and K_5H_5) peptide monomers were synthesized on a solid support of Rink amide resin (100-200 mesh) *via* standard Fmoc/tBu chemistry on an automated peptide synthesizer. Prior to cleavage, peptide monomers were modified with Fmoc-protected 1-aminohexanoic acid (Ahx) or Fmoc-protected cysteine. To provide methacrylamido functionality, peptides were capped with methacryloyl chloride [21] or coupled with *N*-succinimidyl methacrylate. The solid support was then rinsed with DMF, DCM, and methanol, and allowed to dry overnight prior peptide cleavage. Methacrylamido-functionalized $AhxK_{10}$, $AhxK_{12}$, $AhxK_6H_5$, and $AhxK_5H_5$ peptides (termed $MaAhxK_{10}$, $MaAhxK_{12}$, $MaAhxK_6H_5$, and $MaAhxK_5H_5$, respectively) were cleaved off the resin by treating the solid support with TFA/triisopropylsilane (TIPS)/1,3 dimethoxybenzene (DMB) (92.5:2.5:5, v/v/v) for 3 h under gentle mixing. Cys-K_5H_5 (CK_5H_5) was cleaved from resin by treating the solid support with TFA/DMB/TIPS/EDT (90.5:2.5:2.5, v/v/v/v). Cleaved peptide monomers were precipitated in cold ether, dissolved in methanol, re-precipitated in cold ether, dissolved in water, and then lyophilized to obtain a fluffy, white solid. Peptide monomer purity and composition was determined *via* RP-HPLC and MALDI-TOF MS, respectively. Peptides were determined to be $> 90\%$ pure by RP-HPLC after peptide cleavage and used in polymerization reactions as is. MALDI-TOF MS was determined for the following peptides: $MaAhxK_{12}$ (MH^+) calculated [1736.54], found [1736.364]; $MaAhxK_{10}$ (MH^+) calculated [1479.98], found [1480.026]; $MaAhxK_6H_5$ (MH^+) calculated [1653.20], found [1653.129]; $MaAhxK_5H_5$ (MH^+) calculated [1525.01], found [1525.351]; CK_5H_5 (MH^+) calculated [1446.81], found [1446.79].

6.2.3 Synthesis of statistical HPMA copolymers by RAFT polymerization

Copolymers of HPMA-*co*-$AhxK_{12}$ ($pS_{lo}0$), HPMA-*co*-$AhxK_{12}$-*co*-$AhxK_6H_5$ ($pS_{lo}1$ and $pS_{lo}2$), HPMA-*co*-$AhxK_{10}$ ($pS_{hi}0$), HPMA-*co*-$AhxK_{10}$-*co*-$AhxK_5H_5$ ($pS_{hi}1$ and $pS_{hi}2$), or HPMA were synthesized *via* reversible-addition fragmentation chain transfer (RAFT) polymerization as previously described [13], using ethyl cyanovaleric trithiocarbonate (ECT, MW 263.4 g/mol) [22] as the chain transfer agent (*CTA*) and VA-044 as the initiator (*I*). The

monomers were dissolved and sonicated in acetate buffer (1 M in dH_2O, pH 5.1) such that the final monomer concentration was 1 M. For $pS_{lo}0$, $pS_{lo}1$, and $pS_{lo}2$, 26.05 mg (10.66 μmol), 13.02 mg (5.33 μmol), and 19.54 mg (7.99 μmol) of $MaAhxK_{12}$, respectively, and 0 mg, 12.40 mg (6.18 μmol), and 12.40 mg (6.18 μmol) of $MaAhxK_6H_5$, respectively, was used in the polymerization reaction. For $pS_{hi}0$, $pS_{hi}1$, and $pS_{hi}2$, 44.40 mg (21.45 μmol), 38.85 mg (18.77 μmol), and 22.20 mg (10.72 μmol) of $MaAhxK_{10}$, respectively, and 0 mg, 11.44 mg (6.29 μmol), and 45.75 mg (25.14 μmol) of $MaAhxK_5H_5$, respectively, was used. The molar ratio of CTA/I was 10, and the DP used was 190. The reaction mixture was added to a 5 mL reaction vessel in the following order: ECT (100 $^{mg}/_{mL}$ in DMSO), peptide monomer/HPMA mixture, and VA-044 (10 $^{mg}/_{mL}$ in acetate buffer). The reaction vessels were then sealed with a rubber septum and purged with N_2 gas for 10 min prior to incubation in an oil bath (44 °C) for 48 h. The copolymer solution was then dissolved in water, dialyzed against dH_2O to remove unreacted monomers and buffer salts, lyophilized, and stored at -20 °C. The final yield after dialysis ranged from 58% to 86% of the theoretical yield.

6.2.4 Synthesis of oligohistidine-grafted diblock copolymers poly[(HPMA-g-CK_5H_5)-b-(HPMA-co-$AhxK_{10}$)]

The synthesis and characterization of the macroCTA *poly*(HPMA-*co*-PDSMA) and diblock *poly*[(HPMA-*co*-PDSMA)-*b*-(HPMA-*co*-$AhxK_{10}$)] (pB0) was carried out as previously described [23]. Peptide conjugation to the diblock copolymer to obtain *poly*[(HPMA-*g*-CK_5H_5)-*b*-(HPMA-*co*-$AhxK_{10}$)] (pB1) was completed as previously reported, but with a few modifications [23]. In a 10 mL flame-dried pear-shaped flask, 25 mg (0.34 μmol polymer, 2.7 μmol PDS groups) of the diblock copolymer was dissolved in 0.9 mL saline buffer (0.5 M NaCl, 20 mM HEPES, pH 7.1). Afterwards, 9.4 mg (6.48 μmol, 2.3 equiv. relative to the diblock copolymer PDS groups) of Cys-K_5H_5, dissolved in 1.3 mL saline buffer, was added to the flask and allowed to stir under argon at room temperature overnight. The released 2-thio-pyridine was monitored by absorbance at $\lambda_{343\,nm}$ to determine the extent of the conjugation reaction. The reaction mixture was passed through a PD-10 desalting

column to remove unreacted species, and lyophilized.

6.2.5 Polymer characterization

Molecular weight analysis of the copolymers was carried out by gel permeation chromatography (GPC) as previously described, using a miniDAWN TREOS light scattering detector (Wyatt, Santa Barbara, CA) and an Optilab rEX refractive index detector (Wyatt). Absolute molecular weight averages ($\overline{M_N}$ and $\overline{M_W}$) and $^{dn}/_{dc}$ values were calculated using ASTRA software (Wyatt). The $^{dn}/_{dc}$ value for each copolymer was $0.133\,^{mL}/_{g}$. The content of lysine- and histidine-containing peptides within the HPMA copolymers were determined by amino acid analysis, using 1-amino-2-propanol, lysine, and histidine as standards, as previously described [16, 23].

6.2.6 Acid-base titration

The buffering capacity of polymers was determined by acid-base titration. Polymer was dissolved in 15 mL dH_2O to yield a 1 mM lysine concentration. For PEI, 1 mM total amine concentration was used. The pH of the solution was increased to 10.0 with 1 M NaOH, and then titrated with 0.1 N HCl. Buffer capacity, β, was calculated as previously described [24], using the following equation:

$$\beta = \frac{\Delta A_{\text{mol}}}{\Delta pH}$$

where ΔA_{mol} is the change of the moles of acid added. Values were calculated from interpolation with a 3rd-order polynomial from pH 5.1 to 7.4 (GraphPad Prism v.6).

6.2.7 Polyplex formulation and characterization

Stock solutions of polymers and peptides were prepared at $10\,^{mg}/_{mL}$ in 0.1X phosphate buffered saline (PBS), and the pH was adjusted to 6.5 by adding 0.1 N HCl. To formulate polyplexes, pCMV-Luc2 plasmid DNA was diluted to $0.1\,^{mg}/_{mL}$ in DNase/RNase-free H_2O and mixed with an equal volume of polymer at desired lysine to DNA phosphate (N/P) ratios. Polyplexes were then allowed to incubate for 10 min at room temperature. For *in vitro* transfections, 20 μL of the polyplex solution (containing 1 μg DNA) was mixed with

180 μL of Opti-MEM medium (Invitrogen). The particle size of the polyplexes was determined by mixing 20 μL of the polyplex solution with either 20 μL of 0.2 μm-filtered dH_2O or 20 μL of 2X PBS. The polyplex solutions were incubated for 15 min at room temperature prior to particle sizing by dynamic light scattering (DLS) (ZetaPlus, Brookhaven Instruments Corp., Novato, CA). Particle sizing measurements were performed at a wavelength of 659.0 nm with a detection angle of 90° at room temperature, and calculated using the viscosity (0.890 cP) and refractive index (1.330) of water at 25 °C. Particle sizes are expressed as effective diameters using a log-normal distribution. For ζ potential measurements, 20 μL of polyplexes were formulated with 1 μg DNA, incubated for 15 min, diluted with 180 μL dH_2O, and 800 μL 10 mM NaCl. ζ potential was determined using a ZetaSizer Nano ZS (Malvern Instruments Inc., Southborough, MA) using the Smoluchowsky model for aqueous suspensions. Transmission electron microscopy was completed exactly as previously described [23]. The particle width, length, and aspect ratio (length/width) were measured and calculated using ImageJ.

6.2.8 Cell culture

Hela (human cervical carcinoma) and COS-7 (African green monkey kidney fibroblast) cells were grown in minimum essential medium (MEM) and Dulbeccos modified eagle medium (DMEM), respectively, supplemented with 10% FBS and 100 IU penicillin, 100 $\mu g/mL$ streptomycin, and 0.25 $\mu g/mL$ amphotericin B. Cells were passaged when they reached ~80% confluency.

6.2.9 In vitro transfection

HeLa and COS-7 cells were seeded overnight in 24-well plates at a density of 3×10^4 cells per well (1 mL/well) at 37 °C, 5% CO_2. Polyplexes were formulated as described above. After the polyplexes were formed, 20 μL (containing 1 μg DNA) was mixed with 180 μL of Opti-MEM medium (Invitrogen). Seeded cells were washed once with PBS and then treated with 200 μL of polyplexes in Opti-MEM, which was added dropwise on top of the cells. After a 4 h incubation at 37 °C, 5% CO_2 in a humidified environment, the cells

were washed once again with PBS and incubated in 1 mL of fresh complete medium for an additional 44 h. Cells were harvested and assayed for luciferase expression at 48 h. This was done by washing cells once with PBS, adding of 200 μL reporter lysis buffer (Promega, Madison, WI), and then performing one freeze-thaw cycle to complete the lysis of cells. Lysates were collected and centrifuged at 14,000g for 15 min. Luminescence was carried out following the manufacturer's instructions (Promega, Madison, WI). Luciferase activity is reported in relative light units (RLU) normalized by mg protein (RLU/mg), as measured by a microBCA Protein Assay Kit (Pierce).

6.2.10 In vitro transfection with chemical inhibitors

Stock solutions of genistein (5 $^{mg}/_{mL}$ in DMSO), chlorpromazine (1 $^{mg}/_{mL}$ in DMSO), amiloride (2.5 mgmL), chloroquine (20 mM in water), bafilomycin A_1 (0.1 $^{mg}/_{mL}$ in DMSO), and further diluted to working concentrations in OptiMEM (genistein, 50 $^{\mu g}/_{mL}$; chlorpromazine, 10 $^{\mu g}/_{mL}$; amiloride, 25 $^{\mu g}/_{mL}$; chloroquine, 200 μM; bafilomycin A_1, 150 nM), and sterile-filtered for transfections. For transfection with inhibitors, HeLa and COS-7 cells were seeded overnight in 24-well plates at a density of 3×10^4 cells per well (1 mL/well) at 37 °C, 5% CO_2. Polyplexes were formulated as described above. Cells were washed once with PBS and pre-treated with one of the chemical inhibitors (in OptiMEM) for 1 h at 37 °C, 5% CO_2 prior to polyplex transfection. 20 μL of polyplexes were then added to the cells and incubated for an additional 2 h at 37 °C, 5% CO_2. Cells were then washed once with PBS and incubated with fresh complete media for an additional 46 h. Cells were lysed and assayed for luciferase expression as described above.

6.2.11 Statistical analysis

The data are represented as the mean and standard deviations. Data were analyzed using the two-tailed Student's t-test and a p-value of less than or equal to 0.05 was taken as significant.

6.3 Results and discussion

6.3.1 Synthesis of HPMA-co-oligolysine-co-oligohistidine polymers

Three sets of HPMA copolymers with varying percentages of oligo(L-lysine) (K_{12} or K_{10}) peptide and oligo(L-histidine)-containing peptide (K_6H_5 or K_5H_5) were synthesized *via* RAFT polymerization (Figure 6.2, Table 6.1). The pS polymers are statistical copolymers of HPMA, oligo(L-lysine) monomers, and oligo(L-histidine)-containing monomers (Figure 6.2A, molecule **1**). The "lo" and "hi" subscripts refers to the peptide incorporation ratio, where "lo" polymers contain < 3.0 mmol lysine per g polymer and "hi" polymers contain ≥ 3.0 mmol lysine per g polymer. The pB polymers are block copolymers of the aforementioned monomers synthesized by copolymerizing HPMA and pyridyl disulfide methacrylamide (PDSMA) to form one block, and then chain-extending with HPMA and oligo(L-lysine) monomer to form the second block (pB0, Figure 6.2B, molecule **2**). To synthesize pB1, cysteine-modified K_5H_5 was grafted onto the first block *via* disulfide exchange between the pyridyl disulfide moiety on the polymer and cysteine on the oligo(L-histidine)-containing peptide (Figure 6.2B, molecule **3**). K_{12} and K_6H_5 peptides were used in pS_{lo} copolymers as a follow-up to initial studies [13]; however, optimization of oligolysine peptide length in later studies [16] prompted the synthesis of statistical and diblock HPMA copolymers with K_{10} and K_5H_5 peptides in the pS_{hi} and pB copolymers. Therefore, the pS_{hi} and pB polymer series will be the focus of this study.

RAFT polymerization of HPMA, oligolysine, and oligohistidine peptide monomers resulted in statistical copolymers with close to target molecular weights (within ~20% of target M_n) and low polydispersity (≤ 1.2), except for the polymer $pS_{hi}2$, which had a slightly higher polydispersity (PD = 1.54) (Figure 6.1). The relatively high polydispersity of $pS_{hi}2$ may be due to the lower pK_a of oligohistidine residues, which can lead to aminolysis of the trithiocarbonate chain transfer agent during the polymerization reaction [25]. Attempts to incorporate $AhxH_5$ or more $AhxK_5H_5$ (> 1.4 mmol histidine per g polymer) into statistical polymers led to poor conversion (data not shown), further indicating that this phenomenon may be occurring. HPMA, lysine, and histidine concentration in the copolymers was determined by amino acid analysis; the lysine concentration was approximately 2.4-2.7 mmol

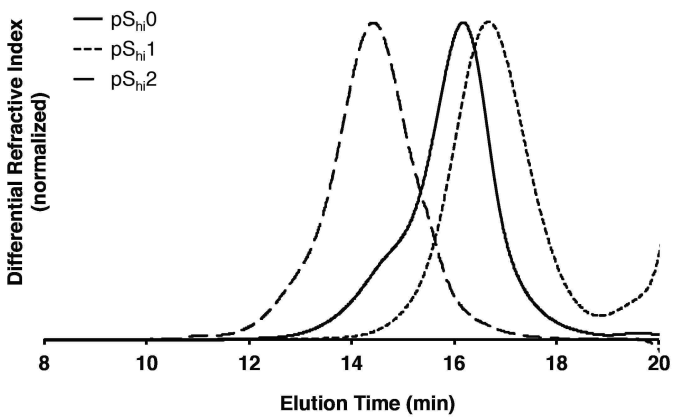

Figure 6.1: **Size exclusion chromatography of pS_{hi} polymers.** Molecular weight analysis of polymers was carried out by size exclusion chromatography with polymers at 10 $^{mg}/_{mL}$ in running buffer (0.15 M sodium acetate buffer, pH 4.4). Absolute molecular weight averages ($\overline{M_N}$ and $\overline{M_W}$), and $^{dn}/_{dc}$ were calculated using ASTRA software. The $^{dn}/_{dc}$ for each copolymer was 0.133 $^{mL}/_{g}$.

Table 6.1: Characterization of HPMA-oligolysine-oligohistidine brush polymers

polymer	targeted M_n (kD)	determined M_n (kD)	M_n/M_w	mol % K_{12}^{*}/K_{10}^{**} monomer	mol % $K_6H_5^{*}/K_5H_5^{**}$ monomer	mmol K/g polymer	mmol H/g polymer
$pS_{lo}0^{*}$	57.48	51.27	1.14	6.74	0	2.71	0
$pS_{lo}1^{*}$	56.69	48.71	1.20	5.80	0.98	2.46	0.206
$pS_{lo}2^{*}$	64.27	54.22	1.03	5.83	2.62	2.36	0.532
$pS_{hi}0^{**}$	78.01	77.60	1.18	20.0	0	3.78	0
$pS_{hi}1^{**}$	84.73	84.79	1.08	17.6	6.21	3.53	0.530
$pS_{hi}2^{**}$	105.1	101.8	1.54	9.53	16.32	2.95	1.36
$pB0^{**}$	78.0	74.0	1.2	17.0	0	3.61	0
$pB1^{**}$	–	76.1	1.2	12.37	4.91	3.28	0.533

[a]Polymers with "lo" lysine incorporation contain $^{*}K_{12}$ and K_6H_5 peptides, while polymers with "hi" lysine incorporation contain $^{**}K_{10}$ and K_5H_5 peptides.

lysine per g polymer for the pS_{lo} series and 3.0-3.8 mmol lysine per g polymer for the pS_{hi} and pB series, while the histidine concentration ranged from 0.21-1.4 mmol histidine per g polymer.

6.3.2 Acid-base titration

Incorporation of histidine into polymers can increase the polymer's ability to buffer in the endosomal pH range. This strategy allows for endosomal buffering when materials are used for intracellular delivery. The pS_{hi} and pB copolymers with higher lysine incorporation were evaluated for buffering capacity using acid-base titration (Figure 6.3A). Lysine-based polymers were diluted to equal molar lysine concentration (0.1 mM lysine), basified to pH 10

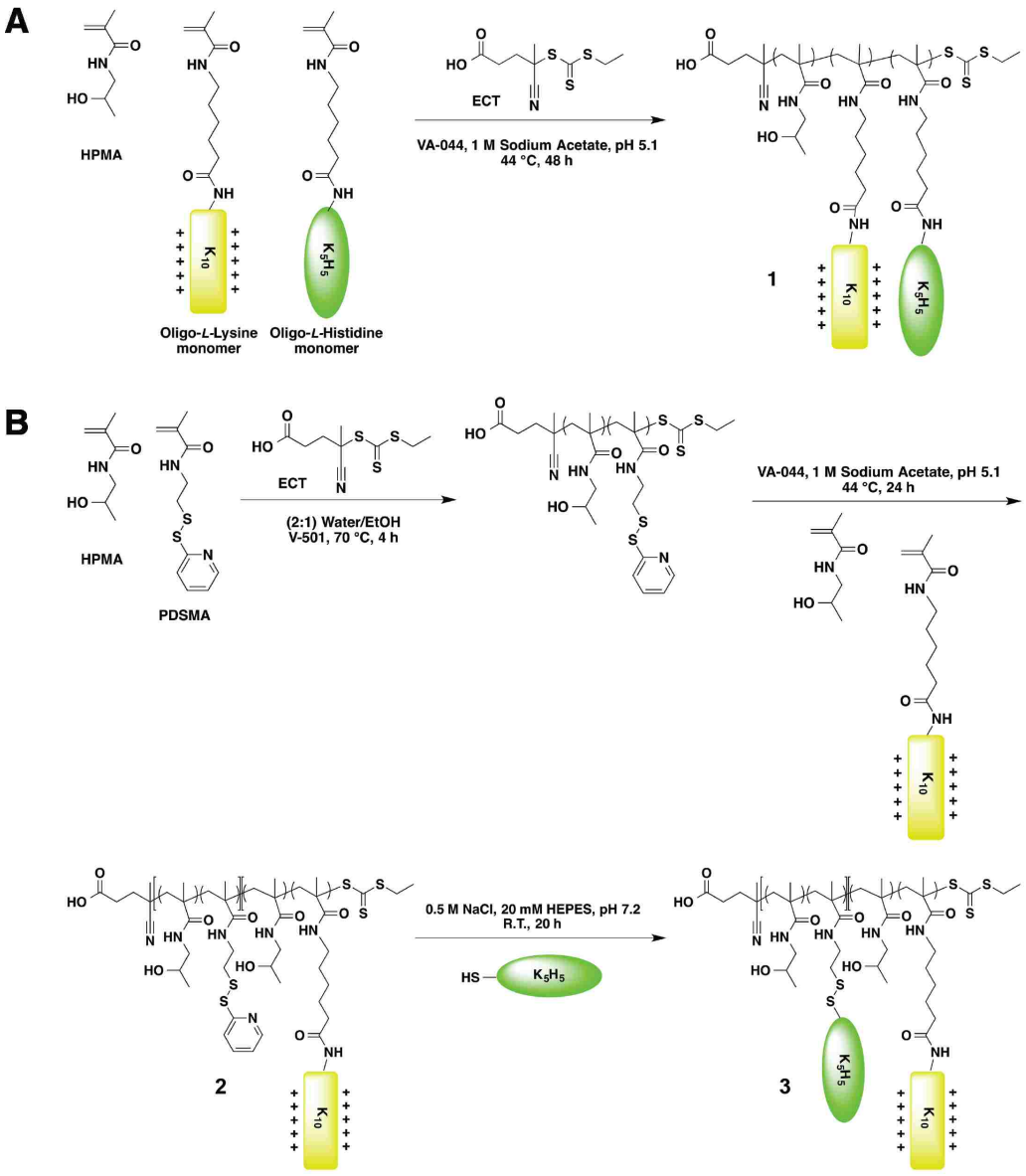

Figure 6.2: **Schematic of statistical and diblock polymer synthesis.** (A) RAFT polymerization of statistical HPMA polymers containing oligo(L-lysine) and oligo(L-histidine) peptides (pS_{lo} and pS_{hi} series, Molecule **1**). (B) RAFT polymerization of HPMA and PDSMA, and then chain-extension with HPMA and oligo(L-lysine) to form pB0 (Molecule **2**). Disulfide exchange between the pyridyl disulfide on **2** and cysteine-functionalized oligo(L-histidine) peptides yields pB1 (Molecule **3**).

with 1 M NaOH, and subsequently titrated with 0.1 N HCl. In general, higher histidine incorporation resulted in greater buffering in the pH range of 5.1-7.4.

We also looked at buffer capacity, β, as a function of environmental pH. Data obtained from the acid-base titration were interpolated from pH 5.1 to 7.4 to generate Figures 6.3B-D. For the pS_{hi} statistical polymers, increasing histidine content only increased buffer capacity in the lower endosomal pH range (pH 5.1-6.6) (Figure 6.3B). In contrast, pB1 had higher buffer capacity in the upper endosomal pH range (pH 5.6-7.4) than pB0 (Figure 6.3C), similarly to PEI (Figure 6.3D). PLL exhibited increased buffer capacity near neutral pH. These results suggest that buffer capacity can be potentially modulated by varying the polymer architecture of oligohistidine polymers and raises the interesting possibility of more specifically directing location of endosomal release (*e.g.*, early *vs.* late endosome) by selection of polymer carrier. Roufa and Midoux reported that the acetylation of the α-amino group of histidine residues substituted on polylysine resulted in a shift of the pK_a to pH 6.0 from pH 6.9 for the non-acetylated polymer, and that this may have led to decreased transfection efficiencies of the acetylated polymer [26]. In addition, the difference in buffer capacity may indicate that histidine residues in block architectures may be more accessible to protonation than those in statistical architectures.

Increases in buffer capacity at the lower endosomal pH range (pH 3.5-6) were also noted when increasing amounts of His_3 was grafted onto PAMAM dendrimer derivatives [27]. Furthermore, Hashemi *et al.* saw significant differences in transfection efficiency between various configurations of lysine-histidine peptides incorporated into 10 kD PEI [10], indicating that varying the amino acid sequence can also potentiate the buffer capacity; however, these differences may be attributed to sequence similarity to naturally-occurring condensing motifs found in histones than differences in endosomal buffering [28]. Interestingly, Mason and coworkers showed that cationic amphipathic histidine-rich peptides transfected less efficiently if the peptide exhibited a low pK_a value, which resulted in delayed and insufficient disruption of endocytic vesicles [29]. Thus, the peptide length and amino acid sequence may also influence the pK_a of the histidine-containing polymers. Furthermore, since endosomal escape may be preferred earlier on during the gene transfection process due to the cytotoxicity of late endosomal/lysosomal proteases [30], lower pK_a values may reduce the

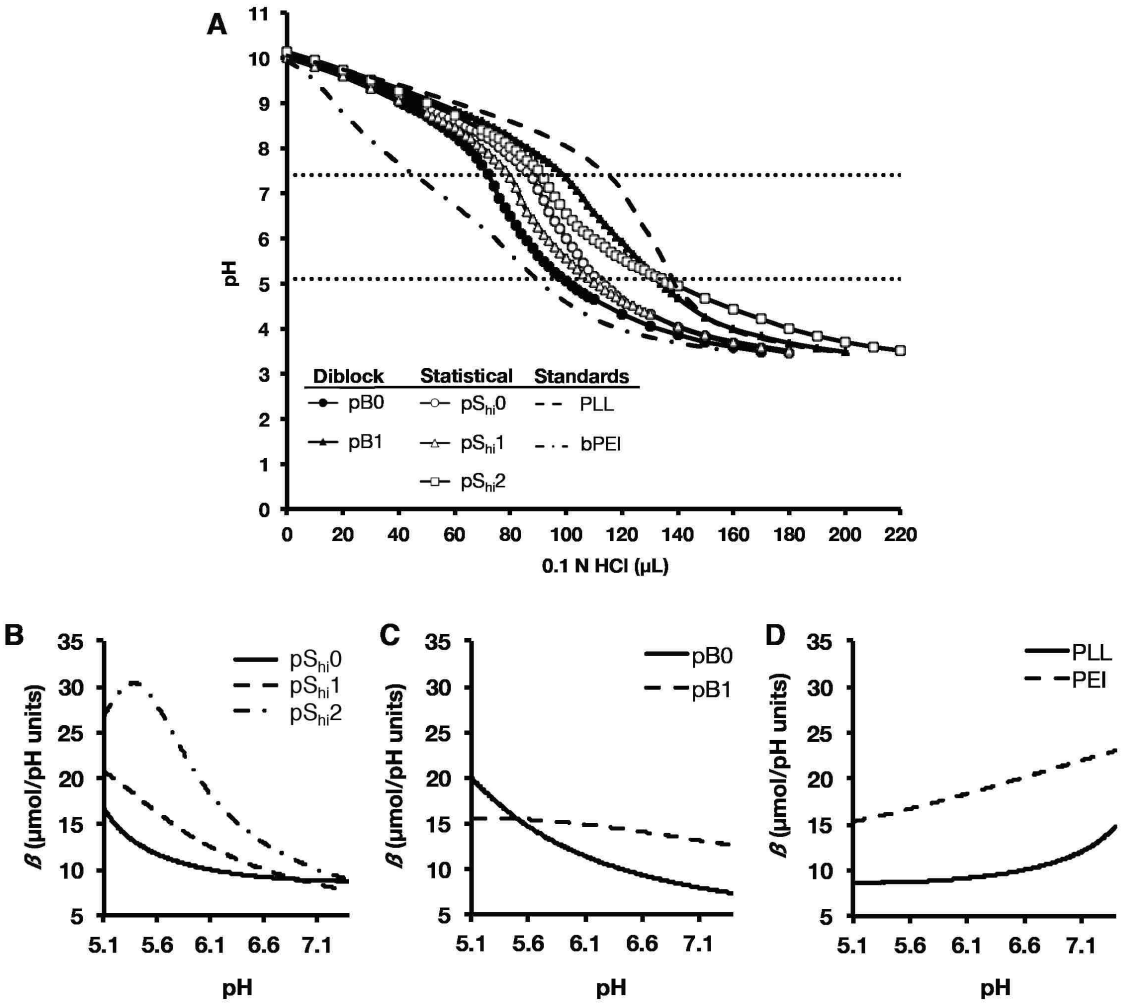

Figure 6.3: **Acid-base titration of HPMA-oligolysine-oligohistidine polymers.** (A) Acid-base titration curves of diblock (pB0, pB1), statistical (pS$_{hi}$0, pS$_{hi}$1, pS$_{hi}$2), and standard polymers (PEI, PLL). Buffer capacity calculated from interpolation of acid-base titration curves of (B) pS$_{hi}$0, pS$_{hi}$1, pS$_{hi}$2, (C) pB0, pB1, and (D) PEI, PLL.

ability of polymer to achieve endosomal escape in a timely manner. These results suggest that designing polymers that can buffer in the upper endosomal pH range (pH ~6-7.4) can enhance gene transfection efficiencies while reducing cytotoxicity.

6.3.3 Polyplex characterization

Polyplex size, surface charge, and morphology were characterized by dynamic light scattering (DLS), ζ potential, and transmission electron microscopy, respectively. For the pS_{hi} series, polymers with lower histidine content produced polyplexes of 170-200 nm in hydrodynamic diameter in water (Figure 6.4A). In contrast, pB1 did not form small particles in water (353-454 nm). All polymers formed stable complexes (< 300 nm) at N/P 5 in the presence of both neutral and acidic PBS (pH 7.4 and 5.5). All polyplexes (N/P 5) also demonstrated positive ζ potentials (11-23 mV) (Figure 6.4B). The increased ζ potential of $pS_{hi}2$ and pB1 over their non-histidylated analogues may be due to the increased display of histidine residues, which are protonated at lower pH, in the polymer architectures. Transmission electron micrographs showed that pS_{hi} polymers and pB0 formed heterogeneous populations of spherical, toroidal, and oblong polyplexes, ranging from 15-52 nm in width and 41-111 nm in length (Figure 6.5A-D, E-G), while pB1 formed more uniform, spherical polyplexes, 24-43 nm in width and 34-55 nm in length (Figure 6.5E-G). Overall, the polyplexes had aspect ratios greater than 1 (Figure 6.5H). The discrepancy between the DLS and TEM results of pB1 polyplexes may be due to particle aggregation that could occur with the block polymer architecture in water, resulting in larger hydrodynamic sizes, as evidenced by TEM.

6.3.4 Delivery of plasmid DNA to cultured cells

The ability of the HPMA-peptide copolymers to transfect cultured HeLa cells was assessed in comparison to PLL and PEI polyplexes in serum-free and 10% serum-containing conditions. Protein content, as measured by the BCA assay, was used as an indicator for polyplex cytotoxicity. Under serum-free conditions, we demonstrated that N/P 5 generally provided the highest transfection efficiency for our HPMA-peptide copolymers, and at higher N/P ratios (Figure 6.6A), cytotoxicity was observed in some formulations (Figure 6.6B). Overall transfection efficiency of the pS_{lo} copolymers was low, although in general, higher incorporation of oligohistidine residues led to slight increases in transfection efficiency. Despite these trends, increases were not statistically significant. The pS_{hi} and pB copolymers, which

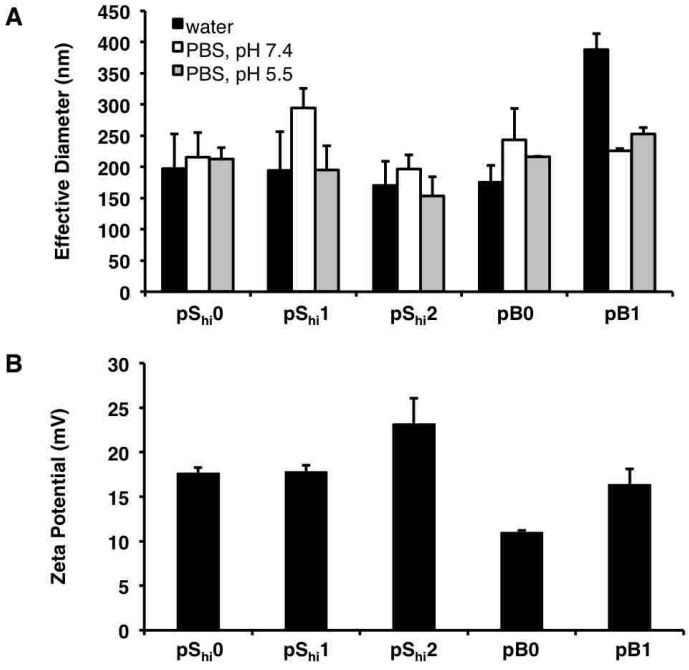

Figure 6.4: **Polyplex characterization by dynamic light scattering and ζ potential.** (A) Effective diameters of polyplexes formulated at N/P 5 in water (black bars), PBS, pH 7.4 (white bars), and PBS, pH 5.5 (grey bars). (B) ζ potential of polyplexes formulated at N/P 5 in water. Data are presented as mean $\pm$ S.D., $n = 3$.

contained higher lysine content, transfected better than the pS_{lo} copolymers (Figure 6.7A) but were also more cytotoxic (Figure 6.7B). The incorporation of 0.53 mmol histidine per g polymer ($pS_{hi}1$ and pB1) did not significantly increase transfection efficiency over the corresponding base polymers, $pS_{hi}0$ and pB0. However, the statistical polymer with the highest oligohistidine content, $pS_{hi}2$, performed significantly better than $pS_{hi}0$, with a 3.0-4.6 fold increase in transfection efficiency. These results suggest that more than 0.53 mmol histidine per g polymer in these brush copolymers is necessary to achieve significant increases in transfection efficiency in the statistical polymer architecture compared to the non-histidylated polymer analogue. Alternatively, the increased ζ potential of $pS_{hi}2$ (Figure 6.4B) may also enhance cellular association and thereby transfection efficiency of the material. Interestingly, even though $pS_{hi}1$ and pB1 showed increased buffer capacity similarly to that of PEI (Figure 6.3B-D), a much greater buffer capacity, which was provided by the $pS_{hi}2$ polymer, was necessary to increase transfection efficiency closer to levels achieved by PEI. Overall, the polymers resulted in some reduced protein content, perhaps due to the large molecular weight of the materials [16]. In the presence of 10% serum, the transfection efficiencies of

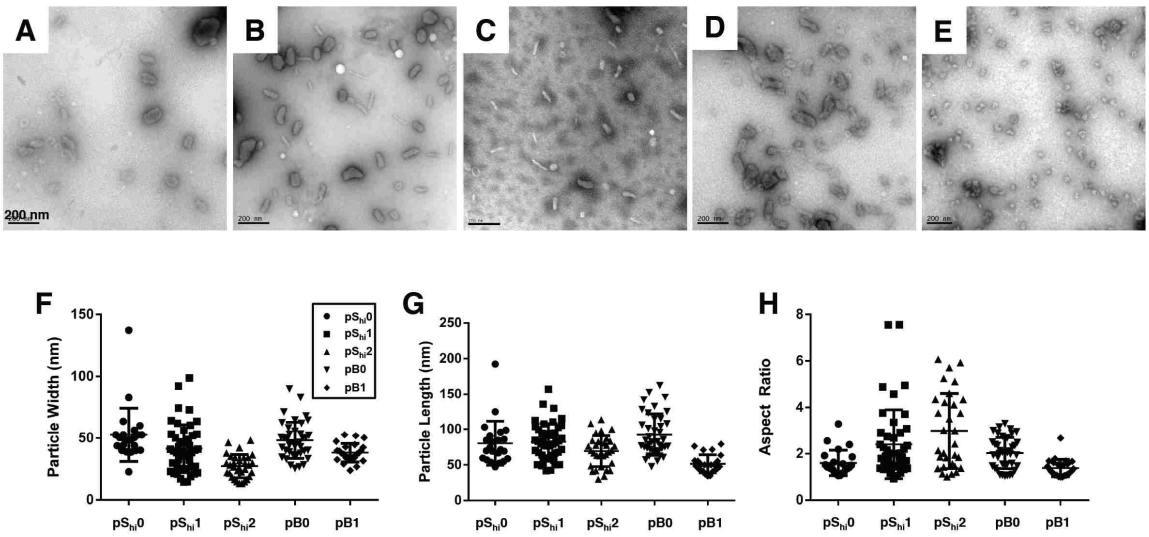

Figure 6.5: **Transmission electron micrographs (TEM) of polyplexes in water.** Representative TEM images of polyplexes (N/P 5) formulated with (A) pS$_{hi}$0, (B) pS$_{hi}$1, (C) pS$_{hi}$2, (D) pB0, and (E) pB1. The (F) particle width, (G) particle length, and (H) aspect ratio were calculated using ImageJ. Data are presented as the mean ± S.D., with n = 23 for pS$_{hi}$0, n = 45 for pS$_{hi}$1, n = 31 for pS$_{hi}$2, n = 39 for pB0, and n = 24 for pB1. Scale bar = 200 nm.

all polymer formulations were decreased and cytotoxicity was limited. In addition, the increase in transfection efficiency achieved by pS$_{hi}$2 over pS$_{hi}$0 was eliminated, indicating that serum proteins may nonspecifically bind to the cationic polyplexes and interfere with overall polyplex uptake [31], thereby reducing the effective concentration of histidine necessary for increased transfection.

Previous reports have also indicated that high levels of histidylation may be needed to significantly impact transfection efficiency. Benns *et al.* synthesized a histidylated version of PLL where 25% of the ϵ-amine groups on the PLL backbone was grafted with poly(L-histidine) that resulted in higher transfection efficiency compared to PLL alone [11]. Additionally, Midoux *et al.* found optimal transfection efficiency when 38% of the ϵ-amines of PLL was substituted with histidyl residues [32]. Reports using polyhistidine peptides for gene delivery have also showed increased transfection efficiencies due to the incorporation of

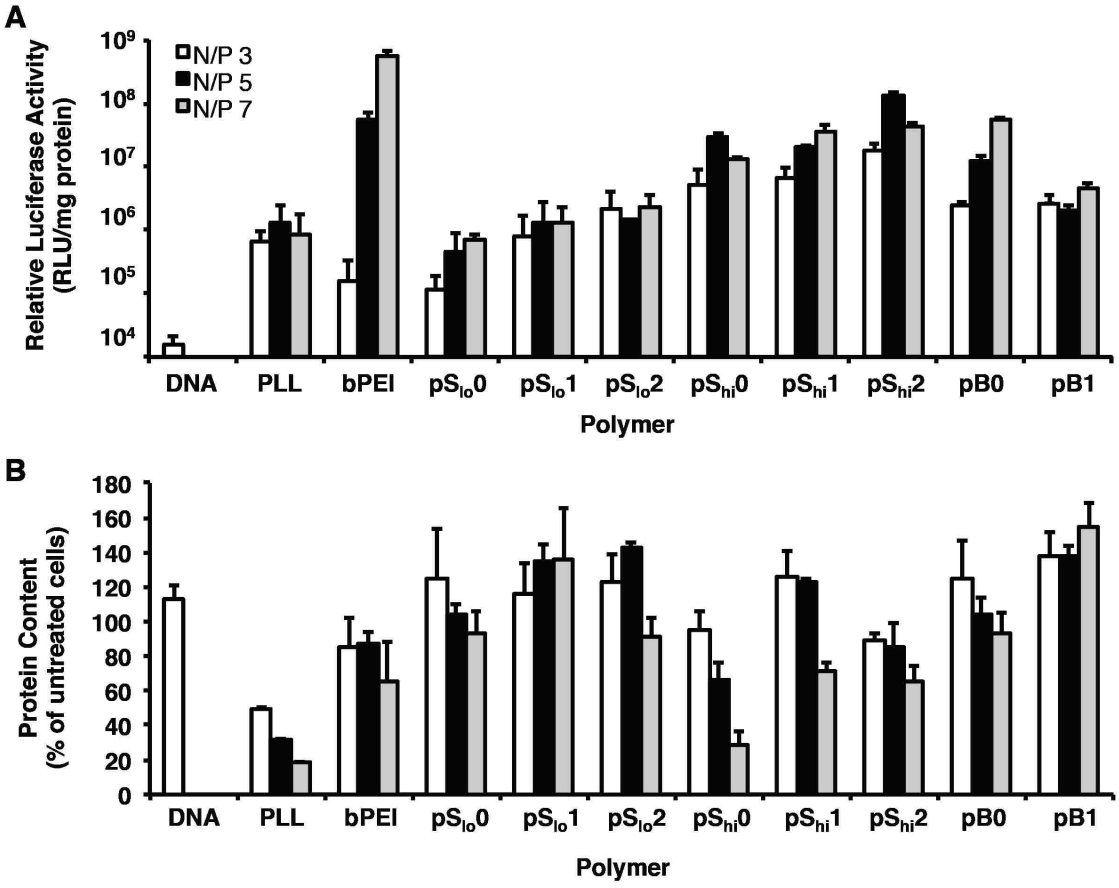

Figure 6.6: **Transfection of HPMA-oligolysine-oligohistidine polyplexes in HeLa cells** (A) Transfection efficiency and (B) protein content of HeLa cells transfected with polyplexes formulated with statistical (pS$_{lo}$0, pS$_{lo}$1, pS$_{lo}$2, and pS$_{hi}$0, pS$_{hi}$1, pS$_{hi}$2) or diblock (pB0, pB1) and DNA (1 μg) at N/P 3, 5, 7 under serum-free conditions. Data are presented as the mean $\pm$ S.D., $n = 3$, and representative of three independent experiments.

histidine [33–35], but shorter peptides (DP 19) were not as efficient gene transfection agents as longer peptides (DP 190) [35].

6.3.5 Delivery of plasmid DNA with bafilomycin A_1 and chloroquine

To determine if the increase in transfection efficiency of pS$_{hi}$2 was a result of effective endosomal buffering, HeLa cells were treated with polyplexes in the presence of bafilomycin A$_1$, an ATPase proton pump inhibitor [36], or chloroquine, a lysosomotropic agent that

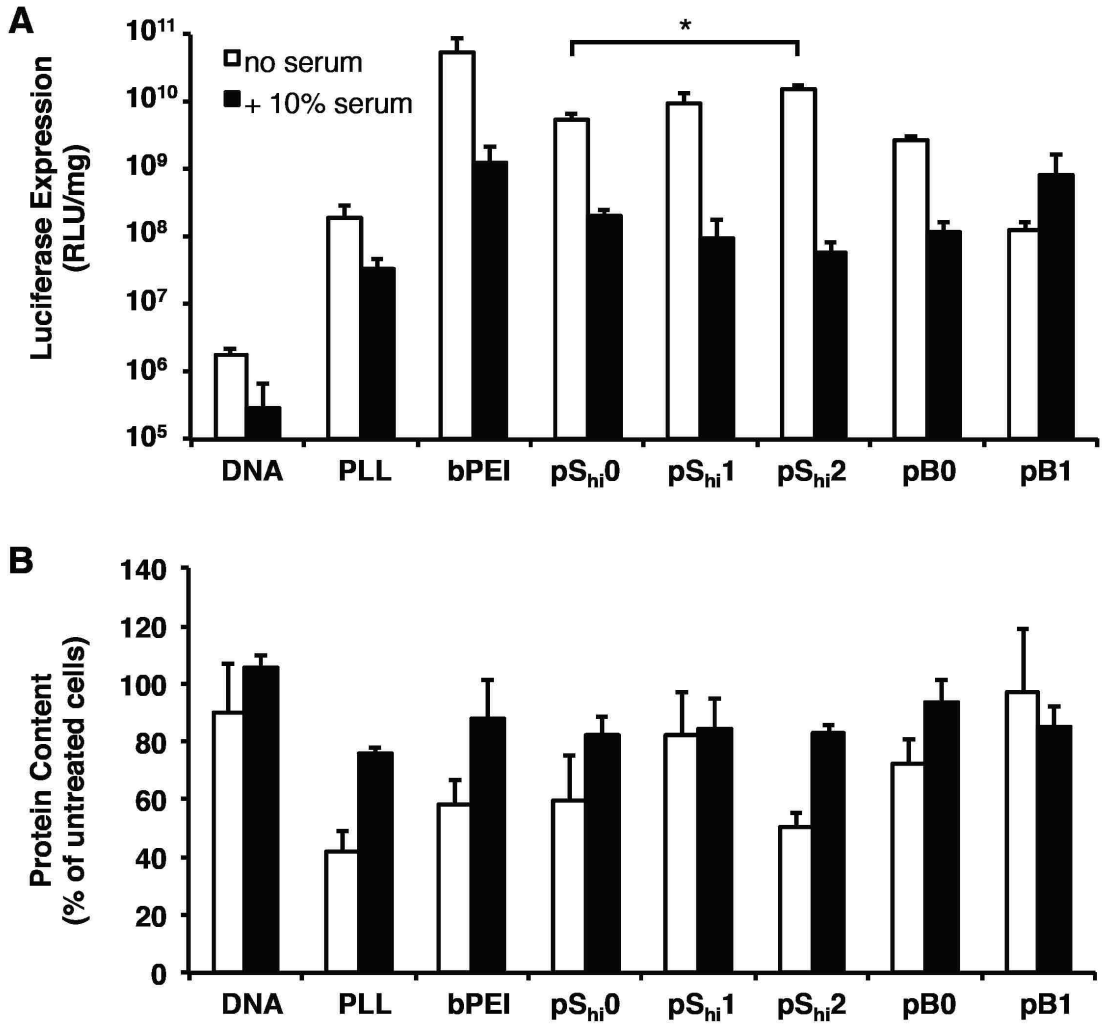

Figure 6.7: **Transfection of HPMA-oligolysine-oligohistidine polyplexes in HeLa cells.** (A) Transfection efficiency and (B) protein content of HeLa cells transfected with polyplexes formulated with statistical ($pS_{hi}0$, $pS_{hi}1$, $pS_{hi}2$) or diblock (pB0, pB1) and DNA (1 μg) at N/P 5 under serum-free (white bars) or 10% serum-containing (black bars) conditions. Data are presented as the mean $\pm$ S.D., $n = 3$, and representative of two independent experiments. (*) $p < 0.05$, as determined by a two-tailed, unpaired Student's t-test with unequal variance.

buffers endosomal vesicles [37]. The transfection efficiencies of $pS_{hi}0$, $pS_{hi}2$, and pB0 in the presence of bafilomycin A_1 decreased to 64.8%, 46.7%, and 68.4%, respectively, of the original transfection efficiency, indicating that polymer protonation does facilitate gene

delivery (Figure 6.8A). As expected, the transfection efficiency of PEI was decreased to 9.4% of the original transfection efficiency, as previously reported [6]. The transfection efficiencies of all polymer formulations were increased 2.0- to 28.8-fold by the addition of chloroquine. These results suggest that further increases in transfection efficiency potentially can be achieved with enhanced endosomal buffering. Similar results were achieved with COS-7 cells (Figure 6.8C). Although inhibitor treatment increased cytotoxicity, the transfection efficiencies were normalized to account for the decreased protein content (Figure 6.8B, D). Additionally, previous reports have shown that buffering ability alone may not be sufficient to increase transfection efficiency [38, 39].

6.3.6 Delivery of plasmid DNA with endocytic uptake inhibitor treatment

Three major cellular uptake pathways have been implicated in polyplex uptake: clathrin-mediated endocytosis, caveolae-mediated endocytosis, and macropinocytosis [40]. Clathrin-mediated endocytosis involves the trafficking of endocytosed materials in increasingly acidified endosomal environments; in this case, the ability of endosomal buffering becomes beneficial as a potential method for endosomal escape. In caveolae-mediated endocytosis and macropinocytosis, endocytosed materials are not subjected to acidic environments. Therefore, the ability to buffer at endosomal pH may not be crucial for gene delivery. To determine if the HPMA-oligolysine copolymers preferred one of these endocytic pathways, transfection studies were conducted in cells treated with the following agents: chlorpromazine, an inhibitor of clathrin-mediated endocytosis [41], genistein, an inhibitor of caveolae-mediated endocytosis [42], and amiloride, an inhibitor of macropinocytosis [43].

For transfections with chemical inhibitors, HeLa cells were treated with chlorpromazine, genistein, or amiloride for 1 h prior to transfection with polyplexes. Since polyplex uptake pathways are highly cell-dependent44, COS-7 cells were also tested since the cell line had also been previously used in inhibitor studies [44, 45]. In HeLa cells, both pS_{hi} and pB polyplexes exhibited decreased transfection when the cells were pre-treated with genistein (Figure 6.9A). When HeLa cells were pre-treated with chlorpromazine, $pS_{hi}2$ and pB0 exhibited a 1.7- and 4.5-fold increase, respectively, in transfection efficiency. No significant

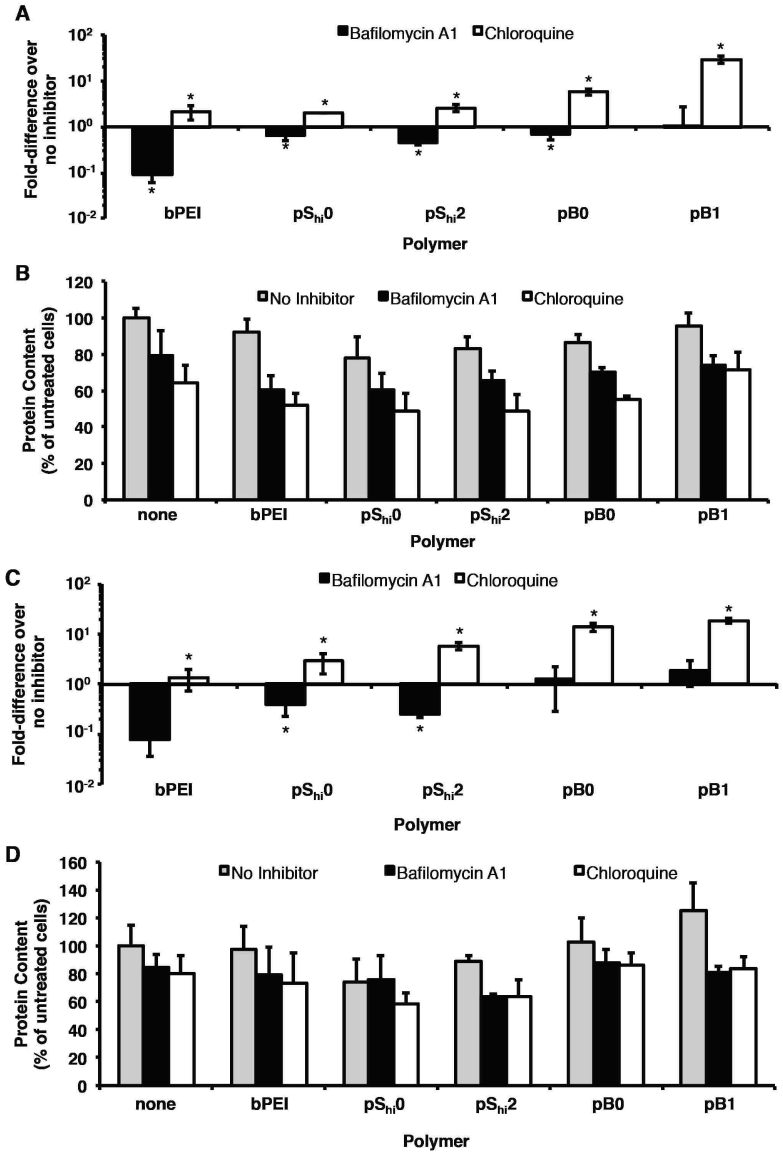

Figure 6.8: **Transfection of HPMA-oligolysine-oligohistidine polyplexes in HeLa and COS-7 cells with bafilomycin A_1 or chloroquine.** (A) Transfection efficiency and (B) protein content of HeLa cells, and (C) transfection efficiency and (D) cell viability of COS-7 cells transfected with polyplexes formulated with statistical ($pS_{hi}0$, $pS_{hi}2$) or diblock (pB0, pB1) and DNA (1 μg) at N/P 5 in the presence of 150 nM bafilomycin A_1 or 200 μM chloroquine under serum-free conditions. Data are presented as the mean $\pm$ S.D., $n = 3$, and representative of three independent experiments. (*) $p < 0.05$, as determined by a two-tailed, unpaired Student's t-test with unequal variance.

differences in transfection efficiency were seen when cells were treated with amiloride. In COS-7 cells, $pS_{hi}0$, $pS_{hi}2$, and pB0 polymers exhibited 2.0-, 2.1-, and 2.4-fold increase, respectively, in transfection efficiency with chlorpromazine pre-treatment (Figure 6.9C). The increases in transfection efficiency observed with chlorpromazine treatment may indicate that compensatory uptake mechanisms are upregulated upon inhibition of clathrin-mediated endocytosis [46]. Decreased transfection efficiency was seen with pS_{hi} polyplexes with genistein pre-treatment. Again, inhibitor treatment slightly increased cytotoxicity and the transfection efficiencies were normalized to account for the reduced protein content (Figure 6.9B, D). While all three internalization routes may be used to varying extents, these results indicate that caveolae-mediated uptake is a significant method of HPMA-peptide copolymer internalization that leads to successful gene transfection. Other reports have demonstrated similar findings for other polymer systems. For example, van de Aa *et al.* demonstrated that pDMAEMA polyplexes had better transfection efficiencies when routed through the caveolar pathway [45]. Hanes and coworkers recently demonstrated that PEGylated polylysine (CK_{30}) particles also trafficked *via* the non-degradative caveolar pathway, leading to efficient transfection [47]. They attribute the method of uptake in HeLa [48] and human bronchial epithelial cells [47] to the rod shape of CK_{30} particles; smaller (24 nm) nanoparticles were also taken up *via* a non-degradative pathway in HeLa cells [49]. A recent study by Herd *et al.* also demonstrated that particle geometry affected cellular uptake mechanism [50], therefore emphasizing the need to further study the role of polyplex morphology on cellular uptake. Statistical polymers ($pS_{hi}1$ and $pS_{hi}2$) and pB0 were seen to have rod-shaped morphologies (Figure 6.5), which may contribute to uptake *via* caveolae. Reilly *et al.* also showed that PEI polyplexes containing histone-mimetic peptides achieved productive transfection when routed through caveolae instead of mainly clathrin-mediated endocytosis with PEI alone [51]. While the increased buffering capacity of $pS_{hi}2$ does enhance transfection efficiency, the increases in transfection efficiency with the incorporation of histidine residues are small (at most, only 4.6-fold), and thus, these structures may be attaining high levels of transfection efficiency through an alternative, non-acidifying pathway, such as the caveolar pathway. Thus, in order to improve the transfection efficiency of HPMA-oligolysine copolymers, methods other than improving endosomal buffering can be

explored.

6.4 Conclusions

In summary, we describe the synthesis of statistical and diblock HPMA-oligolysine-oligohistidine copolymers *via* RAFT polymerization and evaluate these materials as gene delivery vehicles. The copolymers were characterized for buffering ability and polyplex formation, and evaluated for in vitro transfection efficiency. Statistical and diblock copolymers also showed increased, but differential buffering capability in the endosomal pH range. Nevertheless, only the statistical polymer containing the highest oligohistidine content resulted in higher transfection efficiencies than the non-histidylated analogue. Therefore, one possible explanation is that for these polymer architectures, higher histidine content may be required. In addition, endocytic inhibitor studies showed that these HPMA copolymers might achieve greater transfection when routed through the caveolar endocytic pathway, indicating that these polymers minimally benefit from enhanced endosomal buffering capabilities. Therefore, alternative approaches for vesicular escape that do not rely on acidification may further increase gene transfection efficiency for this class of polymers.

6.5 Acknowledgments

This work is supported by NIH/NINDS1R01 NS064404. J.S. is supported by the National Science Foundation Graduate Research Fellowship under Grant No. DGE-0718124 and the Howard Hughes Medical Institute/UW Molecular Medicine Graduate Student Scholarship. B.C. and J.L.C. were supported by the Mary Gates Undergraduate Research Fellowship. E.A. was supported by the Amgen Summer Scholars Program. We thank Profs. Anthony Convertine and Patrick Stayton for the general donation of the ECT reagent, Prof. In-Kyu Park (Chonnam Medical University) and David Chu for helpful discussions, Prof. Shaoyi Jiang (University of Washington) for use of his Malvern Zetasizer, and Dr. Bobbie Schneider (Electron Microscopy Services at the Fred Hutchinson Cancer Research Center) for her help and assistance with TEM imaging.

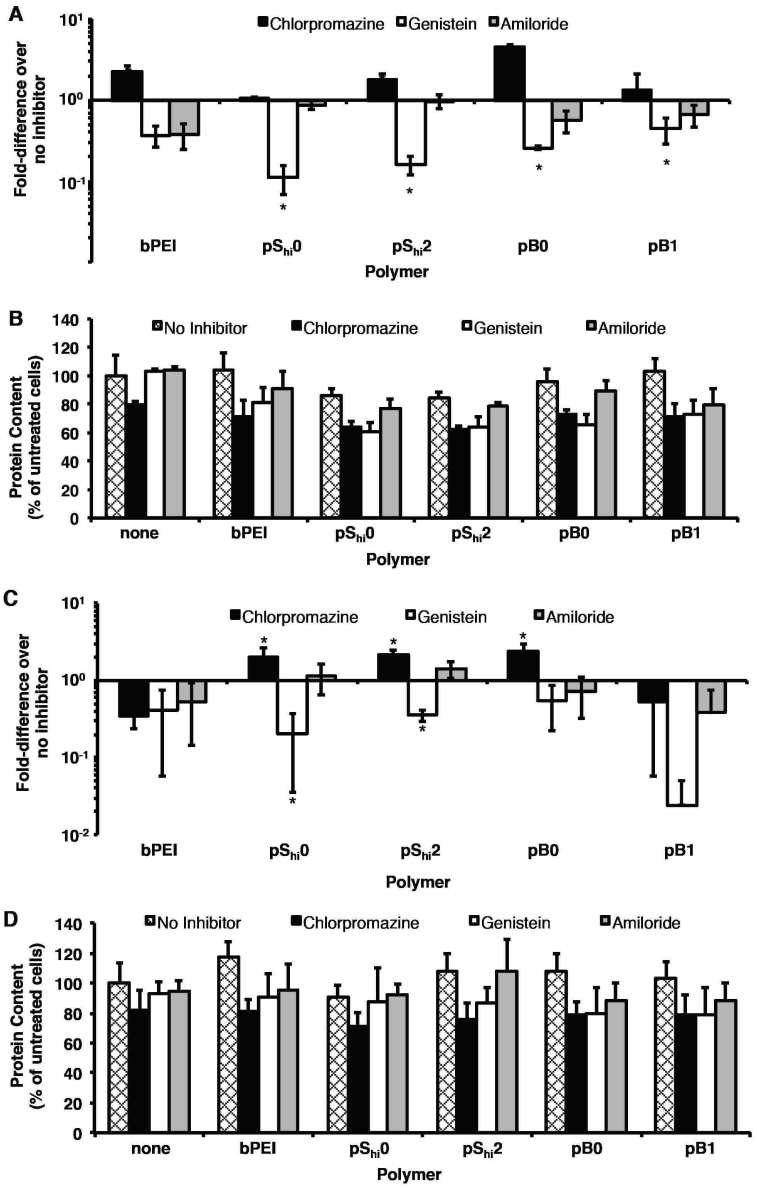

Figure 6.9: **Transfection of HPMA-oligolysine-oligohistidine polyplexes in HeLa and COS-7 cells with chlorpromazine, genistein, or amiloride.** (A) Transfection efficiency and (B) protein content of HeLa cells, and (C) transfection efficiency and (D) cell viability of COS-7 cells transfected with polyplexes formulated with statistical ($pS_{hi}0$, $pS_{hi}2$) or diblock (pB0, pB1) and DNA (1 μg) at N/P 5 in the presence of 10 μg/mL chlorpromazine, 50 μg/mL genistein, or 25 μg/mL amiloride under serum-free conditions. Data are presented as the mean ± S.D., $n = 4$, and representative of four independent experiments. (*) $p < 0.05$, as determined by a two-tailed, unpaired Student's t-test with unequal variance.

References

[1] Pack, D. W., Hoffman, A. S., Pun, S., and Stayton, P. S. (2005) Design and development of polymers for gene delivery. *Nat. Rev. Drug Discov.*, **4**, 581–593.

[2] Ruponen, M., Honkakoski, P., Rönkkö, S., Pelkonen, J., Tammi, M., and Urtti, A. (2003) Extracellular and intracellular barriers in non-viral gene delivery. *J. Control. Release*, **93**, 213–217.

[3] Suh, J., Wirtz, D., and Hanes, J. (2003) Efficient active transport of gene nanocarriers to the cell nucleus. *Proc. Natl. Acad. Sci. U.S.A.*, **100**, 3878–3882.

[4] Varga, C. M., Tedford, N. C., Thomas, M., Klibanov, A. M., Griffith, L. G., and Lauffenburger, D. A. (2005) Quantitative comparison of polyethylenimine formulations and adenoviral vectors in terms of intracellular gene delivery processes. *Gene Ther.*, **12**, 1023–1032.

[5] Behr, J.-P. (1997) The proton sponge: a trick to enter cells the viruses did not exploit. *CHIMIA International Journal for Chemistry*, **51**, 34–36.

[6] Akinc, A., Thomas, M., Klibanov, A. M., and Langer, R. (2005) Exploring polyethylenimine-mediated DNA transfection and the proton sponge hypothesis. *J. Gene Med.*, **7**, 657–663.

[7] Pichon, C., Gonçalves, C., and Midoux, P. (2001) Histidine-rich peptides and polymers for nucleic acids delivery. *Adv. Drug Deliv. Rev.*, **53**, 75–94.

[8] Midoux, P., Pichon, C., Yaouanc, J.-J., and Jaffrès, P.-A. (2009) Chemical vectors for gene delivery: a current review on polymers, peptides and lipids containing histidine or imidazole as nucleic acids carriers. *Br. J. Pharmacol.*, **157**, 166–178.

[9] Chang, K.-L., Higuchi, Y., Kawakami, S., Yamashita, F., and Hashida, M. (2010) Efficient gene transfection by histidine-modified chitosan through enhancement of endosomal escape. *Bioconjug. Chem.*, **21**, 1087–1095.

[10] Hashemi, M., Parhiz, B. H., Hatefi, A., and Ramezani, M. (2011) Modified polyethyleneimine with histidine-lysine short peptides as gene carrier. *Cancer Gene Ther.*, **18**, 12–19.

[11] Benns, J. M., Choi, J. S., Mahato, R. I., Park, J. S., and Kim, S. W. (2000) pH-sensitive cationic polymer gene delivery vehicle: N-Ac-poly(L-histidine)-graft-poly(L-lysine) comb shaped polymer. *Bioconjug. Chem.*, **11**, 637–645.

[12] Chen, Q. R., Zhang, L., Stass, S. A., and Mixson, A. J. (2001) Branched co-polymers of histidine and lysine are efficient carriers of plasmids. *Nucleic Acids Res.*, **29**, 1334–1340.

[13] Johnson, R. N., Burke, R. S., Convertine, A. J., Hoffman, A. S., Stayton, P. S., and Pun, S. H. (2010) Synthesis of statistical copolymers containing multiple functional peptides for nucleic acid delivery. *Biomacromolecules*, **11**, 3007–3013.

[14] Chu, D. S. H., Schellinger, J. G., Shi, J., Convertine, A. J., Stayton, P. S., and Pun, S. H. (2012) Application of living free radical polymerization for nucleic acid delivery. *Acc. Chem. Res.*, **45**, 1089–1099.

[15] Ahmed, M. and Narain, R. (2013) Progress of RAFT based polymers in gene delivery. *Prog. Polym. Sci.*.

[16] Johnson, R. N., Chu, D. S. H., Shi, J., Schellinger, J. G., Carlson, P. M., and Pun, S. H. (2011) HPMA-oligolysine copolymers for gene delivery: optimization of peptide length and polymer molecular weight. *J. Control. Release*, **155**, 303–311.

[17] Parelkar, S. S., Chan-Seng, D., and Emrick, T. (2011) Reconfiguring polylysine architectures for controlling polyplex binding and non-viral transfection. *Biomaterials*, **32**, 2432–2444.

[18] Ahmed, M. and Narain, R. (2011) The effect of polymer architecture, composition, and molecular weight on the properties of glycopolymer-based non-viral gene delivery systems. *Biomaterials*, **32**, 5279–5290.

[19] Yin, L., Song, Z., Kim, K. H., Zheng, N., Tang, H., Lu, H., Gabrielson, N., and Cheng, J. (2013) Reconfiguring the architectures of cationic helical polypeptides to control non-viral gene delivery. *Biomaterials*, **34**, 2340–2349.

[20] Wei, H., Volpatti, L. R., Sellers, D. L., Maris, D. O., Andrews, I. W., Hemphill, A. S., Chan, L. W., Chu, D. S. H., Horner, P. J., and Pun, S. H. Dual-responsive, stabilized nanoparticles for efficient in vivo plasmid delivery.

[21] Burke, R. S. and Pun, S. H. (2010) Synthesis and characterization of biodegradable HPMA-oligolysine copolymers for improved gene delivery. *Bioconjug. Chem.*, **21**, 140–150.

[22] Convertine, A. J., Benoit, D. S. W., Duvall, C. L., Hoffman, A. S., and Stayton, P. S. (2009) Development of a novel endosomolytic diblock copolymer for siRNA delivery. *J. Control. Release*, **133**, 221–229.

[23] Schellinger, J. G., Pahang, J. A., Johnson, R. N., Chu, D. S. H., Sellers, D. L., Maris, D. O., Convertine, A. J., Stayton, P. S., Horner, P. J., and Pun, S. H. (2013) Melittin-grafted HPMA-oligolysine based copolymers for gene delivery. *Biomaterials*, **34**, 2318–2326.

[24] Fischer, D., von Harpe, A., Kunath, K., Petersen, H., Li, Y., and Kissel, T. (2002) Copolymers of ethylene imine and N-(2-hydroxyethyl)-ethylene imine as tools to study effects of polymer structure on physicochemical and biological properties of DNA complexes. *Bioconjug. Chem.*, **13**, 1124–1133.

[25] McCormick, C. L. and Lowe, A. B. (2004) Aqueous RAFT polymerization: recent developments in synthesis of functional water-soluble (co)polymers with controlled structures. *Acc. Chem. Res.*, **37**, 312–325.

[26] Roufaï, M. B. and Midoux, P. (2001) Histidylated polylysine as DNA vector: elevation of the imidazole protonation and reduced cellular uptake without change in the polyfection efficiency of serum stabilized negative polyplexes. *Bioconjug. Chem.*, **12**, 92–99.

[27] Yu, G. S., Bae, Y. M., Choi, H., Kong, B., Choi, I. S., and Choi, J.-S. (2011) Synthesis of PAMAM dendrimer derivatives with enhanced buffering capacity and remarkable gene transfection efficiency. *Bioconjug. Chem.*, **22**, 1046–1055.

[28] Canine, B. F., Wang, Y., and Hatefi, A. (2008) Evaluation of the effect of vector architecture on DNA condensation and gene transfer efficiency. *J. Control. Release*, **129**, 117–123.

[29] Iacobucci, V., Di Giuseppe, F., Bui, T. T., Vermeer, L. S., Patel, J., Scherman, D., Kichler, A., Drake, A. F., and Mason, A. J. (2012) Control of pH responsive peptide self-association during endocytosis is required for effective gene transfer. *Biochim. Biophys. Acta*, **1818**, 1332–1341.

[30] Parhamifar, L., Larsen, A. K., Hunter, A. C., Andresen, T. L., and Moghimi, S. M. (2010) Polycation cytotoxicity: a delicate matter for nucleic acid therapy—focus on polyethylenimine. *Soft Matter*, **6**, 4001–4009.

[31] Burke, R. S. and Pun, S. H. (2008) Extracellular barriers to in vivo PEI and PEGylated PEI polyplex-mediated gene delivery to the liver. *Bioconjug. Chem.*, **19**, 693–704.

[32] Midoux, P. and Monsigny, M. (1999) Efficient gene transfer by histidylated polylysine/pDNA complexes. *Bioconjug. Chem.*, **10**, 406–411.

[33] Chamarthy, S. P., Kovacs, J. R., McClelland, E., Gattens, D., and Meng, W. S. (2003) A cationic peptide consists of ornithine and histidine repeats augments gene transfer in dendritic cells. *Mol. Immunol.*, **40**, 483–490.

[34] McKenzie, D. L., Smiley, E., Kwok, K. Y., and Rice, K. G. (2000) Low molecular weight disulfide cross-linking peptides as nonviral gene delivery carriers. *Bioconjug. Chem.*, **11**, 901–909.

[35] Pichon, C., Roufaï, M. B., Monsigny, M., and Midoux, P. (2000) Histidylated oligolysines increase the transmembrane passage and the biological activity of antisense oligonucleotides. *Nucleic Acids Res.*, **28**, 504–512.

[36] Bowman, E. J., Siebers, A., and Altendorf, K. (1988) Bafilomycins: a class of inhibitors of membrane ATPases from microorganisms, animal cells, and plant cells. *Proc. Natl. Acad. Sci. U.S.A.*, **85**, 7972–7976.

[37] Erbacher, P., Roche, A. C., Monsigny, M., and Midoux, P. (1996) Putative role of chloroquine in gene transfer into a human hepatoma cell line by DNA/lactosylated polylysine complexes. *Exp. Cell Res.*, **225**, 186–194.

[38] Funhoff, A. M., van Nostrum, C. F., Koning, G. A., Schuurmans-Nieuwenbroek, N. M. E., Crommelin, D. J. A., and Hennink, W. E. (2004) Endosomal escape of polymeric gene delivery complexes is not always enhanced by polymers buffering at low pH. *Biomacromolecules*, **5**, 32–39.

[39] Jones, R. A., Poniris, M. H., and Wilson, M. R. (2004) pDMAEMA is internalised by endocytosis but does not physically disrupt endosomes. *J. Control. Release*, **96**, 379–391.

[40] Khalil, I. A., Kogure, K., Akita, H., and Harashima, H. (2006) Uptake pathways and subsequent intracellular trafficking in nonviral gene delivery. *Pharmacol. Rev.*, **58**, 32–45.

[41] Larkin, J. M., Brown, M. S., Goldstein, J. L., and Anderson, R. G. (1983) Depletion of intracellular potassium arrests coated pit formation and receptor-mediated endocytosis in fibroblasts. *Cell*, **33**, 273–285.

[42] Aoki, T., Nomura, R., and Fujimoto, T. (1999) Tyrosine phosphorylation of caveolin-1 in the endothelium. *Exp. Cell Res.*, **253**, 629–636.

[43] Koivusalo, M., Welch, C., Hayashi, H., Scott, C. C., Kim, M., Alexander, T., Touret, N., Hahn, K. M., and Grinstein, S. (2010) Amiloride inhibits macropinocytosis by lowering submembranous pH and preventing Rac1 and Cdc42 signaling. *J. Cell Biol.*, **188**, 547–563.

[44] von Gersdorff, K., Sanders, N. N., Vandenbroucke, R., De Smedt, S. C., Wagner, E., and Ogris, M. (2006) The internalization route resulting in successful gene expression depends on both cell line and polyethylenimine polyplex type. *Mol. Ther.*, **14**, 745–753.

[45] van der Aa, M. A. E. M., Huth, U. S., Häfele, S. Y., Schubert, R., Oosting, R. S., Mastrobattista, E., Hennink, W. E., Peschka-Süss, R., Koning, G. A., and Crommelin, D. J. A. (2007) Cellular uptake of cationic polymer-DNA complexes via caveolae plays a pivotal role in gene transfection in COS-7 cells. *Pharm. Res.*, **24**, 1590–1598.

[46] Vercauteren, D., Vandenbroucke, R. E., Jones, A. T., Rejman, J., Demeester, J., De Smedt, S. C., Sanders, N. N., and Braeckmans, K. (2010) The use of inhibitors to study endocytic pathways of gene carriers: optimization and pitfalls. *Mol. Ther.*, **18**, 561–569.

[47] Kim, A. J., Boylan, N. J., Suk, J. S., Lai, S. K., and Hanes, J. (2012) Non-degradative intracellular trafficking of highly compacted polymeric DNA nanoparticles. *J. Control. Release*, **158**, 102–107.

[48] Chen, X., Shank, S., Davis, P. B., and Ziady, A. G. (2011) Nucleolin-mediated cellular trafficking of DNA nanoparticle is lipid raft and microtubule dependent and can be modulated by glucocorticoid. *Mol. Ther.*, **19**, 93–102.

[49] Lai, S. K., Hida, K., Man, S. T., Chen, C., Machamer, C., Schroer, T. A., and Hanes, J. (2007) Privileged delivery of polymer nanoparticles to the perinuclear region of live cells via a non-clathrin, non-degradative pathway. *Biomaterials*, **28**, 2876–2884.

[50] Herd, H., Daum, N., Jones, A. T., Huwer, H., Ghandehari, H., and Lehr, C.-M. (2013) Nanoparticle geometry and surface orientation influence mode of cellular uptake. *ACS Nano*, **7**, 1961–1973.

[51] Reilly, M. J., Larsen, J. D., and Sullivan, M. O. (2012) Polyplexes traffic through caveolae to the Golgi and endoplasmic reticulum en route to the nucleus. *Mol. Pharm.*, **9**, 1280–1290.

Chapter 7

DEVELOPMENT OF PEPTIDE DISPLAY AND SUBCELLULAR FRACTIONATION TECHNIQUES TO IDENTIFY POTENTIAL TARGETING PEPTIDES TO MITOCHONDRIA

Julie Shi, Jennifer L. Choi, and Suzie H. Pun

Abstract

Approaches to target the mitochondria for drug therapy often take advantage of the mitochondria's negative membrane potential, and thus are generally not targeted to receptors specific for the mitochondria. Therefore, methods to discover new and specific moieties to improve the delivery of mitochondrial-targeted therapeutics are desirable. In this work, we used phage display to identify potential targeting ligands for an altered mitochondrial state using cultured cell lines with a cancerous metabolic state. Mitochondria were isolated from these cell lines using differential centrifugation, and were incubated with an M13 phage library in solution or on a solid surface. After three or more successive subtractive/selection panning steps, no consensus sequences were isolated, possibly due to the numerous targets available and lack of stringency. Therefore, in order to further improve this screening method, increased stringency in the screening process should be explored.

7.1 Introduction

The mitochondria are an important intracellular target for drug therapy [1–3]. Numerous diseases are derived from mitochondrial dysfunction, arising from various defects in metabolic pathways, the synthesis and sequestration of reactive oxygen species (ROS), and mitochondrial DNA. Additionally, pro-apoptotic cancer therapeutics, such as paclitaxel, induce apoptosis by acting on the mitochondrial membrane [4]. Although most studies have focused on determining key design parameters for efficient systemic distribution and cellular uptake of drugs, increasing evidence has shown the importance of intracellular targeting for the delivery of complex biologic therapeutics, such as polymer-drug conjugates. Current approaches for controlling intracellular events in these polymer conjugates include the incorporation of virus-derived peptides [5] or pH-sensitive [6] linkages for endosomal escape and reducible [7] or protease-specific [8–10] linkages for cytosolic release of the drug.

Current approaches to target the mitochondria often take advantage of the mitochondria's negative membrane potential. Amphiphilic molecules, such as rhodamine 123, phosphonium salts, and dequalinium (DQA) [11], have demonstrated localization to the mitochondria, but have shown limited success when chemically conjugated to larger biologics [12]. Recently, a series of mitochondrial-penetrating peptides were designed *de novo* and optimized [13], and have been used to route small molecule drugs to the mitochondria [14–16]. However, methods to discover new and potentially better moieties to improve the intracellular delivery of polymer-based therapeutics are limited.

To address these shortcomings, screening techniques, such as phage display, have been used to find new peptides against purified proteins derived from various organelles, such as the mitochondria [17–19]. However, peptides found in this manner can be limited in applicability since the native intracellular environment is ignored during the screening process. Therefore, methods that involve panning against functional target organelles can potentially allow for the discovery of peptides that can be later used for the delivery of biologics. Recently, the Arap-Pasqualini group reported the use of a modified M13 phage display method to screen for mitochondria-specific peptides *in vitro* [20]; although they identified a peptide that localized to mitochondria and promoted cell death, the identified target was actually

a ribosomal protein. Thus, ligands identified by phage display can potentially enhance the intracellular targeting of various biologic molecules and/or small molecule drugs.

The goal of this work was to combine phage display and subcellular fractionation techniques to identify preferential targeting ligands for mitochondria from tumorigenic cell lines. Primary cell lines derived from foreskin fibroblasts [21] and mammary epithelial cells [22] that were either spontaneously immortalized or introduced with telomerase catalytic subunit (hTERT) for immortalization were used in the subtractive panning process. The transformed versions of these immortalized cells with oncogenic alleles, such as simian virus 40 large and small T antigen and H-ras, were used in the selection panning process. These cell lines have the same genetic background and their metabolic changes have been profiled in depth [21, 22]. Subcellular fractionation was used to isolate mitochondria for phage pannings in solution or with mitochondria applied to a solid surface. Between three to five rounds of subtractive/selection panning rounds were completed, and promising phage clones were evaluated for specific binding to isolated mitochondria.

7.2 Materials and methods

7.2.1 Materials

The Ph.D.-12 and Ph.D.-C7C M13 phage libraries were purchased from New England Biosciences (Ipswitch, MA). The BJ cell lines (EH, EL, and ELR) were generously donated by Prof. William Hahn (Dana Farber Cancer Research Institute, Boston, MA). MCF cell lines (MCF10A, MCF10Ca1) were purchased from the Barbara Ann Karmanos Cancer Institute (Detroit, MI). SuperBlock buffer (no. 37537) and HALT protease inhibitor cocktail were purchased from Thermo Scientific (Rockford, IL). All cell culture reagents were purchased from either Life Technologies (Carlsbad, CA) or Cellgro/Mediatech (Fisher Scientific, Pittsburgh, PA). All other materials were reagent grade or better and were purchased from Sigma-Aldrich (St. Louis, MO) unless otherwise stated.

7.2.2 Cell culture

Foreskin fibroblast cell lines serially transduced with oncogenes (hTERT, simian virus 40 LT & ST, and H-ras, named "BJ EH", "BJ EL", and "BJ ELR", respectively) were maintained in KnockOut-DMEM containing 1X medium 199, 15% fetal bovine serum (FBS), 100 IU penicillin, and 100 $\mu g/mL$ streptomycin. The breast mammary tumorigenic cell line MCF10Ca1 cell line was maintained in DMEM:F12 supplemented with 5% horse serum, 15 mM HEPES, 1.05 mM $CaCl_2$, 100 IU penicillin, and 100 $\mu g/mL$ streptomycin. The MCF10A cell line was maintained in the same media as MCF10Ca1 except supplemented with 10 $\mu g/mL$ insulin, 20 ng/mL EGF, and 0.5 $\mu g/mL$ hydrocortisone. Cells were grown at 37 °C, 5% CO_2 and passaged when they reached ~80% confluency.

7.2.3 Isolation and quantification of mitochondria

Mitochondria were isolated from cells using established protocols Wiekckowski 2009.Two confluent flasks (225 cm^2) of cells were trypsinized and collected. Cells were then pelleted at 180g for 5 min at 4 °C, washed twice with ice-cold isolation buffer (IB) (70 mM sucrose, 220 mM mannitol, 5 mM HEPES, 1 mM EGTA, pH 7.2, 0.5% (w/v) fatty-acid free BSA), resuspended in 2.5X the wet pellet weight in IB containing 1X protease inhibitors, and homogenized with 15 passes through a 25-gauge needle. The homogenate was then centrifuged twice at 600g for 10 min at 4 °C, discarding the pellet, containing unbroken cells and nuclei, each time. The supernatant was then centrifuged at 7000g for 10 min at 4 °C, and the supernatant, containing lysosomes and microsomes, was discarded. The pellet, containing mitochondria, was resuspended in ice-cold IB, pelleted again at 7000g for 10 min at 4 °C, and the supernatant removed, leaving a concentrated mitochondrial pellet. Protein content was measured using a Bradford-based protein assay kit (Bio-Rad) according to the manufacturer's instructions, using immunoglobulin as a standard. The typical yield was ~50 mg/mL protein in a total volume of 5-20 μL.

7.2.4 Solution-phase biopanning

For the initial selection round, 0.5 mg of isolated mitochondria from cancerous cell lines (BJ EL, BJ ELR, or MCF10Ca1) were incubated with 1.5×10^{11} pfu Ph.D.-12 library for 2 h on ice. For subsequent rounds, 1.5×10^{11} pfu of the amplified phage from the previous round was incubated with 0.5 mg of isolated mitochondria from normal cell lines (BJ EH or MCF10A) for 2 h on ice. The mitochondria were then pelleted and washed twice with 250 μL of mitochondrial assay buffer (MAS) (70 mM sucrose, 220 mM mannitol, 10 mM KH_2PO_4, 2 mM HEPES, 1 mM EGTA, pH 7.2, 0.2% (w/v) fatty-acid free BSA), by centrifugation at 7000g for 10 min at 4 °C. The unbound phage (supernatant from washes) was then incubated with 0.5 mg of isolated mitochondria from cancerous cell lines for 1 h on ice. Afterwards, the mitochondria was again pelleted and washed twice with 250 μL MAS containing increasing concentrations of Tween-20. The details for the panning conditions of each round are summarized in Table 7.1. Bound phage was then eluted off the mitochondria by the addition of 100 μL elution buffer (0.2 M glycine, pH 2.2) for 5 min, and then neutralized with 15 μL buffer (1 M Tris-HCl, pH 9.1). Serial dilutions of the eluted phage were incubated with ER2738 *E. coli* and plated on LB plates containing X-gal and IPTG to determine the recovered phage titer. The eluted phage was amplified by adding the remaining phage to early-log phase bacteria (O.D. ~0.2) and grown for 4.5 h at 37 °C. The phage were then recovered by polyethylene glycol/NaCl precipitation, and used for subsequent biopanning rounds.

7.2.5 Solid-phase biopanning

For the initial selection round, the wells of a tissue culture-treated 96-well plate were incubated with 1.5×10^{11} pfu each of the Ph.D.-12 and Ph.D.-C7C libraries in 100 μL MAS for 2 h at 4 °C to deplete the phage library of plate binders. Meanwhile, 10 μg of mitochondria isolated from cancerous cell lines in 50 μL MAS was added into wells of a different tissue culture (TC)-treated 96-well plate, and centrifuged onto the plate at 2000g for 20 min at 4 °C. The phage were then collected off the wells and the wells were washed once with 100 μL MAS. The phage and wash were combined and added to the mitochondria, and allowed

Table 7.1: Biopanning conditions for solution-phase panning

Round	Subtractive (mass, incubation time)	Selection (mass, incubation time)	Wash Conditions
0	-	0.5 mg cancerous mitochondria, 2 h	2X MAS
1	0.5 mg normal mitochondria, 2 h	0.5 mg cancerous mitochondria, 1 h	2X MAS
2	0.5 mg normal mitochondria, 2 h	0.5 mg cancerous mitochondria, 1 h	2X MAS + 0.1% (w/v) Tween-20
3	0.5 mg normal mitochondria, 2 h	0.5 mg cancerous mitochondria, 1 h	2X MAS + 0.3% (w/v) Tween-20

to incubate for 1 h at 4 °C. For subsequent rounds, 1.5×10^{11} pfu of the amplified phage from the previous round were incubated with 10 μg of mitochondria isolated from normal cell lines and applied to TC-treated 96-well plates for 1 h at 4 °C. The phage were then collected off the phage and the wells were washed once with 100 μL MAS. The phage and wash were combined and incubated with 10 μg of mitochondria isolated from cancerous cell lines and applied to TC-treated 96-well plates for up to 1 h at 4 °C. The mitochondria were then washed 3X with 100 μL MAS containing increasing amounts of Tween-20. The details for the panning conditions of each round are summarized in Table 7.2. Bound phage were eluted off the mitochondria, neutralized, titered, and amplified as described above.

7.2.6 Sequencing of phage DNA

Sequencing of phage DNA was carried out as described by the M13 phage display manual (New England Biosciences, Ipswitch, MA) using the -96gIII primer (5'-TCA TAG TTA GCG TAA CG-3'). The purified phage DNA was reconstituted in water and sequenced by a GeneWiz facility (Seattle, WA).

7.2.7 Determination of binding using ELISA

To determine binding of phage-displayed peptides to mitochondria, 10 μg of isolated mitochondria was centrifuged onto individual wells in a 96-well tissue-culture treated plate at 2000g for 20 min at 4 °C. After one wash with 100 μg MAS buffer, mitochondria were

Table 7.2: Biopanning conditions for solid-phase panning

Round	Subtractive (mass, incubation time)	Selection (mass, incubation time)	Wash Conditions
0	plastic plate only	10 μg cancerous mitochondria, 2 h	3X MAS
1	10 μg normal mitochondria, 1 h	10 μg cancerous mitochondria, 1 h	3X MAS
2	10 μg normal mitochondria, 1 h	10 μg cancerous mitochondria, 1 h	3X MAS + 0.1% (w/v) Tween-20
3	10 μg normal mitochondria, 1 h	10 μg cancerous mitochondria, 1 h	3X MAS + 0.3% (w/v) Tween-20
4	10 μg normal mitochondria, 1 h	10 μg cancerous mitochondria, 1 h	3X MAS + 0.5% (w/v) Tween-20
5	10 μg normal mitochondria, 1 h	10 μg cancerous mitochondria, 30 min	3X MAS + 1% (w/v) Tween-20

incubated with serial dilutions of phage in MAS buffer (in 100 mL total volume) for 1 h at 4 °C. The phage solution was then aspirated off, and the mitochondria were washed 3X with MAS containing 1% Tween-20. The mitochondria were then incubated with 200 μL mouse horseradish peroxidase (HRP)-conjugated anti-M13 (1:5000 in Superblock buffer) (GE Healthcare, no. 27-9421-01) for 1 h at room temperature. The wells were then washed 3X with Tris-buffered saline containing 1% Tween-20 (TBS-T), and developed with 100 μL 3,3',5,5'-tetramethylbenzidine (TMB) substrate for 15-30 min. The absorbance was read at 652 nm using a Tecan Safire^2 plate reader.

7.2.8 Mitochondrial respiration measurements

Measurement of the mitochondrial oxygen consumption rate (OCR) was completed with isolated mitochondria using the XF Analyzer (Seahorse Biosciences, North Billerica, MA). Mitochondria were isolated as described above, and diluted 10X in MAS buffer. Various amounts of mitochondria were centrifuged onto an XF cell culture microplate at 2000g for 20 min at 4 °C. After centrifugation, 450 μL of 1X MAS and substrate was added to each well. The mitochondria were viewed briefly under a microscope at 20X to ensure consistent adherence to the well, then placed at 37 °C for 10 min to allow the plate to warm. The plate

was then transferred to the XF24 Analyzer and the experiment initiated. With the initial presence of 10-20 μg mitochondria per well, 10 mM pyruvate, 2 mM malate and 4 μM FCCP, injections were made as follows: port A, 50 μL of 20 μM rotenone (2 μM final); port B, 55 μL of 100 mM succinate (10 mM final); port C, 60 μl of 40 μM antimycin A (4 μM final); port D, 65 μL of 100 mM ascorbate plus 1 mM TMPD (10 mM and 100 μM final, respectively).

For high-throughput measurements, respiration measurements with isolated mitochondria were carried out using the MitoXpress probe (Luxcel Biosciences, Cork, Ireland) according to manufacturer's instructions using succinate as the substrate.

7.3 Results and discussion

7.3.1 Isolation of intact, functional mitochondria

To ensure that peptides were screened to bind functionally-active mitochondria during biopanning rounds, isolated mitochondria were verified for adequate respiration. Since the isolation procedure is similar for all cell lines, and the normal cell lines were probably the most sensitive to the isolation procedure, only the MCF10A and BJ EH cell lines were tested. In general, the oxygen consumption rate (OCR) for isolated mitochondria increased after the addition of ADP, decreased after the addition of oligo, increased after the addition of FCCP, and decreased to baseline after the addition of AA (Figure 7.1).

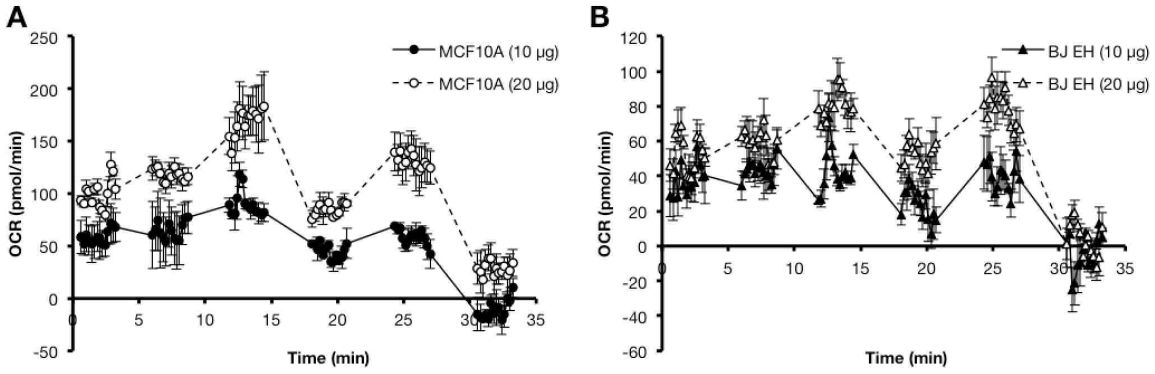

Figure 7.1: **Mitochondrial respiration assay.** Mitochondria were isolated from BJ EH and MCF10A cells and verified for adequate respiration to determine mitochondrial functionality. Data are presented as mean ± S.D., $n = 3$.

7.3.2 Solution-phase biopanning strategy

To selectively isolate peptides that preferentially bound to the altered cancerous mitochondrial phenotype, a consecutive subtractive/selection strategy was used. For the initial selection, a phage library expressing random 12-mer linear peptides was incubated with mitochondria isolated from cancerous cell lines. In subsequent rounds, the amplified phage from the previous round was incubated first with normal mitochondria, and then applied to cancerous mitochondria. The initial selection pan resulted in high titers, indicating the depletion of only 85-97% of the phage library (Figure 7.2). After three additional rounds of panning, 10 clones from each panning was sequenced; no consensus sequences were found (Table 7.3). Several insertless sequences were also found, indicating that the panning conditions may not be sufficiently stringent since ∼5-10% of the phage library consists of insertless phage.

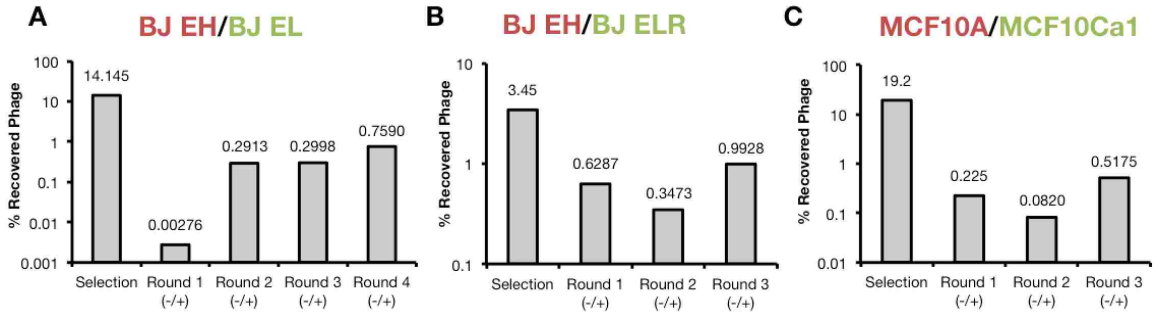

Figure 7.2: **Titers from solution-phase biopanning.** After each round, the recovered phage was titered to calculate enrichment efficiency. Isolated mitochondria from BJ EH cells were used in the subtractive pan in (A) and (B), while isolated mitochondria from MCF10A were used in the subtractive pan in (C). Isolated mitochondria from (A) BJ EL, (B) BJ ELR, and (C) MCF10Ca1 were used in the selection pan.

7.3.3 Solid-phase biopanning strategy

In an effort to decrease the amount of available target for the phage library, isolated mitochondria were applied to wells in the 96-well plate, similarly to preparation of mitochondria for respiration studies. To increase library diversity, the Ph.D.-C7C cyclic 7-mer library

Table 7.3: Sequencing results from solution-phase biopanning

Clone	Sequence[a]		
BJ EH (-)/BJ EL (+)[b,c]		MCF10A (-)/MCF10Ca1 (+)[b]	
EL-01	AFLGPLNALDSY	MCF-01	GNFITDWRSMTN
EL-02	SMLSKQQEVNLR	MCF-02	MHTTIHDIKYSN
EL-03	ALCKGMGPVSVM	MCF-03	NQMWNPSGLRVP
EL-04	VGAAFNVTSLQR	MCF-04	TKLHENNWFMPW
EL-08	EGFHISQRTKML	MCF-05	ITARAYSAYPMS
EL-09	GQWPSQVVEVWL	MCF-06	GLMRMMTSPMPA
BJ EH (-)/BJ ELR (+)[b,c]		MCF-07	TLAGTTIVMKQM
ELR-01	NLMHAPKGGRKQ	MCF-08	GSYTALMVVSQL
ELR-02	SHGYTVVTLQKY	MCF-09	GNVNLLMSNAHS
ELR-03	NLYSYRLDTAVL	MCF-10	SFSYTAMEPPLR
ELR-04	ANDLNETWIPIE		
ELR-07	MIDLRGSPHTVQ		
ELR-08	HGTNWPGHSPMA		
ELR-09	STTFHELQPDVY		
ELR-10	EPHSPNIVWYRQ		

[a] Sequences contain a C-terminal Gly-Gly-Gly-Ser (GGGS) spacer.

[b] The first cell line, followed by a "(-)" was used for the subtractive pan, while the second cell line, followed by a "(+)" was used for the selection pan.

[c] Ten clones were sequenced from each round; clones not listed contained no insert.

was also added to the biopanning rounds. In the modified biopanning strategy (Table 7.2), 50-fold less mitochondria was used for each round. Titers generally increased during the initial subtractive/selection rounds, but then decreased (Figure 7.3). After an initial selection round and five additional subtractive/selection rounds, no consensus sequences were detected again. However, one sequence appeared once in the BJ EH (-)/BJ EL (+) pan (clone EL-04) and again in the BJ EH (-)/BJ ELR (+) pan (clone ELR-08). When the corresponding phage clone was tested for binding affinity using ELISA, no signal was detected (data not shown), indicating a lack of phage binding to the target mitochondria.

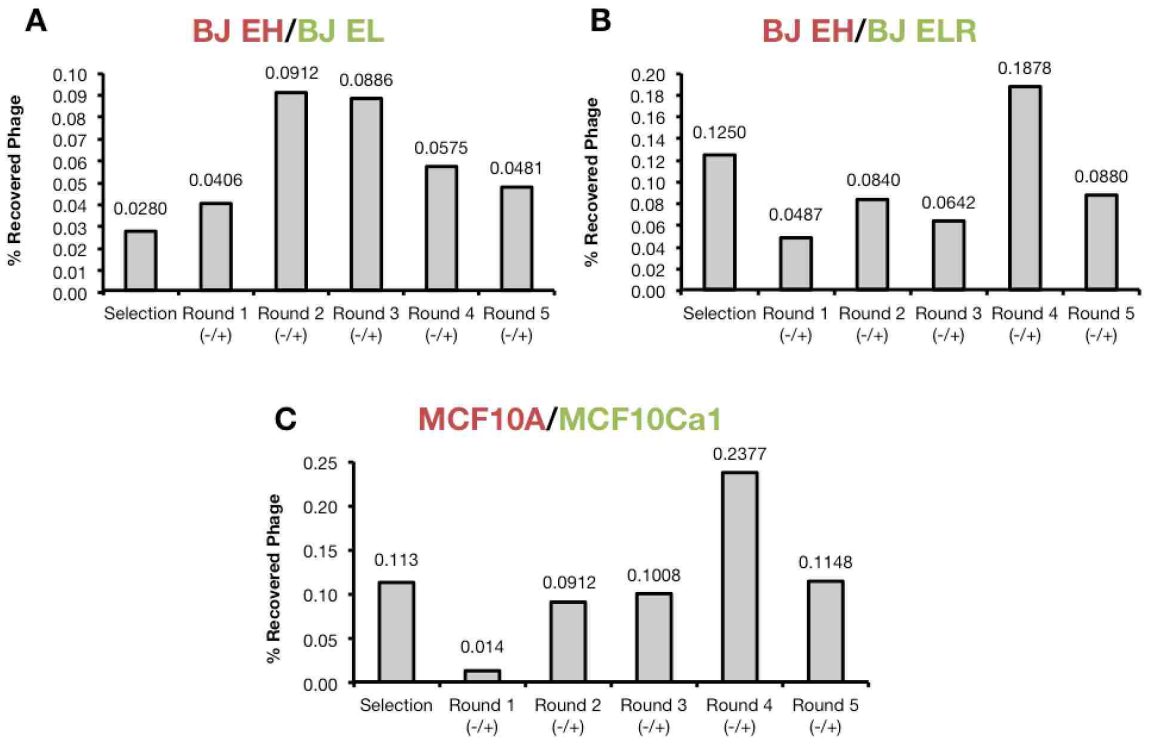

Figure 7.3: **Titers from solid-phase biopanning.** After each round, the recovered phage was titered to calculate enrichment efficiency. Isolated mitochondria from BJ EH cells were used in the subtractive pan in (A) and (B), while isolated mitochondria from MCF10A were used in the subtractive pan in (C). Isolated mitochondria from (A) BJ EL, (B) BJ ELR, and (C) MCF10Ca1 were used in the selection pan.

Table 7.4: Sequencing results from solid-phase biopanning

Clone	Sequence[a]	Clone	Sequence[a]
BJ EH (-)/BJ EL (+)[b,c]		MCF10A (-)/MCF10Ca1 (+)[b,c]	
EL-01	SPSVHLKYGQIW	MCF-01	MNRIQTETTHTP
EL-03	ACSSMPVHTC	MCF-02	NPVANHPAKLAY
EL-04	SPIEPKYQYIRT	MCF-03	QHREIQYNYFWQ
EL-05	SLFVDDHYSQQG	MCF-04	AHFSKAGPXIRS[d]
EL-07	NSHWPXMALQSI[d]	MCF-05	SGNAAHFLSGHR
EL-08	ANHDSTQFNKGW	MCF-07	HTFVNHRPGYNT
EL-09	YNSDLSRYPRIS	MCF-08	ACVGTAALYC
EL-11	QPERPVTGNFTS	MCF-09	ESTRSNSAYTPL
EL-12	TMHSFLSPTIKY	MCF-10	NVNTLLNIYKSR
EL-13	VMPSNVNLPKLW	MCF-11	NHYWLLDHQHNE
EL-14	ITEPPGGPRQIN	MCF-12	AYLSSTEPARHW
EL-15	VSIPTLRTLNYS	MCF-13	QNSTPRGDMSVP
EL-18	AMPKQHTSLFHN	MCF-14	ANRAIQYHVPQE
EL-20	EVSLAPMNQKPE	MCF-15	MPPSLGASQLNT
EL-21	GAAQNPPPAGMR	MCF-16	NSQTFISSMQGQ
BJ EH (-)/BJ ELR (+)[b,c]		MCF-17	TFGVATSGSGWD
ELR-01	HSGVTFKPMPAG	MCF-18	TDHVSSNNKWML
ELR-02	LGHAEQXAFVKR[d]	MCF-19	SAHPLQRYHEMA
ELR-03	GAAYEKAYFSRT		
ELR-04	SLANVPLPLPVS		
ELR-05	ASGPYTNTNYGA		
ELR-07	DTLMLAPNWMRP		
ELR-08	SPIEPKYQYIRT		
ELR-09	FPSHNSWNHNIL		
ELR-12	STHYMAMNFMPT		
ELR-13	NNSYHESSWTNT		
ELR-14	FQETAEVNSSNR		
ELR-15	GASYHQVNGSDA		
ELR-16	FAPQATRTQHPQ		
ELR-17	DFRDWRNDYTIY		
ELR-18	ACLTQAHYTC		
ELR-19	DSLTTKMAMHLH		

[a] Sequences contain a C-terminal Gly-Gly-Gly-Ser (GGGS) spacer.

[b] The first cell line, followed by a "(-)" was used for the subtractive pan, while the second cell line, followed by a "(+)" was used for the selection pan.

[c] Ten clones were sequenced from each round; clones not listed contained no insert.

[d] The amino acid residue "X" corresponds to a stop codon.

7.4 Conclusions

The identification of targeting ligands for the mitochondria can lead to improved therapies for the treatment of diseases that arise from mitochondrial dysfunction. We have demonstrated that using phage display on isolated organelles may be useful in identifying potential targeting ligands to altered mitochondrial states; however, in order to optimize these methods, more stringency will need to be used during the screening process. Alternatively, an additional screening of sequenced peptides can be carried out to determine potential binding to isolated mitochondria of a desired phenotype.

7.5 Acknowledgments

J.S. is supported by the National Science Foundation Graduate Research Fellowship under Grant No. DGE-0718124. J.L.C. were supported by the Mary Gates Undergraduate Research Fellowship. We gratefully thank Prof. William Hahn (Dana-Farber Cancer Research Institute) for the general donation of the BJ cell lines, Dr. David Hockenbery (Fred Hutchinson Cancer Research Center) for helpful discussions, and Dr. Daciana Margineantu (Fred Hutchinson Cancer Research Center) for her help with the mitochondrial respiration studies on the Seahorse XF24 Analyzer.

References

[1] Murphy, M. P. and Smith, R. A. (2000) Drug delivery to mitochondria: the key to mitochondrial medicine. *Adv. Drug Deliv. Rev.*, **41**, 235–250.

[2] Muratovska, A., Lightowlers, R. N., Taylor, R. W., Wilce, J. A., and Murphy, M. P. (2001) Targeting large molecules to mitochondria. *Adv. Drug Deliv. Rev.*, **49**, 189–198.

[3] Armstrong, J. S. (2009) Mitochondrial medicine: pharmacological targeting of mitochondria in disease. *Br. J. Pharmacol.*, **151**, 1154–1165.

[4] Costantini, P., Jacotot, E., Decaudin, D., and Kroemer, G. (2000) Mitochondrion as a novel target of anticancer chemotherapy. *J. Natl. Cancer Inst.*, **92**, 1042–1053.

[5] Nori, A., Jensen, K. D., Tijerina, M., Kopečková, P., and Kopeček, J. (2003) Tat-conjugated synthetic macromolecules facilitate cytoplasmic drug delivery to human ovarian carcinoma cells. *Bioconjug. Chem.*, **14**, 44–50.

[6] Ulbrich, K. and Šubr, V. (2004) Polymeric anticancer drugs with pH-controlled activation. *Adv. Drug Deliv. Rev.*, **56**, 1023–1050.

[7] Saito, G., Swanson, J. A., and Lee, K.-D. (2003) Drug delivery strategy utilizing conjugation via reversible disulfide linkages: role and site of cellular reducing activities. *Adv. Drug Deliv. Rev.*, **55**, 199–215.

[8] Kopecek, J., Kopecková, P., Minko, T., and Lu, Z. (2000) HPMA copolymer-anticancer drug conjugates: design, activity, and mechanism of action. *Eur. J. Pharm. Biopharm.*, **50**, 61–81.

[9] Lee, J. S., Groothuis, T., Cusan, C., Mink, D., and Feijen, J. (2011) Lysosomally cleavable peptide-containing polymersomes modified with anti-EGFR antibody for systemic cancer chemotherapy. *Biomaterials*, **32**, 9144–9153.

[10] Chu, D. S. H., Johnson, R. N., and Pun, S. H. (2012) Cathepsin B-sensitive polymers for compartment-specific degradation and nucleic acid release. *J. Control. Release*, **157**, 445–454.

[11] Torchilin, V. P. (2012) Recent approaches to intracellular delivery of drugs and DNA and organelle targeting. *Annu Rev Biomed Eng*, **8**, 343–375.

[12] Callahan, J. and Kopeček, J. (2006) Semitelechelic HPMA copolymers functionalized with triphenylphosphonium as drug carriers for membrane transduction and mitochondrial localization. *Biomacromolecules*, **7**, 2347–2356.

[13] Horton, K. L., Pereira, M. P., Stewart, K. M., Fonseca, S. B., and Kelley, S. O. (2012) Tuning the activity of mitochondria-penetrating peptides for delivery or disruption. *Chembiochem*, **13**, 476–485.

[14] Fonseca, S. B., Pereira, M. P., Mourtada, R., Gronda, M., Horton, K. L., Hurren, R., Minden, M. D., Schimmer, A. D., and Kelley, S. O. (2011) Rerouting chlorambucil to mitochondria combats drug deactivation and resistance in cancer cells. *Chem. Biol.*, **18**, 445–453.

[15] Pereira, M. P. and Kelley, S. O. (2011) Maximizing the therapeutic window of an antimicrobial drug by imparting mitochondrial sequestration in human cells. *J. Am. Chem. Soc.*, **133**, 3260–3263.

[16] Chamberlain, G. R., Tulumello, D. V., and Kelley, S. O. (2013) Targeted delivery of doxorubicin to mitochondria. *ACS Chem. Biol.*, **8**, 1389–1395.

[17] Takenaka, I. M., Leung, S. M., McAndrew, S. J., Brown, J. P., and Hightower, L. E. (1995) Hsc70-binding peptides selected from a phage display peptide library that resemble organellar targeting sequences. *J. Biol. Chem.*, **270**, 19839–19844.

[18] Gueorguieva, D., Li, S., Walsh, N., Mukerji, A., Tanha, J., and Pandey, S. (2006) Identification of single-domain, Bax-specific intrabodies that confer resistance to mammalian cells against oxidative-stress-induced apoptosis. *FASEB J.*, **20**, 2636–2638.

[19] Serasinghe, M. N., Seneviratne, A. M. P. B., Smrcka, A. V., and Yoon, Y. (2010) Identification and characterization of unique proline-rich peptides binding to the mitochondrial fission protein hFis1. *J. Biol. Chem.*, **285**, 620–630.

[20] Rangel, R., et al. (2012) Combinatorial targeting and discovery of ligand-receptors in organelles of mammalian cells. *Nat. Commun.*, **3**, 788.

[21] Ramanathan, A., Wang, C., and Schreiber, S. L. (2005) Perturbational profiling of a cell-line model of tumorigenesis by using metabolic measurements. *Proc. Natl. Acad. Sci. U.S.A.*, **102**, 5992–5997.

[22] Richardson, A. D., Yang, C., Osterman, A., and Smith, J. W. (2008) Central carbon metabolism in the progression of mammary carcinoma. *Breast Cancer Res. Treat.*, **110**, 297–307.

Part III

FUTURE PERSPECTIVES

The final section summarizes the major findings of the work described in this document, and provides potential project ideas as follow-up experiments to the major findings.

Chapter 8

SUMMARY OF MAJOR FINDINGS AND RECOMMENDATIONS FOR FUTURE WORK

8.1 Summary of major findings

8.1.1 Quantitative assessment of the intracellular trafficking of nonviral vectors and associated cargo

A considerable number of synthetic materials has been developed in the hope of discovering better gene delivery vectors. However, our knowledge of how these vectors behave in biological systems is still limited. Thus, it is imperative to enhance our understanding of how these vectors work in order to engineer more efficient delivery systems. In Chapters 1 and 2, subcellular fractionation methods were developed and used to elucidate the intracellular whereabouts of a commonly used nonviral gene delivery vector, polyethylenimine (bPEI), and its cargo DNA. We found that while a large amount of DNA becomes cell-associated, only a small fraction of the polymer does so, indicating that the polymeric carrier and DNA become dissociated early on in the transfection process. These unexpected results raise important questions of what the role of the polymeric carrier is in the gene delivery process, and shed new insight into how gene delivery vectors and cargo are processed by the cell.

8.1.2 Consideration of particle morphology when designing gene delivery vectors

While several studies have shown that particle morphology can affect cellular internalization rates, the relationship between particle morphology and biologic delivery has not been explored in detail. In Chapter 3, particles of larger aspect ratios (more rod-like) were found to have slower cellular internalization rates. Particle morphology was decoupled from other particle properties, such as particle surface charge, uptake mechanism, and intracellular trafficking kinetics. These fundamental findings are important to further the design and development of non-viral gene delivery vectors.

8.1.3 Peptide-functionalized cationic polymers as nonviral gene delivery vectors

In order to overcome various barriers to gene delivery, synthetic materials have been developed with bioactive peptides to address these barriers. In Chapters 4 through 6, polymers consisting of a hydrophilic backbone of *N*-(2-hydroxypropyl)methacrylamide (HPMA) and several bioactive peptides for DNA condensation, endosomal escape, and degradability were described. In Chapter 5, degradability was introduced into the HPMA-oligolysine base polymer *via* reducible linkers. Although the incorporation of reducible linkers reduced the ability of the polymer to transfect cells efficiently, the reducible polymers were much better tolerated than the non-reducible polymer. The instability of the reducible polymer was attributed to the high concentration of disulfide linkages in the polymer, which led to spontaneous reduction of the disulfide bonds. In Chapter 6, oligohistidine peptides were incorporated into the HPMA-oligolysine base polymer in an effort to increase endosomal escape *via* the proton sponge effect. The polymer architecture (random-statistical *vs.* diblock) was found to affect the buffering range of the oligohistidine-containing polymers. Since the transfection efficiency was only slightly improved with a high incorporation of oligohistidine peptides, the mechanism of cellular uptake was also investigated; the HPMA-oligolysine polymers were found achieve high transfection efficiency through a non-acidifying caveolar pathway. The development of these peptide-polymers are summarized in Chapter 4, which provides insight on the impact of polymer architecture, multivalency effects, and the use of peptides for the continued development of gene delivery vectors.

8.2 Recommendations for future work

8.2.1 Role of excess polymer in polyplex transfection

Background and significance

Excess free polymer is necessary for efficient gene transfer [1]; however, the role of the excess polymer has not been clearly elucidated. Several reports demonstrated that treating cells with polyplexes at an N/P 3, and adding excess polymer (to N/P 10) at various times before or after the main polyplex treatment decreased transfection in all cases [2–4]. However, Bonner *et al.* demonstrated that transfection efficiencies increased with the addition of

excess polymer (to N/P 10) 4 h after an initial transfection with polyplexes at N/P 5 [5]. Furthermore, the amount of internalized DNA is decreased when excess polymer was added after the initial polyplex addition [2]. We also previously showed that very little polymer is internalized in the cell, even after 4 h [6]. Therefore, it is still unclear how the polymeric carrier works to increase transfection.

Preliminary results

Since there are conflicting reports as to whether adding excess polymer does increase gene transfer efficiencies, HeLa cells were transfected with radiolabeled ([^{14}C]) bPEI polyplexes at an initial N/P 3, and excess radiolabeled ([^{3}H]) polymer (to N/P 5) was added immediately after polyplex treatment ($t = 0$) or 4 h later ($t = 4$) (Figure 8.1). As a control, polyplexes were formulated at N/P 5 with the same ratio of [^{14}C]- and [^{3}H]-labeled bPEI. The polyplex solution was then removed after 8 h. The cells were replenished with complete media, and assessed for polyplex transfection and radioactivity at 48 h. In general, less than ~3% of the added polymer was detected in cell lysates. In agreement with previous reports [2–4], transfection efficiencies decreased when excess polymer was added 4 h after the initial polyplex treatment (Figure 8.1A). Similarly to previous results (Section 1.4.8), radiolabeled bPEI was less toxic than unlabeled bPEI (Figure 8.1B). The amount of cell-associated [^{14}C]-labeled bPEI was similar for all treatment groups, but there was less cell-associated [^{3}H]-labeled bPEI in cells dosed with excess polymer at 4 h (Figure 8.1C). However, there are differential amounts of cell-associated bPEI with cells treated at N/P 5, and so these results should be further verified.

Specific aim

To further investigate the role of excess polymer in polyplex transfection, we propose the following specific aim:

Aim 1 *Determine the uptake and transfection efficiencies of dual-labeled bPEI polyplexes with excess polymer pulsed in at different time points.* As an initial step, polyplexes formulated with [^{14}C]- and/or [^{3}H]-labeled bPEI should be confirmed for similar complexation

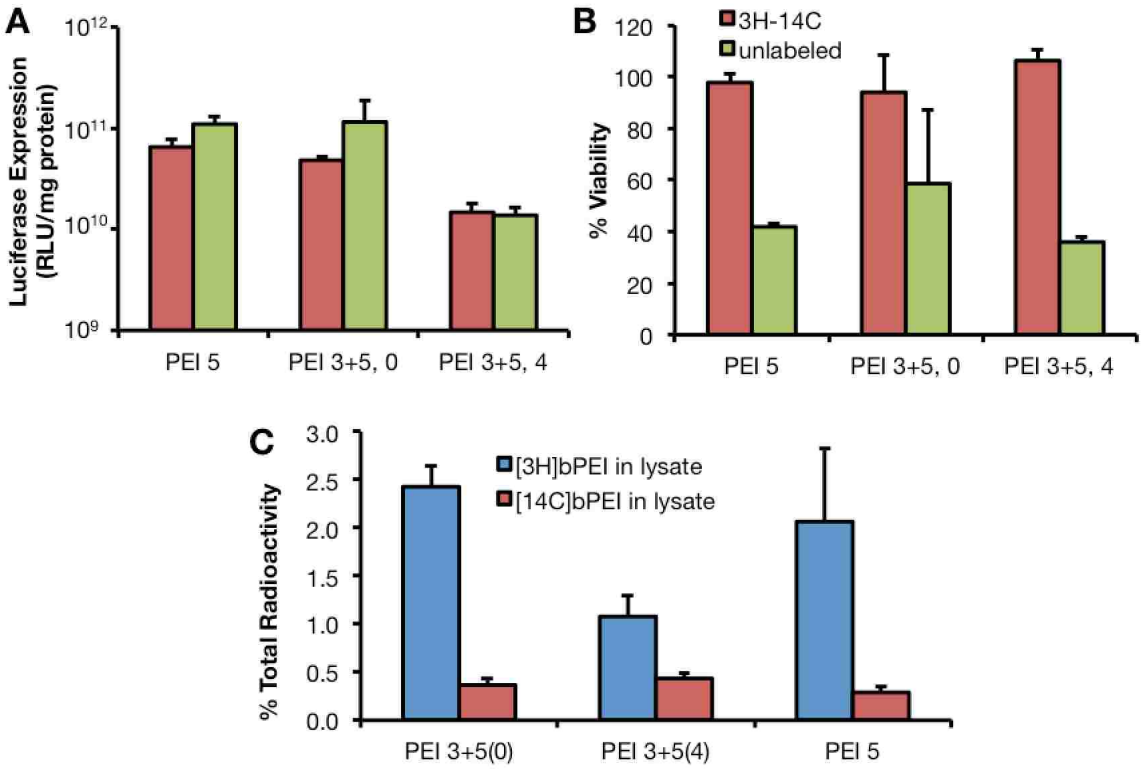

Figure 8.1: **Uptake and transfection of dual-radiolabeled bPEI polyplexes in HeLa cells.** HeLa cells were treated with polyplexes formulated with [^{14}C]-labeled bPEI (N/P 3) (containing 1 μh DNA), and supplemented with [^{3}H]-labeled bPEI (to N/P 5) either immediately after initial polyplex treatment ("PEI 3+5,0"), or 4 h after ("PEI 3+5,4"). As a control, polyplexes were formulated with the same ratio of radiolabeled bPEI at N/P 5 ("PEI 5"). Polyplexes were removed after 8 h, and cells were replenished with complete media. Cells were assessed for radioactivity, luciferase expression, and protein content at 48 h. Data are presented as mean ± S.D., $n = 3$.

behavior, similarly to previous work (Figure 2.5). HeLa cells will be treated with polyplexes formulated with [^{14}C]-labeled bPEI at N/P 5 with excess polymer dosed in either immediately after initial polyplex treatment, or 4 h later (up to N/P 10). For uptake studies, cells will then be washed with CellScrub to remove surface-bound polyplexes, and collected media, wash buffer, and lysate will be quantified for radioactivity. For transfection studies, cells will be assessed for bulk luciferase activity.

8.2.2 Cellular uptake of nonviral vectors and associated DNA cargo in vivo

Background and significance

In Chapter 2 we demonstrated that a relatively small amount of polymer becomes cell-associated in an *in vitro* cell culture model. In order to improve gene delivery *in vivo*, it is important to translate these *in vitro* findings and investigate the amount of polymeric carrier and DNA cargo that is internalized by target cells after *in vivo* administration. Although several reports have tracked the nonviral carrier and nucleic acid cargo in whole organs [7–10], there are currently limited studies on the relative amount of nonviral carrier and nucleic acid cargo in various cell types after *in vivo* administration. We also previously demonstrated that very little polymer becomes internalized in liver cells even though DNA was detected [11]; however, fluorescence-labeling was used, and so relative quantification of the two components was not possible. A previous report demonstrated that about 60% of systemically injected radiolabeled polyplexes were found in the liver after 30 min [12].

Specific aims

To further investigate the intracellular trafficking of polymeric carrier and cargo DNA *in vivo*, we propose the following specific aims:

Aim 1 *Quantify the amount of radiolabeled polymer and DNA associated with hepatocytes after systemic in vivo administration.* Since the majority of polyplexes accumulate in the liver after tail vein injection and hepatocytes are a target cell of interest for therapies, we will focus on quantifying polyplex distribution in hepatocytes. Balb/c mice will receive [^{14}C]bPEI/[^{3}H]DNA polyplex treatment at N/P 3 (containing 25 μg DNA) *via* tail vein injection. The animals will be sacrificed, and livers will be isolated after 20 min and 1 h. Hepatocytes from mouse liver will be extracted using established protocols [13]. Hepatocytes will then be prepared for scintillation counting for determine relative quantities of [^{14}C]bPEI and [^{3}H]DNA.

Aim 2 *Quantify the amount of radiolabeled polymer and DNA associated with neural progenitor cells (NPCs) after intraventricular injection.* In order to improve gene delivery to the brain, it is important to understand the trafficking of materials in an *in vivo* environment. Previous work in the Pun group demonstrated gene delivery to adult NPCs using Tet1-targeted PEI-polyethylene glycol (PEG) as the polymeric carrier [14]. Similarly, untargeted and targeted constructs will be radiolabeled by partial acetylation (Section 2.2.6), used to formulate polyplexes at N/P 15 (containing 2.5 μg) [^{3}H]DNA), and stereotaxically injected into the left side of the skull of C57/BL6 mice. After 24 h, the mice will be sacrificed, the brain will be harvested, and NPCs will be purified using established protocols [15]. NPCs will then be prepared for scintillation counting for determine relative quantities of [^{14}C]bPEI and [^{3}H]DNA.

8.2.3 Role of exocytosis in polyplex trafficking

Background and significance

We previously demonstrated that there was a differential distribution of polymer and DNA in a 5-20% iodixanol gradient, with an overlap of the two components in between the peak intensities of polymer and DNA (Section 2.9) [6]. We hypothesized that polymer may be trafficking through multivesicular bodies (MVBs), which have previously been shown to be distributed amongst endosomal and lysosomal fractions in HeLa cells [16]. Recent reports have also demonstrated the role of MVBs in the recycling of lipid/siRNA complexes. When delivered with lipid/RNA-induced silencing (RISC) complexes, the amount of internalized siRNA in the cytosolic fraction was only $<$ 0.1-1%, while $>$ 75-90% of the internalized siRNA was directed for clearance by lysosomes or secretion by MVBs [17, 18]. The Anderson group recently showed that MVBs were responsible for the recycling of $\sim$70% of the internalized siRNA/lipid complexes [19]. Therefore, it is possible that trafficking through MVBs may also play a role in polymer/DNA polyplex trafficking.

Preliminary results

Since there are conflicting reports as to the presence of MVBs in HeLa cells, HeLa cell lysate was separated according to the density-gradient fractionation (Section 2.2.15), and the fractions were probed for the presence of CD63 (Santa Cruz Biotechnology, no. sc-5275, 1:500 dilution), a marker for MVBs. CD63 was detected lesser dense fractions compared to hexosaminidase A, an enzymatic marker for lysosomes (Figure 8.2). These results suggest that polymer may be preferentially trafficking through MVBs and recycled out of the cell. A low amount of polymer was detected in cell-associated fractions, also suggesting rapid exocytosis of the polymer (Figure 2.8). However, organelle distribution have been shown to shift after polyplex treatment (Figure 2.9), and thus, CD63 distribution should also be quantified upon polyplex treatment.

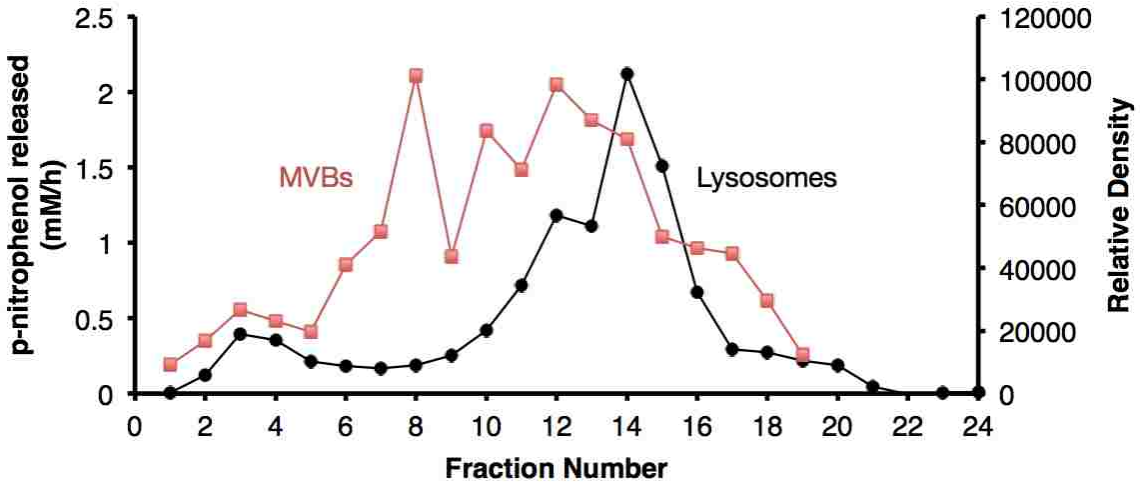

Figure 8.2: **Distribution of CD63 and hexosaminidase A in a 5-20% iodixanol gradient.** 2×10^7 HeLa cells were homogenized, and fractionated according to the methods in Section 2.2.15. Collected fractions were immunoprecipitated and probed for CD63 using a chemiluminscent substrate. The intensity of each band was quantified using ImageJ. Hexosaminidase A activity was also determined for each fraction.

Specific aims

To further investigate the role of MVBs in polyplex trafficking and pinpoint the intracellular site of polyplex dissociation, we propose the following specific aims:

Aim 1 *Determine the distribution of radiolabeled bPEI/DNA polyplexes in polyplex-treated cells over time.* HeLa cells will be treated with [^{14}C]bPEI/[^{3}H]DNA at N/P 5 (containing 100 μg DNA) for 30 min, 2 h, and 4 h, and subsequently homogenized and fractionated using a 10-30% iodixanol gradient to promote better resolution between endocytic organelles [16]. Fractions collected will analyzed by marker enzyme markers, as described previously [6], and will be probed for CD49 (plasma membrane), Rab5 (early endosome), CD63 (MVBs), LAMP2 (lysosomes). Radiolabeled bPEI and DNA will also be quantified in extracellular exosomes by collecting the supernatant after polyplex treatment and isolating extracellular exosomes according to established protocols [20].

Aim 2 *Determine the uptake of radiolabeled bPEI/DNA polyplexes after downregulating MVB formation.* To determine if downregulation of MVB biogenesis would increase the amount of internalized polymer, HeLa cells will be pre-treated with siRNA against *Hrs* (si*Hrs*), which is necessary for MVB formation [21], and subsequently treated with radiolabeled bPEI/DNA polyplexes for 30 min, 2 h, or 4 h. Radiolabeled bPEI and DNA will also be quantified in media, cell wash buffer, and cell lysate. Furthermore, to determine if downregulating MVB formation can increase polyplex transfection, HeLa cells pre-treated with si*Hrs* will be used for transfection analysis. As an alternative approach, downregulation of Neimann-Pick type C1 (NPC1) may be used instead of Hrs since it has been shown to be an important regulator of lipid/siRNA complex recycling [19].

8.2.4 Alternative methods for the analysis of materials in subcellular organelles

Subcellular fractionation, while a robust method for quantifying the intracellular distribution of various biologics, is a very tedious and time-consuming process, and inefficient for high-throughput analysis of multiple gene delivery vectors. In order to facilitate the establishment of property-structure-function relationships, an improved method for the analysis

of materials in subcellular organelles is needed. Fluorescence-assisted organelle sorting (FAOS) may be a higher-throughput method where fluorescently-labeled compounds can be detected with fluorescently-labeled organelles. Organelles can be labeled with fluorescent protein constructs, or with various fluorescent organelle markers (*e.g.* MitoTracker for mitochondria, LysoTracker for lysosomes, etc.). Colocalization of the organelle fluorescence and fluorscently-labeled compound can then be quantified. Although this method is significantly less quantitative, it may be ideally used as an initial screen to determine the optimal fractionation procedure to use in later studies, and may be useful for discerning potential property-structure-function relationships.

8.2.5 HPMA-oligolysine brush polymers with a reducible polymer backbone

In Chapter 5, we described the development of a HPMA-oligolysine brush polymer with reducible disulfide linkages between the HPMA backbone and pendant oligolysine moeity. These polymers were sensitive to spontaneous reduction from trace metals in solution, and thus, better methods for introducing degradable segments into the polymer may be attractive. Recent reports have shown various methods for incorporating degradable structures into polymers. For example, novel cyclic monomers were developed to incorporate cleavable functional groups, *e.g.* esters and disulfides [22]. These cyclic monomers were efficiently incorporated into linear copolymers *via* radical ring-opening polymerization (Figure 8.3). Therefore, incorporating cyclic monomers of HPMA into the polymer backbone may enhance degradability of the polymer while maintaining transfection efficiency.

References

[1] Boeckle, S., von Gersdorff, K., van der Piepen, S., Culmsee, C., Wagner, E., and Ogris, M. (2004) Purification of polyethylenimine polyplexes highlights the role of free polycations in gene transfer. *J. Gene Med.*, **6**, 1102–1111.

[2] Dai, Z., Gjetting, T., Mattebjerg, M. A., Wu, C., and Andresen, T. L. (2011) Elucidating the interplay between DNA-condensing and free polycations in gene transfection through a mechanistic study of linear and branched PEI. *Biomaterials*, **32**, 8626–8634.

[3] Yue, Y., Jin, F., Deng, R., Cai, J., Chen, Y., Lin, M. C. M., Kung, H.-F., and Wu, C. (2011) Revisit complexation between DNA and polyethylenimine - Effect of uncom-

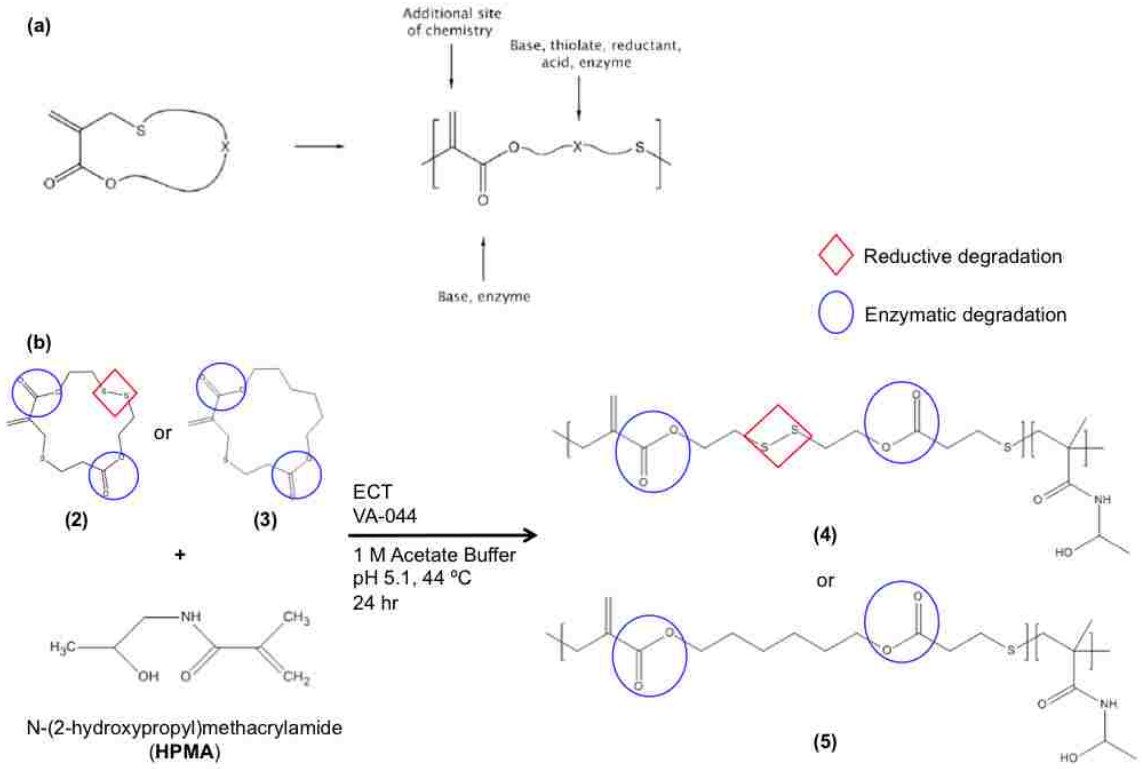

Figure 8.3: **Synthesis of cyclic monomers and polymerization of cyclic monomer with HPMA.** (A) Radical ring-opening polymerization of cyclic monomers, as described in [22], and (B) RAFT polymerization of HPMA and cyclic monomers.

plexed chains free in the solution mixture on gene transfection. *J. Control. Release*, **155**, 67–76.

[4] Yue, Y., Jin, F., Deng, R., Cai, J., Dai, Z., Lin, M. C. M., Kung, H.-F., Mattebjerg, M. A., Andresen, T. L., and Wu, C. (2011) Revisit complexation between DNA and polyethylenimine–effect of length of free polycationic chains on gene transfection. *J. Control. Release*, **152**, 143–151.

[5] Bonner, D. K., Zhao, X., Buss, H., Langer, R., and Hammond, P. T. (2013) Crosslinked linear polyethylenimine enhances delivery of DNA to the cytoplasm. *J. Control. Release*, **167**, 101–107.

[6] Shi, J., Chou, B., Choi, J. L., Ta, A. L., and Pun, S. H. (2013) Investigation of polyethylenimine/DNA polyplex transfection to cultured cells using radiolabeling and subcellular fractionation methods. *Mol. Pharm.*, **10**, 2145–2156.

[7] Barron, L. G., Meyer, K. B., and Szoka, F. C. (1998) Effects of complement depletion on the pharmacokinetics and gene delivery mediated by cationic lipid-DNA complexes. *Hum. Gene Ther.*, **9**, 315–323.

[8] Shenoy, D., Little, S., Langer, R., and Amiji, M. (2005) Poly(ethylene oxide)-modified poly(beta-amino ester) nanoparticles as a pH-sensitive system for tumor-targeted delivery of hydrophobic drugs: part 2. In vivo distribution and tumor localization studies. *Pharm. Res.*, **22**, 2107–2114.

[9] Merkel, O. M., Librizzi, D., Pfestroff, A., Schurrat, T., Buyens, K., Sanders, N. N., De Smedt, S. C., Béhé, M., and Kissel, T. (2009) Stability of siRNA polyplexes from poly(ethylenimine) and poly(ethylenimine)-g-poly(ethylene glycol) under in vivo conditions: effects on pharmacokinetics and biodistribution measured by Fluorescence Fluctuation Spectroscopy and Single Photon Emission Computed Tomography (SPECT) imaging. *J. Control. Release*, **138**, 148–159.

[10] Merkel, O. M., Beyerle, A., Librizzi, D., Pfestroff, A., Behr, T. M., Sproat, B., Barth, P. J., and Kissel, T. (2009) Nonviral siRNA delivery to the lung: investigation of PEG-PEI polyplexes and their in vivo performance. *Mol. Pharm.*, **6**, 1246–1260.

[11] Burke, R. S. and Pun, S. H. (2008) Extracellular barriers to in vivo PEI and PEGylated PEI polyplex-mediated gene delivery to the liver. *Bioconjug. Chem.*, **19**, 693–704.

[12] Nishikawa, M., Yamauchi, M., Morimoto, K., Ishida, E., Takakura, Y., and Hashida, M. (2000) Hepatocyte-targeted in vivo gene expression by intravenous injection of plasmid DNA complexed with synthetic multi-functional gene delivery system. *Gene Ther.*, **7**, 548–555.

[13] Li, W.-C., Ralphs, K. L., and Tosh, D. (2010) Isolation and culture of adult mouse hepatocytes. *Methods Mol. Biol.*, **633**, 185–196.

[14] Kwon, E. J., Lasiene, J., Jacobson, B. E., Park, I.-K., Horner, P. J., and Pun, S. H. (2010) Targeted nonviral delivery vehicles to neural progenitor cells in the mouse subventricular zone. *Biomaterials*, **31**, 2417–2424.

[15] Benedetti, S., et al. (2000) Gene therapy of experimental brain tumors using neural progenitor cells. *Nat. Med.*, **6**, 447–450.

[16] Gibbings, D. J., Ciaudo, C., Erhardt, M., and Voinnet, O. (2009) Multivesicular bodies associate with components of miRNA effector complexes and modulate miRNA activity. *Nature*, **11**, 1143–1149.

[17] Stalder, L., et al. (2013) The rough endoplasmatic reticulum is a central nucleation site of siRNA-mediated RNA silencing. *EMBO J.*, **32**, 1115–1127.

[18] Gilleron, J., et al. (2013) Image-based analysis of lipid nanoparticle-mediated siRNA delivery, intracellular trafficking and endosomal escape. *Nat. Biotechnol.*, **31**, 638–646.

[19] Sahay, G., et al. (2013) Efficiency of siRNA delivery by lipid nanoparticles is limited by endocytic recycling. *Nat. Biotechnol.*, **31**, 653–658.

[20] van den Boorn, J. G., Schlee, M., Coch, C., and Hartmann, G. (2011) SiRNA delivery with exosome nanoparticles. *Nature*, **29**, 325–326.

[21] Bache, K. G., Brech, A., Mehlum, A., and Stenmark, H. (2003) Hrs regulates multivesicular body formation via ESCRT recruitment to endosomes. *J. Cell Biol.*, **162**, 435–442.

[22] Paulusse, J. M. J., Amir, R. J., Evans, R. A., and Hawker, C. J. (2009) Free radical polymers with tunable and selective bio- and chemical degradability. *J. Am. Chem. Soc.*, **131**, 9805–9812.